

İSTANBUL TECHNICAL UNIVERSITY ★ INSTITUTE OF SCIENCE AND TECHNOLOGY

**IMPROVEMENT OF THERMAL AND ELECTRICAL PROPERTIES OF
PNVC_z BY COPOLYMERS AND COMPOSITES**

**Ph.D. Thesis by
Argun T. GÖKÇEÖREN**

Department : Polymer Science and Technology

Programme : Polymer Sciene and Technology

OCTOBER 2010

**IMPROVEMENT OF THERMAL AND ELECTRICAL PROPERTIES OF
PNVCz BY COPOLYMERS AND COMPOSITES**

**Ph.D. Thesis by
Argun T. GÖKÇEÖREN
(515032001)**

**Date of submission : 10 September 2010
Date of defence examination: 21 October 2010**

**Supervisor (Chairman) : Prof. Dr. Candan ERBİL (ITU)
Members of the Examining Committee : Prof. Dr. A. Sezai SARAÇ (ITU)
Prof.Dr. Gülten ATUN (IU)
Prof.Dr. B.Filiz ŞENKAL (ITU)
Prof.Dr. Ülker BEKER (YTU)**

OCTOBER 2010

İSTANBUL TEKNİK ÜNİVERSİTESİ ★ FEN BİLİMLERİ ENSTİTÜSÜ

**KOPOLİMER VE KOMPOZİTLER VARLIĞINDA PNVCz'ÜN TERMAL VE
ELEKTRİKSEL ÖZELLİKLERİNİN İYİLEŞTİRİLMESİ**

DOKTORA TEZİ
Argun T. GÖKÇEÖREN
(515032001)

Tezin Enstitüye Verildiği Tarih : 10 Eylül 2010

Tezin Savunulduğu Tarih : 21 Ekim 2010

Danışman : Prof. Dr. Candan ERBİL (İTÜ)
Diğer Jüri Üyeleri : Prof. Dr. A. Sezai SARAÇ (İTÜ)
Prof.Dr. Gülten ATUN (İÜ)
Prof.Dr. B.Filiz ŞENKAL (İTÜ)
Prof.Dr. Ülker BEKER (YTÜ)

EKİM 2010

FOREWORD

I would like to express my deep appreciation and thanks for the infinite support, and sharing of her experience during my thesis, to my advisor Prof.Dr. Candan ERBİL.

I would like to thank my friends Erdem YAVUZ, Deniz TOPUZ, Kübra YUMAKGİL, Fatma DURAP,

I am very pleased of the support of Yasin ARSLANOĞLU and Birgül ARSLANOĞLU all along my thesis.

Thanks to Prof. Dr. Ahmet GÜL and friends in anorganic chemistry for their support.

I would like to thanks Prof. Dr. Yaşar Yılmaz for his help on conductivity measurements. And a special thanks for Esra Alveroğlu, who made clear the basics of electrical conductivity and beyond for me.

Thanks to Prof. Dr. Belkıs USTAMEHMETOĞLU and Prof.Dr. Esmâ SEZER for potentiostatic measurements.

I would like also to thanks Neslihan YUCA and Assoc.Prof..Dr. Nilgün YAVUZ for their help on TGA measurements.

I also would like to thanks my family for their support during my thesis.

September 2010

Argun.T. GÖKÇEÖREN

Chemist

TABLE OF CONTENTS

	<u>Page</u>
FOREWORD	v
TABLE OF CONTENTS	vii
ABBREVIATIONS	ix
LIST OF TABLES	xi
LIST OF FIGURES	xiii
SUMMARY	xix
ÖZET	xxvii
1. INTRODUCTION	1
2. THEORETICAL PART	7
2.1 Conductive polymers.....	7
2.2 N-Vinyl Carbazole	11
2.2.1 Electrochemical Polymerization	11
2.2.2 Chemical polymerization	13
2.3 Itaconic acid and Its Ester Derivatives	14
2.4 N-isopropylacrylamide	16
2.5. Monomer Reactivity Ratios	16
2.6. Dopamine	18
2.5 Poly(dimethylsiloxane) PDMS	19
2.6 Composites and Nanocomposites.....	20
2.6.1 Clay	25
2.6.2 Organo modified clays	26
2.6.3 Polymer / Clay Nanocomposites.....	28
2.6.4 Graphite.....	31
2.6.5 Graphite/Polymer Composites	33
2.6.6 Carbon Nanotubes.....	35
2.6.7 CNT/Polymer Composites	37
2.7 Conductivity	41
2.7.1 Voltammetric Techniques	42
2.7.2 Cyclic Voltammetry (CV).....	44
2.7.3 Other Pulse Methods	45
2.7.3.1 Normal Pulse Voltammetry (NPV)	45
2.7.3.2 Differential Pulse Voltammetry (DPV)	46
2.7.3.3 Square-Wave Voltammetry (SWV).....	46
2.8 Electrochemical Impedance Spectroscopy Theory and applications	46
2.8.1 Theory	46
2.8.2 Applications	49
3. COPOLYMERS OF N-VINYLCARBAZOLE WITH ACRYLIC ACID, ITACONIC ACID AND N-ISOPROPYL ACRYLAMIDE: SYNTHESIS, DETERMINATION OF MONOMER REACTIVITY RATIOS AND ELECTROCHEMICAL PROPERTIES	51
3.1 Experimental	51

3.2 Copolymerization.....	51
3.3 Copolymer Characterization	53
3.4 Results.....	56
3.5 Discussion.....	65
4. MORPHOLOGICAL CHARACTERIZATION AND ELECTROCHEMICAL / ELECTRICAL PROPERTIES OF POLY (N-VINYL CARBAZOLE) / MONTMORILLONITE COMPOSITES	67
4.1 Experimental	67
4.2. Preparation of PNVCz and PNVCz/MMT composites.....	67
4.3. Analysis and characterization techniques	70
4.4. Results.....	72
4.4.1. FTIR Analysis.....	72
4.4.2. X-Ray Diffraction Analysis	76
4.4.3. Morphological and Thermal Analysis	78
4.4.4. Electrochemical Properties	82
4.4.5. Electrochemical Impedance Spectroscopy (EIS) Measurements	84
4.5 Discussion	87
5. POLY(N-VINYL CARBAZOLE) (PNVCZ) BASED COMPOSITE MATERIALS: ELECTRICAL PROPERTIES, MORPHOLOGIC AND THERMAL CHARACTERIZATION OF PNVCZ/ MULTIWALLED CARBON NANOTUBE AND PNVCZ/GRAPHITE SYSTEMS.....	89
5.1 Experimental	89
5.1.1 Free radical polymerization PNVCz and P(NVCz-co-MCeI)	89
5.1.2 Oxidative polymerization of PNVCz.....	90
5.1.3 Oxidation of GLs and MWCNTs.....	91
5.1.4 Preparation of PNVCz / graphite composites	93
5.1.5 Preparation of PNVCz / MWCNT composites.....	94
5.2 Analysis and characterization techniques	95
5.3 Results and Discussion.....	96
5.3.1 XRD patterns of PNVCz/ graphite and PNVCz/carbon nanotube composites	96
5.3.2 Morphological image studies of PNVCz/graphite and PNVCz/carbon nanotube composites	99
5.3.3 Glass transition behavior of PNVCz/ graphite and PNVCz/carbon nanotube composites	101
5.3.4 Thermal Stability of PNVCz/carbon nanotube and PNVCz/ graphite composites.....	103
5.3.5 Electrical conducting properties of PNVCz/carbon nanotube and PNVCz/ graphite composites	105
5.3.6 Proposed polymerization mechanisms for PNVCz/o-GL and PNVCz/o-MWCNT composites	107
6. ELECTROCHEMICAL IMPEDANCE SPECTROSCOPY AND IN-SITU UV-VIS SPECTROELECTROCHEMISTRY STUDIES OF POLYDIMETHYLSILOXANE / POLY (N-VINYL CARBAZOLE) COMPOSITE ELECTRODES	109
6.1. Experimental.....	109
6.1.1. Electrochemical Polymerization and EIS Measurements.....	109
6. 2. Results and Discussion	110
7. CONCLUSION	124
REFERENCES.....	127
CURICULUM VITAE.....	147

ABBREVIATIONS

Cz	: Carbazole
NVCz	: N-vinyl Carbazole
NIPAAm	: N-Isopropylacrylamide
IA	: Itaconic Acid
MCeI	: Monocetyl Itaconate
ACN	: Acetonitrile
THF	: Tetrahydrofuran
EG	: Expanded Graphite
o-GL	: Oxidized Graphite
CNT	: Carbon Nanotube
MMT	: Montmorillonite
ODA-MMT	: Octadecylamine modified montmorillonite
TMSA-MMT	: Trimethylstearylammmonium modified montmorillonite
PDMS	: Polydimethylsiloxane

LIST OF TABLES

	<u>Page</u>
Table 2.1 : A Listing of the Various Methods Used to Estimate the Reactivity Ratios	18
Table 2.2 : Structure and chemical of layered silicates.....	26
Table 3.1 : Polymerization Conditions of PIA and NVCz / IA Copolymers	52
Table 3.2 : Polymerization Conditions of PAA and NVCz/AA Copolymers.....	52
Table 3.3 : Polymerization Conditions of PNIPAAm and NVCz/NIPAAm Copolymers.....	53
Table 3.4 : FTIR and DSC Results of the Samples in Tables 1 and 2	56
Table 3.5 : Copolymerization Composition Data for Reactivity Ratio Calculation of Copolymers of NVCz (1) and NIPAAm (2)	59
Table 3.6 : UV Spectroscopy Data for Determining of Composition of IA(2)/NVCz(1) and AA(2) / NVCz(1) Copolymers Synthesized from Various Initial Monomer Mixtures.....	59
Table 3.7 : Extended Kelen-Tüdós parameters for NIPAAm (2) and NVCz (1) using FTIR analysis data	61
Table 3.8 : Extended Kelen-Tüdós Parameters for IA (2) and NVCz (1) using UV-vis. Spectroscopy Data	62
Table 3.9 : Monomer Reactivity Ratios for the Copolymerization of NVCz (monomer 1) with NIPAAm, IA and AA (monomer 2), Using FTIR and UV Spectroscopy Techniques	62
Table 3.10 : The changes of peak potentials and currents of DA for three different PMEs at 500 mV/s scan rate.....	64
Table 3.11 : The changes of peak potentials and currents of dopamine for three different PMEs at 50 mV s ⁻¹ scan rate.....	64
Table 4.1 : Voltammetric and gravimetric results of PNVCz/MMT composites	68
Table 4.2 : Voltammetric and gravimetric results of PNVCz/ODA-MMT composites	69
Table 4.3 : Voltammetric and gravimetric results of PNVCz/TMSA-MMT composites	70
Table 4.4 : Conductivity results	85
Table 5.1 : Reaction possibilities between NVCz and conducting fillers.....	95
Table 6.1 : The effect of the coating temperature of PMDS, electropolymerization temperature of PNVCz and PDMS concentration on the charge, thickness and weight of the films	114
Table 6.2 : EIS fitting data of PDMS/PNVCz bilayers coated on Pt disc electrode and tested in 0.1 mol/L NaClO ₄ + ACN system.....	120
Table 6.3 : EIS fitting data of PDMS/PNVCz bilayers coated on GC disc electrode and tested in 0.1mol/L NaClO ₄ + ACN system	121
Table 6.4 : Effect of PDMS content, PNVCz and PDMS coating temperatures, and electrode material on the real impedances and specific capacitances of Pt/PDMS/PNVCz and GC/PDMS/PNVCz bilayer electrodes	122

LIST OF FIGURES

	<u>Page</u>
Figure 2.1: Conductivity range of conjugated polymers.....	7
Figure 2.2: n- and p- doped polymers	8
Figure 2.3: Tinted windows by on-off switch.....	9
Figure 2.4: Old fashion electric circuits.....	10
Figure 2.5: Illustration of electrochemical propagation of NVCz	12
Figure 2.6: Representative illustration of NVCz electrodeposition.....	13
Figure 2.7: Mono Itaconate derivatives	14
Figure 2.8: Representation of Poly(dimethylsiloxane)	20
Figure 2.9: Nanocomposite by melt blending	22
Figure 2.10: Nanocomposite by solution blending	23
Figure 2.11: Nanocomposite by In-situ polymerization	24
Figure 2.12: Montmorillonite Clay	25
Figure 2.13: Structure of 2:1 phyllosilicates Reproduced from Beyer	26
Figure 2.14: Intercalation by surfactant	27
Figure 2.15: Illustration of different states of dispersion of organoclays in polymers with corresponding WAXS and TEM results	28
Figure 2.16: Schematic illustration of two different types of thermodynamically achievable polymer/layered silicate nanocomposites	31
Figure 2.17: A schematic showing the formation of expanded graphite (EG) from natural flake graphite	32
Figure 2.18: graphite-polymer interaction	34
Figure 2.19: SEM images of purified SWCNT grown in using Alumina supported Fe-Mo catalyst on a patterned silicon substrate: (a) SWCNT at magnification of x200,000 and (b) SWCNT grown between catalyst particles at magnification x50,000.....	35
Figure 2.20: Schematic presentation of MWCNT	36
Figure 2.21: Proposed interaction of polymer and CNT.....	38
Figure 2.22: Schematic presentation of MWCNT-PNVCz interaction	39
Figure 2.23: Proposed interaction of polymer and CNT by electrochemical method	40
Figure 2.24: Electrical conductivity as a function of reduced mass fraction of nanotubes, showing a threshold of 0.11 wt %.	41
Figure 2.25: Different voltametric step models	45
Figure 2.26: Sinusoidal Current Response in a Linear System	47
Figure 2.27: Nyquist Plot with Impedance Vector	49
Figure 3.1: Schematic illustration of used chemicals	51
Figure 3.2: FTIR spectra of NVCz /AA copolymers, which are given in Table 3.2	54
Figure 3.3: FTIR spectra of NVCz / NIPAAm copolymers, which are given in Table 3	55
Figure 3.4: Relationship between $1/T_g$ and w_{IA}	57

Figure 3.5: Calibration curves for NVCz / AA, NVCz / IA and NVCz / NIPAAm copolymers.....	58
Figure 3.6: UV spectra of NVCz/IA copolymers ($\lambda_{\text{max}} = 295 \text{ nm.}$), which are given in Table 1	59
Figure 3.7: EKT Method for determining monomer reactivity ratios in the copolymerization of NVCz (1) and NIPAAm (2) by using FTIR spectroscopy data ($\alpha = 0.3104$)	60
Figure 3.8: EKT Method for determining monomer reactivity ratios in the copolymerization of NVCz (1) and NIPAAm (2) by using UV spectroscopy data ($\alpha = 0.3299$)	61
Figure 3.9: EKT Method for determining monomer reactivity ratios in the copolymerization of NVCz (1) and IA (2) by using UV spectroscopy data ($\alpha = 0.3106$)	61
Figure 3.10: The CVs of $9.0 \times 10^{-4} \text{ mol/L}$ of DA on the the PNVCz, NVCz/NIPAAm and NVCz/IA modified electrodes in phosphate buffer solution (pH 7.0) at 50 mV / s scan rate.....	63
Figure 3.11: The CVs of $9.0 \times 10^{-4} \text{ mol/L}$ of DA on the PNVCz, NVCz/NIPAAm and NVCz/IA modified electrodes in phosphate buffer solution (pH 7.0) at 500 mV /s scan rate.....	63
Figure 3.12: Scan rate dependence of DA response on NVCz/NIPAAm coated electrode	65
Figure 4.1: Schematic illustration of used chemicals.....	67
Figure 4.2: FTIR spectra of Na^+MMT , ODA-MMT and TMSA-MMT.....	73
Figure 4.3: FTIR spectra of PNVCz/ODA-MMT, 15.0 wt %, composites prepared by sonication for 5 min. (a), by sonication for 1 hour (b) and by mechanical stirring for 1 hour	74
Figure 4.4: FTIR spectra of PNVCzs synthesized with AIBN and CAN (a, b) and, PNVCz/ Na^+MMT composites synthesized by using CAN to initiate the polymerization and by mixing with magnetic stirrer (c), sonic tip (d) and homogenizator (e) to obtain homogeneous dispersions of Na^+MMT (15.0 wt %, based on NVCz concentration) in ACN	75
Figure 4.5: X-ray diffraction patterns of Na^+MMT (a), ODA-MMT (b) and TMSA-MMT (c)	76
Figure 4.6: XRD patterns in the range of 2θ from 2° to 10° of PNVCz/ Na^+MMT (a), PNVCz/ODA-MMT (b) and PNVCz/TMSA-MMT (c) composites intercalated by sonication for 5 min (MMT content = 15.0 wt % of NVCz concentration).....	76
Figure 4.7: XRD patterns in the range of 2θ from 2° to 10° of PNVCz/ODA-MMT (a) and PNVCz/TMSA-MMT (b) composites intercalated by mechanical stirring for 1 hour (MMT content = 15.0 wt % of NVCz concentration)	77
Figure 4.8: DSC thermograms of PNVCzs initiated with AIBN (a) and CAN (b) and, Sample 1 (c), Sample 4 (d), Sample 2 (e), Sample 5 (f), Sample 3 (g) and Sample 6 (h) in Table I.....	79
Figure 4.9: SEM micrograph of PNVCz/ Na^+MMT (15.0 wt %) prepared with magnetic stirring for 17 hours (Sample 1 in Table I).....	80
Figure 4.10: SEM micrograph of PNVCz/ Na^+MMT (15.0 wt %) prepared with ultrasonic agitation for 5 min (Sample 4 in Table I).....	80

Figure 4.11: Optical microscope images for PNVCz/MMT composites containing (a, c) 15.0 wt % ODA-MMT and TMSA-MMT, respectively ; for 17 hours magnetic stirring, (b, d) 15.0 wt % ODA-MMT and TMSA-MMT, respectively ; for 5 min ultrasonic agitation, (e, f) 1.0 wt % ODA-MMT ; for 5 min ultrasonic agitation. Image (f) is the same position with the others but under cross-polarized light condition.....	81
Figure 4.12: Cyclic voltammograms of GC electrode during electrochemical deposition of chemically synthesized PNVCz/TMSA-MMT composite (Sample 22 in Table III) in ACN + NaClO ₄ solution. Scan rate: 50 mV / s. Inset: Cyclic voltammograms of PNVCz/TMSA-MMT coated GC electrode in three different scan rates (50, 250 and 500 mV/s). Supporting electrolyte: NaClO ₄ in ACN.....	82
Figure 4.13: Cyclic voltammograms of Pt electrode during electrochemical deposition of chemically synthesized PNVCz/TMSA-MMT composite (Sample 18 in Table III) in NaClO ₄ + ACN solution. Scan rate: 50 mV / s. Inset: Cyclic voltammograms of PNVCz/TMSA-MMT coated Pt electrode in three different scan rates (50, 250 and 500 mV/s). Supporting electrolyte: NaClO ₄ in ACN.....	83
Figure 4.14: Bode plots showing change in phase angle of bare GC disc electrode (a) and GC electrode coated on PNVCz polymerized chemically (b) and electrochemically (c), PNVCz / TMSA-MMT composites mixed with sonicator (d), homogenizator (e) and magnetic stirrer (f) (Samples 6, 11 and 3, respectively, in Table I) during dispersion of silicate layers	85
Figure 4.15: Nyquist plots of PNVCz / ODA-MMT composites containing 15.0 (a), 5.0 (b) and 1.0 (c) wt % of layered silicate (Samples 5, 12 and 13, respectively, in Table II) coated on Pt electrode. Their corresponding equivalent circuit and the enlarged data in high frequency are shown in insets. Symbols Z' and Z'' refer to the real and imaginary components.....	86
Figure 5.1: Schematic illustration of used chemicals	89
Figure 5.2: Polymerization reaction of P(NVCz-co-MCeI) copolymer	90
Figure 5.3: Possible mechanism for the polymerization of NVCz by Ce (IV) ion.....	91
Figure 5.4: FTIR spectra of o-GLs (a) and o-MWCNT (b).....	91
Figure 5.5: Proposed mechanism for the in situ polymerization of NVCz without CAN by sonicated o-GLs in ACN/water/SDS (10.0 wt % of NVCz) mixture at room temperature	94
Figure 5.6: Proposed mechanism for the in situ polymerization of NVCz without CAN by sonicated o-MWCNTs in ACN at room temperature	95
Figure 5.7: XRD patterns of (a) o-GLs, (b) PNVCz initiated with CAN and, PNVCz/o-GLs composites prepared by in-situ polymerization (c) without CAN and (d) with CAN as oxidant, respectively.....	97

Figure 5.8: XRD patterns of (a) P(NVCz-co-MCeI), (b) and (c) P(NVCz-co-MCeI)/MWCNT (1.0 and 15.0 wt %, respectively) composites prepared by solution blending, (d) and (e) PNVCz(initiated with CAN)/MWCNT (1.0 and 15.0 wt %, respectively) composites prepared by solution blending and (f) MWCNT	98
Figure 5.9: Polarizing microscope images of PNVCz/o-GLs composites prepared by in situ polymerization method in ACN/water mixture (a) without CAN in the presence of 10.0 wt % of SDS and (b) with CAN in the presence of 1.0 wt % of SDS, respectively.....	99
Figure 5.10: Polarizing microscope images of (a) PNVCz/MWCNT, (b) P(NVCz-co-MCeI)/MWCNT and (c) P(NVCz-co-MCeI)/o-GLs composites prepared by solution blending method in THF containing 1.0 wt % o-GLs	100
Figure 5.11: DSC thermograms of (a) PNVCz prepared by oxidative polymerization, (b) and (c) PNVCz/o-GLs composites prepared by in situ polymerization method in ACN/water mixture with CAN in the presence of 1.0 wt % of SDS and without CAN in the presence of 10.0 wt % of SDS, respectively	102
Figure 5.12: DSC thermograms of PNVCz initiated with AIBN and PNVCz/MWCNT composite (a,b), P(NVCz-co-MCeI) initiated with AIBN and P(NVCz-co-MCeI)/MWCNT composite (c, d), PNVCz initiated with CAN and PNVCz/MWCNT composite (e, f) (preparation method = solution blending in THF; filler content = 1.0 wt %).....	103
Figure 5.13: TGA thermograms of poly(N-vinyl carbazole)s initiated with AIBN and CAN (a, b), PNVCz/o-GLs composites prepared by in situ polymerization method in ACN/water mixture without CAN in the presence of 10.0 wt % of SDS (c) and with CAN in the presence of 1.0 wt % of SDS (d), respectively, under air atmosphere	104
Figure 5.14: TGA thermograms of PNVCz and P(NVCz-co-MCeI) initiated with AIBN (a, b) and, PNVCz/MWCNT and P(NVCz-co-MCeI)/MWCNT composites under air atmosphere (preparation method = solution blending in THF; filler content = 1.0 wt %)	105
Figure 5.15: Electrical conductivities plotted as a function of filler volume fraction: (a) PNVCz/MWCNT composites prepared by solution blending, (b) PNVCz/o-GLs/SDS/CAN composites prepared by in situ polymerization and (c) PNVCz/o-GLs/SDS composite prepared by in situ polymerization	106
Figure 5.16: Electrical conductivities plotted as a function of MWCNT weight fraction: (a) PNVCz (initiator: AIBN) /MWCNT, (b) P(NVCz-co-MCeI) (initiator: AIBN)/MWCNT and (c) PNVCz (initiator: CAN) /MWCNT composites prepared by solution blending method in THF.....	107
Figure 6.1: FTIR spectra of (a) PNVCz/o-MWCNT composite, (b) PNVCz extracted from PNVCz/o-MWCNT composite and (c) PNVCz/o-GLs composite prepared by in situ polymerization without CAN and, (d) PNVCz synthesized by CAN in ACN	111
Figure 6.2: Cyclic voltammogram of NVCz in 0.1mol/L TBABF ₄ +ACN at 50mV/s scan rate on PDMS (5.0 wt %) coated Pt electrode.....	111

Figure 6.3: Cyclic voltammogram of NVCz in 0.1mol/L TBABF ₄ +ACN system at 50mV/s scan rate on PDMS (5.0 wt %) coated GC electrode.....	112
Figure 6.4: Cyclic voltammograms of (a) GC/PNVCz, (b) GC/PDMS(5.0 wt %)/PNVCz, (c) GC/PDMS(10.0 wt %)/PNVCz and (d) GC/PDMS(15.0 wt %)/PNVCz electrodes in MF solution at 50mV/s scan rate (0.1mol/L NaClO ₄ +ACN system; 25°C was chosen as PDMS coating and NVCz electropolymerization temperatures)	113
Figure 6.5: Cyclic voltammograms of (a) Pt/PNVCz, (b) Pt/PDMS (5.0 %; 25°C)/ PNVCz (25°C) and (c) Pt/PDMS (5.0 %; -15°C)/ PNVCz (-15°C) electrodes in MF solution (0.1mol/L NaClO ₄ +ACN) at 50mV/s scan rate.....	115
Figure 6.6: Bode phase plots of (a) Pt and (b) Pt/PNVCz , (c) Pt/PDMS (5.0 wt/v %; 25°C)/PNVCz (25°C), (d) Pt/PDMS (5.0 wt/v % ; 25°C)/PNVCz (0°C), (e) Pt/PDMS(5.0 wt/v % ; 25°C)/PNVCz (-15°C) and (f) Pt/PDMS(5.0 wt/v % ; -15°C)/PNVCz (-15°C) composite electrodes in ACN containing 0.1 mol/L NaClO ₄	115
Figure 6.7: Bode phase plots of (a) GC and (b) GC/PNVCz , (c) GC/PDMS (5.0 wt %) /PNVCz, (d) GC/PDMS (10.0 wt %) /PNVCz and (e) GC/PDMS(15.0 wt %) /PNVCz electrodes in ACN containing 0.1 mol/L NaClO ₄ at 25°C.....	117
Figure 6.8: Nyquist plots of (a) Pt, (b) Pt/PNVCz, (c) Pt/PDMS(5.0 wt/v % ; 25°C)/PNVCz (25°C), (d) Pt/PDMS(5.0 wt/v % ; -15°C)/PNVCz (-15°C), (e) Pt/PDMS(10.0 wt/v % ; 25°C)/PNVCz (25°C), (f) Pt/PDMS(10.0 wt/v % ; -15°C)/PNVCz (-15°C) electrodes in ACN containing 0.1 mol/L NaClO ₄ . The points denote the experimental data while the line represents the fitting obtained using the equivalent circuit in Figure 9	117
Figure 6.9: Equivalent circuit for PDMS / PNVCz composite electrodes: R _{el} / R _{pol} refer electrode resistance (bare electrode)/bulk resistance (polymer coated electrode). R _{sol} / R _{ct} denote solution/charge-transfer resistances	118
Figure 6.10: In-situ UV spectra of PDMS (5.0 wt/v % in THF) / PNVCz composites coated on ITO, at four different potentials between 800 mV and 1400 mV	121
Figure 6.11: Absorption spectra of (a) PNVCz and (b) PNVCz/PDMS films at different potentials	122

NANOSTRUCTURED MATERIALS BASED ON CARBAZOLE COPOLYMERS

SUMMARY

The interaction between the components of composites have generated a new domain to materials with uncommon properties. The composites are prepared by various nanostructured components such as inorganic oxides, organically modified clays, carbon nanotubes and graphite.

Clays are composed of layered silicates. The more commonly used layered silicates (montmorillonite, hectorite, and saponite) are tetrahedrally substituted. Organically modified clays are produced from natural smectite clays consisting of two fused silicate tetrahedral sheets sandwiching between octahedral sheet of either magnesium or aluminium hydroxide, by substituting the alkali and alkaline earth cations situated inside the layers with organic ammonium or quaternized ammonium salts

Carbon nanotubes (CNTs) have received much attention for their many potential applications such as nanoelectronic and photovoltaic devices, superconductors, electromechanical actuators, electrochemical capacitors, nanowires and nanocomposite materials.

Graphite is like CNT, a carbon allotrop used to improve conductivity. Pristine graphite is composed of carbon sheets separated by layers such as smectite clays.

Poly(N-vinyl carbazole) PNVCz is a well known photoconductive polymer with high Tg (227°C) and low conductivity in the insulating state ($\sim 10^{-15}$ S/cm).

In this thesis, we have mainly tried to improve the conductive properties of PNVCZ, by using nanostructured materials such as montmorillonite (MMT), multiwall carbonnanotube (MWCNT) and graphite and so by synthesizing copolymers and/or composites.

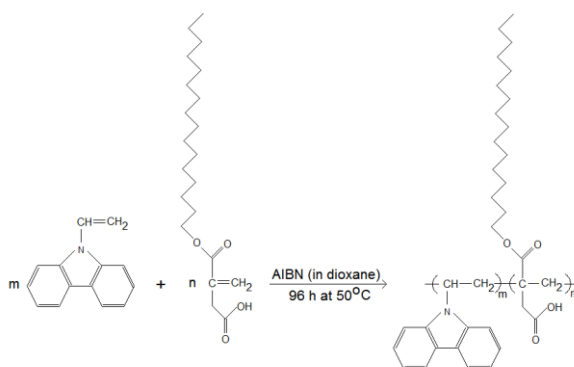


Figure 1: Free radical polymerization of N-vinyl carbazole with monocetyl itaconate.

The copolymers of NVCz with acrylic acid(AA), itaconic acid (IA), N-isopropylacrylamide (NIPAAm) and monocetyl itaconate (MCI) as hydrophilic ,

hydrophobic and hydrophilic / hydrophobic comonomers having different composition were synthesized by free radical solution polymerization in 1,4-Dioxane with AIBN (1.0×10^{-3} mol / L) at 50°C under nitrogen atmosphere (Figure 1). The total monomer concentration of 1.0 mol / L was kept constant while the feed ratio of the monomers was varied.

The compositions of these copolymers were determined by Ultraviolet (UV) and Fourier transform infrared (FTIR) spectroscopies (Figure 2).

The monomer reactivity ratios were computed by application of extended Kelen-Tüdös (EKT) method at high conversion, which is one of the conventional linearization methods, and found to be $r_{\text{NVCz}} = 0.29$ and $r_{\text{NIPAAm}} = 0.12$, $r_{\text{NVCz}} = 0.84$ and $r_{\text{IA}} = 0.12$, $r_{\text{NVCz}} = 0.86$ and $r_{\text{AA}} = 0.31$ by UV, $r_{\text{NVCz}} = 0.32$ and $r_{\text{NIPAAm}} = 0.07$ by FTIR, respectively (Figure 3).

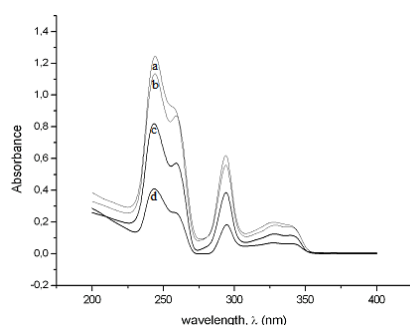


Figure 2: NVCz/IA kopolimerlerine ait UV spektrumları % (a)20.0, (b)40.0, (c)60.0 and (d) 80.0 IA mol içeriğinde. ($\lambda_{\text{max}} = 295$ nm.).

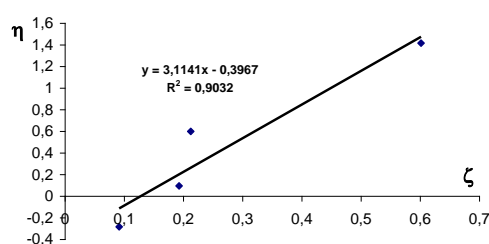


Figure 3:EKT Method for determining monomer reactivity ratios in the copolymerization of NVCz (1) and IA (2) by using UV spectroscopy data ($\alpha = 0.3106$).

Polymer modified electrodes having electroactive, ionic and hydrophobic properties were prepared by electrooxidation using PNVCz, NVCz/NIPAAm and NVCz/IA copolymers and tested as sensor electrodes to dopamine (DA).

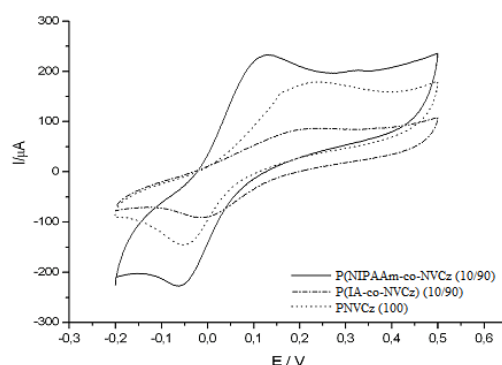


Figure 4: The CVs of 9.0×10^{-4} mol/L of DA on the PNVCz, NVCz/NIPAAm and NVCz/IA modified electrodes in phosphate buffer solution (pH 7.0) at 50 mV / s scan rate.

It can be said that the electrochemical responses of DA were remarkably enhanced in the cases of copolymers coated electrodes. It is probably due to the adsorption,

resulting from the hydrophobic isopropyl group of NIPAAm or hydrophilic carboxyl groups of IA.

The composites of P(N-vinyl carbazole-co-monoethyl itaconate) P(NVCz-co-MCeI) copolymer with multi walled carbon nanotube (MWCNT) were prepared by solution blending process.

In a beaker, 10 ml of THF and a certain amount of MWCNTs (to yield the desired loading of MWCNTs from 0.5 to 2.0 wt % in 100 mg of PNVCz and P(NVCz-co-MCeI)) were mixed and dispersed by sonication. Then, 0,1 g of PNVCz and its copolymers, P(NVCz-co-MCeI) were dissolved in the MWCNT/THF dispersions and stirred using magnetic stirrer for 1 h. After that, PNVCz/MWCNT/THF and P(NVCz-co-MCeI)/MWCNT/THF mixtures were transferred into glass petri dishes. Remaining THF was first evaporated in the petri dishes at room temperature for 1 d and then in a vacuum oven at 25° C for 2 d to yield PNVCz /carbon nanotube composites prepared by solution blending process.

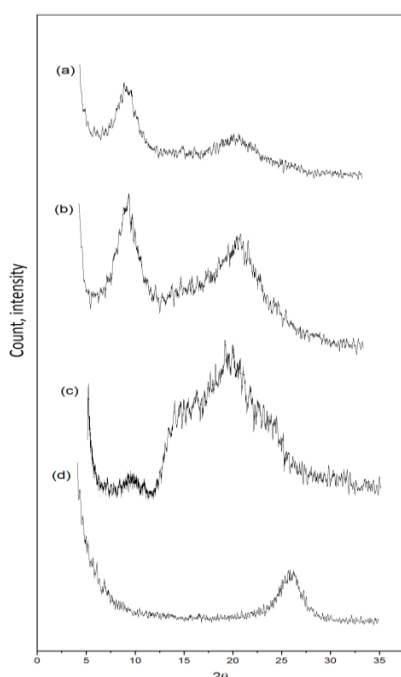


Figure 5: XRD patterns for, P(NVCz-co-MCeI) (a), MWCNT/P(NVCz-co-MCeI) composites for 1.0 (b) and 15.0 wt % (c) filler and MWCNT (d) prepared by solution blending in THF.

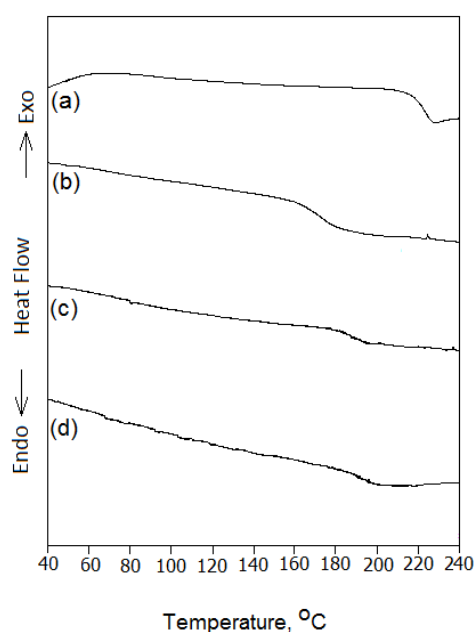


Figure 6: DSC thermograms of PNVCz initiated with AIBN and PNVCz/MWCNT composite (a,b), P(NVCz-co-MCeI) initiated with AIBN and P(NVCz-co-MCeI)/MWCNT composite (c, d), (preparation method = solution blending in THF; filler content = 1.0 wt %).

XRD patterns for MWCNT, P(NVCz-co-MCeI) and their composites prepared by solution blending in THF (carbon nanotube content = 1.0 and 15.0 wt %, based on polymer) are shown in Figure 5.

The copolymer of NVCz clearly illustrated two diffraction peaks at $2\theta = 7.5^\circ$ and 23.5° , while the MWCNT demonstrated the diffraction peak at $2\theta = 26^\circ$. The three peaks appeared at different locations ($2\theta = 12.5^\circ$, 17.5° and 22.5°) in the P(NVCz-co-MCeI)/MWCNT composite (Figure 5) clearly support that the introduction of PNVCz-co-MCeI affects the structure of both MWCNTs and PNVCz-co-MCeI chains. These three diffraction peaks may be an indication of the crystalline behavior of PNVCz-co-MCeI.

Figure 6 shows the DSC curves of PNVCz/MWCNT composites prepared by solution blending process in THF. It was found that the T_g s of PNVCz after being added a 1.0 wt % of MWCNTs strongly decreased comparing with pristine polymer whereas the T_g of the composite based on the copolymer of NVCz with monocetyl itaconate slightly increased. These results were attributed to the characteristics of the composites and indicated that the quality of dispersion shifted T_g but the direction of shifts were dependent on the intermolecular interactions between the MWCNTs and polymer chains. As to the DSC thermograms in Figure 6, the compatibility between PNVCz and MWCNT were highly improved by the addition of 5.0 mol % of MCeI, bearing a long hydrophobic chain and a hydrophilic group, to the PNVCz chains.

The conductivity at room temperature of the PNVCz/MWCNT composites prepared by solution blending is shown in Figure 7 as a function of the weight fraction of the MWCNTs. The conductivities of PNVCz initiated with N,N'-azobisisobutyronitrile (AIBN) (a) and cerium ammonium nitrate (CAN) (c), and P(NVCz-co-MCeI) initiated with AIBN (b) are 2.1×10^{-13} , 2.3×10^{-11} and 3.2×10^{-10} S/cm, respectively. According to the percolation theory, the percolation threshold corresponds to the onset of the transition from an insulator to a semi-conductor. At low MWCNT content less than 0.12 vol %, the conductivities resemble to that of an insulator. Between 0.24 and 0.95 vol % of filler, the composites exhibit smooth transition from insulator state to semi-conducting region and then at higher concentrations than 0.95 vol %, their conductivities reach 10^{-6} - 10^{-5} S/cm and steady-state region occurs, which are consistent with that of a semi-conductor.

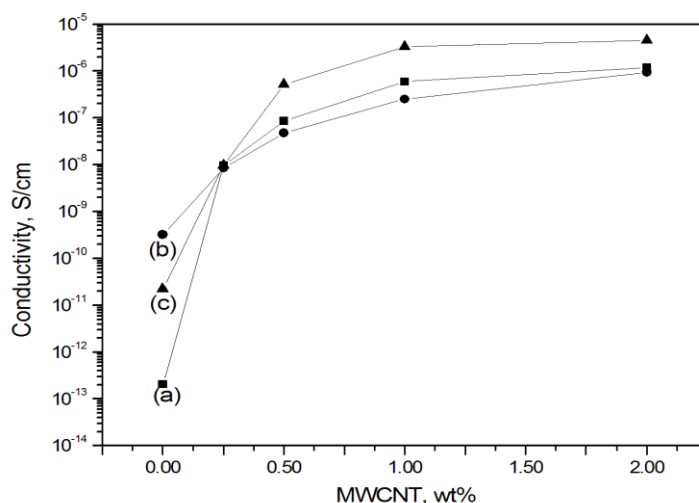


Figure 7: Electrical conductivities plotted as a function of MWCNT weight fraction: (a) PNVCz (initiator: AIBN) /MWCNT, (b) P(NVCz-co-MCeI) (initiator: AIBN)/MWCNT and (c) PNVCz (initiator: CAN) /MWCNT composites prepared by solution blending method in THF.

The oxidative polymerization process was as follows: NVCz monomer with a known weight was dissolved in ACN. Then, CAN as an oxidizing agent was added into the NVCz/ACN solution to initiate the polymerization. The mol ratio of monomer to oxidizing agent was kept at 200:1. 1.0 mol /L concentration of NVCz was used. The synthesis was carried out at 25°C under atmospheric conditions.

The oxidized graphite is a strongly oxygenated, highly hydrophilic layered material. In this part of the thesis, it was dispersed in ACN/water mixture containing sodium dodecyl sulphate (SDS). NVCz monomer and o-GLs/ACN/water/SDS(10 wt %) dispersion at room temperature produced PNVCz/o-GLs composite by in situ polymerization method without CAN (Figure 8).

The polymerization mechanism between the dispersion of o-GLs and NVCz in the presence of 10.0 wt % of SDS is not clear. It is assumed that during sonication, SDS molecules help to disperse o-GLs, and afterwards they are adsorbed on the surfaces of o-GLs and prevent the aggregation of graphite layers by repulsive forces and then, the direct interaction of NVCz, being an electron donor molecule with the graphite layers (sonicated and so strongly activated, and decorated with functional groups) creates charge transfer between them (Figure 9).

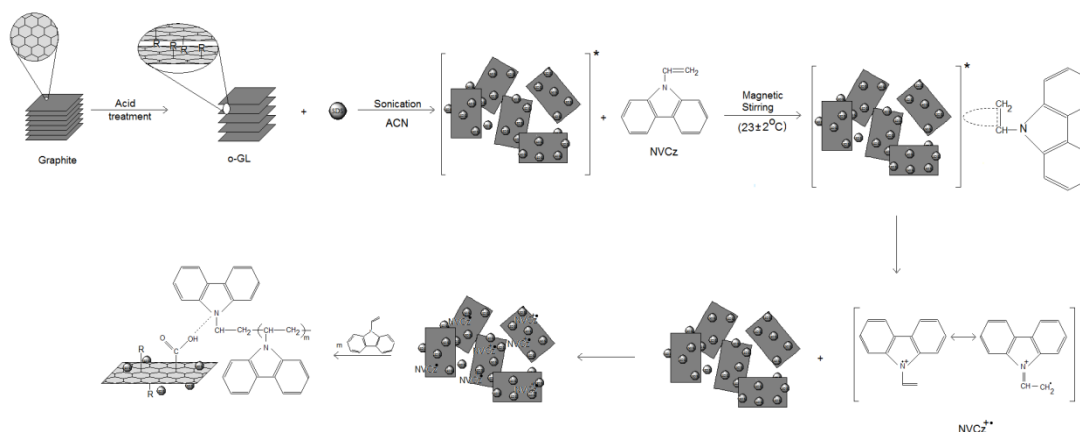


Figure 8: Proposed mechanism for the in situ polymerization of NVCz without CAN by sonicated o-GLs in ACN/water/SDS (10.0 wt % of NVCz) mixture at room temperature.

In the FTIR spectra of the composites, the presence of characteristic bands of PNVCz ($1600 - 1450 \text{ cm}^{-1}$ for aromatic stretching and aromatic $-\text{CH}$ in plane bending, and 750 cm^{-1} for aromatic $-\text{CH}$ out of plane bending), together with the peaks around 1750 cm^{-1} and 3450 cm^{-1} , which are attributed to the o-GLs also confirms the formation of PNVCz/o-GLs composite without CAN.

PNVCz / MMT composites were also prepared by the heterogeneous solution polymerization. First, Na+MMT, octadecylamine-MMT (ODA-MMT) and trimethyl stearyl ammonium-MMT (TMSA-MMT) with known weight were dispersed into ACN using magnetic stirrer, homogenizator (GN 125, 230V/50/60 Hz, 8000-30000 rpm) and high-power sonic tip (Sonopuls HD 2200, 200W/20kHz). Then, the monomer was added into these dispersions before the polymerization in the presence of CAN. After completed reaction period, the precipitate was santrifugated and washed with ACN at least 3 times to remove any unreacted NVCz and dried under vacuum at room temperature. The same process was used to prepare the PNVCz homopolymer.

Their morphologies and electrochemical / electrical properties were characterized by Fourier Transform Infrared Spectroscopy (FTIR), X-Ray Diffractometer (XRD), Differential Scanning Calorimetry (DSC), Polarized Optical Microscope (POM), Scanning Electron Microscope (SEM), Electrochemical Impedance Spectroscopy (EIS) and Cyclic Voltammetry (CV).

The chemically polymerized PNVCz and its composites with layered silicates were deposited at 1.2 V by electrooxidation in ACN containing 0.1 mol/L NaClO₄ on platinum (Pt) and glassy carbon (GC) disc electrodes. Cyclic voltammograms (CVs) of the working electrodes were obtained between 0.5 to 1.5 V at the scan rate 50 mV/s by using a Gamry Reference 600 potentiostat. A three-electrode cell containing Pt or GC disc electrodes that have diameters 1.6 and 3.0 mm, respectively, as working electrode, a Pt wire as the counter electrode, and a silver (Ag) wire as the pseudo-reference electrode were used for all electrochemical characterizations.

The electrochemical activity of the PNVCz/MMT composites was evaluated from the current–voltage curves obtained by cyclic voltammetry. After 6 scans, GC and Pt disc electrodes coated with composite films were taken out of electrochemical cell, washed with ACN, and placed in a monomer free solution. CVs of PNVCz and PNVCz/MMT composites in ACN+0.1 mol/L NaClO₄ system were recorded in 0.5 – 1.5 V potential range at three different scan rate.

EIS is an effective method to study the interfacial properties of surface-modified electrodes. Bode and Nyquist plots are constructed, and appropriate equivalent circuit model is used to correlate the impedance measurements with the capacitance and the resistance of the film. Special attention is paid to obtain a relationship between the type of conductivity (electronic and/or ionic) and the shape of impedance spectra.

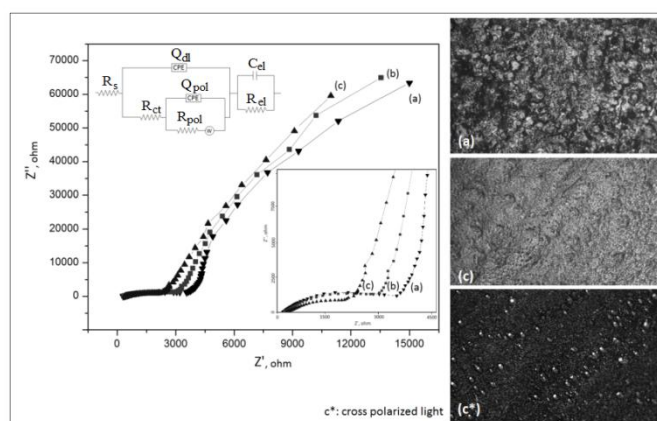


Figure 9: Nyquist plots of PNVCz / ODA-MMT composites containing 15.0 (a), 5.0 (b) and 1.0 (c) wt % of layered silicate coated on Pt and their polarized optic micrographs.

Nyquist plots of PNVCz/ODA-MMT composites prepared using sonicator with three different clay content (1.0, 5.0 and 15.0 wt % of ODA-MMT based on NVCz concentration in the feed) at room temperature are shown in Figure 9. All three plots exhibit a semicircular arc in the high frequency region and an oblique line in the low frequency region. In another word, these Nyquist plots are characterized by two regions: a semicircle at high frequencies associated with charge transfer (R_{dl}) at the polymer/solution interface and an oblique line indicating a diffusion-controlled process at the electrode, i.e., R_{pol} (or R_b). The interactions between solution -

PNVCz/ODA-MMT - Pt interfaces were modelled as an equivalent circuit consisting of the parallel combination of the double-layer constant phase element (CPE- Q_{dl}) and charge transfer resistance (R_{ct}), in series with parallel circuit of bulk-polymer constant phase element (CPE- Q_{pol}), the bulk-polymer resistance (R_{pol}) and Warburg impedance (W).

The morphological images of the composites containing 15.0 and 1.0 wt % clay show more ordered morphology for PNVCz/ODA-MMT composites. The addition of the inorganic particles into the polymer matrix promoted not only an improvement on the morphological properties but also contributed to the increase in the conductivity of PNVCz. From EIS and DC-measurements, it has been shown that the conductivity of PNVCz in the presence of ODA-MMT between 15.0 and 1.0 wt % at room temperature increased from 10^{-13} S/cm to 10^{-5} S/cm.

Poly(N-vinyl carbazole) / Poly(dimethylsiloxane) (PNVCz/PDMS) composite electrodes were also prepared by electrochemical polymerization of NVCz monomer onto PDMS coated platinum (Pt) and glassy carbon (GC) electrode surfaces to investigate the influence of the insulating constituent, PDMS and process temperature on the capacitive performance of the coated layers. The electrochemical properties of the bilayer coatings were studied by electrochemical impedance spectroscopy and UV-vis spectroelectrochemistry measurements. The specific capacitance values of composite electrodes indicated that the capacitive behaviors of the composites decreased with increasing PDMS content in coating solutions (from 5.0 to 10.0; in wt/v %) and with decreasing coating temperatures of PDMS and PNVCz (from 25°C to -15°C) and, more resist PDMS/PNVCz layers are formed (Figure 10).

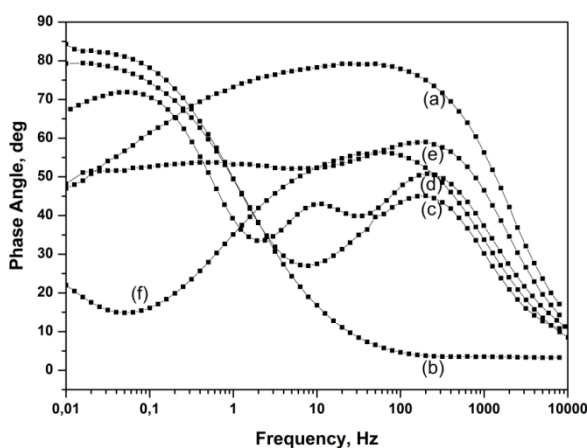


Figure 10: Bode phase plots of (a) Pt and (b) Pt/PNVCz, (c) Pt/PDMS (5.0 wt/v %; 25°C)/PNVCz (25°C), (d) Pt/PDMS (5.0 wt/v %; 25°C)/PNVCz (0°C), (e) Pt/PDMS(5.0 wt/v %; 25°C)/PNVCz (-15°C) and (f) Pt/PDMS(5.0 wt/v %; -15°C)/PNVCz (-15°C) composite electrodes in ACN containing 0.1 mol/L NaClO₄.

KARBAZOL KOPOLİMERLERİNE DAYALI NANOYAPILI MALZEMELER

ÖZET

Kompozitleri oluşturan bileşenler arasındaki etkileşimler farklı özelliklere sahip yeni malzemelerin olduğu bir alan yaratmıştır. Kompozitler inorganik oksitler, organik modifiye killer, karbon nanotüpler ve grafit gibi birçok farklı nano yapıya sahip bileşen kullanılarak elde edilirler.

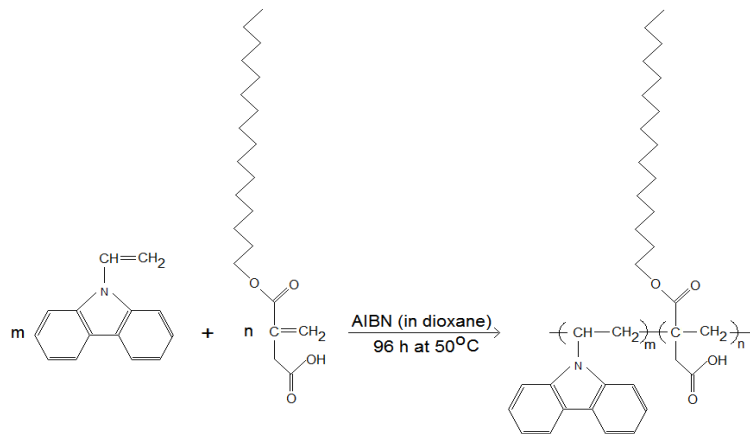
Killer tabakalı silikatlardan oluşmaktadır. En sık kullanılan tabakalı silikatlar (montmorillonite, hektorit ve saponite) tetrahedral yapıdadır. Organik olarak değiştirilmiş killer tetrahedral yapıdaki iki silikat tabakası arasındaki oktahedral yapıdaki magnezyum veya alüminyum hidroksit içeren tabakadaki alkali ve toprak alkali kationlarının organik amonyum veya kuaterner amonyum tuzları ile süstitüe edilmesiyle elde edilir.

Karbon nanotüpler (CNT) nanoelektronik ve fotovoltaik malzemeler, süperiletkenler, elektrokimyasal kapasitörler, nanokablolar ve nanokompozit malzemeler gibi birçok potansiyel uygulamaya dikkat çekmiştir.

CNT gibi bir karbon allotropu olan grafit de iletkenliği iyileştirmede kullanılır. Ayrıca grafit de kile benzer şekilde tabakalı bir yapıdan oluşmaktadır.

Yüksek camısı geçiş sıcaklığına, T_g (227°C) sahip olan Poli(N-vinil karbazol) (PNVCz) yalıtkan haldeyken düşük iletkenliğe ($\sim 10^{-15}$ S/cm) sahip fotoiletken bir polimerdir.

Bu tezde, PNVCz'ün elektriksel özelliklerinin iyileştirilebilmesi için kimyasal ve elektrokimyasal yöntemlerle MMT, çok katmanlı karbon nanotüp ve grafit gibi nano yapıya sahip malzemeler ve PNVCz'ün kopolimerleri kullanılarak kompozitleri sentezlendi.

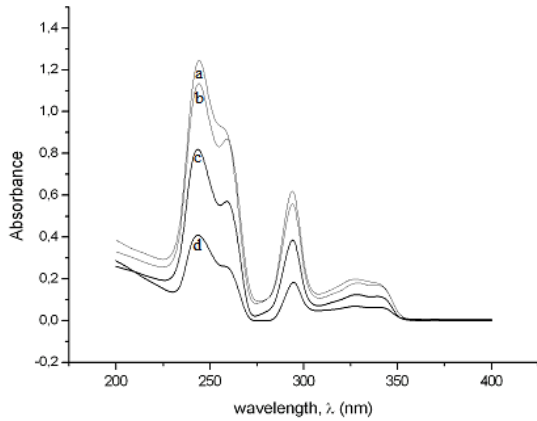


Şekil 1: NVCz ile Monosetil itakonate (MCEI)'nin serbest radikal polimerizasyonu.

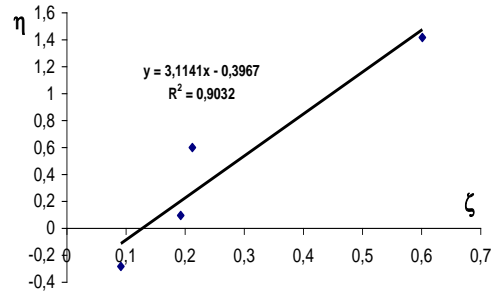
PNVCz ve kopolimerleri, NVCz ile hidrofilik, hidrofobik ve hidrofilik/hidrofobik yapıdaki itakonik asit(IA), akrilik asit (AA), N-izopropilakrilamid (NIPAAm) ve Monosetil itakonat (MCeI) komonomerleri (Şekil 1) kullanılarak çözelti polimerizasyonu ile 1,4 dioksanda ve başlatıcı olarak AIBN(1.0×10^{-3} mol / L) kullanılarak 50°C 'de ve azot atmosferinde, sentezlendi. Monomer oranı değişmekle birlikte toplam monomer konsantrasyonu 1.0 mol / L olarak tutuldu.

Kopolimer kompozisyonu morötesi (UV) ve Fourier dönüşümlü kızılötesi (FTIR) spektroskopisi ile tespit edildi (Şekil 2).

Yüksek dönüşümler için sıkça kullanılan genişletilmiş Kelen Tüdos (EKT) yöntemi ile hesaplanan monomer reaktiflik oranları, FTIR için $r_{\text{NVCz}} = 0.29$ ve $r_{\text{NIPAAm}} = 0.12$, $r_{\text{NVCz}} = 0.84$ ve $r_{\text{IA}} = 0.12$, $r_{\text{NVCz}} = 0.86$ ve $r_{\text{AA}} = 0.31$ ve UV için $r_{\text{NVCz}} = 0.32$ ve $r_{\text{NIPAAm}} = 0.07$ olarak bulundu (Şekil 3).

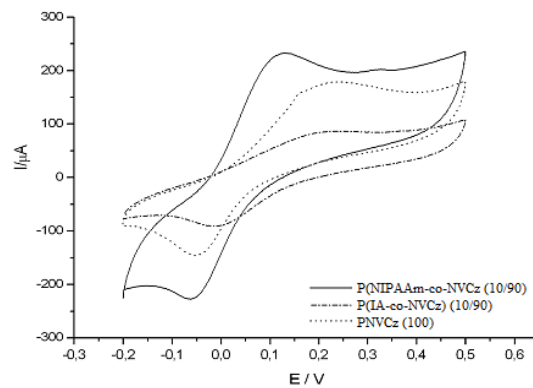


Şekil 2: (a)%20.0, (b)%40.0, (c)%60.0 ve (d) %80.0 mol IA içeren NVCz/IA kopolimerlerine ait UV spektrumları. ($\lambda_{\text{max}} = 295$ nm.).



Şekil 3: UV spektroskopik verileri ve EKT yöntemi kullanılarak NVCz (1) ve IA (2) monomer reaktivite oranlarının belirlenmesi ($\alpha = 0.3106$).

Elektroaktif, iyonik ve hidrofobik özellikleri PNVCz, NVCz/NIPAAm ve NVCz/IA kopolimerleri ile modifiye edilmiş elektrotlar dopamin'e karşı sensor elektrot olarak test edildi.

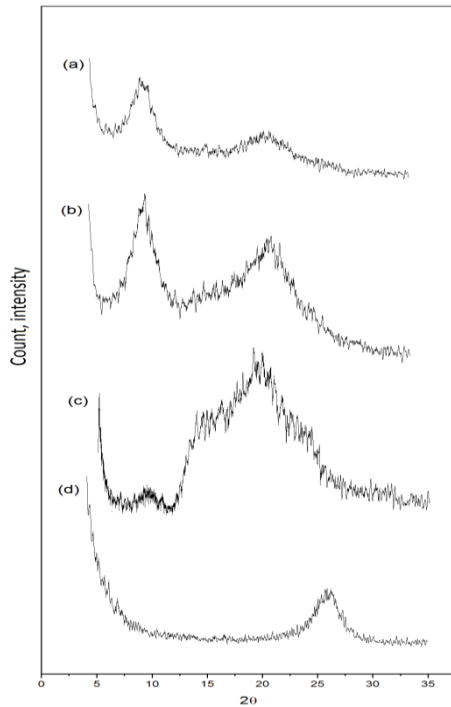


Şekil 4: PNVCz, NVCz/NIPAAm ve NVCz/IA modifiye elektrotlar ile fosfat tampon çözeltide (pH=7) ve $50\text{mV} / \text{s}$ tarama hızında elde edilen, 9.0×10^{-4} mol/L DA' e ait CV'ler.

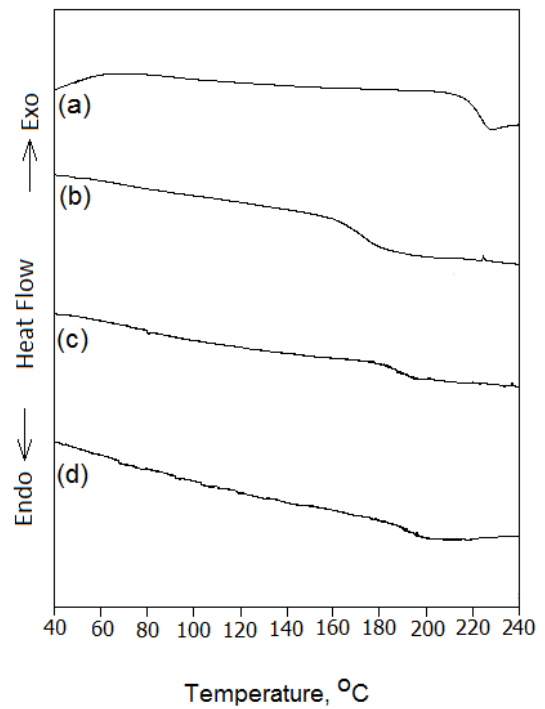
Kopolimer kaplı elektrotlar durumunda DA'ya karşı elektrokimyasal duyarlılığın önemli ölçüde değiştiği, ve bu değişimin NIPAAm'a ait hidrofobik izopropil veya IA'ya ait hidrofilik karboksil grupları ile DA moleküllerine ait etkileşimden kaynaklandığı söylenebilir.

P(N-vinil karbazol-ko-monosetil itakonat) kopolimerinin MWCNT ile kompoziti çözelti karıştırma yöntemi ile hazırlandı.

Bir behere, 10 ml THF ve belli miktarda MWCNT karıştırıldı ve sonikatör ile dispers edildi. Daha sonra 10 mg PNVCz veya kopolimeri P(NVCz-ko-MCeI), MWCNT/THF dispersiyonu içinde çözüldü ve 1 saat manyetik karıştırıcı ile karıştırıldı. Sonrasında PNVCz/MWCNT/THF ve P(NVCz-co-MCeI)/MWCNT/THF karışımları petri kaplarına aktarıldı ve kalan THF oda sıcaklığında 1 gün, 25°C sıcaklıkta vakum etüvünde bekletilerek ve 2 gün bekletilerek uçuruldu ve çözelti karıştırma yöntemiyle hazırlanan PNVCz/MWCNT kompozitleri elde edildi.



Şekil 5: Çözelti karıştırma yöntemi ile THF'de hazırlanan P(NVCz-ko-MCeI)'a (a), P(NVCz-ko-MCeI) / MWCNT kompozitlerine. MWCNT miktarı = polimere göre ağırlıkça %1.0 (b) ve %15.0 (c), ve MWCNT (d)'e ait XRD grafikleri.



Şekil 6: AIBN başlatıcısı ile sentezlenen PNVCz'ün ve PNVCz/MWCNT kompozitinin (a,b), AIBN başlatıcısı ile sentezlenen P(NVCz-co-MCeI)'in ve P(NVCz-co-MCeI)/MWCNT kompozitine (c, d) ait DSC termogramları, (kompozit hazırlama yöntemi = THF varlığında çözelti karıştırma ile; MWCNT miktarı = %1.0, ağırlıkça).

P(NVCz-ko-MCeI), MWCNT'e ve bu bileşenlerin THF içinde çözelti karıştırma yöntemi ile hazırlanan kompozitlerine ait XRD'leri Şekil 5'de gösterilmiştir. (karbon nanotüp içeriği: polimere göre ağırlıkça %1.0 ve %15.0).

NVCz kopolimeri iki ($2\theta = 7.5^\circ$ ve 23.5°), MWCNT tek bir pik ($2\theta = 26^\circ$) gösterirken, P(NVCz-ko-MCeI)/MWCNT kompoziti için gözlenen üç ayrı pik ($2\theta = 12.5^\circ$, 17.5° ve 22.5°), PNVCz-ko-MCeI ilavesinin hem MWCNT'ün hem de PNVCz-ko-MCeI zincir yapısını etkilediğini göstermektedir. Kompozit durumunda piklerin kayması ve üçüncü bir pikin gözlenmesi PNVCz-co-MceI kristallenmesine ait bir bulgu olarak değerlendirilebilir.

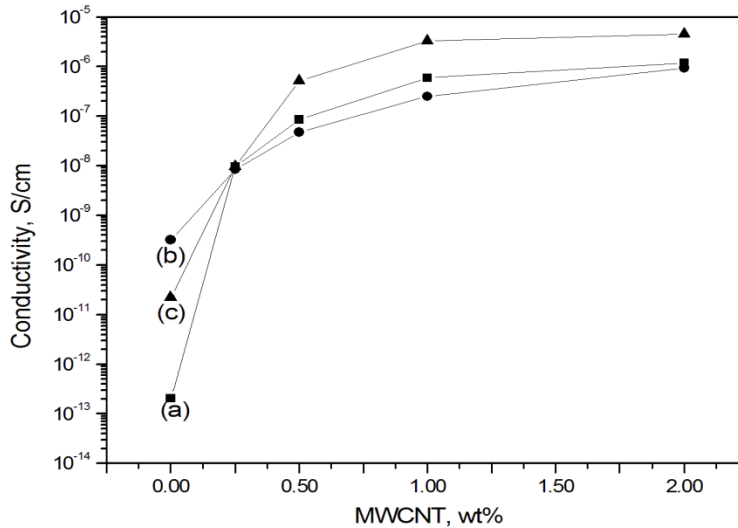
Şekil 6 THF içinde çözelti karıştırma yöntemiyle hazırlanan PNVCz/MWCNT kompozitlerine ait DSC termogramlarını göstermektedir.

Ağırlıkça %1.0 MWCNT ilavesi ile PNVCz'ün ait camsı geçiş sıcaklığı (T_g)'nın azaldığı, MceI içeren kopolimeri ile hazırlanan kompozitin, T_g 'sinin ise yükseldiği gözlemlendi. Bu sonuçlar dispersiyon kalitesinin T_g kaymasına etkide bulunduğunu ve, kaymanın yönünün MWCNT ile polimer zincirleri arasındaki etkileşime bağlı olduğunu göstermektedir. Şekil 6'deki DSC termogramları incelendiğinde, NVCz birimleri ile MWCNT'ler arasındaki uyumluluğun, uzun hidrofobik bir zincir ve hidrofilik bir grup taşıyan MceI'in (%5 mol) ilavesiyle iyileştiği gözlemlendi.

Şekil 7'de, çözelti karıştırma yöntemi ile hazırlanan PNVCz/MWCNT kompozitlerinin oda sıcaklığında, MWCNT ağırlık miktarına bağlı olarak ölçülen iletkenlikleri görülmektedir.

AIBN ve seryum amonyum nitrat başlatıcısı (CAN) ile sentezlenen PNVCz'lerin ve AIBN başlatıcısı ile sentezlenen P(NVCz-co-MCeI)'in iletkenlikleri, sırasıyla, 2.1×10^{-13} , 2.3×10^{-11} ve 3.2×10^{-10} S.cm⁻¹'dir.

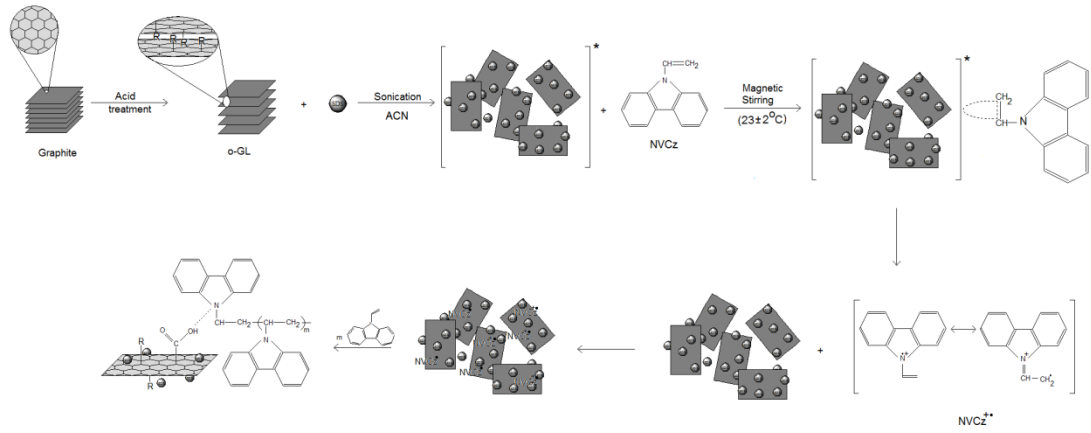
Perkolasyon teorisine göre, perkolasyon eşiği yalıtkan bir yapıdan iletken yapıya geçişi tanımlar. Hacimce %0.12'den daha düşük miktarda MWCNT içeren kompozitlerin iletkenliği yalıtkan seviyesindedir. Hacimce %0.24 ile %0.95 aralığında iletken katkı maddesi içeren kompozitlerinse yalıtkindan yarı-iletken yapıya geçiş gösterdiği, hacimce %0.95 ve üzeri konsantrasyonda ise iletkenliklerinin 10^{-6} - 10^{-5} S.cm⁻¹ seviyesine ulaştığı gözlemlendi.



Şekil 7: THF'de, çözelti karıştırma yöntemi ile hazırlanan kompozitlerinin MWCNT ağırlık kesrine bağlı elektriksel iletkenlikleri: (a) PNVCz (başlatıcı: AIBN) /MWCNT, (b) P(NVCz-co-MCeI) (başlatıcı: AIBN)/MWCNT and (c) PNVCz (başlatıcı: CAN) /MWCNT.

NVCz'ün oksidatif polimerizasyonu ACN'de CAN varlığında gerçekleşti. Monomerin oksidana oranı 200:1 ve NVCz konsantrasyonu 1.0 mol/L olarak alındı. Sentez 25°C ve atmosfer koşulları altında yapıldı.

Oksitlenmiş grafit hidrofilik yapıda tabakalı bir malzemedir. Tezin bu kısmında, o-GL, sodyum dodesil sülfat içeren ACN/su karışımında dispers edildi. Daha sonra, NVCz monomeri ve o-GL/ACN/su/SDS(10 wt %) dispersiyonunda, oda sıcaklığında CAN başlatıcısı kullanılmadan polimerleştirilerek PNVCz/o-GL kompoziti sentezlendi (Şekil 8). Sonik karıştırma işlemi esnasında, SDS molekülleri o-GL dispersiyonuna katkıda bulunmakta, sonrasında ise o-GL yüzeyine adsorbe olmakta, itme kuvvetleriyle grafit tabakalarının yığılmasını önlemekte ve sonuçta elektron verici NVCz molekülleri ile hem sonik karışma ile aktive edilmiş, hem de fonksiyonel gruplara sahip, grafit tabakaları arasında yük transferine imkan tanıdığı düşünülmektedir (Şekil 8).



Şekil 8: CAN yokluğunda ACN/su/SDS (NVCz'e göre ağırlık % 10.0) karışımında oda sıcaklığında in situ polimerizasyonu için önerilen mekanizma.

Kompozitin FTIR spektrumu, karakteristik PNVCz bantları (aromatik gerilme ve aromatik -CH düzlemi için $1600-1450\text{ cm}^{-1}$, ve aromatik -CH düzlemdışı bükülme için ise 750 cm^{-1}) ile 1750 cm^{-1} ve 3450 cm^{-1} 'de o-GL'e ait olduğu bilinen piklerin gözlenmesi PNVCz/o-GL kompozitinin oluştuğunu göstermektedir.

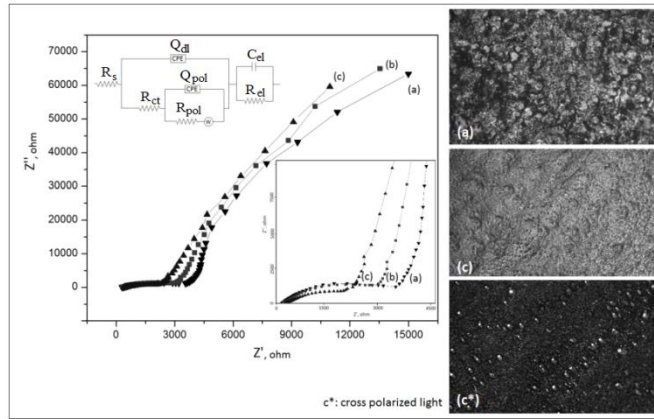
PNVCz/MMT kompozitleri de benzer şekilde, heterojen çözelti polimerizasyonu ile hazırlandı. İlk olarak, ağırlığı bilinen Na^+MMT , ODA-MMT ve TMSA-MMT örnekleri ACN içinde üç farklı yöntem kullanılarak (manyetik karıştırıcı, homojenizatör (GN 125, 230V/50/60 Hz, 8000-30000 rpm) ve yüksek güçlü sonik uç (Sonopuls HD 2200, 200W/20kHz)) dispers edildi. Dispers edilen kil örneklerine NVCz ilave edilerek CAN varlığında polimerizasyonu gerçekleştirildi. Reaksiyon sonunda elde edilen ürün, monomerinin giderilmesi için, birkaç kez ACN ile yıkanarak santrifüjlenmiş ve sabit tartıma gelene kadar oda sıcaklığında, vakumda kurutulmuştur. PNVCz homopolimeri için de benzer yöntem uygulanmıştır.

Morfolojik yapıları ve elektrokimyasal/elektriksel özellikleri Fourier dönüşümlü Kızılötesi Spektroskopisi (FTIR), X-ışını kırılımı (XRD), Diferansiyel Taramalı Kalorimetre (DSC), Polarize Optik Mikroskop (POM), Taramalı Elektron Mikroskobu (SEM), Elektrokimyasal Empedans Spektroskopisi (EIS) ve Döngü Voltametri (CV) ile incelendi.

Kimyasal polimerizasyonla elde edilen PNVCz ve tabakalı silikat kompozitleri 0.1 mol/L NaClO₄ destek elektrolit varlığında ACN içinde 1.2 V'da elektrokimyasal olarak oksitlenerek platin (Pt) ve camı karbon (GC) disk elektrotlara kaplandı. 0.5 ile 1.5V aralığında 50mV/s tarama hızında Gamry Reference 600 potansiyostat kullanılarak döngülü voltamogramları alındı. Elektrokimyasal ölçümlerde, çalışma elektrodu olarak Pt (ø:1.6mm) ve GC (ø:3.0mm) disk elektrotlar, karşıt elektrot olarak Pt tel ve referans elektrot olarak gümüş (Ag) tel elektrot kullanıldı.

PNVCz/MMT kompozitlerinin elektrokimyasal aktiviteleri döngülü voltametri sonuçlarından elde edilen akım-gerilim verileri incelenerek belirlendi. PNVCz ve PNVCz/MMT kompozitlerinin ACN içindeki çözeltileri Pt ve GC elektrotlara 6 döngüde kaplandı. Kaplanan filmler, ACN ile yıkandı ve monomersiz ortamda, destek elektrolit varlığında (ACN+0.1 mol/L NaClO₄) 50, 250 ve 500 mV/s tarama hızlarında, 0.5-1.5V aralığında CV ölçümleri alındı.

Yüzey modifiye elektrotların ara yüzeylerinin incelenmesinde EIS etkin bir yöntemdir. Bode ve Nyquist eğrileri hazırlanarak ve empedans ölçümlerine uyumlu eşdeğer devreler çizilerek, filmlere ait kapasitans ve direnç değerleri bulunur. Yöntemde esas olan, filmlerdeki iletkenlik yapısı ile (elektronik ve/veya iyonik) empedans spektrumu arasındaki uyumun gösterilmesidir.



Şekil 9: Pt elektrota kaplanan ağırlıkça % 15.0 (a), %5.0 (b) ve %1.0 (c) tabakalı silikat içeren PNVCz / ODA-MMT kompozitlerine ait Nyquist eğrileri ve polarize optik mikrografları.

Sonik karıştırma ile hazırlanmış PNVCz/ODA-MMT kompozitlerinin Nyquist grafikleri Şekil 9'da gösterilmektedir. Her üç eğri de yüksek frekans bölgesinde ydairesel ve düşük frekans bölgesinde ise doğrusal yapıdadırlar.

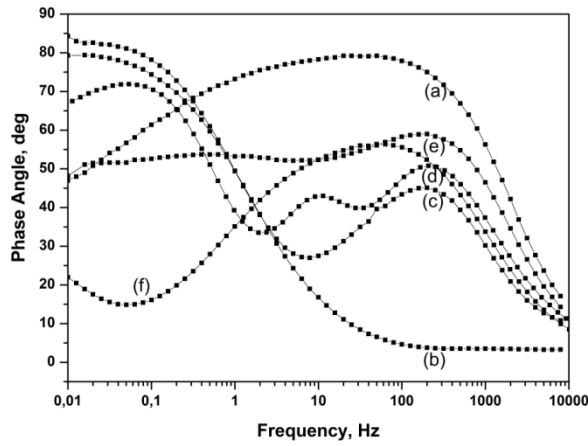
Bir başka deyişle Nyquist eğrileri iki farklı bölgeye sahiptirler. Yük transfer direncini (R_{ct}) belirten yarıdairesel bölge ve elektroda ait difüzyon prosesini gösteren (R_{pol} veya R_b) doğrusal bölgeden oluşmaktadır. Bu çalışmadaki deneysel verileri kullanarak, Çözelti-PNVCZ/ODA-MMT-Pt ara yüzeylerini modelleyen bir eşdeğer devre oluşturuldu. Devre, çift tabaka faz elemanına (CPE-Q_{dl}) paralel yük transfer direnci (R_{ct}) ve buna seri bağlı polimer direnci (R_{pol}) ve Warburg elemanı (W) ile paralel polimer sabit faz elemanından (CPE-Q_{pol}) oluşmaktadır.

Ağırlıkça %15.0 ve %1.0 kil içeren kompozitlere ait morfolojik görüntüler incelendiğinde PNVCz/ODA-MMT kompozitleri daha düzenli bir yapı göstermektedir (Şekil 9). Polimer matrisine inorganik tanecik ilavesi sadece morfolojik özellikleri iyileştirmekle kalmayıp, aynı zamanda PNVCz'ün iletkenliğini

de arttığı bulgugulandı. EIS ve DC ölçümlerine göre, ağırlıkça %15.0 ve %1.0 ODA-MMT içeren örneklerin iletkenliği 10^{-13} S/cm'den 10^{-5} S/cm'ye yükseldi.

PDMS kaplı Pt ve GC elektrot yüzeylerine, NVCz monomerinin elektrokimyasal olarak polimerleştirilmesiyle elde edilen Poli(N-vinil karbazol) / Polidimetilsiloksan kompozit elektrotlarının kapasitifi özelliklerine, yalıtkan PDMS tabakasının ve kaplama sıcaklığının etkileri incelendi.

Çift tabakalı kaplamaların elektrokimyasal özellikleri elektrokimyasal empedans spektroskopisi ve UV-vis spektroeletrokimya ölçümleri ile incelendi. Kompozit elektrotların, spesifik kapasitanslarının, artan PDMS içeriği (% 5.0'den % ve 10.0) ve azalan PDMS ve PNVCz kaplama sıcaklıkları ile (25°C 'den -15°C 'e) azaldığı, ve daha dirençli bir PDMS/PNVCz tabakası oluştuğu görülmektedir (Şekil 10).



Şekil10: (a) Pt ve (b) Pt/PNVCz , (c) Pt/PDMS (%5.0; 25°C)/PNVCz (25°C), (d) Pt/PDMS (%5.0; 25°C)/PNVCz (0°C), (e) Pt/PDMS(%5.0; 25°C)/PNVCz (-15°C) ve (f) Pt/PDMS(%5.0; -15°C)/PNVCz (-15°C) ACN'de 0.1 mol/L NaClO_4 varlığındaki Bode faz eğrileri.

1. INTRODUCTION

N-vinylcarbazole (NVCz) molecules are nitrogen-containing heterocyclic compounds and, poly(N-vinylcarbazole) (PNVCz) is one of the number of vinyl polymers with aromatic pendant groups. The aromatic unit provides a better chemical and environmental stability while the nitrogen atom that can be easily substituted with a wide variety of functional groups help to tune the optical and electrical properties.

PNVCz has recently gained considerable interest as photoactive and electroactive systems because of its optoelectronic, photoconductive and thermal properties. Its composites with inorganic oxides, layered silicates and carbon nanotubes, and copolymers with vinyl monomers such as N-isopropylacrylamide, methyl methacrylate and acrylonitrile lead to materials that have improved bulk properties.

It can be obtained by three different polymerization techniques: free radical, cationic and charge-transfer. Polymerization of NVCz through vinyl group gives white insulating PNVCz with interesting photoconducting properties while when the polymerization occurs through the aromatic rings, the main product is a green, cross-linked polymer. Also, polymerization of NVCz is possible by electrochemical oxidation. Direct anodic oxidation leads mainly to the green conducting form of the polymer.

In this thesis, the synthesis and characterization of PNVCz and its copolymers with acrylic acid (AA), itaconic acid (IA) and N-isopropylacrylamide (NIPAAm) using different feed ratios are reported. The compositions of these copolymers were determined by Ultraviolet (UV) and Fourier transform infrared (FTIR) spectroscopies. The monomer reactivity ratios were computed by extended Kelen-Tüdós method at high conversion. The present study is also concerned with the use of Pt electrodes coated with PNVCz, N-vinyl carbazole/itaconic acid (NVCz/IA) and N-vinylcarbazole/N-isopropylacrylamide) (NVCz/NIPAAm) copolymer films as dopamine(DA) sensors. It is expected that DA molecules are confined in these polymer films by electrostatic attraction and hydrophobic interaction, resulting from molecular structures of monomer (NVCz, hydrophobic) and comonomers (IA,

weakly acidic and NIPAAm, hydrophobic/hydrophilic, depending on the processing temperature).

The poor mechanical strength and high processing temperature being a defect on proper use of NVCz as electrode material could be overcome by preparation of its copolymers or composites that have lower T_g s and improved mechanical properties. Therefore, new types of materials that consist of PNVCz and inorganic (and/or organic) components have been designed to combine processability and thermal stability with modified electrical and optical properties. An interesting approach for obtaining such materials is to incorporate PNVCz into an inorganic component at molecular level. Their properties are varied by changing the ratio of the inorganic and organic parts.

Montmorillonite (MMT) is a natural clay mineral which has a large layer space and some excellent properties such as good water absorption, swelling, cation-exchange and drug delivery. In general, MMT, which is a hydrophilic natural clay, is treated by alkylammonium salts to improve hydrophobic compatibility with organic polymers. The organic modifier may either enhance the interaction between the clay layers and the polymer chains, producing more exfoliated structure, or it may favour the intercalation of the polymer chain into the layer spaces.

In this thesis, the effect of both the mixing methods used to prepare homogeneous dispersions of layered silicates in polymerization solutions and the structure of cationic surfactants attached to MMT layers on the morphological characteristics and electrochemical/electrical properties of PNVCz have also been investigated.

The conductivity and material properties of a conducting polymer depend mainly on the arrangement of its chains. Therefore, the presence of MMT particles may influence the arrangement of PNVCz chains, as they keep within the clay layers. In the work reported in the present study, it is expected to obtain a useful combination of thermal and electrical properties in the PNVCz/MMT composites. To do so, PNVCz and its composites were prepared by using cerium ammonium nitrate, $(\text{NH}_4)_2\text{Ce}(\text{NO}_3)_6$ to initiate oxidative polymerization and by using magnetic stirrer, homogenizer and a sonic tip to disperse the three different concentrations of ODA-MMT, TMSA-MMT and Na^+MMT . Their morphologies and electrochemical/electrical properties were characterized by Fourier Transform

Infrared Spectroscopy (FTIR), X-Ray Diffractometer (XRD), Differential Scanning Calorimetry (DSC), Polarized Optical Microscope (POM), Scanning Electron Microscope (SEM), Electrochemical Impedance Spectroscopy (EIS) and Cyclic Voltammetry (CV).

Conducting polymer composites made from carbon based electrically conductive fillers such as graphite particles and carbon nanotubes may have improved thermal properties and electrical conductivity beyond a threshold level of loading. However, it is difficult for a monomer to load on their surfaces because of the lack of the reactive groups on the natural graphite and carbon nanotubes (CNTs). Therefore, they are oxidized by various methods.

Graphite platelets, which are two dimensional and layered conductive materials, are one of the carbon based conductive fillers for polymer composites with a low percolation threshold. The graphite layers (GLs) are bound by van der Waals forces while carbon atoms within a layer are covalently bonded. The GLs are oxidized by using an intercalating agent, which enter between the carbon layers. It is similar to the preparation of organically modified layered silicate from sodium montmorillonite by using alkyl ammonium salts, to form homogeneous dispersion in monomer or polymer and/or to intercalate monomer or polymer into the clay layers.

The preparation of homogeneous dispersions of CNTs in organic polymer matrix also is difficult and results in the aggregate formations due to both van der Waals attractions among CNTs and weak intermolecular interactions between polymer and CNT. In order to improve the dispersion of CNTs in polymer matrix, their surfaces are treated by strong acids. The purification/oxidation methods of CNTs create carboxylic groups on the tubewalls. The activation of the carboxylic groups by acylation and coupling reactions increases their solubility/stability in organic solvents. To overcome the van der Waals interactions between the CNTs/GLs, sonication process is also applied. It leads to stable dispersions because of the provided mechanical energy.

Another procedure, which is used to incorporate CNTs and GLs into polymer systems, includes the addition of surfactants. To enhance the electrostatic forces and improve the stability of graphite / polymer and carbon nanotube / polymer composites, the surfaces of GLs, CNT walls, oxidized graphite layers (o-GLs) and

oxidized (o-CNT) walls are modified with neutral, cationic or anionic surfactants. The adsorption of ionic surfactant molecules, which consist of a hydrophilic head, a long hydrophobic tail and an ionic group, on the surfaces of GLs, o-GLs and CNT walls creates a distribution of negative or positive charge and so, the repulsive forces between them prevent (or reduce) aggregation and produces homogeneous dispersions. The studies on surfactant adsorption revealed that CNTs are covered by surfactant layers oriented vertically on the tube surfaces. Further, it was observed that the sonication procedure has an important role in the dispersion of CNTs but surfactant alone can not be able to produce the uniform dispersions of CNTs without sonication.

Graphite particles and carbon nanotubes have been widely used as conducting fillers in preparing polymer composites. They can be designed using both conductive polymers such as polyaniline, polypyrrole and polythiophene, and insulating polymers. The latter ones can be converted into the conductive forms by addition of carbon based conductive fillers.

Conducting polymer composites are characterized by a limit at which the conductivity starts to increase as a function of filler contents. The critical value which is known as percolation threshold concentration of conductive filler depends on its dispersion into polymer matrix and the preparation method of composites.

The present thesis reports a comparative study of PNVCz/graphite and PNVCz/carbon nanotube composites prepared with GLs and MWCNTs treated by acidic oxidative reagents. The composites were prepared by both solution blending procedure and in situ oxidative chemical polymerization. The morphology, thermal stability, glass transition behavior and electrical property of the film and fine powder forms of the composites were characterized by Fourier transform infrared spectroscopy (FTIR), X-ray diffractometer (XRD), thermogravimetric analysis (TGA), differential scanning calorimetry (DSC), polarized optical microscope (POM) and direct current conductivity measurements.

The physical and chemical insufficiencies of PNVCz such as poor mechanical property and high glass transition temperature can be modified by using polydimethylsiloxane (PDMS), being an elastomer that have high chain mobility and lower glass transition temperature ($\approx -130^{\circ}\text{C}$). The PDMS based hybrids have not

only the properties such as flexibility and thermal stability but also water-repellency as expected from the hydrophobic nature of dimethylsiloxane units. Therefore, PDMS layered electrodes may be designed and integrated into many optical and microfluidic devices due to their hydrophobic, mechanic and optic properties.

The last part of the thesis mainly focused on the preparation of PNVCz/PDMS composite electrodes by electrochemical polymerization of NVCz monomer onto PDMS coated electrode surface and, the investigation their electrochemical and spectroelectrochemical responses by mean of electrochemical impedance spectroscopy (EIS) and in situ UV-vis spectroelectrochemistry techniques.

2. THEORETICAL PART

2.1. Conductive polymers

Although the polymers that were eventually going to be known as conducting polymers have been known for at least 100 years it wasn't until 1977 that by accident the high conductivity of polyacetylene was discovered after the over addition of iodine catalyst for the polymerization of polyacetylene [1]. While the exact manner in which conductive polymers (CP) conduct electricity is not fully understood, it is generally said to be due to the delocalization of π -bonded electrons along the conjugated polymer chain backbone where the delocalization can extend over many monomer unit lengths [2]. Conjugated polymers spread over a wide region from insulators to up to metal conductivity limits (Fig 2.1.).

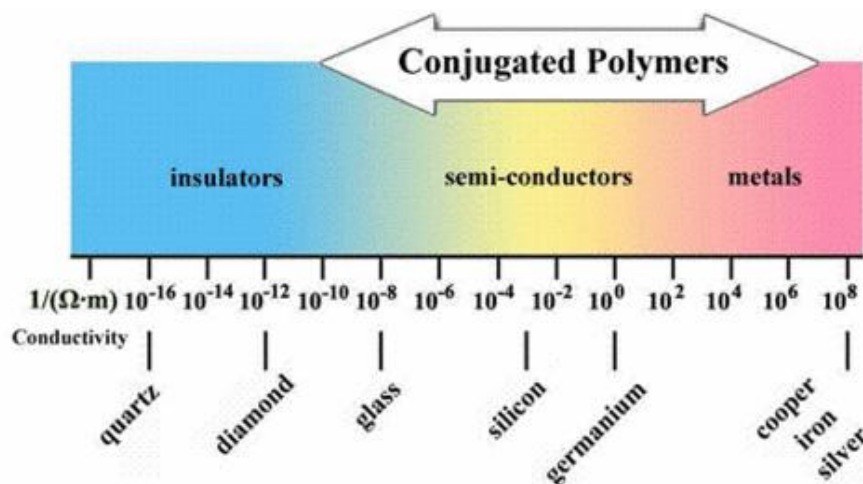


Figure 2.1: Conductivity range of conjugated polymers.

There are two main ways of preparing conducting polymers: chemical and electrochemical polymerization [3]. The principal advantage of the chemical methods of synthesis is that they offer possibilities of mass production at low cost. But, the electrochemical methods offer materials with better conducting properties in a form of thin film for different applications. Electrochemical experiments also offer a great deal of controllability during the preparation of these polymers. By controlling the potential or the current at the working electrode, the thermodynamics

of the system or the kinetics of the reaction is better controlled for specific purposes. These features of electrochemistry give a number of ways to control the quality of polymerized products.

Polymers are generally with insulating nature. But, they can be generated with conductive property by doping. The doping of polymers is what transforms a naturally insulating polymer into a polymer capable of conducting an electric current. Conducting polymers are not conducting until they are doped either via oxidative doping (n-type doping) or protonic doping (p-type doping) where either type of doping will increase the number of charge carriers and in effect lowering the band gap therefore allowing conduction. n-type dopants introduce extra electrons to carry the electric current and p-type dopants use positively charged holes to carry electric current (Figure 2.2).

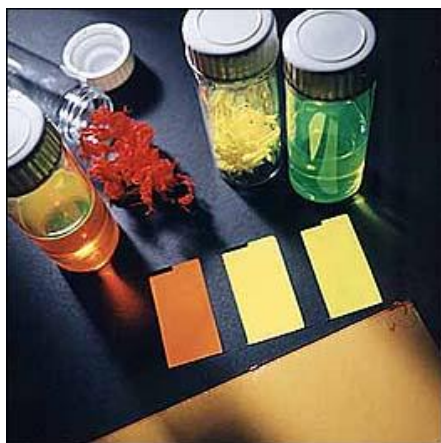
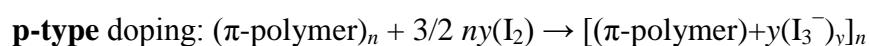


Figure 2.2: p- and n- doped polymers

There is two specific methods to dope polymers. These procedures can be summarized as chemical or electrochemical doping.

The chemical doping by charge transfer is as follow. Conjugated polymers were initially doped by a charge-transfer chemistry with a proper electron donors or acceptor by oxidation (**p-type** doping) or reduction (**n-type** doping). These procedures are illustrated by the following chemical reactions [4].



Although chemical doping (charge transfer reaction) is an efficient and straightforward process, it is difficult to control the degree of doping. Complete

doping with high charge concentrations yields to reasonably high-quality materials. However, attempts to obtain intermediate doping levels often result in electrically inhomogeneous materials. Electrochemical doping was explored to solve this particular problem. In the electrochemical doping, the electrode supplies the charges to the polymer *via* electron transfer reactions, in which ions diffuse into (or out of) the polymer matrix from the nearby electrolyte to compensate the electronic charge introduced.

In contrast to the chemical doping the doping level could be determined by the voltage between the polymer film and the counter electrode. Electrochemical doping is illustrated by the following reactions [5]:



By adjusting the doping level, a change in conductivity between that of the undoped (insulating or semiconducting) and that of the fully doped (highly conducting) form of the polymer can be easily obtained.

Due to the fact that, electronically conducting polymers are electroactive materials, their electrochemical characterization would be a first step in describing their electrical properties. For this reason, the polymer films have been characterized by either electrochemical or electrical measurements either on the electrode surface in electrolyte solutions or in solid states to establish the electrochemical activity of the polymer films [6] or to determine its conductivity [7].



Figure 2.3: Tinted windows by on-off switch. Ref. [11]

Since their discovery, conductive polymers are used at everyday applications.

An example of this is the development of gas sensors. It has been shown that polypyrrole behaves as a quasi 'p' type material. Its resistance increases in the presence of a reducing gas such as ammonia, and decreases in the presence of an oxidizing gas such as nitrogen dioxide.

Conducting polymers can also be used to directly convert electrical energy into mechanical energy. Electrochemical actuators can function by using changes in a dimension of a conducting polymer as microtweezers, microvalves, micropositioners for microscopic optical elements, and actuators for micromechanical sorting [8-10].

Tinting windows is the latest application of conductive polymers (Figure 2.3) [11]

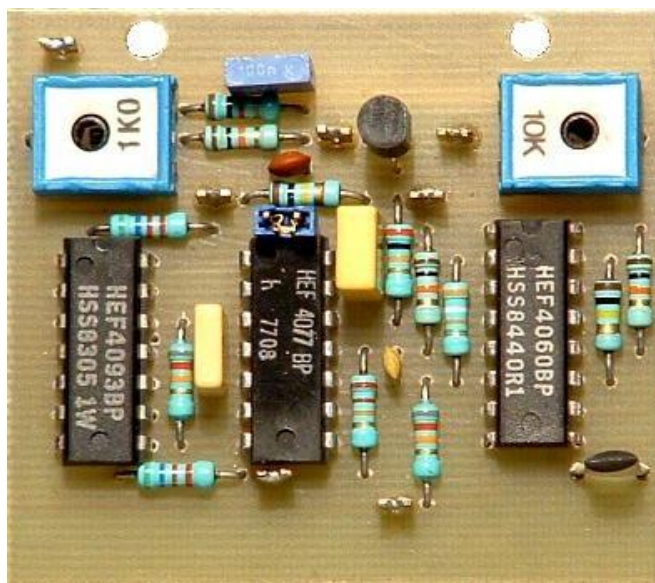


Figure 2.4: Old fashion electric circuits.

But probably the most publicized and promising of the current applications are light weight rechargeable batteries. Some prototype cells are comparable to, or better than nickel-cadmium cells now on the market. The polymer battery, such as a polypyrrole lithium cell operates by the oxidation and reduction of the polymer backbone. During charging the polymer the oxidized anions in the electrolyte enter the porous polymer to balance the charge created [12].

The capacitors used on computer and electronic devices were replaced for a decade by its polymer analogues. But new researches are intensified to fit the obtained data from the EIS plots for equivalent circuit's modeling. Then in a not distant future, it could be used to substitute already used circuits by its polymer analogues. This method will reduce the cost of electronic devices and lower the weight (fig 2.4).

2.2. N-vinyl carbazole

N-vinyl carbazole (NVCz) is a white crystalline material that melts at 65°C. It is soluble in most aromatic, chlorinated and polar organic solvents. The material has to be handled with care since it may cause severe skin irritations. Like other aromatic amines NVCz, is suspected to cause cancer [13].

Poly (N-vinylcarbazole) (PNVCz) is a well known polymer since 1940, with high thermal stability but very low dc conductivity (10^{-12} to 10^{-16} S/cm) [14].

Due to the bulkiness of the carbazole groups, main chain and side group motions are severely restricted in PNVCz. The chains are stiff and the polymer has a glass transition temperature of 227 °C which is among the highest known for vinyl polymers but depending on the molecular weight (ca.2000) lower to ca. 70°C. PNVCz exhibits an excellent thermal stability up to at least 300 °C [15–17].

Unfortunately this property has never been fully utilized because of the extreme brittleness of the material. Many attempts have been made to improve the mechanical and processing characteristics of PNVCz by plastification, orientation, blending and copolymerization. PNVCz is soluble in common organic solvents like benzene, toluene, chloroform and tetrahydrofuran.

Considerable research attention has been paid over the past few years, after the discovery of its distinctive optoelectronic properties, to the modification of specialty, vinyl addition polymers, and condensation polymers to improve their bulk properties [18-21].

2.2.1. Electrochemical Polymerization

PNVCz gives two different products on electrochemical polymerization (Figure 2.5). During the direct electrolysis of NVCz a green electro conductive crosslinked insoluble polymer occurs, as presented in the study published by Papez *et al.*, [22] and deposits on the surface of the electrode, while the polymerization through vinyl groups give a non conductive white polymer which precipitate into the solution [23]. The non conductive polymer is photoconductive with UV light and soluble in most common organic solvents. Two polymerization stages are mainly observed, depending on the experimental setups: in the first, a thin layer of very compact

(PNVCz) is formed, on which, in the second stage, a polymer with a globular structure grows [24].

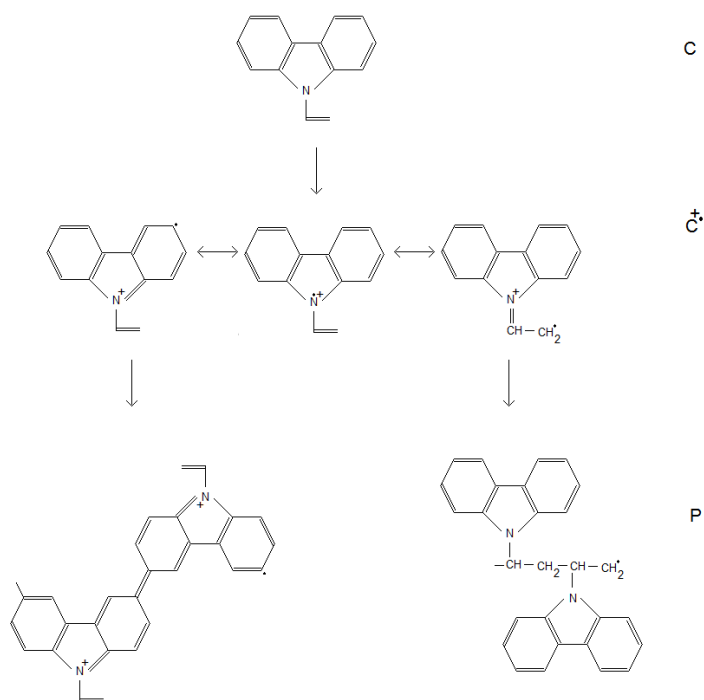


Figure 2.5: Illustration of electrochemical polymerization of NVCz.

The cyclic voltammograms obtained for NVCz attached to a platinum electrode is as shown in Figure 2.6. The cyclic voltammograms and their changes during repetitive cycling are quite similar to those for carbazole oxidation in acetonitrile [25] or in mixed media [26], although no tendency towards passivation [27] was observed. A high, irreversible oxidation peak appears at ca. $E=0.9$ V vs. SCE, which is in connection with the formation of NVCz cation radicals, the C-C dimerization of these cation radicals resulting in 3,3'-divinylcarbazyl and/or polymer of similar structure and the further oxidation of the dimer polymer) [25-28]. The progressively developing waves ($E_{\text{anodic}}=0.4$ V, $E_{\text{cathodic}}=0.82$ V,) belong to the reversible redox processes of the dimer or of the polymer. The formation of polymer can be assumed because of the permanent growth of these waves. The redox processes were accompanied by a color change from a pale yellow/ colorless (reduced) to a dark green (oxidized) form.

The irreversible wave at 0.9 V gradually decreases, attesting that the NVCZ attached to the platinum surface is transformed into dimer (polymer), and eventually the total amount will be consumed.

The oxidation of NVCz can be described by an electron transfer-chemical reaction-electron transfer (ECE) mechanism where each electrochemical step involves one electron per parent molecule and the coupling reaction is very rapid. Consequently, the primary oxidation wave is a mixture of ECE and EC processes [25].

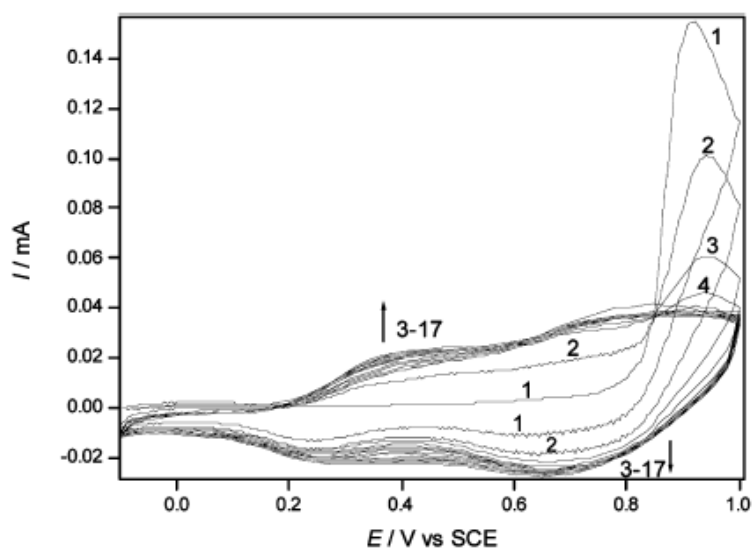


Figure 2.6: Representative illustration of NVCz electrodeposition.ref 29.

2.2.2. Chemical Polymerization

NVCz polymerizes with azo compounds, peroxides and similar radical generating initiators in bulk, solution, suspension and emulsion methods to give high molecular weight [30-36] products. It also yields low molecular weight polymers with chain transfer agent [37].

It was reported recently [38] that ultrahigh molecular weight PNVCz can be obtained using low temperature initiation with 2,2-azobis(2,4-dimethylvaleronitrile). The weight average molecular weight and the polydispersity index of the polymer obtained were 3×10^6 g/mol and 2.4, respectively. *o*-Chlorohexaphenylbis-imidazole [39], 2-benzyl-2-dimethylamino-1-(4-morpholinophenyl)butanone-1 [40] and other photoinitiators were used as initiators for the radical photopolymerization of NVCz. Besides of the bulk polymerization which is carried out as a technical process,

PNVCz can also be obtained in solution [41] or by precipitation polymerization [42,43], suspension polymerization [44–46] as well as by photopolymerization [47].

Wang et al. [48] reports that ceric ammonium nitrate, ferric nitrate and cupric nitrate are capable of polymerizing NVCz in methanol solution and also of polymerizing completely the mixture of NVCz and styrene. Such metal salts can accept electrons leading to oxidation of NVCz during which radical ion might be formed as an intermediate. The polymerization of NVCz in ethylene dichloride, acetone, benzene and dioxane with cupric nitrate, ferric nitrate, and ceric ammonium nitrate catalysts were also studied [49]. In all of these cases, polymerization seemed to be cationic in type and yields are around 20%-50% for ceric ammonium nitrate (CAN) in 2 hours.

NVCz monomer, which exhibits base character, give cationic polymerization in the presence of protonic acids, Lewis bases and carbocations. Initiation is relatively high, and propagation rate constant was found to be five times higher. The polydispersity index is high ($M_w/M_n > 3$) [50]

The cationic polymerization of *N*-vinyl carbazole, initiated by $\text{Ph}_3\text{C}^+ \text{AsF}_6^-$ and $\text{Ph}_3\text{C}^+ \text{PF}_6^-$ in methylene dichloride is an example for this polymerization [51] So NVCz can be polymerized by hydrochloric acid [52], perchloric acid [53] and several other Brønsted acids [54].

Probably the most obvious method for the cationic polymerization of NVCz involves the treatment of the monomer with acids. So NVCz can be polymerized by hydrochloric acid [55], perchloric acid [56] and several other Brønsted acids [57]. Due to the nucleophilicity of NVCz even relatively weak carboxylic acids cause polymerization [58]. Cationic polymerization of NVCz is also initiated by carbon whiskers (vapor-grown carbon fibers) [59] and by g-poly(glutamic acid) [60].

These polymerizations are heterogeneous processes during which carboxylic groups on the surface of the carbon whiskers and g-poly (glutamic acid) particles are responsible for the initiation of NVCz polymerization.

2.3. Itaconic Acid and its Ester Derivatives

Itaconic acid (IA) is an unsaturated dicarboxylic acid with one carboxyl attached to methylene group.

Itaconic acid and its derivatives polymerizes by various methods. Bulk, suspension and emulsion are techniques used for polymerization of its esters. High melting point and isomerization compromise the use of emulsion and solution methods for acids [62].

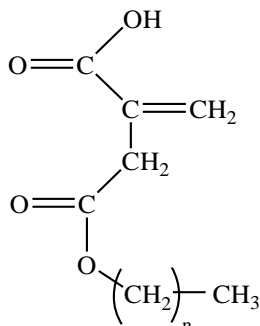


Figure 2.7: Mono Itaconate derivatives.

Mono and dialkyl itaconates (Figure 2.7) were mainly prepared by esterification of IA with different alcohols such as, butyl, octyl and cetyl using acetyl chloride as a catalyst to ensure slightly acidic conditions, according to the general methods previously reported by Gargallo and coworkers [63].

Work on polymerization of diester derivatives with side chains lengths from methyl to hexyl [64], dibenzyl itaconates [65], diitaconate esters containing methylterminated poly(ethyleneoxide) side chains [66], dialkylitaconic acid esters with side chain lengths C7 to C20 [67] were synthesized.

Although monoester derivatives were found to polymerize more rapidly than the corresponding diesters, they were less investigated [68]. Since, the radical polymerization of monoitaconate esters is known to be very sensitive to steric effects due to the influence of the side group [69].

Filler such as CNT and Graphite have hydrophobic character. Although natural graphite is hydrophobic, the oxidized graphite layers (o-GL) prepared from the oxidation of graphite shows hydrophilic properties due to polar groups such as; -COOH, -OH etc [70].

This new property facilitates the dispersion of graphite but lowers the interaction with polymers. So, polymers with hydrophilic and hydrophobic side groups could enhance the homogeneity of the composite.

2.3.2. N-isopropylacrylamide

N-isopropylacrylamide (NIPAAm) is the most prominent member of the N-alkyl acrylamides used to prepare temperature responsive hydrogel.

NIPAAm molecule is composed of two strictly opposite groups. While the hydrophilic group enhance the interaction with hydrogen bondings, the hydrophobic counterpart enhance the interaction with organic matrix. This property was in great part used to synthesis pH and thermo sensitive hydrogels. Its pH and temperature dependent swelling-shrinking behavior offers many potential applications such as biotechnological devices, immobilization of enzymes, etc [71-74].

Further, it is reported that the amphiphilic property of NIPAAm resulting from the hydrophobic and hydrophilic groups, enhance the interaction with inorganic fillers (i.e. montmorillonite, CNT, etc) and improve the physical properties [75].

2.4. Monomer Reactivity Ratios

The copolymerization with various monomers lead the possibility to enrole the properties of each component on the same polymer backbone. The synthesis of those new polymers has lead to another problem. Determine the composition and the activity of each monomer to be part on the copolymer backbone.

The estimation of copolymerization reactivity ratios is an area of interest to both academia and industry.

The terminal unit modeling [76] assumes that the reactivity of the propagating species depends only to the monomer unit at the end of chain. The propagating chain that ends in $M_A\cdot$ can either add a monomer of type M_A or of type M_B . Also, the propagating chain that ends in $M_B\cdot$ can add a monomer unit of type M_B or of type M_A .

The rate constant for the reaction of the propagating chain that ends in M_A and adds another M_A to the end of the chain is k_{AA} , and the rate constant for the reaction of the propagating chain that ends in M_B and adds M_A to the end of the chain is k_{BA} , and so on.

The copolymerization composition equation is given as (2.1)

$$\frac{d[M_A]}{d[M_B]} = \frac{[M_A] (r_A [M_A] + [M_B])}{[M_B] ([M_A] + r_B [M_B])} \quad (2.1)$$

As, F_A and F_B are the mole fractions of M_A and M_B in the copolymer, and f_A and f_B are the mole fractions of monomers M_A and M_B in the feed. Therefore:

$$f_A = 1 - f_B = \frac{[M_A]}{[M_A] + [M_B]} \quad (2.2)$$

$$F_A = 1 - F_B = \frac{d[M_A]}{d[M_A] + d[M_B]} \quad (2.3)$$

Then, by combining the equations gives [76]:

$$F_A = \frac{r_A f_A^2 + f_A f_B}{r_A f_A^2 + 2f_A f_B + r_B f_B^2} \quad (2.4)$$

A perfectly random copolymerization is achieved when the r_A and r_B values are both equal to one. On this type the monomer show the exact same preference for the addition of each type of monomer. In other words, the growing radical chains do not prefer to add one of the monomers more than the other monomer, which results in perfectly random incorporation into the copolymer.

An alternating copolymerization is defined as $r_A = r_B = 0$. The polymer product in this type of copolymerization shows a non-random equimolar amount of each comonomer that is incorporated into the copolymer. This may occur because the growing radical chains will not add to its own monomer. Therefore, the opposite monomer will have to be added to produce a growing chain and a perfectly alternating chain.

When $r_A > 1$ and $r_B > 1$, both of the monomers want to add to themselves and in theory could produce block copolymers. But in actuality, because of the short lifetime of the propagating radical, the product of such copolymerizations produces very undesirable heterogeneous products that include homopolymers. Therefore, macroscopic phase separation could occur and desirable physical properties such as transparency would not be achieved.

Most existing procedures for calculating r_A and r_B can be classified as linear least-squares (LLS), and non-linear least-squares (NLLS) methods. It is accepted that LLS methods such as those proposed by Finemann and Ross [77], and by Kelen and Tudos [78], can only be applied to experimental data at sufficiently low conversion,

because the calculation is based on the differential copolymerization equation [79]. The only LLS method, as an exception, is the extended Kelen-Tudos method [80], which involves a rather more complex calculation. It could be applied to medium-high conversion experimental data (40% conversion) without sufficient systematic error.

In 1993, Mao and Huglin represented a new calculation method, which can provide the determination of reactivity ratios at high conversion and still uses the LLS method without systematic error [81].

Mortimer and Tidwell, calculated r_A and r_B by the nonlinear least squares method [82]. This method can be considered to be a modification or extension of the curve fitting method. For selected values of r_A and r_B , the sum of the squares of the differences between the observed and the computed polymer compositions is minimized. Using this criterion for the nonlinear least squares method of analysis, the values for the reactivity ratios are unique for a given set of data, where all investigators arrive at the same values for r_A and r_B by following the calculations.

Table 2.1: A Listing of the Various Methods Used to Estimate the Reactivity Ratios

Method Description	Reference
BF Barson–Fenn	Barson and Fenn85
EVM error-in-variables model	Dube et al.86
ex-KT extended Kelen–Tudos	Tudos et al. 80
FR Fineman–Ross	Fineman and Ross 77
KT Kelen–Tudos	Kelen and Tudos 78
MH Mao–Huglin	Mao and Huglin81
ML Mayo–Lewis	Mayo and Lewis83
TM Tidwell–Mortimer	Tidwell and Mortimer82
YBR Yezrielev–Brokhina–Roskin	Yezrielev et al.84

2.5. Dopamine

DA is one of the most significant catecholamine, belongs to the family of excitatory chemical neurotransmitter [87] and plays a very important role in the function of central nervous, renal, hormonal and cardiovascular system [88].

When dopamine is released it provides also feelings of enjoyment and reinforcement to motivate us to do, or continue doing, certain activities. Dopamine is released by naturally rewarding experience. This pre-programmed reward system makes sure that people do eat, do desire to procreate, and basically survive. Without enough dopamine, people feel the opposite of enjoyment and motivation. They feel fatigued and depressed, and experience a lack of drive and motivation.

Which is symptom of several diseases such as schizophrenia and Parkinsonism and HIV infection [89]. Various methods have been proposed to detect DA [90-91].

The major problem encountered with the detection of DA is the interference from ascorbic acid (AA), which largely coexists with DA in brain tissue and has an overlapping oxidation potential on the solid electrodes, so it is very difficult to determine DA directly [92].

In order to resolve this problem, many different strategies have been used to modify the electrode, which include self-assembled monolayer [93], electrochemical pretreatment [94], polymer film [95 - 98] and by covalent modified [99] glassy carbon electrode.

Zhang et al. determined dopamine in the presence of ascorbic acid using the glassy carbon electrode modified with poly(styrene sulfonic acid) film and single-wall carbon nanotube [100]. Poly(hippuric acid) [101], poly(2-picolinic acid) [102], poly(p-aminobenzenesulfonic acid) [103], poly(amidosulfonic acid) [104], and poly(o-aminobenzoic acid) [105] film-coated electrodes have also been developed by Zhang et al. to monitor dopamine in the presence of ascorbic acid.

2.6. Poly (dimethylsiloxane)

Since their discovery in 1940's, functionally terminated silicone oligomers were used to synthesis silicon rubbers, but only recently the importance of organofunctionally terminated polysiloxanes get attention, due to their ability in block, segmented or grafted copolymers synthesis [106].

Most polydimethylsiloxane (PDMS) fluids are non-volatile polymeric organosilicon materials consisting of $(\text{CH}_3)_2\text{SiO}$ structural units (Figure 2.8).

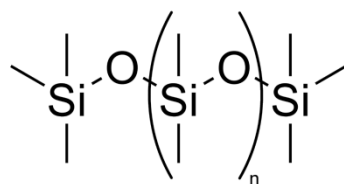


Figure 2.8: Representation of Poly (dimethylsiloxane).

Polysiloxanes are used in a wide range of applications due to their properties such as low surface energy, low glass transition temperature, high chain flexibility, thermal and UV stability. These properties lead to the thermodynamic incompatibility of polysiloxanes with almost all other organic polymers. Using polysiloxanes, especially PDMS in copolymer systems overcomes their incompatibility problem. In siloxane containing copolymers siloxane segments migrate to the air surface; while the organic segments in the copolymer act as anchoring groups for the siloxane blocks [108].

The major problem with pristine conducting polymers is that they are insoluble and infusible materials and not quite suitable for electronic device applications. Their processing could be improved by the synthesis of block and graft copolymers containing insulating and conducting sequences [109-112]. Blending of conducting polymers with thermoplastic polymers is another attempt to modify their mechanical properties [113]. So, PDMS blends and copolymers could be an answer for that problem [114].

Küçükyavuz et al. prepared a PDMS/carbon fiber (CF)/Polythiophene (Pth) composite coated on Pt electrode. The first attempts with PDMS/Pth showed high flexibility due to the rubbery properties of PDMS. But, tensile properties were poor. Therefore the tensile property was reinforced by using carbon fiber [115-117].

2.7. Composites and Nanocomposites

Many potential applications of conducting polymers are limited because of their general insolubility in common organic solvents, poor mechanical properties vis-a-vis their insufficient environmental stability. To overcome this problem a special class of materials has originated by the combinations of two or more nanosized particles with polymers resulting in materials having unique physical properties and

wide application potential in diverse areas. Novel properties of nanocomposites can be derived from the successful combination of the characteristics of parent constituents into a single material [118].

Based on the filler geometries, nanocomposites can be classified into three primary categories. Fumed silica dioxide and nanometallic powder are particles, which are characterized by three dimensions in the nanometer range [119 - 120]. Carbon nanotube (CNT) and whiskers possess two dimensions in the nanometer range [121, 122]; whereas clay, mica and expanded graphite layered structural fillers [123 – 125] possess only one dimension in the nanometer range.

The nanocomposite materials of PNVCz have been prepared with nanodimensional fillers such as; metal oxides (ZrO_2 , MnO_2 , Al_2O_3 , SiO_2 , etc.) [126-128], montmorillonite (MMT) clay [129,130], zeolites [131], and allotropes of carbon such as carbon black (CB) [132], acetylene black (AB) [133], and Buckminster fullerene [134].

The physical mixture of a polymer and nano structured fillers is not always enough to define as a nanocomposite. This mixture, defined as polymer blends could have a discrete phase separation. The resulting material will have a poor physical interaction between the organic and the inorganic components and leads to poor mechanical and thermal properties. In contrast, if stronger interactions between the polymer and the filler were to be created it will lead to the organic and inorganic phases being dispersed at the nanometer level. As a result, nanocomposites will exhibit unique properties not shared by their micro counterparts or conventionally filled polymers [135].

Polymer composites could generally be obtained by three main methods.

While solution processing is a valuable technique for both nanotube dispersion and composite formation, it is less suitable for industrial scale processes, where melt processing is preferred because of its speed and simplicity. In this case, the strategy consists in blending a molten thermoplastic with the nanotubes in order to optimize the polymer-nanotubes interactions and form a nanocomposite. The polymer chains experience a dramatic loss of conformational entropy during the process. The proposed driving force for this mechanism is the important enthalpic contribution of the polymer nanotube interactions during the blending step. Figure 2.9 shows the

flowchart presenting different steps of melt processing. Melt blending can be used to produce either isotropic composites or composite fibers. In order to exploit the intrinsic potentials of CNTs, composite fibers are more suitable than isotropic materials, since fiber production techniques tend to align the nanotubes themselves within the fibers.

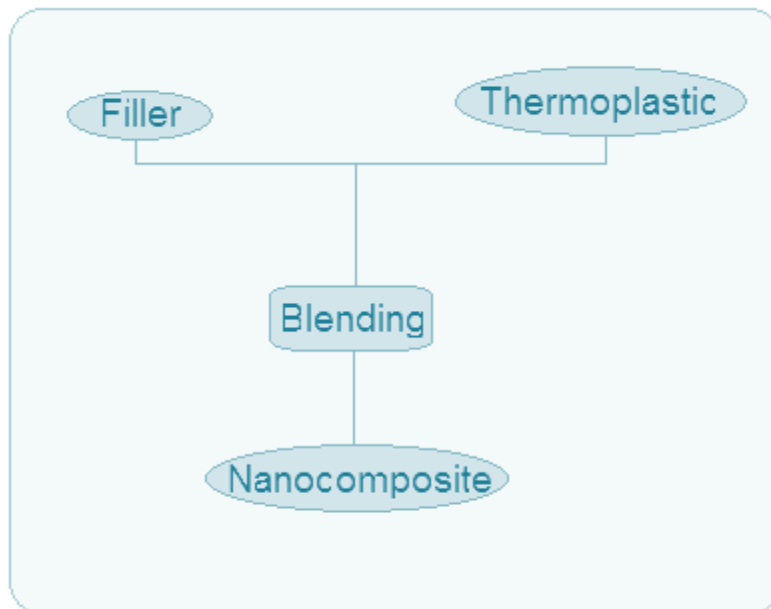


Figure 2.9: Nanocomposite preparation by melt blending.

An interesting finding was reported by Meincke et al. [136]. They prepared polyamide/ acrylonitrile-butadiene–styrene blends containing CNTs and they observed a double percolation effect. Due to the confinement of the nanotubes in the polyamide component, these materials showed an onset in the electrical conductivity at lower filler loadings (2–3 wt %) as compared to pure polyamide/CNTs composites (4–6 wt %).

On the second method shown in Figure 2.10, the filler such as silicates, CNT, graphite, Al_2O_3 etc. is dispersed by mean of different methods (sonic bath, high power sonicator, mechanical stirrer, magnetic stirrer etc.) and the obtained solution is mixed with the polymer. The obtained product is precipitated and dried to obtain the final composite or blend. This is the most common method for fabricating polymer nanocomposites because it is both amenable to small sample sizes and effective. Solution blending involves three major steps: disperse nanotubes in a suitable solvent, mix with the polymer (at room temperature or elevated temperature), and recover the composite by precipitating or casting a film.

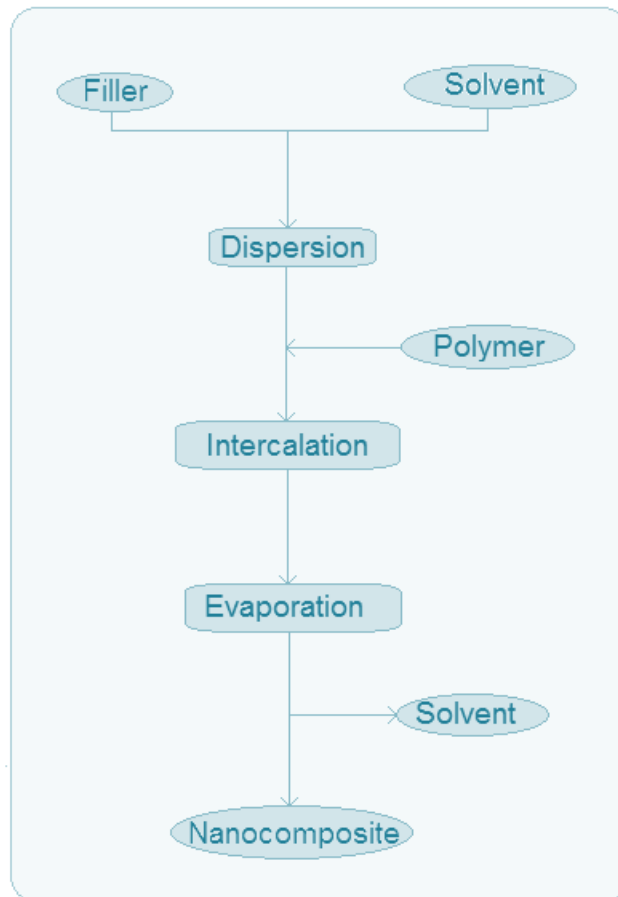


Figure 2.10: Nanocomposite preparation by solution blending.

On the last method, called as the in-situ polymerization has been extensively explored for the preparation of polymer nanocomposites. Its main advantage being the creation of a covalent bond between the filler and the matrix. The presence of polymeric chain onto the filler surface facilitates their dispersion providing a strong interface at the same time.

First, the particles of filler are swollen in the monomer. Then, the reaction is initiated. For the thermosets such as epoxies or unsaturated polyesters, a curing agent or a peroxide, is added to initiate the polymerization. For thermoplastics, the polymerization can be initiated either by the addition of an initiator or by an increase of temperature. Figure 2.11 shows the flowchart for in-situ polymerization processing.

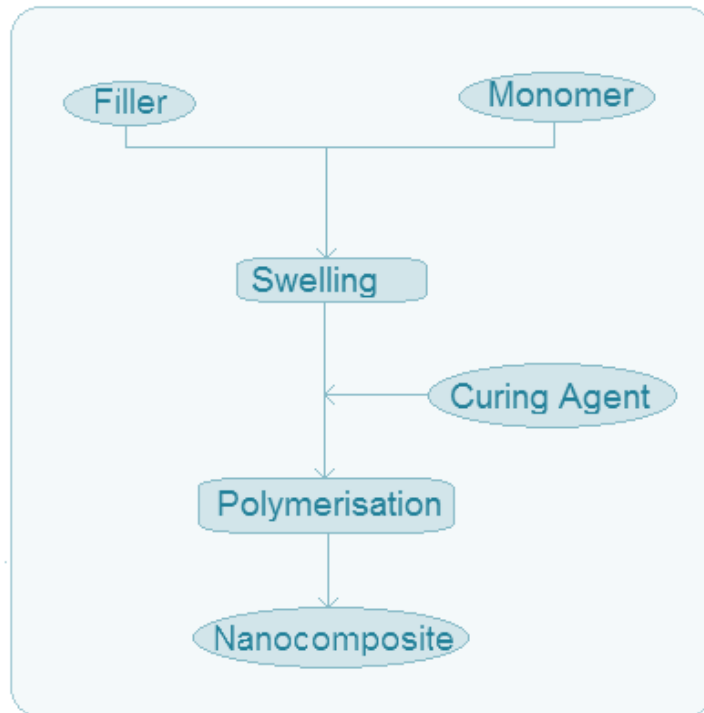


Figure 2.11: Nanocomposite preparation by in-situ polymerization.

The first challenge for researchers is to disperse the filler (silicates, carbon nanotube, and graphite). Although examples could be given for silicates, pristine CNT cannot be dispersed homogeneously by a simple stirring. High-power ultrasonication had to be used to make suspensions of nanotubes in different solvents. But, high-power ultrasonication for a long period of time shortens the nanotube length, i.e., reduces the aspect ratio, which is very important to the composite properties [137]. The minimum sonication conditions (time, power) that produce CNT degradation are yet to be determined and will certainly depend on nanotube concentration and initial nanotube length distribution.

Another possibility is to use surfactants to disperse higher loadings of CNT [138-140]. Sodium dodecyl sulfate (SDS) is one of them. SDS is a typical and easily commercially available anionic surfactant. Although surfactants are used in suspension polymerization systems to form micelles at a specific concentration known as critical micelle concentration, they could be used with much different applications. SDS like surfactant could be used to disperse inorganic fillers. It is thought that during sonication, the provided mechanical energy overcomes the van der Waals interactions in the bundles and leads to exfoliation, whereas at the same time, surfactant molecules adsorb onto the surface of the filler particles to stabilize it.

But, using surfactants to improve should be done with care. At high concentration the remains in the resulting nanocomposite might degrade transport properties. The thermal conductivity of the surfactant-SWCNT/epoxy composites was found lower than the same loading composite without surfactant [140].

2.7.1. Clay

Clays are composed of layered silicates. Those layered silicates have two types of structure: tetrahedral-substituted and octahedral substituted. In the case of tetrahedrally substituted layered silicates the negative charge is located on the surface of silicate layers; as a result polymer matrices can react and interact more easily with these than with octahedrally-substituted one. MMT, hectorite, and saponite are the most commonly used layered tetrahedral silicates (Figure 2.12).



Figure 2.12: Montmorillonite Clay.

MMT is a clay mineral consisting of stacked silicate sheets with high aspect ratio (220) and with a plate like morphology [141]. The layer thickness is around 1 nm, and the lateral dimensions of these layers may vary from 30 nm to several microns or larger, depending on the layered silicate. This high aspect ratio (ratio of length to thickness) plays an important role for the enhancement of mechanical and physical properties. As mentioned before, MMT consists of two fused silicate tetrahedral sheets sandwiching an edge-shared octahedral sheet of either magnesium or aluminum hydroxide phyllosilicates with 2:1 ratio. The conformation of the layers leads to a regular van der Waals gap between those layers called as interlayer or gallery. In this interlayer region there exist Na^+ and Ca^{2+} ions [142].

In the crystal structure of MMT clays, some of the atoms of aluminum can be replaced by magnesium (Mg), lithium (Li) or iron (Fe) by isomorphic substitution. This process generates negative charges that are counterbalanced by alkali and alkaline earth cations situated inside the galleries. This type of layered silicate is

characterized by a moderate surface charge known as the cation exchange capacity (CEC), and generally expressed as mequiv/100 g. This charge is not constant and varies from layer to layer, and must be considered as an average value over the whole crystal. Details regarding the structure and chemistry for these layered silicates are provided in Figure 2.13 and Table 2.1, respectively.

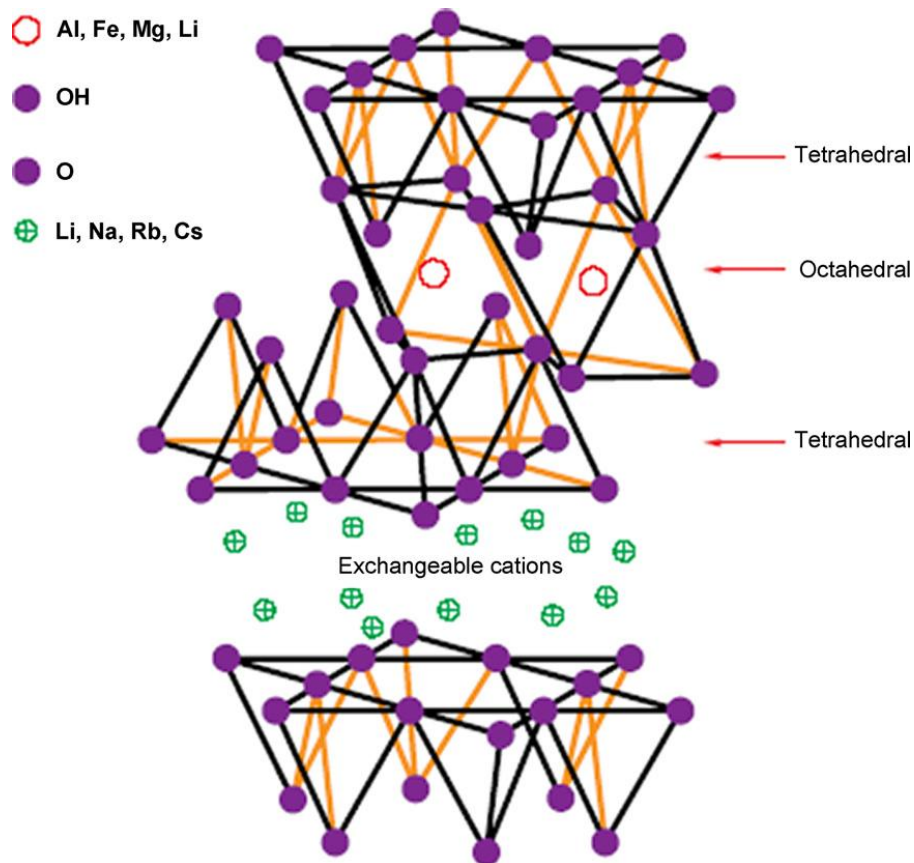


Figure 2.13: Structure of 2:1 phyllosilicates Reproduced from Beyer [143].

Table 2.2: Structure and chemical of layered silicates.

2:1 phyllosilicates	Chemical formula	CEC (mequiv/100 g)	Particle length (nm)
Montmorillonite	$M_x(\text{Al}_{4-x}\text{Mg}_x)\text{Si}_8\text{O}_{20}(\text{OH})_4$	110	100–150
Hectorite	$M_x(\text{Mg}_{6-x}\text{Li}_x)\text{Si}_8\text{O}_{20}(\text{OH})_4$	120	200–300
Saponite	$M_x\text{Mg}_6(\text{Si}_8-x\text{Al}_x)\text{Si}_8\text{O}_{20}(\text{OH})_4$	86.6	50–60

M, monovalent cation; x, degree of isomorphous substitution (between 0.5 and 1.3).

2.7.2. Organo modified clays

In their natural form the clay excess negative charge is balanced by cations (Na^+ , Li^+ , Ca^{2+}) which exist hydrated in the interlayer [144]. Unfortunately, pristine layered silicates are only miscible with hydrophilic polymers, such as poly(ethylene oxide)

(PEO) [145], or poly(vinyl alcohol) (PVA) [146]. To render layered silicates miscible with other polymer matrices, one must convert the normally hydrophilic silicate surface to an organophilic one, making the intercalation of many engineering polymers possible. Generally, this can be done by ion-exchange reactions with cationic surfactants including primary, secondary, tertiary, and quaternary alkylammonium or alkylphosphonium cations. Alkylammonium or alkylphosphonium cations in the organosilicates rendering the clay into organophilic nature [147-148], lower the surface energy of the inorganic host and improve the wetting characteristics of the polymer matrix, and result in a larger interlayer spacing. Additionally, the alkylammonium or alkylphosphonium cations can provide functional groups that can react with the polymer matrix, or in some cases initiate the polymerization of monomers to improve the strength of the interface between the inorganic and the polymer matrix [149].

The organic modifier plays an important role for producing the nanocomposite. It may either enhance the interaction between the clay and the polymer, making it more suitably mixed, or it may favor the intercalation of the polymer chain by dictating the gallery spacing (Figure 2.14).

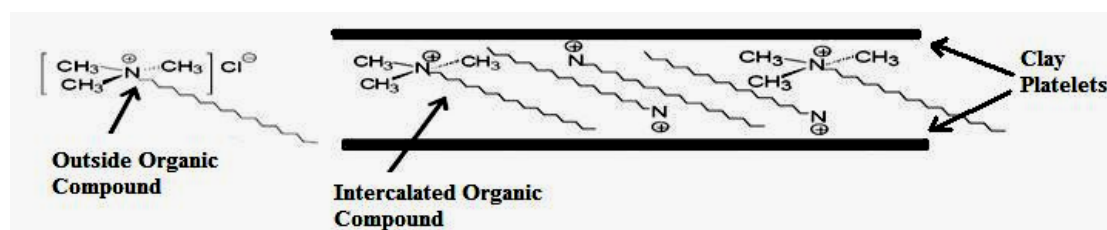
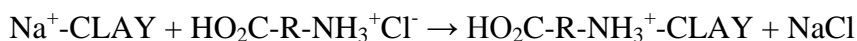


Figure 2.14: Intercalation by surfactant ref. [150].

For example, in montmorillonite, the sodium ions in the clay can be exchanged for an amino acid such as 12-aminododecanoic acid (ADA):



The way in which this is done has a major effect on the formation of particular nanocomposite product forms and this is discussed further below. Although the organic pre-treatment adds to the cost of the clay, the clays are nonetheless relatively cheap feedstock with minimal limitation on supply. Montmorillonite is the most common type of clay used for nanocomposite formation; however, other types of clay can also be used depending on the precise properties required from the product.

These clays include hectorites (magnesium silicates), which contain very small platelets, and synthetic clays, which can be produced in a very pure form and can carry a positive charge on the platelets, in contrast to the negative charge found in montmorillonites [151].

While far from a completely accurate or descriptive nomenclature, the literature commonly refers to three types of morphology: immiscible (conventional or microcomposite), intercalated, and miscible or exfoliated. These are illustrated schematically in Figure 2.15 along with example transmission electron microscopic, TEM, images and the expected wide angle X-ray scans [152].

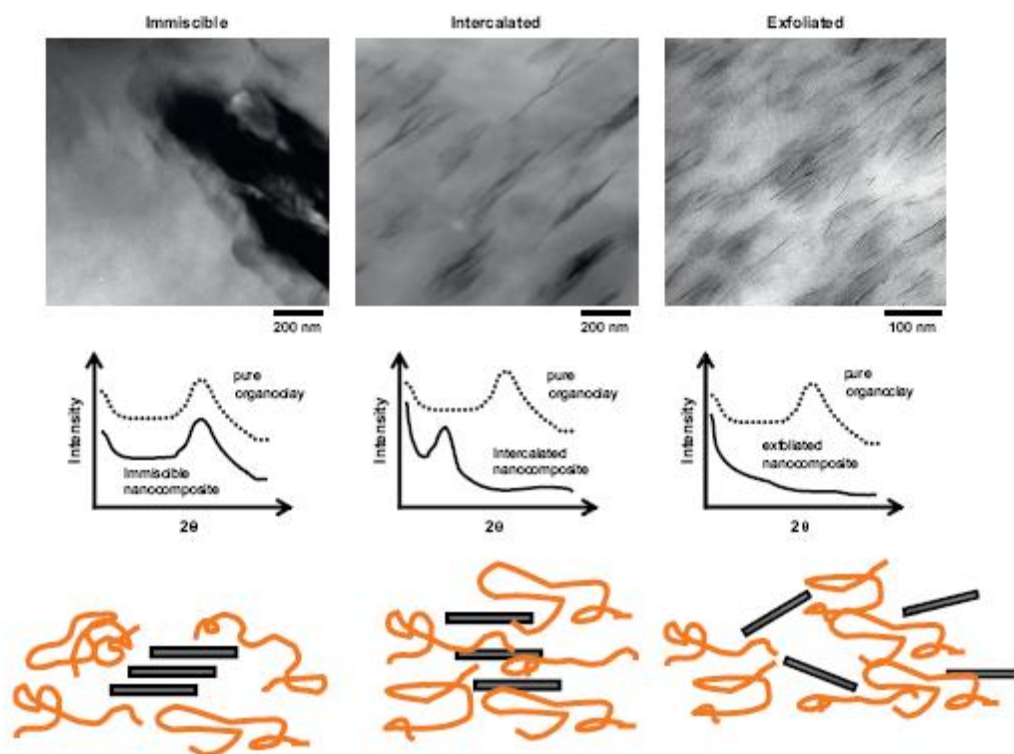


Figure 2.15: Illustration of different states of dispersion of organoclays in polymers with corresponding WAXS and TEM results [152].

2.7.3. Polymer / Clay Nanocomposites

Polymer/layered silicates (PLS) nanocomposites have attracted great interest, because they exhibit remarkable improvement in materials properties when compared with virgin polymer or conventional micro and macro-composites. These improvements can include high moduli [153 - 154], increased strength and heat resistance [155], decreased gas permeability [156–159] and flammability [160–162], and increased biodegradability of biodegradable polymers [163]. On the other hand,

there has been considerable interest in theory and simulations addressing the preparation and properties of these materials, and they are also considered to be unique model systems to study the structure and dynamics of polymers in confined environments [164–168].

Although the intercalation chemistry of polymers when mixed with appropriately modified layered silicate and synthetic layered silicates has long been known [169, 170], the field of PLS nanocomposites has gained momentum recently. Two major findings have stimulated the interest in these materials: in first, very small amounts of layered silicate loadings resulted in remarkable improvements of thermal and mechanical properties; and second, that it is possible to melt-mix polymers with layered silicates, without the use of organic solvents.

Polymer-clay nanocomposites have attracted much attention in recent years due to their ability to achieve increased properties from pure polymer with the addition of a small volume percentage of nanometer-sized particles.

The creation of a so-called “nanocomposite” composed of polymer and a layered silicate has received much more attention since some of the first research on this type of composite was undertaken by Toyota Motor Company researchers in the 1980s and 1990s by creating the nylon 6/montmorillonite nanocomposite [171]. Nanocomposite research grew in interest because of the enhanced properties obtained over bulk properties being separated including: mechanical, chemical, and barrier properties [172 – 175]. Through the years polymer/layered silicate nanocomposite research has opened up not only to conductive polymer / layered silicate nanocomposite research and but also to using in non conductive polymers like: polyurethanes [176], nylons [177-179], polypropylene [180], polystyrene [181-182], polyisoprene [183], phenolic resins [184], epoxies [185-186], poly (methyl methacrylate) [187 - 189], polyimides [190 - 192], polyethylene [193], and polyethylene terephthalate [194].

Layered silicates should possess two particular characteristics to be considered for polymer/layered silicate nanocomposites.

1. The ability of the silicate particles to disperse into individual layers.
2. The ability to fine-tune their surface chemistry through ion exchange reactions with organic and inorganic cations.

These two characteristics are, of course, interrelated since the degree of dispersion of layered silicate in a particular polymer matrix depends on the interlayer cation.

Most of the layered silicates used for polymer / clay nanocomposites are members of the 2:1 phyllosilicates family like hectorite and montmorillonite. Smectite or layered silicates are of special interest for formation of polymer / clay nanocomposites for a number of reasons including: cation exchange capacity, surface area, surface reactivity, adsorption properties, viscosity properties, and transparency. Dispersion or intercalation of monomer and / or polymer and ultimately formation of a nanocomposite is largely dependent on the aforementioned ion exchange to create interactions between the inorganic clay and the organic polymer otherwise a phase separated / immiscible system would be created.

The clay nanoparticles may influence the arrangement of polymer chains, as it may become confined into the clay plates.

In general, layered silicates have layer thickness on the order of 1 nm and a very high aspect ratio (e.g. 10–1000). A few weight percent of layered silicates that are properly dispersed throughout the polymer matrix thus create much higher surface area for polymer/filler interaction as compared to conventional composites. Depending on the strength of interfacial interactions between the polymer matrix and layered silicate (modified or not), three different types of PLS nanocomposites are thermodynamically achievable (Figure 2.16):

1. Intercalated nanocomposites: in intercalated nanocomposites, the insertion of a polymer matrix into the layered silicate structure occurs in a crystallographically regular fashion, regardless of the clay to polymer ratio. Intercalated nanocomposites are normally interlayer by a few molecular layers of polymer.
2. Flocculated nanocomposites: conceptually this is same as intercalated nanocomposites. However, silicate layers are sometimes flocculated due to hydroxylated edge–edge interaction of the silicate layers.
3. Exfoliated nanocomposites: in an exfoliated nanocomposite, the individual clay layers are separated in a continuous polymer matrix by an average distances that depends on clay loading.

Usually, the clay content of an exfoliated nanocomposite is much lower than that of an intercalated nanocomposite.

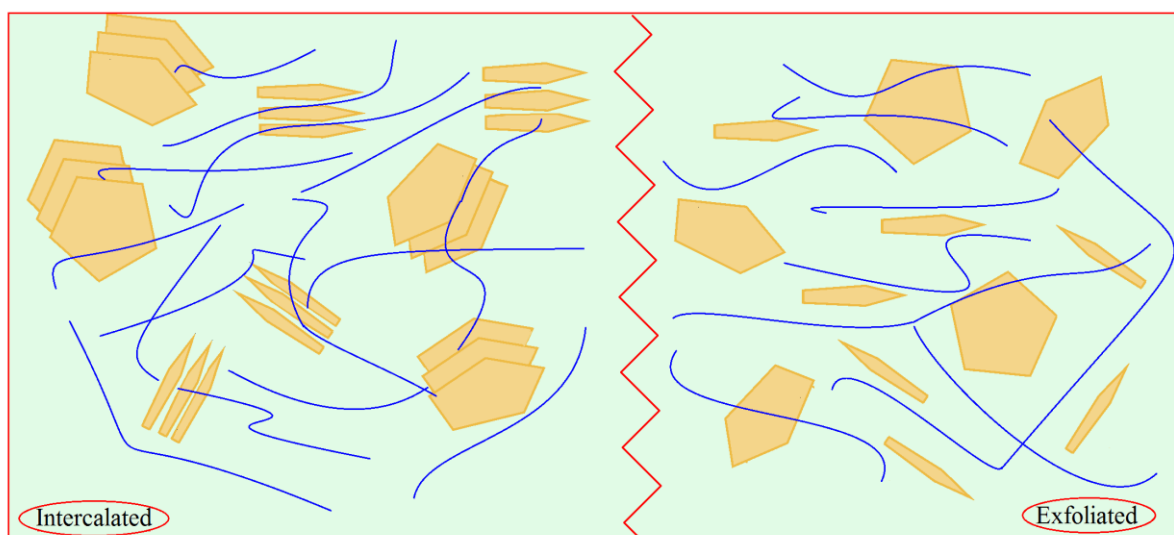


Figure 2.16: Schematic illustration of two different types of thermodynamically achievable polymer/layered silicate nanocomposites.

The synthesis of MMT/PNVCz composite was one of the different attempts tried to enhance the conductivity and other defective properties of PNVCz. Biswas et al. polymerized NVCz with no other initiator in the presence of MMT at mild temperatures (70°C) in solid state [195]. Their other attempt was to polymerise NVCz in aqueous media with FeCl_3 as initiator with success at 10^{-5} S/cm conductivity [196].

The conductivity and optical properties of a conducting polymer depend mainly on the arrangement of its chains. On the other hand, it is essential to control the molecular orientation and the arrangement at the monomolecular level in order to drive the functionality of these organic molecular devices in an efficient manner. However, in many cases, it is difficult to control the molecular arrangement and the homopolymer packing because PNVCz itself easily forms an amorphous polymer [197].

2.7.4. Graphite

The nanocomposites containing layered silicates exhibit markedly superior mechanical, thermal and barrier performance in comparison with conventional micro composites [198 – 201]. Unfortunately, nanoclay reinforced polymers do not possess electrical conductivity, photonic and dielectric properties that are as good as some functional polymers such as graphite-containing polymers.

Graphite is a layered material, consisting of a structure where carbon atoms are bound by covalent bonds to other carbons in the same plane and only van der Waals forces are acting between successive layers. Since the van der Waals forces are relatively weak, it is possible for a wide range of atoms, molecules, and ions to intercalate between graphite sheets [202-204]. In contrast to the clays, there is no net charge on graphite; thus, ion exchange processes like those used to organically modify clays, are not possible for graphite.

Different conductive fillers such as carbon black (CB) etc. have been extensively explored for composite components. These fillers effectively improve the conductivity of polymers [205 - 206]. Usually rather high filler content is needed to increase the conductivity because the filler size is only in the micrometer range.

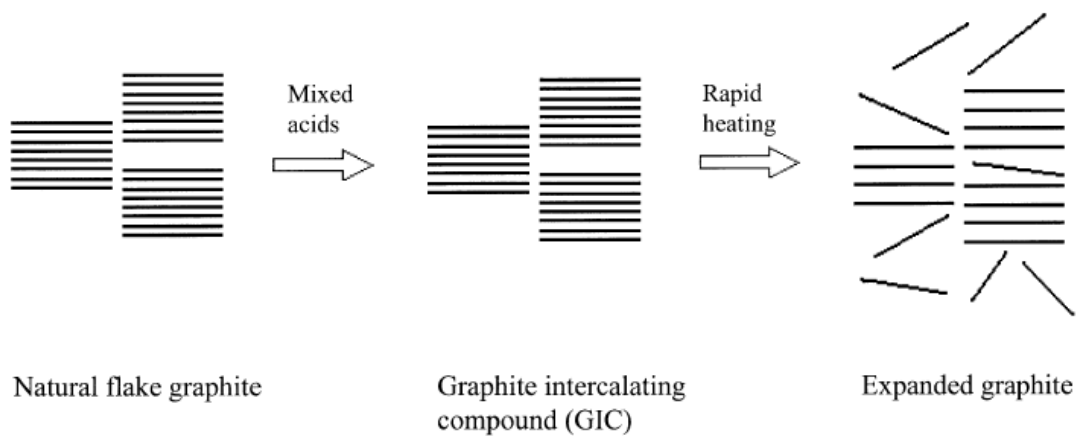


Figure 2.17: A schematic showing the formation of expanded graphite from natural flake graphite.ref 207.

The significant improvement in electrical conductivity arising from the increase of filler content was observed for most composites and it was explained by the percolation transition of the conductive network formation. In most cases, relatively large quantities of fillers were needed to reach the critical percolation value.

Composites containing conducting fillers in insulating polymers become electrically conductive when the filler content exceeds a critical value, known as a percolation threshold. The percolation threshold is characterized by a sharp jump in the conductivity by many orders of magnitude which is attributed to the formation of a three-dimensional conductive network of the fillers within the matrix.

Percolation theory [208-209] can be employed to explain the insulator–conductor transition occurring in the composite systems when a critical of conducting fillers is reached, using the following equation:

$$\sigma = \sigma_0 (p - p_c)^n \quad (2.5)$$

Where n is a critical exponent of conductivity, which depends only on the dimensionality of the systems.

2.7.5. Graphite/Polymer Composites

Although natural graphite/polymer composites were reported, expanded graphite (EG) has been shown to possess better interaction with polymer chains [210-212]. Because there are no reactive groups on the natural graphite layers, it is difficult for a monomer to load on its surface. In addition, natural graphite particles are difficult to be dispersed because they have large volume and their shapes are regular [213].

EG is generally obtained by an acid treatment at low temperature followed by a high temperature ($\sim 900^\circ\text{C}$) thermal process on a short period (5 - 30 seconds) (Figure 2.17) [214-216].

The obtained EG contains abundant multi-pores ranging from 2 to 10 nm. The properties of multi-pores, functional acids and the OH groups promote a good affinity of EG to both the organic compounds and the polymers. Therefore, EG is able to adsorb some monomers, initiators and polymers resulting in conductive polymer/graphite nanocomposites.

EG has a huge specific surface area, high adsorptive capacity, and large occluded volume. It has strong tendency for nonpolar molecules. During the acidizing process, the groups of -OH and -COOH form at the surface of the graphite. In a certain environment, EG can also adsorb the polar molecules, and it has the characteristics of macroporous structure and physical adsorption effect [217, 218].

For instance, FTIR spectrum of graphite shows the presence of an intense peak around 1740 cm^{-1} , which may be attributed to the oxidized graphite phase. For example in the preparation of PANI/ EG composites, the presence of characteristic peaks of graphite and aniline confirms the presence of both phases in the composite. However, all these bands show a systematic shifting that indicates the existence of significant interaction. These interaction between graphite (electron acceptor) and

doped polyaniline (donor or p-type material) may be attributed to the formation of charge transfer complex and thought to occur due to partial transfer of lone pair of electrons of amine nitrogen atoms to the graphite particles. As a result amine nitrogen acquires partial positive charge whereas graphite particles develop equivalent negative charge (Figure 2.18) [219]. Such complex formation between donor and acceptor molecules has been well documented in case of other conducting polymers and could also be expanded to NVCz molecules.

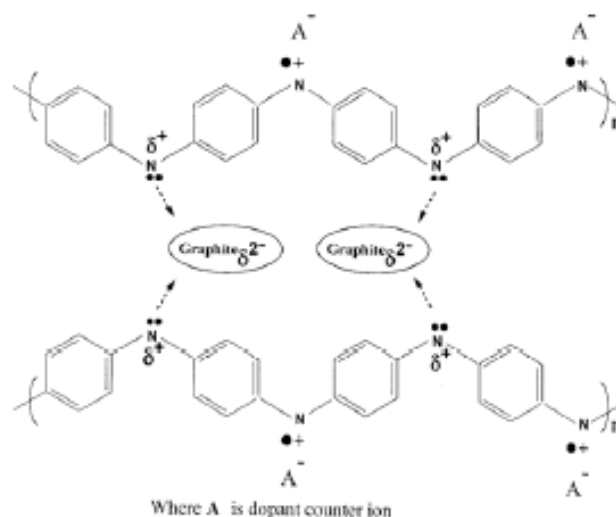


Figure 2.18: graphite-polymer interaction. Ref. [219].

Using EG, both polymer/graphite nanocomposites and macrocomposites with a good electrical conductivity and high thermal storage properties have been reported [220–223].

PMMA/expanded graphite (EG) composites were prepared by direct solution blending of PMMA with the expanded graphite filler. Electrical conductivity and dielectric properties of the composites were measured by a four-point probe resistivity determiner and a dielectric analyzer (DEA). Interestingly, only 1 wt% filler content was required to reach the percolation threshold (Φ) of transition in electrical conductivity from an insulator to a semiconductor using PMMA/EG. The thickness of the interlayer of the expanded graphite was shown to be close to the nanometer scale. The reported filler content was much lower than that required for conventional PMMA/carbon black (8 wt% carbon) and PMMA/graphite (3.5 wt% graphite) composites. The improvements in both electrical conductivity and structural integrity were attributed to the difference in filler geometry (aspect ratio and surface area) and the formation of conductive networks in the composites [224].

2.7.6. Carbon Nanotubes

CNT, discovered in 1991 [225] possess unique properties including high tensile strength, chemical stability and electrical conductivity [226] that may prove useful in the fields of biomedical materials and devices.

Since the discovery of CNTs (Figure 2.19), extensive research in the fields of applied physics, chemistry and materials science and engineering has rapidly emerged [227–229].

The extreme mechanical and transport properties of the carbon nanotubes (CNTs) have inspired scientists and engineers for a wide range of potential applications [230].

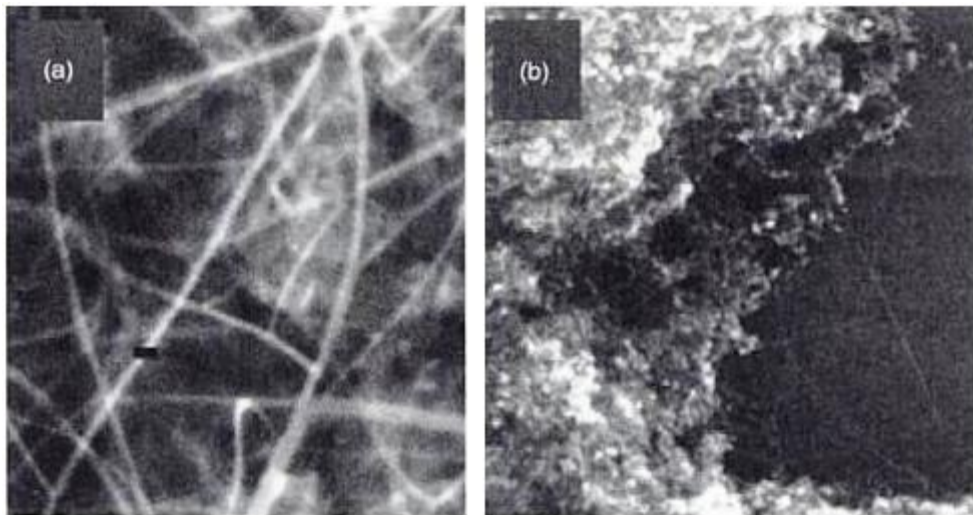


Figure 2.19: SEM images of purified SWCNT grown in using Alumina supported Fe-Mo catalyst on a patterned silicon substrate: (a) SWCNT at magnification of x200,000 and (b) SWCNT grown between catalyst particles at magnification x50,000.

CNTs exist in two main categories: a single-walled nanotube which possess the fundamental cylindrical structure, and the multi-walled nanotube which are made of coaxial cylinders, with spacing between the layers close to that of the interlayer distance in graphite (0.34 nm) (Figure 2.20).

CNTs was produced on first by the arc discharge and laser vaporisations processes, but more and more work has been devoted to chemical vapor deposition (CVD) techniques.

In this process, a mixture of inert gases is decomposed at high temperature (1000°C). A substrate (silicon, glass or aluminium) containing a layer of metal catalyst (Fe, Co or Ni), by sputtering, solution or electron beam evaporation, is placed inside the reactor vessel. At high temperatures, the carbon forms tubes because of a free energy decrease and a lack of dangling bonds [231].

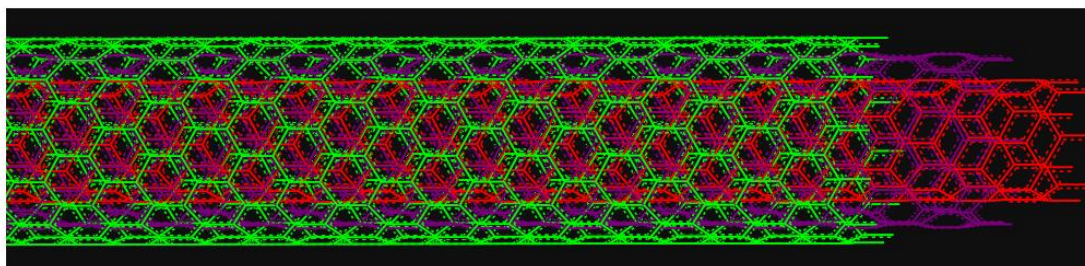


Figure 2 20: Schematic presentation of MWCNT.

In most of the cases the solubility of the CNTs is assessed qualitatively, based on visual appearance. Recently, methods based on sedimentation combined with gravimetric [232, 233] or spectroscopic [234] techniques were proposed to determine quantitatively the CNT solubility.

In some of the cases the optical microscope was used in conjunction with the above methods to construct phase-diagrams [232, 233] or to evaluate the suspension quality [235]. Generally, these methods were used to evaluate the solubility of SWCNT, and the maximum solubility measured was around 2 mg/ml [234].

It is well known that CNT dispersion is not a true solution in the molecular sense, but a colloidal suspension.

However, throughout the literature the terms solution, solubility, solubilisation are widely used to describe CNT dispersions.

Despite the outstanding properties of the individual CNTs their insolubility hinders the transfer of those properties into the bulk. Covalent functionalisation represents an efficient way to render the CNTs soluble either in aqueous or organic phase, by attaching different functional groups directly to the CNTs [236].

Pristine CNTs can be effectively purified with acid to result oxygen-containing groups, mainly carboxyl and hydroxyl, have been found to decorate the graphitic surface[237-239].

Literature screening shows that nitric acid is extensively used to oxidize CNTs. Nitric acid or/and sulphuric acid treatment produces mainly carboxylic groups [237–240] which contribute to the solubilisation of the nanotubes [240, 241]. The reaction conditions differ largely from one author to another, e.g., the acid concentration varies in the range of 15– 70 wt%, the initial concentration of the CNTs varies from 0.1 to 10 mg/ml, and the treatment duration from 1 to 48 h. Up to now there are no dedicated studies on the MWCNT oxidation in nitric acid [242].

The alignment of the MWCNTs is important for certain applications, but there are only a few studies concerning the alignment [243, 244]. The presence of oxygen-containing groups facilitates the exfoliation of CNT bundles, and increases the solubility in polar media [245, 246]. This, in turn, affects the processing of CNTs and increases the possibility of further modification/functionalisation depending on application [247, 248].

2.7.7. CNT/Polymer Composites

Research on CNT incorporated polymer composites has intensified by folds on the last decade. Researches were scoped in generally into two domains related with each other. The increase of the polymer conductivity creates a lack on the physical properties due to their poor stability during cycling. Conductive polymer films, because of volumetric changes during the doping/dedoping process (insertion/deinsertion of counter ions), undergo swelling, shrinkage, cracks, or breaking, which in consequence gradually degrades their conducting properties. Although this drawback, they can be used in many applications such as supercapacitors, sensors, advanced transistors, high-resolution printable conductors, electromagnetic absorbers, photovoltaic cells, photodiodes and optical limiting devices [249].

Despite that, there is limited article on PNVCz/CNT composites, a special attention has been given to CNTs functionalized with poly(N-vinyl carbazole) nowadays [250–251]. Two different methods of synthesis of CNT composites have been reported: direct mixing of the polymer with CNTs, and chemical polymerization of monomer in the presence of carbon nanoparticles [252, 253].

Carbazole moieties are well-known electron donors and hole transporters in organic electronics. While on the other hand CNT's, due to the strong electron-withdrawing

ability and the extensive π -conjugation along the CNT axis, electrons are deeply trapped in the CNT network. The π electron rich surface and the methyl groups of polymers are thought to triggered an interaction known as the CH- π interaction. This interaction is a weak hydrogen bond between soft acids and soft bases. They are largely due to dispersion forces and partly to charge transfer and electrostatic forces.

This behavior permit polymerization of NVCz with slightly acceptable conditions (65°C, in toluene) without any external oxidant. On the other hand, the melt polymerisation is an alternative process having recently close intention. NVCz monomer in the presence of CNT could be synthesized via solid state polymerisation at high temperature without further oxidant [254]. The polymerization procedure is defined for Aniline (ANI) as follows. The mechanism is depicted with the presence of CNT's π - π^* interaction with Aniline. Such strong interaction ensure that the aniline monomers are absorbed on the surface of MWCNT's, which serve as the core and the self-assembly template during the formation of the tubular nanocomposites. The interaction with NVCz is thought to be similar. The addition of external oxidant or else a reflux process enable a bond creation with the vinyl group and the CNT π bond (Figure 2.21).

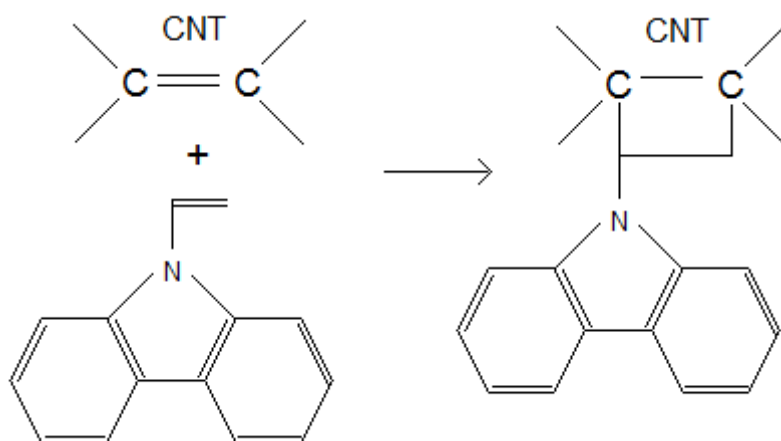


Figure 2.21: Proposed interaction on polymer and CNT. Ref 255.

The main objective is to increase the polymer conductivity. To achieve this goal one must not forget that it exist some drawbacks. Well-dispersed nanotubes generally have higher aspect ratios than nanotube aggregates, so the percolation threshold mentioned earlier decreases with better dispersion. But, in an inverse case where slight aggregation [256] produces a lower percolation threshold by increasing the local interactions between nanotubes. Alignment of the nanotubes in the polymer

matrix has a profound effect on the electrical conductivity and its percolation threshold. When the nanotubes are highly aligned in the composites, there are fewer contacts between the tubes, which results in a reduction in electrical conductivity and a higher percolation threshold as compared to those in a composite with randomly oriented nanotubes.

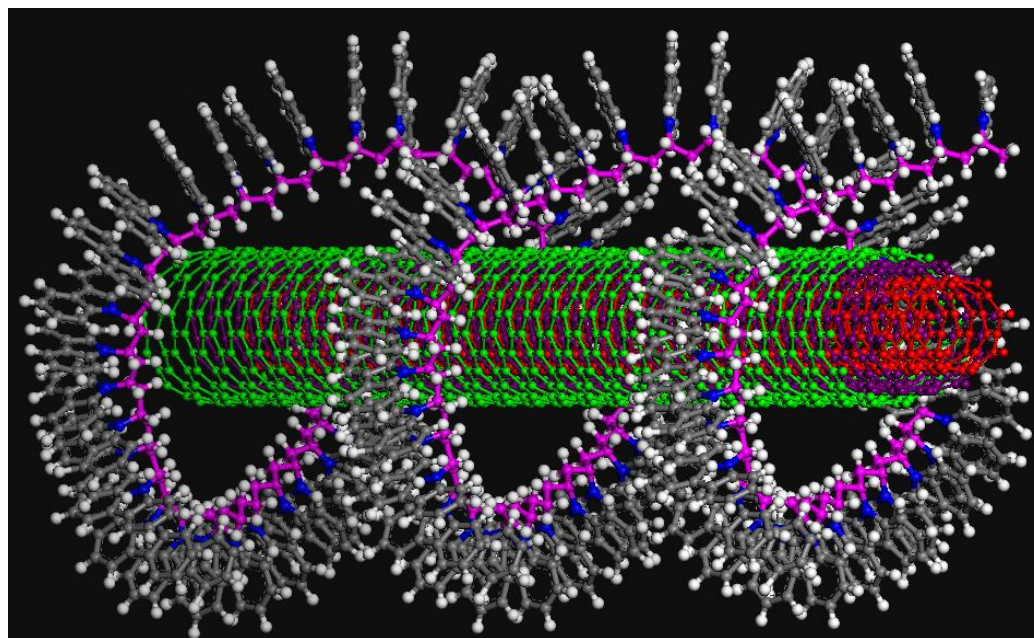


Figure 2.22: Schematic presentation of MWCNT-PNVCz interaction.

It is widely accepted that chemical functionalisation disrupts the extended π -conjugation of nanotubes and thereby reduces the electrical conductivity of isolated nanotubes. But, Tamburri et al. [257] found that extensive functionalisation of SWCNT with -OH and -COOH groups enhances the current in a conducting polymer (1,8-diaminophthalene) by factors of 90 and 140, respectively, whereas the untreated tubes showed an enhancement of only 20. It appears that the disadvantages of functionalisation with respect to SWCNT conductivity are outweighed by the improved dispersion enabled by functionalisation.

Functional groups such as COOH, C=O, and OH are generated on the CNTs as a result of surface treatment [258-259]. These functional groups have some nucleophilicity, which induces polar interactions with electrophilic groups (Figure 2.22). Epoxide/CNT composites, can form nucleophile–electrophile complexes between functional groups and epoxides due to these polar interactions. In the polymer–carbon nanotube system, homogeneous dispersion of carbon nanotubes in

the polymer matrix is a critical factor for improving the performance of materials. Surface treatment of CNTs is a facile way to disperse CNTs more effectively.

Due to the nucleophilicity of NVCz even relatively weak carboxylic acids can cause polymerization [260]. For example, the cationic polymerization of NVCz is initiated by carbon whiskers (vapour-grown carbon fibres) [261] and by g-poly(glutamic acid) [262]. These polymerizations are heterogeneous processes during which carboxylic groups on the surface of the carbon whiskers and g-poly(glutamic acid) particles are responsible for the initiation of NVCz polymerization.

Prog. Polym. Sci. 28 (2003) 1297–1353

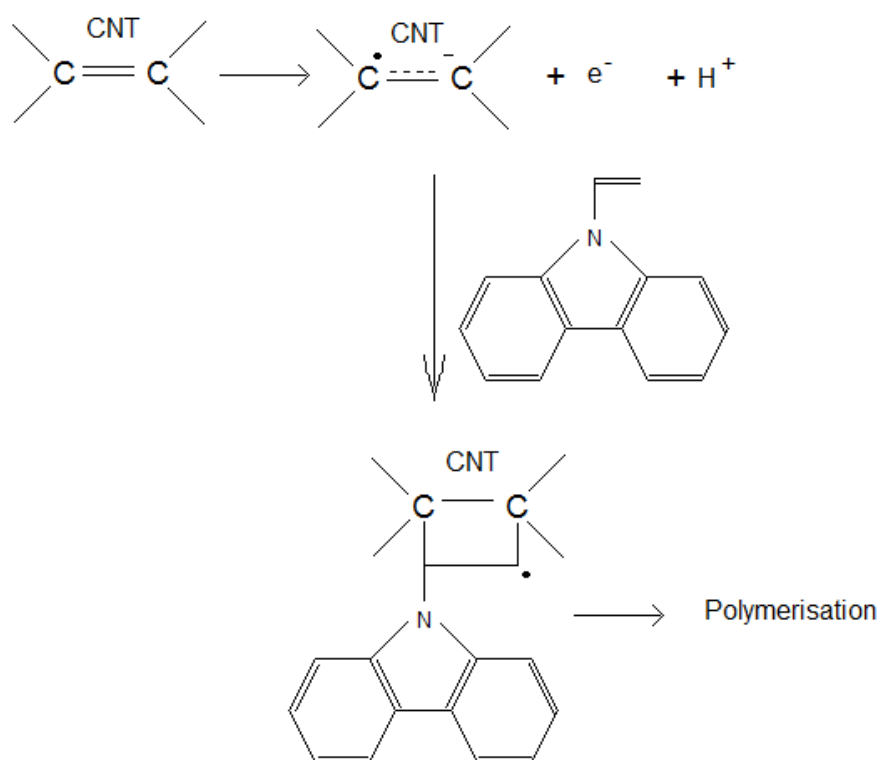


Figure 2.23: Proposed interaction of polymer and CNT by electrochemical methods.

The electrochemical polymerization of NVCz in the presence of CNT is defined by the following mechanism (Fig 2.23) by Islam et al. The ablation of electron creates radicalic gaps on nanotube walls initiating the polymerization of NVCz from the wall sides. The acidic functionalisation could on some case create defects on CNT walls. Those defects could generate radical groups similar to the electrochemical procedure, allowing the polymerization with no further oxidant [263].

2.8. Conductivity

After the discovery of conductive polymers, the main objective has come to improve the conductivity of those polymers. The addition of filler has become a common method nowadays. Different fillers usually used are metal powder [264, 265], carbon black [266], graphite [267], carbon fibers [268], and so forth [269]. Many factors made a dramatic impact on the conductivity of the composites, such as characteristics of fillers and polymers, diameter and structure of fillers, concentration of fillers, dispersion, processing methods, temperature, and pressure [270-273].

The potential of nanotubes as conducting fillers in multifunctional polymer composites has been successfully realized. Several orders of magnitude enhancement in electrical conductivity (σ) has been achieved with a very small loading (0.1 wt% or less) of nanotubes in the polymer matrices, while maintaining the other performance aspects of the polymers such as optical clarity, mechanical properties, low melt flow viscosities, etc.

However, the mechanical properties decrease seriously at high filler contents (~15 wt %, usually).

Therefore, much attention has been centered on the preparation of conducting composites with a low percolation threshold [274- 275]

For example, the electrically conductive percolation threshold at room temperature is 0.75 vol% and the electrical conductivity (σ) reaches 10^{-4} S/cm when EG concentration is 2.0 vol%, which reveals the tremendous potentials and values of Thiophene/EG nanocomposites [276].

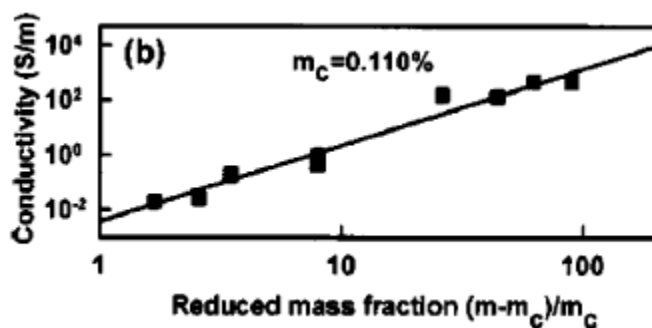


Figure 2.24: Electrical conductivity as a function of reduced mass fraction of nanotubes, showing a threshold of 0.11 wt %.

The percolation threshold is typically determined by plotting the electrical conductivity as a function of the reduced mass fraction of nanotubes and fitting with a power law function (Figure 2.24). The nanotube/polymer composites exhibit very low percolation threshold for electrical conductivity because of the large aspect ratio and the nanoscale dimension of nanotubes. For SWNT/polymer composites, the reported percolation thresholds range from 0.005 vol % to several vol %. Percolation thresholds as low as 0.002 vol % have been achieved in the polymer composite with long flexible ropes of aligned MWCNT [277].

Volumetric conductivity measurement is a common method to determine the conductivity of solid state compounds. On this method, the samples are consolidated in the form of cylindrical compacts with a thickness of generally 1mm by applying a uniaxial pressure using a hydraulic press. The formed pellet is sandwiched between generally two Pt electrodes. The conductivity is measured from the reciprocal of the slope from the applied potential versus intensity [278].

There are also different voltammetric methods to determine and investigate the conductivity.

2.8.1. Voltammetric Techniques

Historically, the branch of electrochemistry we now call voltammetry developed from the discovery of polarography in 1922 by the Czech chemist Jaroslav Heyrovsky, for which he received the 1959 Nobel Prize in chemistry. The early voltammetric methods experienced a number of difficulties, making them less than ideal for routine analytical use. However, in the 1960s and 1970s significant advances were made in all areas of voltammetry (theory, methodology, and instrumentation), which enhanced the sensitivity and expanded the repertoire of analytical methods. The coincidence of these advances with the advent of low-cost operational amplifiers also facilitated the rapid commercial development of relatively inexpensive instrumentation.

The common characteristic of all voltammetric techniques is that they involve the application of a potential (V) to an electrode and the monitoring of the resulting current (i) flowing through the electrochemical cell. In many cases the applied potential is varied or the current is monitored over a period of time (t). Thus, all voltammetric techniques can be described as some function of E , i , and t . They are

considered active techniques (as opposed to passive techniques such as potentiometry) because the applied potential forces a change in the concentration of an electroactive species at the electrode surface by electrochemically reducing or oxidizing it.

The analytical advantages of the various voltammetric techniques include excellent sensitivity with a very large useful linear concentration range for both inorganic and organic species (10^{-12} to 10^{-1} M), a large number of useful solvents and electrolytes, a wide range of temperatures, rapid analysis times (seconds), simultaneous determination of several analytes, the ability to determine kinetic and mechanistic parameters, a well-developed theory and thus the ability to reasonably estimate the values of unknown parameters, and the ease with which different potential waveforms can be generated and small currents measured.

Analytical chemists routinely use voltammetric techniques for the quantitative determination of a variety of dissolved inorganic and organic substances. Inorganic, physical, and biological chemists widely use voltammetric techniques for a variety of purposes, including fundamental studies of oxidation and reduction processes in various media, adsorption processes on surfaces, electron transfer and reaction mechanisms, kinetics of electron transfer processes, and transport, speciation, and thermodynamic properties of solvated species. Voltammetric methods are also applied to the determination of compounds of pharmaceutical interest and, when coupled with HPLC, they are effective tools for the analysis of complex mixtures.

A typical electrochemical cell consists of the sample dissolved in a solvent, an ionic electrolyte, and three (or sometimes two) electrodes. Cells (that is, sample holders) come in a variety of sizes, shapes, and materials. The type used depends on the amount and type of sample, the technique, and the analytical data to be obtained. The material of the cell (glass, Teflon, polyethylene) is selected to minimize reaction with the sample. In most cases the reference electrode should be as close as possible to the working electrode; in some cases, to avoid contamination, it may be necessary to place the reference electrode in a separate compartment.

The reference electrode should provide a reversible half-reaction with Nernstian behavior, be constant over time, and be easy to assemble and maintain.

The counter electrode consists of a thin Pt wire, although Au and sometimes graphite have also been used.

The working electrodes are of various geometries and materials, ranging from small Hg drops to flat Pt disks. Other commonly used electrode materials are gold, platinum, and glassy carbon [279].

2.8.2. Cyclic Voltammetry (CV)

Cyclic voltammetry (CV) has become an important and widely used electroanalytical technique in many areas of chemistry. It is rarely used for quantitative determinations, but it is widely used for the study of redox processes, for understanding reaction intermediates, and for obtaining stability of reaction products.

This technique is based on varying the applied potential at a working electrode in both forward and reverse directions (at some scan rate) while monitoring the current. The important parameters in a cyclic voltammogram are the peak potentials (E_{pc} , E_{pa}) and peak currents (i_{pc} , i_{pa}) of the cathodic and anodic peaks, respectively. If the electron transfer process is fast compared with other processes (such as diffusion), the reaction is said to be electrochemically reversible.

Thus, for a reversible redox reaction at 25 °C with n electrons ΔE_p should be $0.0592/n$ V or about 60 mV for one electron. In practice this value is difficult to attain because of such factors as cell resistance.

Irreversibility due to a slow electron transfer rate results in $\Delta E_p > 0.0592/n$ V, greater, say, than 70 mV for a one-electron reaction.

For a reversible reaction, the concentration is related to peak current by the Randles–Sevcik expression (at 25 °C):

$$i_p = 2.686 \times 10^5 n^{3/2} A c_0 D^{1/2} \nu^{1/2} \quad (2.10)$$

Where i_p is the peak current in amps, A is the electrode area (cm^2), D is the diffusion coefficient ($\text{cm}^2 \text{s}^{-1}$), c_0 is the concentration in mol cm^{-3} , and ν is the scan rate in V s^{-1} .

Cyclic voltammetry is carried out in quiescent solution to ensure diffusion control. A three-electrode arrangement is used. Mercury film electrodes are used because of

their good negative potential range. Other working electrodes include glassy carbon, platinum, gold, graphite, and carbon paste [279].

2.8.3. Other Pulse Methods

In order to increase speed and sensitivity, many forms of potential modulation have been tried over the years. Three of these pulse techniques are widely used (Figure 2.25).

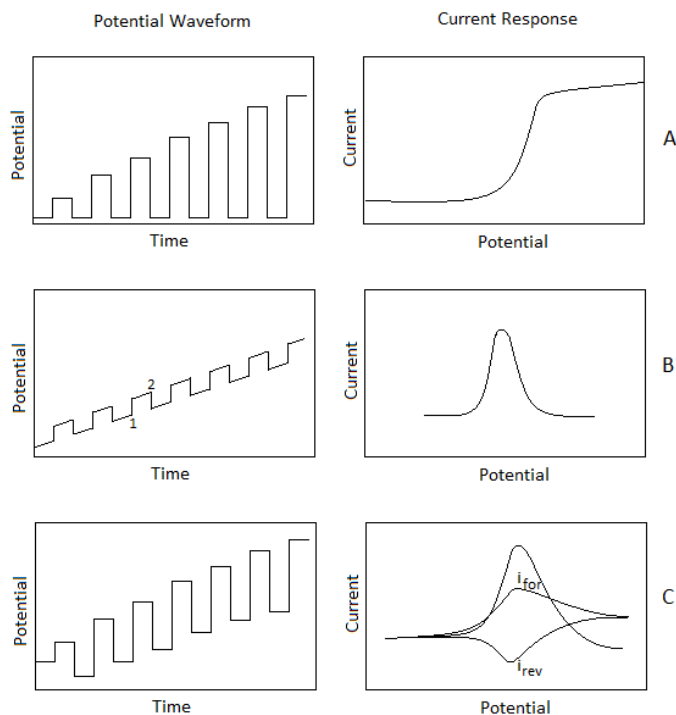


Figure 2.25: Different voltammetric step models.

2.8.3.1. Normal Pulse Voltammetry (NPV)

This technique uses a series of potential pulses of increasing amplitude. The current measurement is made near the end of each pulse, which allows time for the charging current to decay. It is usually carried out in an unstirred solution at either DME (called normal pulse polarography) or solid electrodes.

The potential is pulsed from an initial potential E_i . The duration of the pulse, t , is usually 1 to 100 msec and the interval between pulses typically 0.1 to 5 sec. The resulting voltammogram displays the sampled current on the vertical axis and the potential to which the pulse is stepped on the horizontal axis.

2.8.3.2. Differential Pulse Voltammetry (DPV)

This technique is comparable to normal pulse voltammetry in that the potential is also scanned with a series of pulses. However, it differs from NPV because each potential pulse is fixed, of small amplitude (10 to 100 mV), and is superimposed on a slowly changing base potential. Current is measured at two points for each pulse, the first point (1) just before the application of the pulse and the second (2) at the end of the pulse. These sampling points are selected to allow for the decay of the nonfaradaic (charging) current. The difference between current measurements at these points for each pulse is determined and plotted against the base potential.

2.7.3.3. Square-Wave Voltammetry (SWV)

The excitation signal in SWV consists of a symmetrical square-wave pulse of amplitude E_{sw} superimposed on a staircase waveform of step height ΔE , where the forward pulse of the square wave coincides with the staircase step. The net current, i_{net} , is obtained by taking the difference between the forward and reverse currents ($i_{for} - i_{rev}$) and is centered on the redox potential. The peak height is directly proportional to the concentration of the electroactive species and direct detection limits as low as $10^{-8}M$ is possible.

Applications of square-wave voltammetry include the study of electrode kinetics with regard to preceding, following, or catalytic homogeneous chemical reactions, determination of some species at trace levels, and its use with electrochemical detection in HPLC [279].

2.9. Electrochemical Impedance Spectroscopy Theory and applications

2.9.1. Theory

The EIS theory summarized by Gamry Instruments [280] is as follows.

Ohm's law defines resistance in terms of the ratio between voltage V and current I . This well known relationship is limited to only one circuit element. But, the real world contains circuit elements that exhibit much more complex behavior. We use impedance instead of resistance factor.

$$Z = \frac{V}{I} \tag{2.11}$$

Like resistance, impedance is a measure of the ability of a circuit to resist the flow of electrical current. Electrochemical impedance is usually measured by applying an AC potential to an electrochemical cell and measuring the current through the cell. If we apply a sinusoidal potential excitation; the response to this potential is an AC current signal. This current signal can be analyzed as a sum of sinusoidal functions (a Fourier series).

Electrochemical Impedance is normally measured using a small excitation signal. This is done so that the cell's response is pseudo-linear. In a linear (or pseudo-linear) system, the current response to a sinusoidal potential will be a sinusoid at the same frequency but shifted in phase (Figure 2.26).

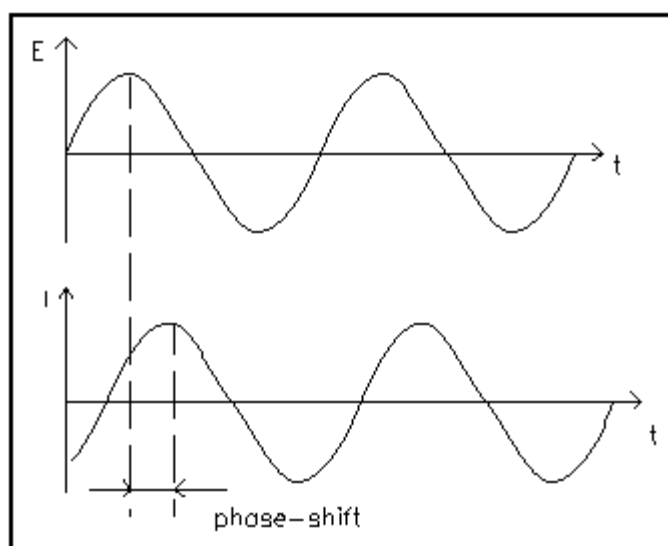


Figure 2.26: Sinusoidal Current Response in a Linear System.

The excitation signal, expressed as a function of time, has the form

$$V(t) = V_0 \cos(\omega t) \quad (2.12)$$

$V(t)$ is the potential at time t , V_0 is the amplitude of the signal, and ω is the radial frequency. The relationship between radial frequency ω (expressed in radians/second) and frequency f (expressed in hertz) is:

$$\omega = 2\pi f \quad (2.13)$$

In a linear system, the response signal, I_t , is shifted in phase (ϕ) and has different amplitude, I_0 :

$$I(t) = I_0 \cos(\omega t - \phi) \quad (2.14)$$

An expression analogous to Ohm's Law allows us to calculate the impedance of the system as:

$$Z = \frac{V(t)}{I(t)} = \frac{V_0 \cos(\omega t)}{I_0 \cos(\omega t - \phi)} = Z_0 \frac{\cos(\omega t)}{\cos(\omega t - \phi)} \quad (2.15)$$

The impedance is therefore expressed in terms of a magnitude, Z_0 , and a phase shift, ϕ .

Using Euler's relationship,

$$\exp(j\phi) = \cos\phi + j\sin\phi \quad (2.16)$$

It is possible to express the impedance to a complex function.

$$Z = \frac{V(t)}{I(t)} = Z_0 \exp(j\phi) = Z_0 (\cos\phi + j\sin\phi) \quad (2.17)$$

From a physical point of view, impedance is just a totally complex resistance (measured in Ohms, Ω) that appears when an AC current flows through a circuit made of resistors, capacitors, inductors or any combination of these. This magnitude shows a complex notation, with a resistive or real part attributable to resistors (in phase with the applied voltage) and a reactive or imaginary part attributable to the contribution of capacitors (out of phase with the applied voltage by $+\pi/2$) and/or inductors (out of phase with the applied voltage by $-\pi/2$):

$$Z = Z' + jZ'' \quad j = \sqrt{-1} \quad (2.18)$$

Where Z' is the resistance (measured in Ω), Z'' the reactance. [281]

Electrochemical impedance spectroscopy (EIS) measurement provides a lot of plot like as Nyquist plot, Bode plot, Warburg plots. Researches can be analyzing their data with respect to these plots.

The Nyquist impedance spectrum consists of a semicircle at high frequencies followed by a linear spike at low frequencies. The diameter of the semicircle has been considered as the charge-transfer resistance (R_{ct}) and the high frequency intercept is due to the solution resistance (R_s).

If the real part is plotted on the Z axis and the imaginary part on the Y axis of a chart, we get a "Nyquist plot" (Figure 2.27). Notice that in this plot the y-axis is negative and that each point on the Nyquist plot is the impedance at one frequency.

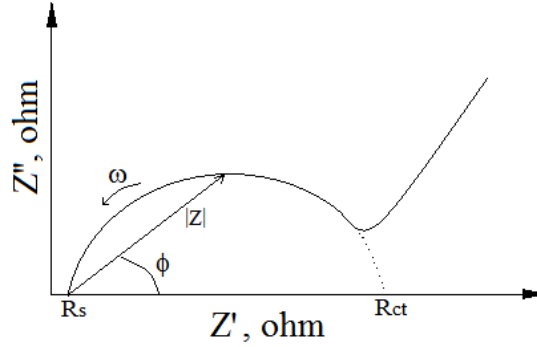


Figure 2.27: Nyquist Plot with Impedance Vector.

Figure 2.27 has been annotated to show that low frequency data are on the right side of the plot and higher frequencies are on the left.

It can be obtained information about time constant (τ) from the frequency corresponding to the maximum of the imaginary component of the semi circle. The time constant is calculated using the expression [282];

$$\tau = \frac{1}{2\pi f} \quad (2.19)$$

Low values of τ are preferred for electrochemical capacitors in order to ensure charge/discharge characteristics.

2.9.2. Applications

When a conducting polymer is either synthesized or characterized by an electrochemical method, one uses an electrochemical cell with an appropriate electrolyte and necessary electrodes. This system is represented by an electrical circuit and the reactions taking place across the electrode/electrolyte interfaces are often interpreted in terms of an equivalent circuit. Indeed, an electrode/electrolyte interface cannot be fully described without making impedance measurements [283].

Electrochemical impedance spectroscopy (EIS) appears to be an excellent technique for the investigation of bulk and interfacial electrical properties of any kind of solid or liquid material connected to or being part of an appropriate electrochemical transducer [284]. Any intrinsic property of a material or a specific process that could affect the conductivity of an electrochemical system can potentially be studied by EIS.

There are countless techniques available for electrochemical sensor development/optimization (i.e., cyclic voltammetry, scanning electrochemical microscopy, etc.) [285–287]. A majority of these methods probe the membrane/electrolyte interface by using a large perturbation, which is designed to provide mechanistic information by driving the reaction to a condition far from equilibrium. Another approach, however, is to apply a small perturbation to ensure that the kinetic information pertaining to the membrane/electrolyte interface is at near zero current conditions. Subsequently, electrochemical impedance spectroscopy (EIS) is a non-destructive steady-state technique that is capable of probing the relaxation phenomena over a range of frequencies [287]. The power of EIS lies in its ability to provide in situ information on relaxation times over the frequency range 10^6 to 10^{-4} Hz. It is a tool that has been used to identify and separate different contributions to the electric and dielectric responses of a material.

Another advantage of the latter technique is that the measurement of the complex impedance behavior in the form of Nyquist plot could be made at a desired DC potential bias. Thus, the electrical behavior of the material could be studied as a function of the applied DC bias and hence several useful items of information could be extracted from a single experiment. [288]

3. COPOLYMERS OF N-VINYL CARBAZOLE WITH ACRYLIC ACID, ITACONIC ACID AND N-ISOPROPYLACRYLAMIDE: SYNTHESIS, DETERMINATION OF MONOMER REACTIVITY RATIOS AND ELECTROCHEMICAL PROPERTIES

3.1 Experimental

N-vinylcarbazole (NVCz; from Aldrich), acrylic acid (AA; from Fluka), itaconic acid (IA; from Fluka) and N-isopropylacrylamide (NIPAAm; from Aldrich) were used as monomers. THF, 1, 4-Dioxane (copolymerization solvent), potassium persulfate (KPS; initiator), tetrabutylammonium tetrafluoroborate (TBABF₄; supporting electrolyte), dichloromethane (CH₂Cl₂) and Dopamine (DA) were used as received (from Merck). The initiator, α , α' -azobisisobutyronitrile (AIBN; from Merck) was recrystallized from methanol.

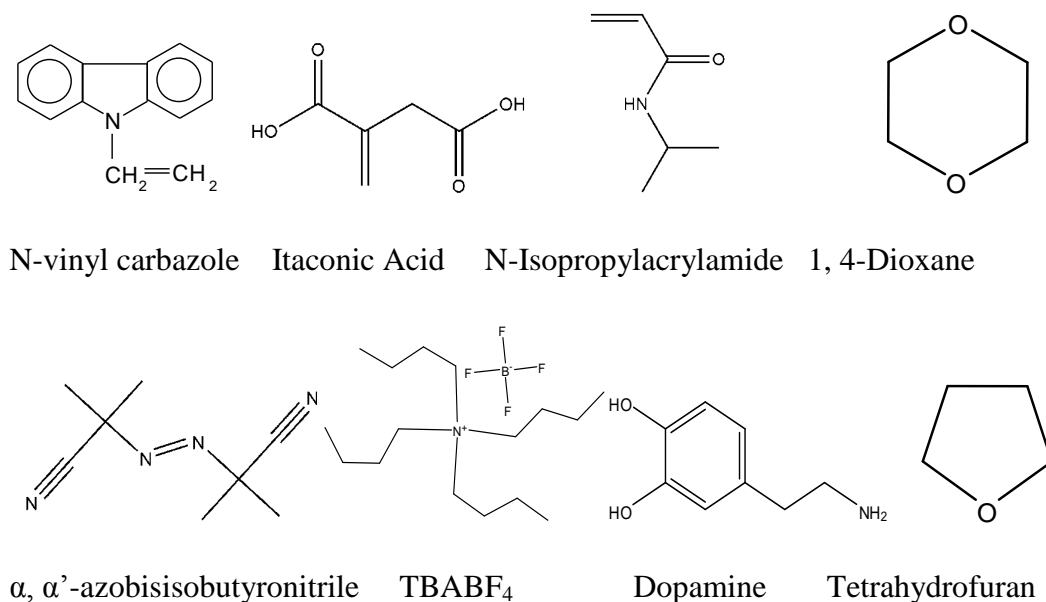


Figure 3.1: Schematic illustration of used chemicals.

3.2 Copolymerization

Copolymers of NVCz with IA, AA (weakly-acidic comonomers) and NIPAAm (hydrophobic/hydrophilic comonomer) having different composition were synthesized by free radical solution polymerization in 1,4-Dioxane with AIBN (1.0×10^{-3} mol / L) at 50°C under nitrogen atmosphere. The total monomer concentration of 1.0 mol / L was kept constant while the feed ratio of the monomers was varied. Further, homopolymers of NVCz, NIPAAm, AA and IA were synthesized using AIBN (1.0×10^{-3} mol / L) in 1, 4-Dioxane and potassium persulphate (KPS) in water as initiators under identical experimental conditions. The polymerization mixtures were introduced into large glass tubes with ~30 mm diameter equipped with a rubber cap and a syringe. Solutions were degassed by bubbling nitrogen for about 20 min. Hexane was used to precipitate the polymers. The homopolymers and copolymers were filtered and washed with hexane. The products were dried under vacuum at room temperature to constant weight. The solid samples were reprecipitated by hexane from the solution in THF and finally dried. Tables 3.1-3.3 summarize the feed compositions of NVCz and comonomers (NIPAAm, IA and AA), experimental conditions, gravimetric (yield, %) and viscometric results ($[\eta]$, mL / g).

Table 3.1: Polymerization Conditions of PIA and NVCz / IA Copolymers.

Sample No	Feed Composition (mole %)	Solvent	Time (h)	Yield (%)	$[\eta]$ (mL/g)	MW (g/mol)
1	IA(100) /NVCz (0)	Water ^a	48	50.4	6.1	3400
2	IA (100) / NVCz (0)	Dioxane	96	42.9	1,1	770
3	IA (80) / NVCz (20)	Dioxane	96	71.3	9.5	-
4	IA (60) / NVCz (40)	Dioxane	30	70.0	29.5	-
5	IA (40) / NVCz (60)	Dioxane	24	83.9	55.7	-
6	IA (20) / NVCz (80)	Dioxane	12	53.7	69.9	-
7	IA (10) / NVCz (90)	Dioxane	6	52.1	-	-
8	IA (5) / NVCz (95)	Dioxane	6	49.7	-	-
9	IA (0) / NVCz (100)	Dioxane	96	86.7	29.2	122000

^a KPS was used as initiator

PNVCz, NVCz/IA and NVCz/NIPAAm copolymers having electroactive, ionic and hydrophobic properties were deposited by electrooxidation in CH_2Cl_2 containing 0.1 M TBABF₄ on Pt wire electrode. Cyclic voltammograms of PMEs were obtained at a scan rate 100 mV / s between 0 - 1800 mV, by using a Model 2263 Parstat potentiostat. The working electrode (area = 3.14×10^{-2} cm²) and counter electrode

were Pt wires. In all cases, Ag wire was used as a pseudo reference electrode. Electrochemical detection of DA was examined in phosphate buffer at pH 7.0.

Table 3.2: Polymerization Conditions of PAA and NVCz/AA Copolymers.

SampleNo	Feed Composition (mole %)	Time (h)	Yield (%)	[η] (mL/g)	MW (g/mol)
10	AA (100) / NVCz (0)	96	75.4	7.07	54500
11	AA (80) / NVCz (20)	96	80.0	22.6	-
12	AA (60) / NVCz (40)	21	72.0	26.0	-
13	AA (40) / NVCz (60)	31	63.9	52.7	-
14	AA (20) / NVCz (80)	12	53.7	61.8	-
15	AA (10) / NVCz (90)	24	51.3	-	-
16	AA (5) / NVCz (95)	24	49.7	-	-
9	AA (0) / NVCz (100)	96	86.7	29.2	122000

Table 3.3: Polymerization Conditions of PNIPAAm and NVCz/NIPAAm Copolymers.

SampleNo	Feed Composition (mol %)	Time (h)	Yield (%)
17	NIPAAm(100)/NVCz(0)	96	75.0
18	NIPAAm(95)/NVCz(5)	72	80.1
19	NIPAAm(90)/NVCz(10)	72	68.3
20	NIPAAm(80)/NVCz(20)	72	67.9
21	NIPAAm(60)/NVCz(40)	72	75.0
22	NIPAAm(45)/NVCz(55)	72	77.4
23	NIPAAm(30)/NVCz(70)	96	78.0
24	NIPAAm(20)/NVCz(80)	96	64.0
25	NIPAAm(10)/NVCz(90)	96	80.3
9	NIPAAm(0)/NVCz(100)	96	86.7

3.3 Copolymer characterization

FTIR spectra of the samples were recorded on Mattson 3000 and Perkin Elmer Spectrum One (FTIR-reflectance, Universal ATR with diamond and ZnSe) spectrophotometers using KBr pellets and the samples in powder form (Figures 3.2 and 3.3), respectively. Viscosity measurements were performed by an Ubbelohde viscometer. The intrinsic viscosities of the homopolymers and copolymers were determined by using single-point method ($c = 0.5$ % w/v). They were converted to molecular weight by using the following relations for PIA, PAA and PNVCz [22-24].

$$[\eta] = 15.47 \times 10^{-3} M^{0.90} \quad (25^\circ\text{C}; 1\text{M NaCl for PIA and PAA}) \quad (1)$$

$$[\eta] = 14.40 \times 10^{-3} M^{0.65} \quad (25^\circ\text{C}, \text{THF for PNVCz}) \quad (2)$$

The compositions of copolymers were determined using a Shimadzu UV-visible 160A double beam spectrophotometer, equipped with a temperature controlled cell. UV spectra of the copolymers and the blends of PAA / PNVCz, PIA / PNVCz and PNIPAAm / PNVCz, which were used to draw the calibration curves, were measured in the range of 200-400 nm. The glass transition temperatures (T_g s) of the samples

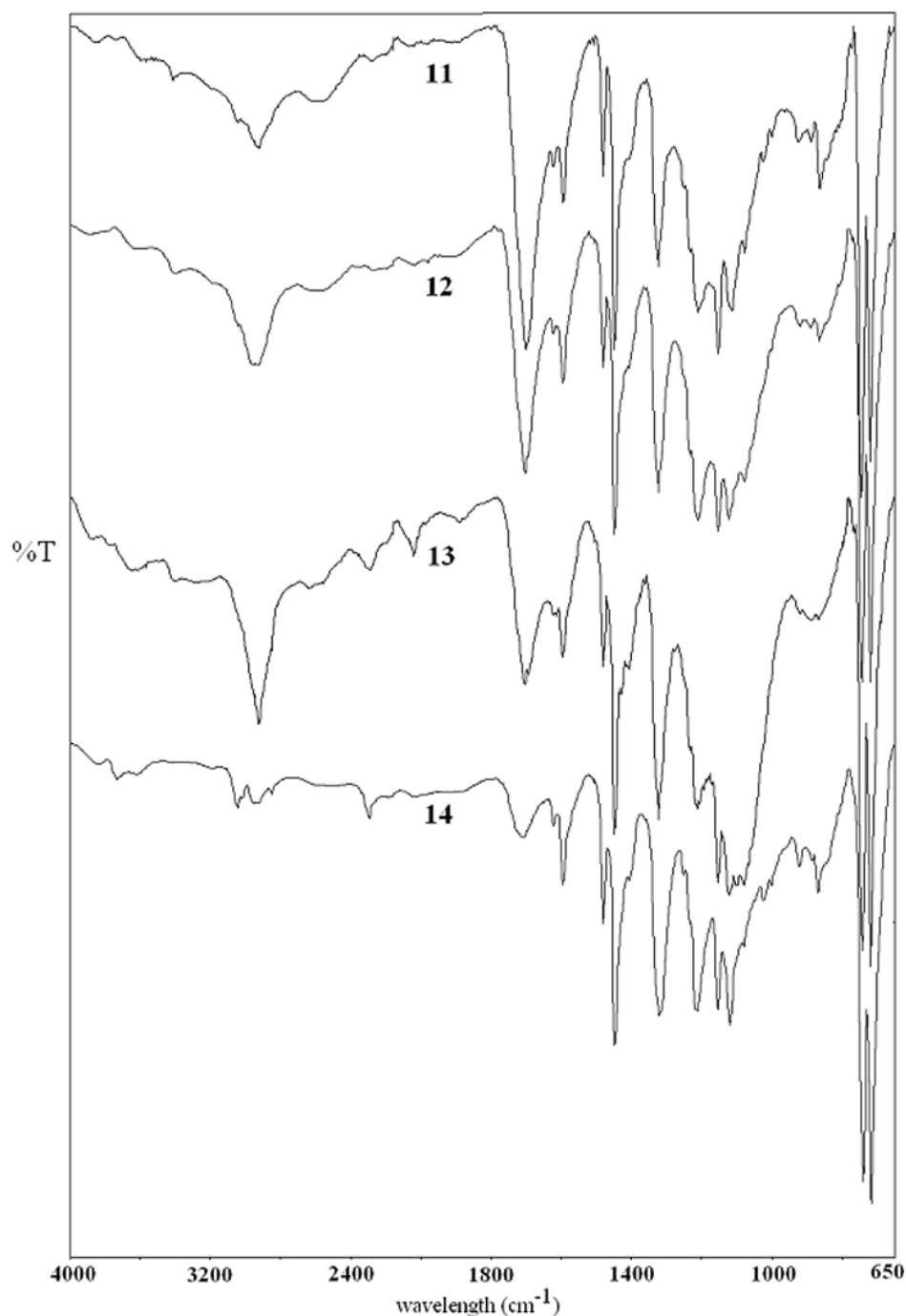


Figure 3.2: FTIR spectra of NVCz /AA copolymers, which are given in Table 3.2.

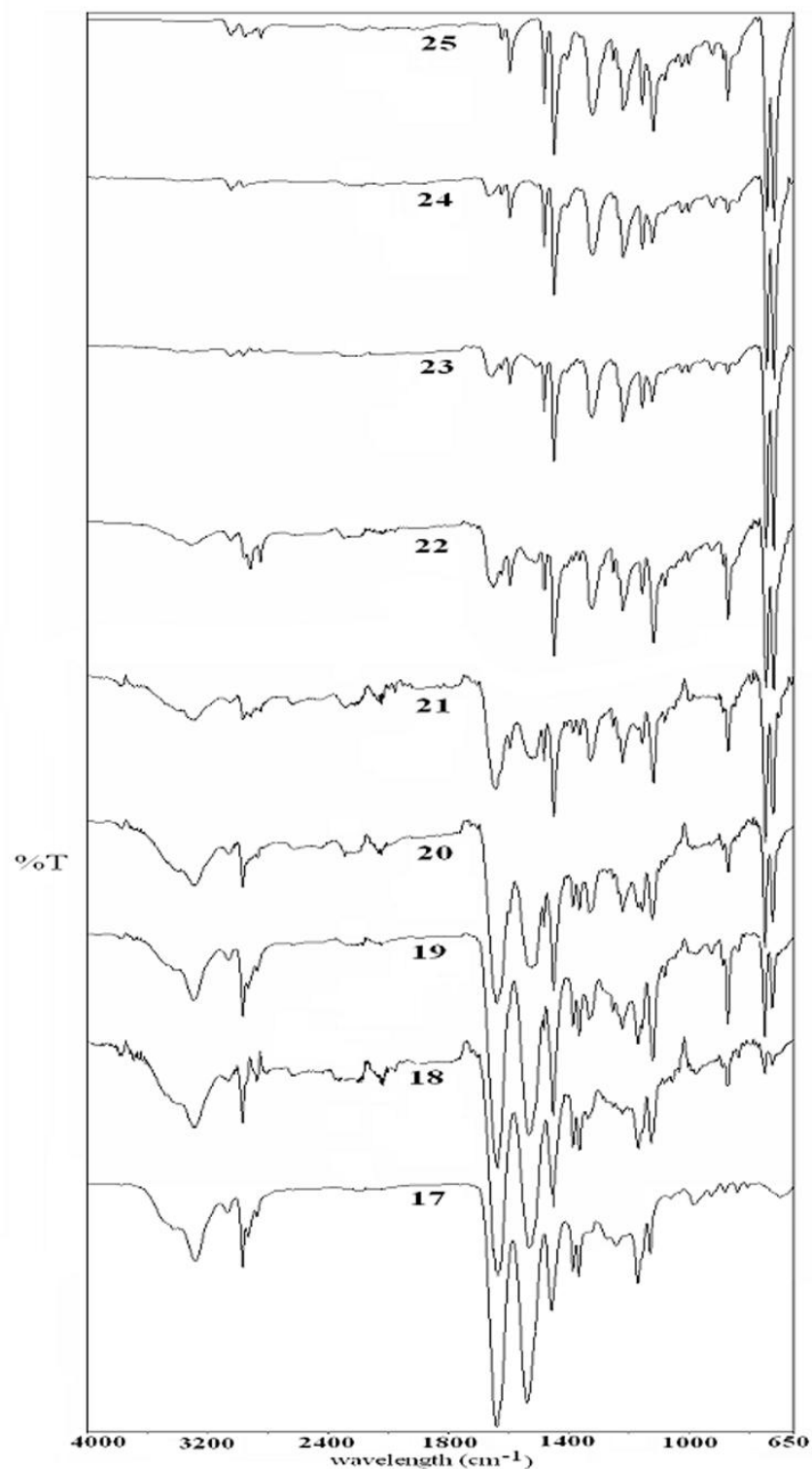


Figure 3.3: FTIR spectra of NVCz / NIPAAm copolymers, which are given in Table 3.3.

were determined using a Perkin Elmer differential scanning calorimeter (Model DSC 6). All thermograms were taken between 25°C and 250°C in nitrogen atmosphere at a heating rate of 10°C / min.

3.4 Results

The chemical structures of PNVCz, PAA, PIA and PNIPAAm are shown in Scheme 1. The free radical polymerization of NVCz gave a white product, being p-type semi-conductive with photoconductive and insulating character. In addition, NVCz can be polymerized by chemical and electrochemical oxidation of the ring to produce a conductive polymer [5, 6, 25]. Copolymers of NVCz with IA, AA and NIPAAm were prepared at high yields and were characterized by measurements of the intrinsic viscosity and the glass transition temperature. In the case of IA, chain transfer to the monomer because of the presence of allylic hydrogens in the molecular structure results in the production of PIA chains with low molecular weight while its copolymers with the vinyl monomers producing more stable radicals have higher molecular weights. The viscosity results of NVCz/IA and NVCz/AA copolymers show that the molecular weights of copolymers increased on increasing the mole fraction of NVCz in the feed (Tables 3.1 and 3.2).

FTIR and UV spectroscopic techniques were employed to determine the copolymer compositions and to calculate the reactivity ratios of monomer pairs. C=O stretching (1730 cm^{-1}) and -OH dimerization ($3500\text{-}2500\text{cm}^{-1}$) bands in the FTIR spectra of PAA and its copolymers indicate the presence of AA units in the chains while the bands at $1600\text{ -}1450\text{ cm}^{-1}$ for aromatic stretching and aromatic -CH in plane bending, 750 cm^{-1} for aromatic -CH out of plane bending are characteristic for PNVCz (Figure 3.1). Further, the bands due to -C=O stretching and NH- bending for secondary amides at 1660 and 1540 cm^{-1} and, a double band for isopropyl group at 1385 and 1370 cm^{-1} are characteristic absorptions of PNIPAAm (Figure 3.2).

Table 3.4: FTIR and DSC Results of the Samples in Tables 1 and 2.

Sample no.	C=O/C=C	Tg ^a	Tg	Sample no.	C=O/C=C	Tg
2	-	-	141	10	-	
4	4.339	158.4	158	12	1.893	
5	2.268	166.4	164	13	1.618	140
6	1.212	173.9	170	14	1.239	144
7	0.469	-	-	15	0.555	
9	-	-	181	9	-	181

^a calculated from the Fox equation

The comparison of the ratios of the absorption intensities of $\text{C}=\text{O}$ stretching at 1730 cm^{-1} to those of $\text{C}=\text{C}$ aromatic stretching at 1600 cm^{-1} that are the characteristic bands of the polyelectrolytes (PAA and PIA) and PNVCz, respectively, would give a qualitative information about the reactivities of IA and AA units in the copolymeric structures. The ratios of the absorption intensities of the $\text{C}=\text{O}$ and $\text{C}=\text{C}$ peaks and the variation of the T_g s of copolymers with the mole fraction of IA and AA units in the copolymers are given in Table 3.4. All the copolymers showed a single T_g , indicating the absence of formation of a mixture of homopolymers or the formation of a block copolymer. According to the results obtained from the $\text{C}=\text{O}/\text{C}=\text{C}$ ratios, AA and IA have nearly same reactivities for the same feed compositions and their T_g s decrease with increasing AA and IA contents. The T_g values of copolymers can be described by using Fox equation ($1/T_g = (w_1/T_{g1}) + (w_2/T_{g2})$), where w_1 and w_2 are the weight fractions of monomer (NVCz) and comonomers (IA, AA and NIPAAm) in the copolymers, respectively. The T_g of PIA (T_{g2}) was measured as 141°C and that of PNVCz (T_{g1}) was 181°C . The T_g values calculated by Fox equation were slightly higher than those of the ones obtained from DSC thermograms for NVCz/IA copolymers (Table 3.4). Figure 3.4 shows the relationship between $1/T_g$ and w_{IA} . It can be seen that good linear relation can be obtained. This implies that the structure of NVCz/IA copolymers is random in nature.

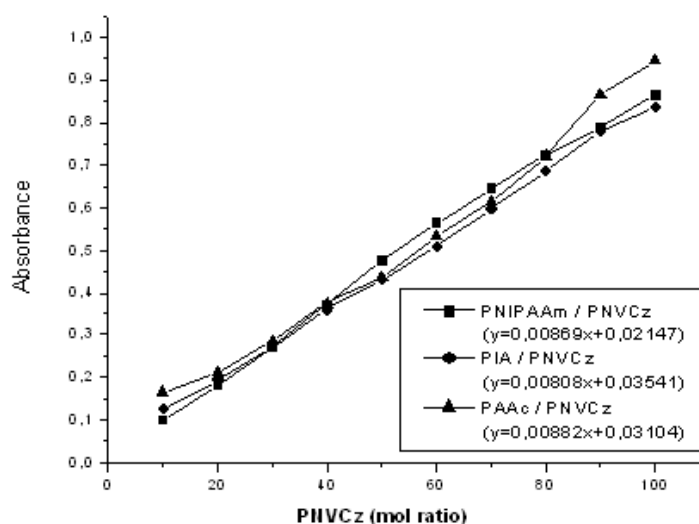


Figure 3.4: Relationship between $1/T_g$ and w_{IA} .

In addition, the quantitative composition of copolymers for a wide range of monomer feed can be determined by FTIR spectroscopy through recorded analytical absorption bands for comonomers [26-28]. For compositional analysis of NVCz / NIPAAm

copolymers, characteristic absorption bands of 747 cm^{-1} (for NVCz units) and 1635 cm^{-1} (for NIPAAm units) were chosen as analytical bands. The least changing absorption band of 1447 cm^{-1} were used as a standard band ($A = \log I_0/I$, $\Delta A^C = A^C/A^{1447}$) to calculate the copolymer composition. The ratios of mole fractions of comonomer units (F_1 and F_2) in NVCz (1) / NIPAAm (2) copolymers were calculated using the following relation:

$$F_1 / F_2 = [\Delta A^{747} / M_1] / [\Delta A^{1635} / M_2] \quad (3)$$

The mole fractions (in mole %) of NIPAAm (2) and NVCz (1) in the copolymers of various compositions, calculated by using FTIR analysis data are given in Table 3.5.

The copolymer compositions are also determined quantitatively by means of the UV spectroscopy [29-31]. UV spectra of homopolymer blends, i.e., the physical mixtures of PNVCz / PNIPAAm, PNVCz / PIA and PNVCz / PAA, prepared in THF were used to draw the calibration curves. It is known that four absorption bands which are observed at 345, 295, 262 and 237 nm are attributed to $\pi \rightarrow \pi^*$ electronic transitions of PNVCz homopolymer [32]. Calibration curves for NVCz/NIPAAm, NVCz/AA and NVCz/IA copolymers were obtained by chosen only one of these characteristic transitions of PNVCz. The maximum absorbances at 295 nm were plotted against mole percent of PNVCz in the physical mixtures (Figure 3.5). All the graphs showed linear dependence to composition and regression coefficients were in the range of 0.991-0.997. From these calibration curves, the composition of the copolymers was determined by using the maximum absorbance values at 295 nm of the copolymer solutions in THF (Figure 3.6).

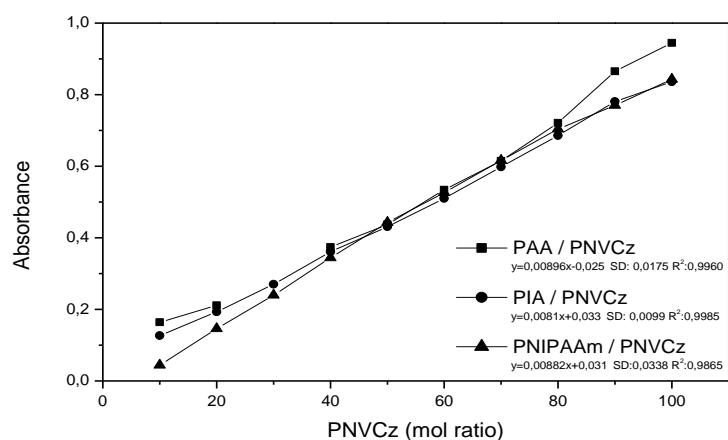


Figure 3.5: Calibration curves for NVCz / AA, NVCz / IA and NVCz / NIPAAm copolymers.

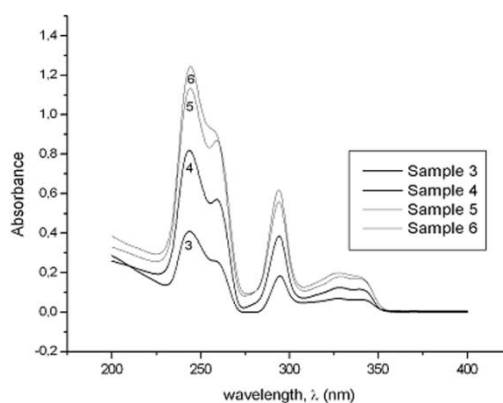


Figure 3.6: UV spectra of NVCz/IA copolymers ($\lambda_{\max} = 295$ nm.), which are given in Table 3.1.

The results, which are summarized in Tables 3.5 and 3.6, indicate that IA and AA have almost the same reactivities and their reactivities are smaller than NVCz.

Table 3.5: Copolymerization Composition Data for Reactivity Ratio Calculation of Copolymers of NVCz (1) and NIPAAm (2).

Sample no.	^a f ₁	f ₂	ΔA^{747} (by FTIR)	ΔA^{1635} (by FTIR)	^b F ₁	F ₂	^b F ₁ (by UV-vis)	F ₂
20	20	80	1.5143	0.8571	29.25	70.75	29.14	70.86
21	40	60	1.0781	1.4468	50.85	49.15	45.51	54.49
22	55	45	-	-	-	-	56.72	43.28
23	70	30	1.3733	0.4533	71.66	28.34	70.48	29.52
24	80	20	1.6171	0.1943	82.98	17.02	82.35	17.65

^a f₁ and f₂ are the mol fractions of NVCz and NIPAAm in the feed. ^b F₁ and F₂ are the mol fractions of NVCz and NIPAAm in the copolymer

Table 3.6: UV Spectroscopy Data for Determining of Composition of IA(2)/NVCz(1) and AA(2) / NVCz(1) Copolymers Synthesized from Various Initial Monomer Mixtures.

Sample no	f _{IA} (mol %)	Abs. $\lambda_{\max}=295$ nm	F _{IA}	Sample no	f _{AA} (mol %)	Abs. $\lambda_{\max}=295$ nm	F _{AA}
6	20	0.759	10.45	14	20	0.797	13.16
5	40	0.661	22.58	13	40	0.607	34.70
4	60	0.483	44.61	12	60	0.512	45.47
3	80	0.277	70,10	11	80	0.225	78.01

The extended Kelen-Tüdös method considers the drifts of copolymer composition with conversion [33]. Therefore, it is suitable for our high conversion data. The extended Kelen-Tüdös copolymer composition equation is

$$\eta = [(r_1 + r_2) / \alpha] \zeta - r_2 / \alpha \quad (5)$$

where $\eta = G / (\alpha + H)$; $\zeta = H / (\alpha + H)$; $X = f_1 / f_2$; $Y = F_1 / F_2$; $G = (Y-1) / z$; $H = Y / z^2$ and $\alpha = (H_{\min} H_{\max})^{1/2}$.

H_{\min} and H_{\max} are the lowest and the highest values of H . The effect of conversion is given by partial molar conversion

$$\xi_2 = w (\mu + X) / (\mu + Y) \quad (6)$$

Where w is the weight conversion of polymerization and μ is the ratio of molecular weight of IA, AA or NIPAAm (2) to that of NVCz (1). The partial molar conversion of NVCz is

$$\xi_1 = \xi_2 Y / X \quad (7)$$

Then,

$$z = \log (1 - \xi_1) / \log (1 - \xi_2) \quad (8)$$

The extended Kelen-Tüdös parameters were calculated from the above equations using experimental data in Tables 3.1-3.3, 3.5 and 3.6. They are summarized in Tables 3.7 and 3.8. η versus ζ plots of NVCz / NIPAAm and NVCz / IA copolymers are shown in Figures 3.7-3.9. In all cases, the plots were linear, indicating that the reactivity of a polymer radical is determined only by the terminal monomer unit.

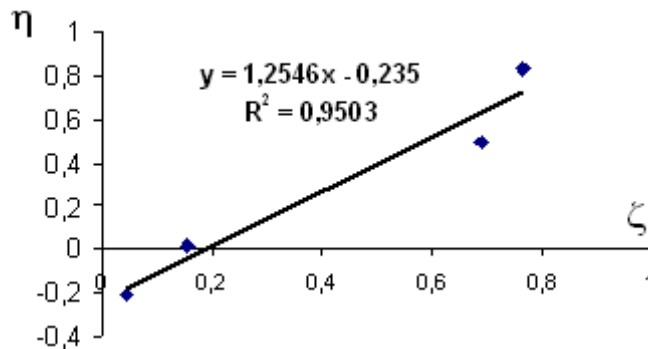


Figure 3.7: EKT Method for determining monomer reactivity ratios in the copolymerization of NVCz (1) and NIPAAm (2) by using FTIR spectroscopy data ($\alpha = 0.3104$).

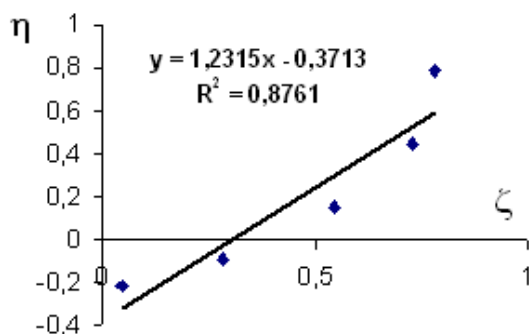


Figure 3.8: EKT Method for determining monomer reactivity ratios in the copolymerization of NVCz (1) and NIPAAm (2) by using UV spectroscopy data ($\alpha = 0.3299$).

Table 3.7: Extended Kelen-Tüdös parameters for NIPAAm (2) and NVCz (1) using FTIR analysis data.

Sample No.	X	Y	ξ_2	ξ_1	z	G	H	ζ	η
20	0.25	0.41	0.57	0.94	3.33	-0.176	0.037	0.044	-0.211
21	0.67	1.03	0.58	0.90	2.65	0.013	0.147	0.156	0.014
23	2.33	2.53	0.73	0.79	1.19	1.278	1.768	0.689	0.498
24	4.00	4.87	0.53	0.64	1.37	2.825	2.591	0.764	0.833

The reactivity ratios of monomer pairs (r_1 and r_2) were evaluated, using the data in Tables 3.1-3.3 and 3.5-3.8 from η vs ζ plots for the NIPAAm (2) - NVCz (1), IA (2) - NVCz (1) and AA (2) - NVCz (1) pairs. The results are summarized in Table 3.9. The fact that $r_1 > r_2$, indicates that NVCz is the more active comonomer in the copolymerization with IA, AA and NIPAAm. For all the copolymers $r_1 < 1$ and $r_2 < 1$ with $r_2 < r_1$, showing that the homopolymerisation of the two monomers is not favored. The probability for the incorporation of IA and AA units is greater than for the incorporation of NIPAAm units.

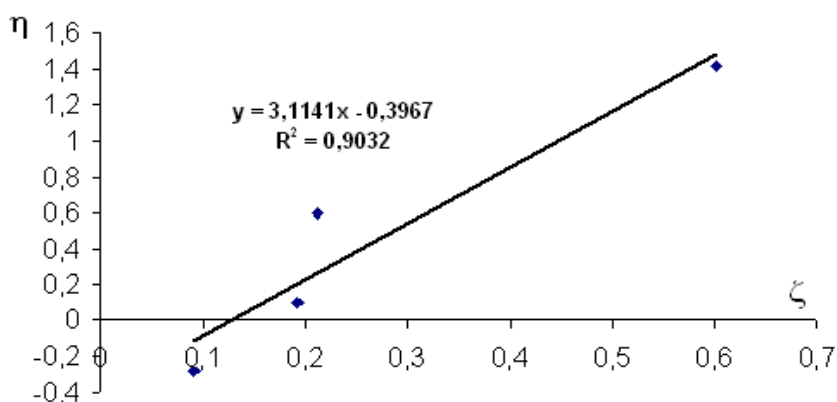


Figure 3.9: EKT Method for determining monomer reactivity ratios in the copolymerization of NVCz (1) and IA (2) by using UV spectroscopy data ($\alpha = 0.3106$).

Table 3.8: Extended Kelen-Tüdös Parameters for IA (2) and NVCz (1) using UV-vis. Spectroscopy Data.

Sample No.	X	Y	ξ_2	ξ_1	z	G	H	ζ	η
3	0.25	0.4265	0.41	0.713	2.307	-0.248	0.080	0.091	-0.283
4	0.67	1.2417	0.37	0.700	2.554	0.095	0.190	0.193	0.096
5	1.50	3.4287	0.36	0.839	3.993	1.608	0.215	0.212	0.600
6	4.00	8.5694	0.25	0.537	2.668	2.837	1.203	0.601	1.417

Table 3.9: Monomer Reactivity Ratios for the Copolymerization of NVCz (monomer 1) with NIPAAm, IA and AA (monomer 2), Using FTIR and UV Spectroscopy Techniques.

Method	NIPAAm / NVCz		IA / NVCz		AA / NVCz	
	(r_2)	(r_1)	(r_2)	(r_1)	(r_2)	(r_1)
UV-vis.	0.12	/ 0.29	0.12	/ 0.84	0.31	/ 0.86
FTIR	0.07	/ 0.32	-	-	-	-

It is known that the product of the monomer reactivity ratios (r_1r_2) for a given binary copolymerization is often used to indicate the sequencing in the resultant copolymer composition, i.e., random, alternating and ideal. Further, it depends only on the difference in the polarity for the two monomers and generally believed that $r_1r_2=1$ represents the upper limit for proper copolymerization. As evidenced from the values of monomer reactivity ratios, which is given in Table 3.9, random copolymerization is realized in AA-NVCz and IA-NVCz systems ($r_1r_2 \approx 0.20$) while the product of r_1r_2 is nearly zero ($r_1r_2 \approx 0.020$), which indicate that the NIPAAm-NVCz system follows an alternative distribution of monomeric units.

The preliminary information about the electrochemical behaviors and biological applications of PNVCz and, NVCz/NIPAAm and NVCz/IA copolymers containing 10 mol % of comonomers in the feed were obtained by using simple, rapid and sensitive electrochemical procedure.

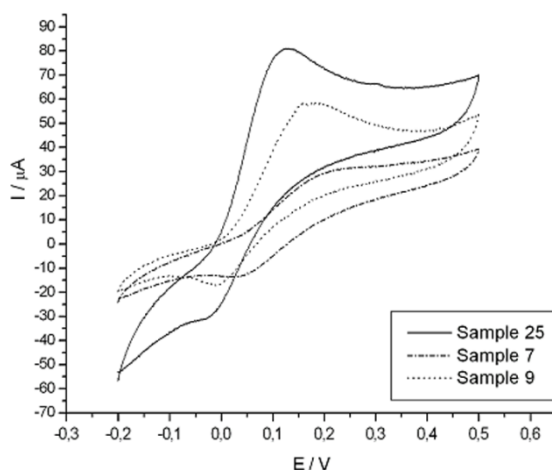


Figure 3.10:The CVs of 9.0×10^{-4} mol/L of DA on the the PNVCz, NVCz/NIPAAm and NVCz/IA modified electrodes in phosphate buffer solution (pH 7.0) at 50 mV / s scan rate.

Figures 3.10 and 3.11 show the cyclic voltammograms (CVs) of DA obtained on the PNVCz, NVCz/NIPAAm and NVCz/IA polymer modified electrodes (PMEs) in phosphate buffer solution (pH = 7.0) at two different scan rates (50 and 500 mV / s).

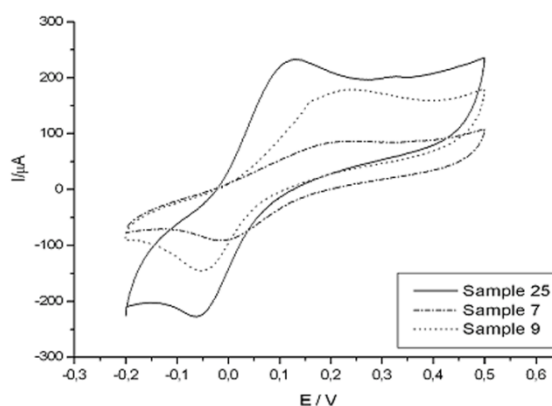


Figure 3.11:The CVs of 9.0×10^{-4} mol/L of DA on the PNVCz, NVCz/NIPAAm and NVCz/IA modified electrodes in phosphate buffer solution (pH 7.0) at 500 mV /s scan rate.

The cyclic voltammetric curves of DA on these modified electrodes showed an anodic peak that corresponds to two-electron oxidation of DA to dopaquinone, which then undergoes deprotonation to produce an imine as suggested in literature, whereas the CVs of PME's did not show any signals in the absence of DA [34-36].

The peak potentials and currents at two different scan rates (50 and 500 mV/s) for the PME prepared by electrochemical deposition of PNVCz and its copolymers on Pt wire electrode were collected in Tables 3.10 and 3.11. From these tables, it is seen that the electrochemical behavior of DA at these electrode surfaces is a quasireversible process in all cases, because the electrode potential differences is about 200 mV and I_{pc} / I_{pa} is close to 1. Dopamine is an electron deficient species and it reacts with nucleophiles in the medium to produce leucochrome by a cyclisation process which can be easily oxidized to dopamine-chrome [37]. This reaction is responsible for the quasireversibility.

Table 3.10: The changes of peak potentials and currents of DA for three different PMEs at 500 mV/s scan rate.

Polymer	E_a (mV)	E_c (mV)	ΔE (mV)	I_{pa} (μA)	I_{pc} (μA)
NVCz / IA (90/10)	188	-2	190	84	-90
NVCz / NIPAAm) (90/10)	125	-60	185	233	-227
PNVCz	218	-49	267	178	-146

Table 3.11: The changes of peak potentials and currents of dopamine for three different PMEs at 50 mV s⁻¹ scan rate.

Polymer	E_a (mV)	E_c (mV)	ΔE (mV)	I_{pa} (μA)	I_{pc} (μA)
NVCz -co- IA (90/10)	201	49	152	29.3	-12.7
NVCz / NIPAAm)(90/10)	127	-25	152	80.9	-30.8
PNVCz	165	-8	173	58.7	-16.9

ΔE values decreased from 267 mV on PNVCz electrode to 190 mV and 185 mV on the NVCz/IA and NVCz/NIPAAm coated electrodes, respectively. The oxidations observed at lower potentials for NVCz/NIPAAm copolymer, which indicate the ease of electron transfer reaction, demonstrate its superiority to PNVCz and NVCz/IA copolymer electrodes. . Further, the highest currents were observed in the case of the NVCz/NIPAAm coated electrode. This means that the presence of hydrophobic isopropyl group in the structures of electrode coating materials provides better electrochemical reactivity than that of the hydrophilic carboxyl groups of IA.

The electrochemical oxidation of DA was also examined as a function of scan rates (Figure 3.11). Current intensities and reversibility increased as the scan rate increased, owing to a decreased extent of internal cyclisation, as expected. The

oxidation peak currents varied linearly with the square root of scan rate in the range of 50-500 mV/s ($r > 0.9967$), indicating semi-infinite linear diffusion of the reactant to the interface.

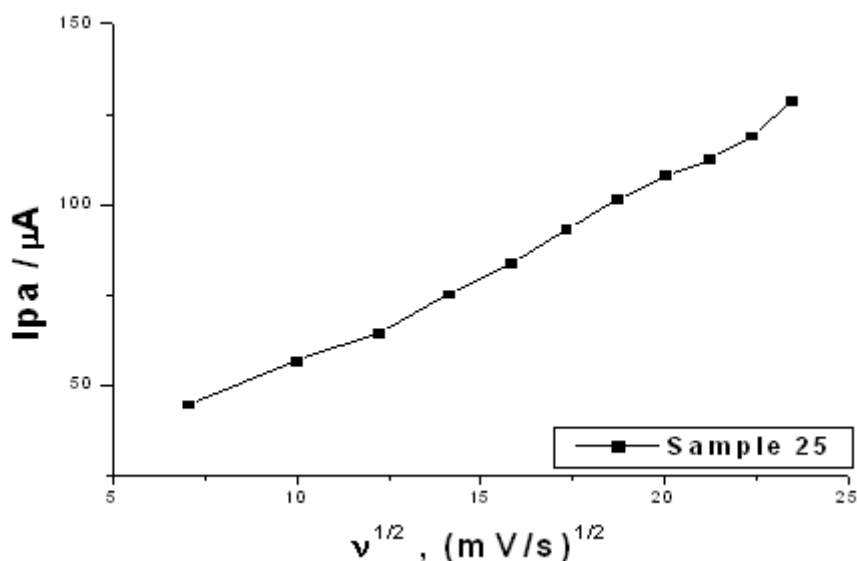


Figure 3.12: Scan rate dependence of DA response on NVCz/NIPAAm coated electrode.

3.5 Discussion

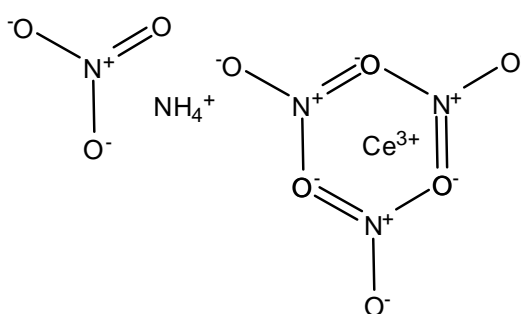
PNVCz, PIA, PAA and PNIPAAm homopolymers and, NVCz/IA, NVCz/AA and NVCz/NIPAAm copolymers having different compositions were synthesized by free radical polymerization in solution, using AIBN as initiator. These homopolymers and copolymers were characterized by calorimetric (DSC) and spectroscopic (FTIR and UV) methods. Analysis of the data by the extended Kelen-Tüdös (for high conversion) yields $r_1 = 0.29$ and $r_2 = 0.12$, $r_1 = 0.84$ and $r_2 = 0.12$, $r_1 = 0.86$ and $r_2 = 0.31$ by UV (for NVCz/NIPAAm, NVCz/IA and NVCz/AA copolymers, respectively), $r_1 = 0.32$ and $r_2 = 0.07$ by FTIR (for NVCz/NIPAAm copolymers). From these results, it was observed that in the case of NVCz-IA and NVCz-AA systems there is a tendency to obtain random copolymers while NIPAAm-NVCz system follows an alternative distribution of monomeric units. In addition, the relationship between T_g^{-1} (obtained from DSC thermograms and Fox equation) and w_{IA} supported that NVCz/IA copolymer chains have a random distribution of monomeric units.

Electrochemical behavior of NVCz/IA and NVCz/NIPAAm coated electrodes was studied by CV measurements and found dependent on the type of comonomer. The present work provides useful data for biological application of new DA-sensitive materials based on copolymers of NVCz with IA and NIPAAm.

4. MORPHOLOGICAL CHARACTERIZATION AND ELECTROCHEMICAL / ELECTRICAL PROPERTIES OF POLY(N-VINYL CARBAZOLE) / MONTMORILLONITE COMPOSITES

4.1 Experimental

The monomer, N-vinylcarbazole (NVCz; Aldrich) was used without further purification. Cerium ammonium nitrate ((NH₄)₂Ce (NO₃)₆, CAN; BDH Chemicals Ltd.) was chosen as initiator. Na⁺-montmorillonite (Na⁺MMT) was synthesized from natural bentonite with stepwise purification by Süd-Chemie (Trademark = Nanofil 757; the cation exchange capacity = 80 meq. /100 g and particle size <10 μm). Octadecyl amine (ODA) and trimethyl stearyl ammonium (TMSA) modified MMTs (Product Name = Nanoclay and particle size ≤ 20 μm) were purchased from Aldrich Chemical and used without further purification



Cerium ammonium nitrate

Figure 4.1: Schematic illustration of used chemicals.

4.2 Preparation of PNVCz and PNVCz/MMT composites

PNVCz was synthesized by free-radical polymerization method. The heterogeneous solution process was as follows: NVCz monomer with a known weight was dissolved in acetonitrile (ACN). Then, ceric ammonium nitrate (Ce (NH₄)₂(NO₃)₆, CAN) as an oxidizing agent was added into the monomer solution to initiate the polymerization. The mole ratio of monomer to oxidizing agent was kept at 200:1. 1.0 mol /L concentration of NVCz was used. The synthesis was carried out at 25°C under atmospheric conditions. After completed reaction period, the precipitate was santrifugated and washed with ACN at least 3 times to remove any unreacted NVCz,

and then nonconductive-white powder was dried to constant weight under vacuum at room temperature. Polymerization yield was 98.6 %. Intrinsic viscosity measurements were carried out using an Ubbelohde capillary viscometer in solvent THF with concentration of 0.5 g /dL at 25°C. The limiting viscosity number of PNVCz in THF was converted to molecular weight that has been calculated as nearly 9000 g/mol by using the following relation [28]. This viscosity average molecular weight indicated that the oxidative polymerization gave PNVCz of low molecular weight.

$$[\eta] = 14.40 \times 10^{-3} M^{0.65} \quad (1)$$

Table 4.1: Voltammetric and gravimetric results of PNVCz/MMT composites.

Sample	Electrode	^a Clay	Mixing method & time	^b Yield	E _a (mV)	E _c (mV)	I _a (μA/cm ²)	I _c (μA/cm ²)
1	GC	Na ⁺ -MMT	Magnetic stirring/17 hrs	79.4	889	747	240	278
1	Pt	Na ⁺ -MMT	Magnetic stirring/17 hrs	79.4	1005	879	567	857
2	GC	ODA-MMT	Magnetic stirring/17 hrs	72.6	951	876	150	233
2	Pt	ODA-MMT	Magnetic stirring/17 hrs	72.6	756	714	358	449
3	GC	TMSA-MMT	Magnetic stirring/17 hrs	68.5	825	798	310	269
3	Pt	TMSA-MMT	Magnetic stirring/17 hrs	68.5	777	739	295	375
4	GC	Na ⁺ -MMT	Sonication /5min	66.0	823	720	377	572
4	Pt	Na ⁺ -MMT	Sonication /5min	66.6	977	748	1558	1855
5	GC	ODA-MMT,	Sonication/5 min	81.7	811	716	375	575
5	Pt	ODA-MMT	Sonication/5 min	81.7	812	716	213	307
6	GC	TMSA-MMT	Sonication/5 min	97.6	861	717	761	1102
6	Pt	TMSA-MMT	Sonication/5 min	97.6	-	-	-	-
10	GC	ODA-MMT	Mechanical stirring/1 hr	66.8	901	788	572	716
10	Pt	ODA-MMT	Mechanical stirring/1 hr	66.8	836	793	674	883
11	GC	TMSA-MMT	Mechanical stirring/1 hr	81.6	796	700	933	1216
11	Pt	TMSA-MMT	Mechanical stirring/1 hr	81.6	836	747	1688	1647

[NVCz] = 1.0 M ; T = 25 ± 2°C ; [NVCz] : [CAN] = 200 :1

^a15.0 wt % (based on NVCz concentration in the feed)

^b[(PNVCz / MMT : NVCz + MMT)x100]

PNVCz / MMT composites were also prepared by heterogeneous solution polymerization. First, Na⁺MMT, ODA-MMT and TMSA-MMT with known weight were dispersed into ACN using magnetic stirrer, homogenizator (GN 125, 230V/50/60 Hz, 8000-30000 rpm) and high-power sonic tip (Sonopuls HD 2200, 200W/20kHz). Then, monomer was added into these dispersions before the polymerization in the presence of CAN. After completed reaction period, the precipitate was santrifugated and washed with ACN at least 3 times to remove any unreacted NVCz and dried under vacuum at room temperature. The detailed processing conditions and conversion percentages for the products obtained by chemical polymerization are provided in Tables 4.1-4.3.

Table 4.2: Voltammetric and gravimetric results of PNVCz/ODA-MMT composites.

Sample	Electrode	Clay & wt %	Mixing method & time	Yield (%)	E _a (mV)	E _c (mV)	I _a (μA/cm ²)	I _c (μA/cm ²)
5	GC	ODA-MMT, 15.0	Sonication/5 min	81.7	811	716	375	575
12	GC	ODA-MMT, 5.0	Sonication/5 min	73.3	835	786	721	721
13	GC	ODA-MMT, 1.0	Sonication/5 min	72.9	902	784	1077	1225
5	Pt	ODA-MMT, 15.0	Sonication/5 min	81.7	812	716	213	307
12	Pt	ODA-MMT, 5.0	Sonication/5 min	73.3	796	736	499	718
13	Pt	ODA-MMT, 1.0	Sonication/5 min	72.9	892	857	1526	1444
10	GC	ODA-MMT, 15.0	Mechanical stirring/1 hr	66.8	901	788	572	716
16	GC	ODA-MMT, 5.0	Mechanical stirring/1 hr	62.6	846	792	717	855
17	GC	ODA-MMT, 1.0	Mechanical stirring/1 hr	55.9	844	766	238	325
10	Pt	ODA-MMT, 15.0	Mechanical stirring/1 hr	66.8	836	793	674	883
16	Pt	ODA-MMT, 5.0	Mechanical stirring/1 hr	62.6	828	792	1060	949
17	Pt	ODA-MMT, 1.0	Mechanical stirring/1 hr	55.9	868	792	324	358

Table 4.3: Voltammetric and gravimetric results of PNVCz/TMSA-MMT composites.

Sample	Electrode	Clay & wt %	Mixing method & time	^b Yield	E _a (mV)	E _c (mV)	I _a (μA/cm ²)	I _c (μA/cm ²)
6	GC	TMSA-MMT, 15.0	Sonication/5 min	97.6	861	717	761	1102
18	GC	TMSA-MMT, 5.0	Sonication/5 min	92.1	899	796	209	256
19	GC	TMSA-MMT, 1.0	Sonication/5 min	84.2	838	785	117.6	162
6	Pt	TMSA-MMT, 15.0	Sonication/5 min	97.6	-	-	-	-
18	Pt	TMSA-MMT, 5.0	Sonication/5 min	92.1	882	799	195	263
19	Pt	TMSA-MMT, 1.0	Sonication/5 min	84.2	828	763	162	246
11	GC	TMSA-MMT, 15.0	Mechanica 1 stirring/1 hr	81.6	796	700	933	1216
20	GC	TMSA-MMT, 5.0	Mechanica 1 stirring/1 hr	79.3	787	759	324	308
21	GC	TMSA-MMT, 1.0	Mechanica 1 stirring/1 hr	72.9	786	775	133	183
11	Pt	TMSA-MMT, 15.0	Mechanica 1 stirring/1 hr	81.6	836	747	1688	1647
20	Pt	TMSA-MMT, 5.0	Mechanica 1 stirring/1 hr	79.3	788	744	385	489
21	Pt	TMSA-MMT, 1.0	Mechanica 1 stirring/1 hr	72.9	-	-	-	-

4.3 Analysis and characterization techniques

PNVCz/MMT composites were analyzed and characterized by using Fourier Transform Infrared Spectroscopy (FTIR), X-Ray diffractometer (XRD), Differential Scanning Calorimetry (DSC), Polarized Optical Microscope (POM), Scanning Electron Microscopy (SEM), Cyclic Voltammetry (CV) and Electrochemical Impedance Spectroscopy (EIS). FTIR, XRD, DSC and SEM measurements were carried out using dried and milled samples of polymer and composites in order to describe their structural properties. For POM studies, PNVCz/MMT composites were dissolved in dichloromethane to give the 4.0 g/L solutions. After casting onto a microscope slide glass, they were dried under vacuum to obtain coatings for polarizing microscope observations.

FTIR spectra of the samples were recorded on Perkin Elmer Spectrum One (FTIR-reflectance, Universal ATR with diamond and ZnSe) spectrophotometer using the samples in powder form. XRD patterns were obtained by Bruker X-ray diffractometer (XRD), a conventional copper target X-ray tube set to 40 kV and 40 mA. The X-ray source was CuK α radiation ($\lambda = 0.154$ nm). Data were collected from 2θ of 2.00° to 10.00° (θ being the angle of diffraction) with a step width of 0.02° and step time of 12 s, scanning speed of $0.1^\circ/\text{min}$. Scanning electron micrographs were taken on a Jeol JSM-T33 model scanning electron microscope. Optical micrographs were taken with a Leica DM-2500P model polarized optical microscope, under bright field and cross-polarized light conditions. DSC was performed on a Mettler Toledo DSC-821 under a continuous flow of nitrogen (60 mL/min). All the samples (about 10 mg in weight) were heated from 40°C to 250°C and the thermograms were recorded at a heating rate of $10^\circ\text{C}/\text{min}$. After cooling to 40°C , heating procedure was repeated. DSC thermograms revealed glass transition temperatures (T_g) and melting temperatures (T_m) of the samples. T_g was selected as the middle point of the transition region at the respective curves while the maximum of the endothermic peak was taken as T_m . All DSC thermograms in Figure 7 were obtained from the second heatings.

The chemically polymerized PNVCz and its composites with layered silicates were deposited at 1.2 V by electrooxidation in ACN containing 0.1 mol/L NaClO $_4$ on platinum (Pt) and glassy carbon (GC) disc electrodes. Cyclic voltammograms (CVs) of the working electrodes were obtained between 0.5 to 1.5 V at the scan rate 50 mV/s by using a Gamry Reference 600 potentiostat. A three-electrode cell containing Pt or GC disc electrodes that have diameters 1.6 and 3.0 mm, respectively, as the working electrodes, a Pt wire as the counter electrode, and a silver (Ag) wire as the pseudo-reference electrode were used for all electrochemical characterizations.

The electrochemical activity of the PNVCz/MMT composites was evaluated from the current–voltage curves obtained by cyclic voltammetry. After 6 scans, GC and Pt disc electrodes coated with composite films were taken out of electrochemical cell, washed with ACN, and placed in a monomer free solution. CVs of PNVCz and PNVCz/MMT composites in ACN+ 0.1 mol/L NaClO $_4$ system were recorded in 0.5 – 1.5 V potential range at three different scan rate, i.e., 50 , 250 and 500 mV/s.

Pt foil (in dimension 10 x 20 x 3 mm) was used as a working electrode to measure the electrical conductivities. The electrode was placed into the cell containing PNVCz/MMT composite in ACN together with the supporting electrolyte, 0.1 mol/L NaClO₄. The constant potential electrolysis was carried out at or above the peak potential of PNVCz. The amount of conducting composite deposited on the Pt foil was controlled by stopping the electrolysis. After the electrodeposition was stopped, the films were washed with ACN and peeled off from the electrode. Samples used for DC electrical-conductivity measurements were in the form of compressed pellets (13 mm in diameter and about 0.2 mm in thickness) obtained by applying a hydraulic pressure of about 10 MPa. The pellets were placed between two identical Pt electrodes in a conductivity cell. The slope of the potential vs current plot in the range of 1.0 – 10.0 V yields the resistance. The conductivities of electrodeposited-composites were evaluated from the surface resistance by means of Meter Scan Scientific software. The conductivity measurements were evaluated as a function of MMT content in the PNVCz/MMT composites.

The conductivities of the materials were also calculated from the data obtained by EIS in the frequency of 10 mHz to 10 kHz. Equivalent circuit was used to fit the experimental data, with the help of the ZsimpWin software. The bulk conductivities were calculated from the bulk resistance value obtained from the complex impedance diagram.

4.4 Results and discussion

4.4.1 FTIR Analysis

FTIR analysis is sensitive to both intra- and inter-molecular interactions. FTIR spectra of unmodified and organically modified montmorillonites (i.e., Na⁺MMT, ODA-MMT and TMSA-MMT), PNVCz and PNVCz/MMT composites synthesized with three different clay content and mixing methods, using CAN as initiator (i.e., PNVCz/Na⁺MMT, PNVCz/ODA-MMT and PNVCz/TMSA-MMT) are given in Figures 4.2-4.4 The band at 1040 cm⁻¹ in the spectra of Na⁺MMT, ODA-MMT and TMSA-MMT is attributed to Si-O stretching vibration The peaks at 1600 –1450 cm⁻¹ for aromatic stretching and aromatic –CH in plane bending, at 750 cm⁻¹ for aromatic -CH out of plane bending are characteristic for PNVCz. The spectra of PNVCz/MMT composites appeared the characteristic absorptions of both PNVCz

and the clay; indicate that both of them are present in structure. In addition, in the case of the composites prepared by using organically modified MMT the two peaks around 2924 and 2854 cm^{-1} along with the one at 1465 cm^{-1} reflect the asymmetric and symmetric stretching vibrations and bending vibration modes of methylene units, respectively.

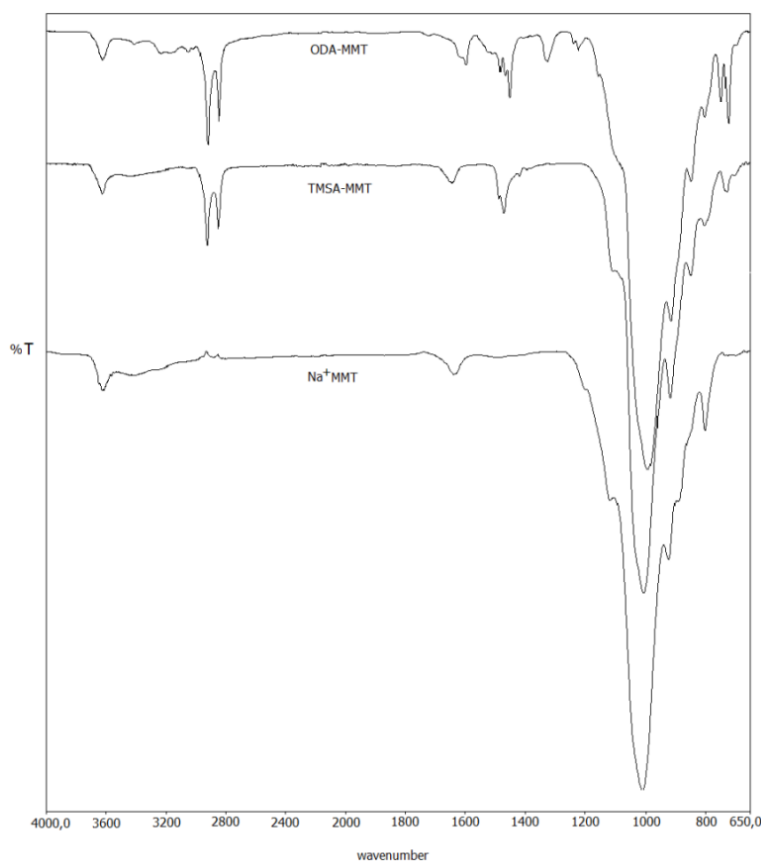


Figure 4.2: FTIR spectra of Na⁺MMT, ODA-MMT and TMSA-MMT.

It is known that there are lots of free molecular water and hydroxyl groups on the surface and edges of clay layers, respectively [29]. The two peaks around 3450 and 3620 cm^{-1} correspond to -OH groups indicated above. The absorption peak at 3620 cm^{-1} attributing to -OH groups on surface and edges of clay layers diminished while the shape and intensity of the absorption peak at 3450 cm^{-1} belonging to -OH groups of free molecular water changed with the type of mixing method. Further, the intensity of Si-O bond was dependent on both dispersion time and mixing method. These results suggested that the intermolecular interactions in the structures of PNVCz/MMT composites prepared by means of magnetic stirrer, high-power sonic

tip and homogenizer should mainly occur between the -OH groups on the surfaces or edges of MMT layers and PNVCz.

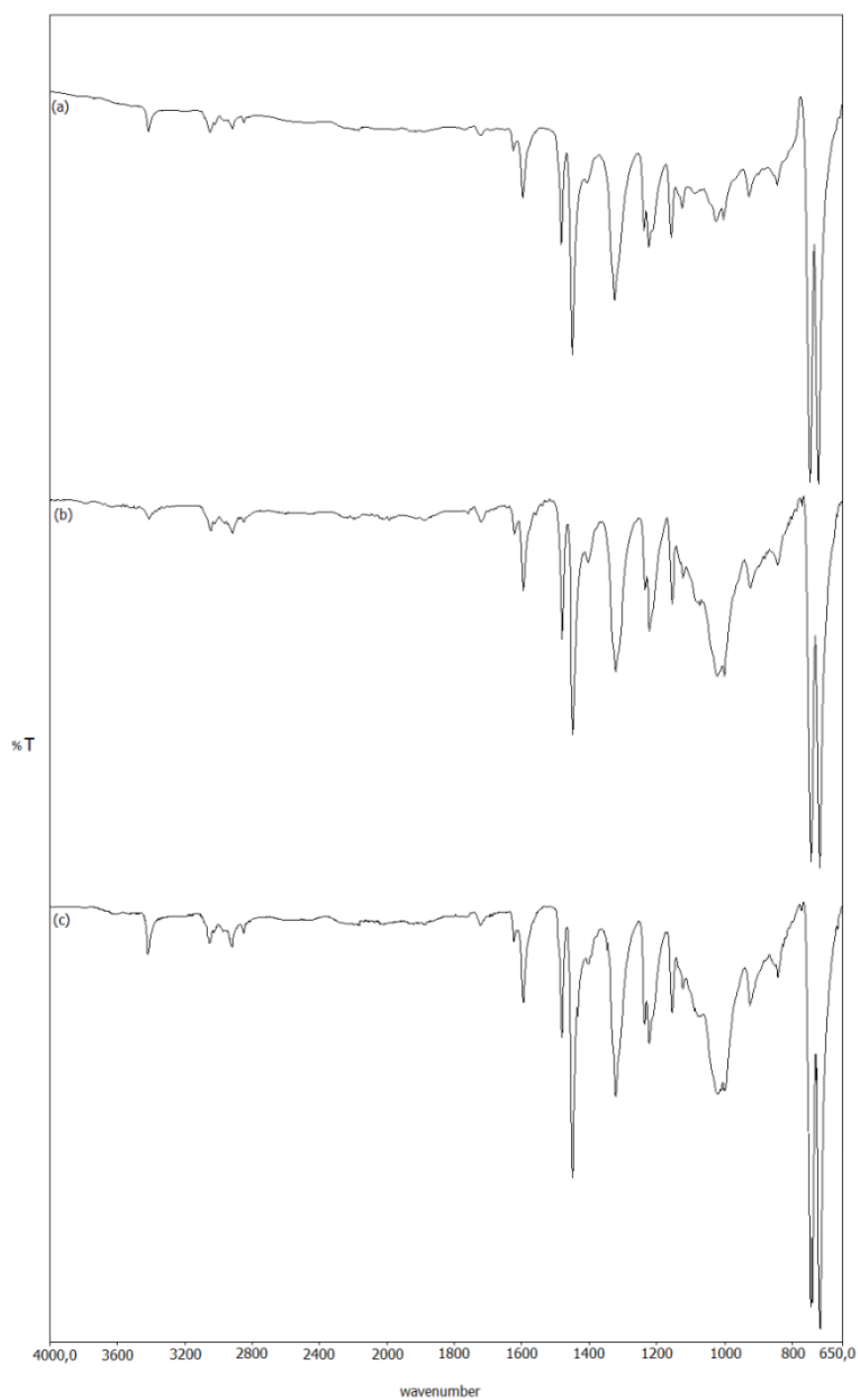


Figure 4. 3: FTIR spectra of PNVCz/ODA-MMT, 15.0 wt %, composites prepared by sonication for 5 min. (a), by sonication for 1 hour (b) and by mechanical stirring for 1 hour.

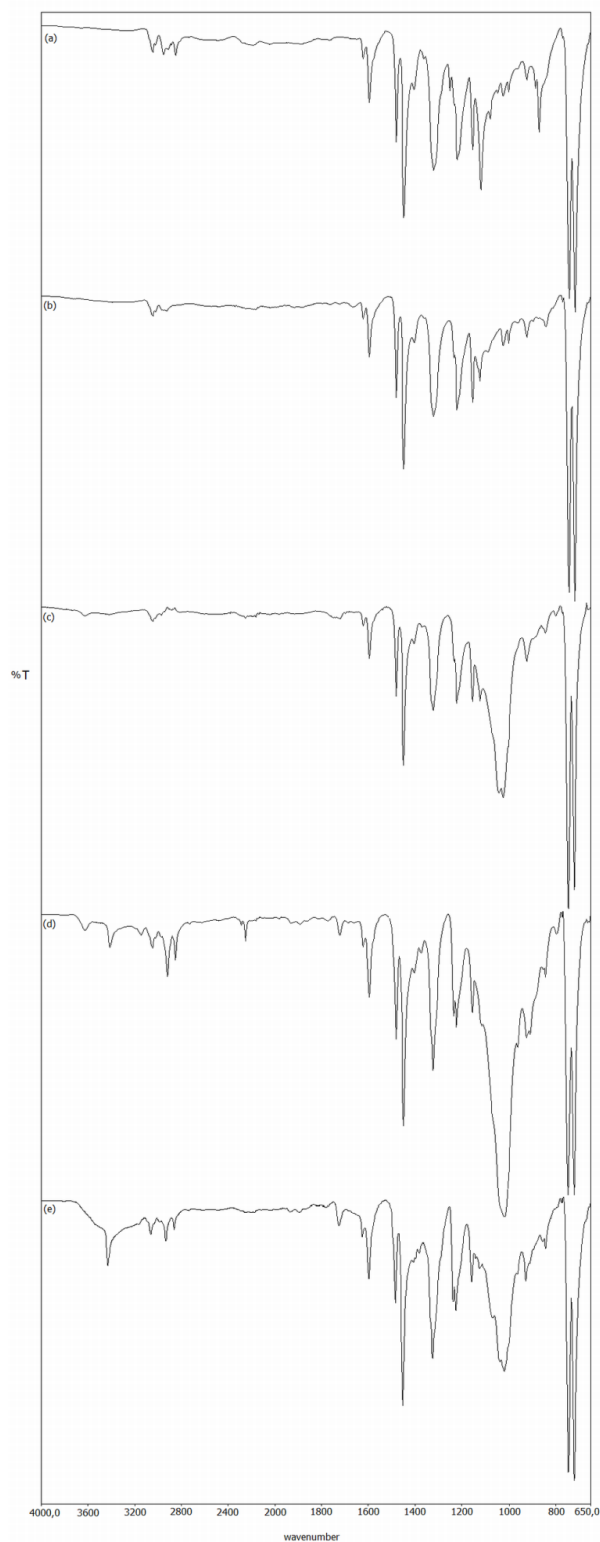


Figure 4.4: FTIR spectra of PNVCzs synthesized with AIBN and CAN (a, b) and, PNVCz/Na⁺MMT composites synthesized by using CAN to initiate the polymerization and by mixing with magnetic stirrer (c), sonic tip (d) and homogenizer (e) to obtain homogeneous dispersions of Na⁺MMT (15.0 wt %, based on NVCz concentration) in ACN.

4.4.2 X-Ray diffraction analysis

XRD was used to follow the clay interlayer spacing, d in Na^+MMT , modified MMTs (Figure 4.5) and their composites with PNVCz (Figures 4.6 and 4.7). The XRD patterns which are given in Figures 4.5-4.7 also gave qualitative information, indicating whether intercalated or exfoliated structure of the composites.

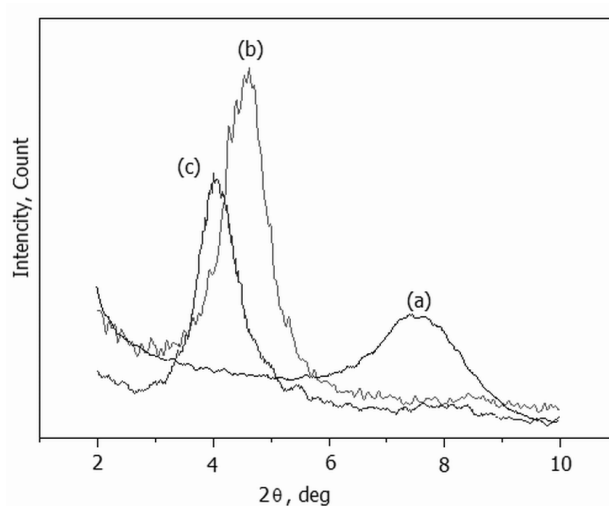


Figure 4. 5: X-ray diffraction patterns of Na^+MMT (a), ODA-MMT (b) and TMSA-MMT (c).

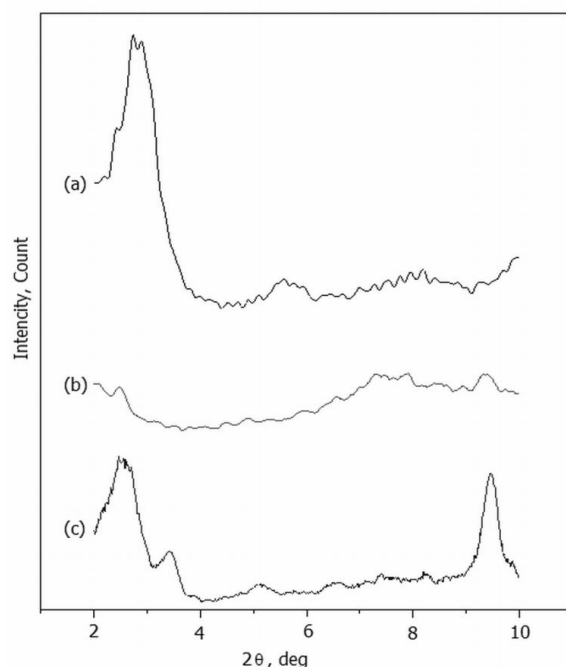


Figure 4.6: XRD patterns in the range of 2θ from 2° to 10° of PNVCz/ Na^+MMT (a), PNVCz/ODA-MMT (b) and PNVCz/TMSA-MMT (c) composites intercalated by sonication for 5 min (MMT content = 15.0 wt % of NVCz concentration).

Na⁺MMT, ODA-MMT and TMSA-MMT were dispersed into ACN using magnetic stirrer, homogenizator and high-power sonic tip before polymerization of NVCz. The d spacing between clay layers was calculated from peak positions using Bragg's law ($d = n\lambda / 2 \sin \theta$), where λ is the X-ray wavelength (1.5418 Å). The interlayer spacing of Na⁺MMT was determined as 11.8 Å (= 1.18 nm) by XRD. As the d-spacing of modified MMTs expands or contracts, the reflection of XRD will shift proportionally to the left or right on the corresponding diffractograms. Figure 3.15 shows X-ray diffraction patterns of ODA and TMSA cation exchanged MMTs along with Na⁺MMT. The peaks on the XRD patterns of ODA-MMT and TMSA-MMT were centered nearly at $2\theta = 4.5^\circ$ ($d = 1.96$ nm) and 3.8° ($d = 2.32$ nm), respectively. Expansion of d-spacing suggests that organo-modifiers successfully intercalated between layers of MMT. The peak positions shifted to lower angles and so the increments of d-spacing were related to both alkyl chain lengths and structures of the surfactants [30].

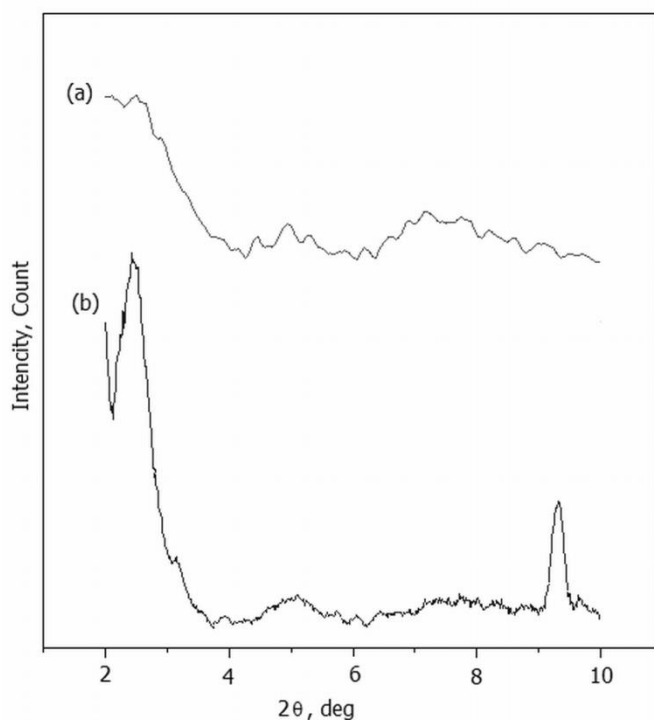


Figure 4.7: XRD patterns in the range of 2θ from 2° to 10° of PNVCz/ODA-MMT (a) and PNVCz/TMSA-MMT (b) composites intercalated by mechanical stirring for 1 hour (MMT content = 15.0 wt % of NVCz concentration).

XRD were also used to characterize the dispersions of the organoclays in PNVCz. Figures 4.6 and 4.7 show XRD patterns of PNVCz/MMT composite materials containing 15.0 wt % of Na⁺MMT and organoclays. The sharp peak located at $2\theta = 2.5^\circ$ by incorporation of Na⁺MMT and organo-MMTs into PNVCz indicated the possibility of intercalated silicate layers of MMT. The changing intensity of this XRD diffraction peak by depending on the type of surfactants and the mixing methods can be shown as an indicator for intercalation degree. Further, the presence of two broad peaks and one sharp peak around 5.5° , 8.0° and 9.5° that correspond to interlayer structure and crystallinity, respectively, indicate some amount of the clay that exists in original clay particles and tactoids. Also, crystalline behavior is suppressed by the introduction of organophilic clay into polymer matrix in the form of an intercalated layer structure. This means that even after sonication and mechanical stirring, organically modified clay particles are still present together with intercalated platelets, i.e. clay layers. The sharp peak appeared nearly $2\theta = 9.5^\circ$ can be related to crystallization induced by the presence of the quaternary alkyl ammonium groups, i.e., TMSA.

4.4.3. Morphological and thermal analysis

To obtain more insight into the interlayer of PNVCz/MMT composites, DSC analyses were performed. Since inorganic montmorillonite is infusible in the measurement temperature range, the melting peaks around 100°C were attributed to the melting of surfactants. The thermograms obtained from the second runs indicated that the thermal properties of the PNVCz within the clay platelets were different from that around their outside, and strongly dependent on the type of both cationic surfactants attached to the MMT platelets and mixing methods used for composite preparation (Figure 4.8). This may be associated with the dispersion of the clay layers. In the cases of ultrasonic agitation using high power sonic tip for all MMTs, some portion of clay platelets maintained the layer structure of MMT while their large amounts displayed highly ordered dispersion of the clay layers that cause the higher T_{ms} than T_g of pure PNVCz synthesized by oxidative polymerization in the presence of Ce (IV) ions. For nanocomposites prepared with TMSA-MMT and Na⁺MMT by using magnetic stirrer for 17 hours, homogeneously dispersed structures and slightly increased T_g s than that of PNVCz were obtained. The absence of any melting peak indicates that both the cationic surfactant, TMSA and PNVCz

chains attach mainly to the outsides of the clay layers, and so their presence are not effected on the motions of the polymer chains. POM and SEM images of the indicated composites also support the observations obtained from DSC thermograms.

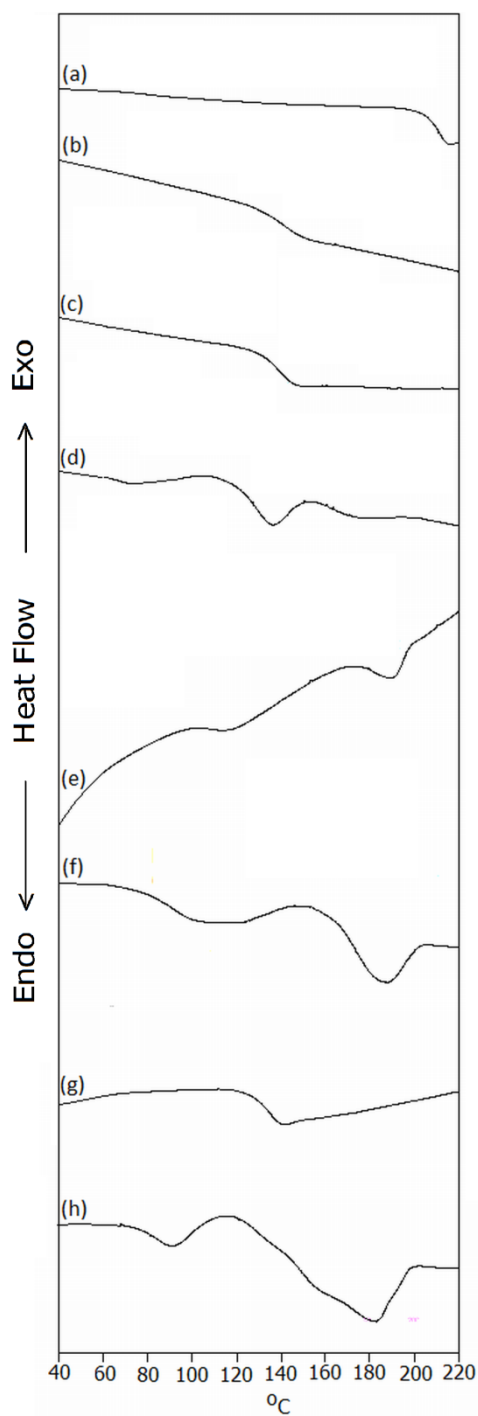


Figure 4.8: DSC thermograms of PNVCzs initiated with AIBN (a) and CAN (b) and, Sample 1 (c), Sample 4 (d), Sample 2 (e), Sample 5 (f), Sample 3 (g) and Sample 6 (h) in Table 4.1.

In addition, from the comparison of the DSC thermograms poly(N-vinyl carbazole)s synthesized with AIBN and CAN, it is seen that T_g values, i.e. thermal stabilities directly reflect the effect of polymerization procedure and initiator type on the molecular weight of PNVCz. This means that the molecular weight of PNVCz initiated with AIBN may be higher than the one obtained with oxidative polymerization in the presence of CAN.

Figures 4.9-4.11 show the SEM and POM images of PNVCz/MMT structures prepared by magnetic stirring and by mixing with high power sonic tip.

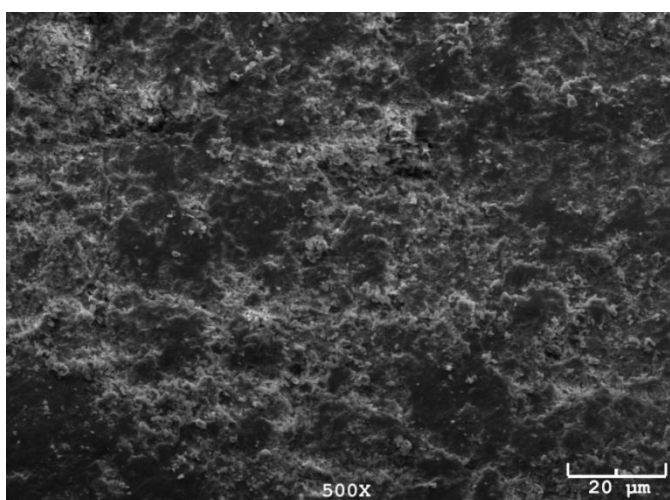


Figure 4.9: SEM micrograph of PNVCz/Na⁺MMT (15.0 wt %) prepared with magnetic stirring for 17 hours (Sample 1 in Table 4.1).

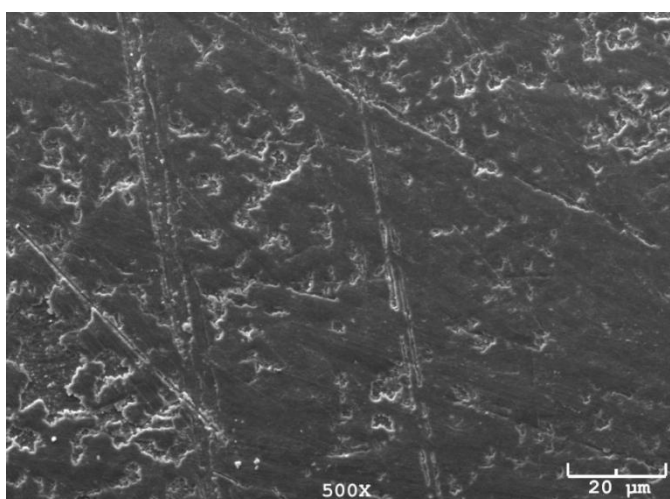


Figure 4.10: SEM micrograph of PNVCz/Na⁺MMT (15.0 wt %) prepared with ultrasonic agitation for 5 min (Sample 4 in Table 4.2).

20 micron square regions on the SEM micrographs had different morphologies (Figures 3.19 and 3.20). The darker areas correspond to PNVCz, while the lighter

areas indicate silicate layers. The micrograph for the PNVCz / Na⁺MMT composite synthesized by sonication revealed more oriented and ordered morphology while for the one obtained with magnetic stirring, homogeneous distributions of darker and lighter regions were observed.

The morphological images of the PNVCz/ODA-MMT and PNVCz/TMSA-MMT composites containing 15.0 and 1.0 wt % of clay were studied with a POM. The micrographs in Figure 3.21 show more ordered morphology for PNVCz/ODA-MMT composites, being different than the morphologies of PNVCz/TMSA-MMT. It is clearly seen that the ordered morphologies of PNVCz/ ODA-MMT composites are independent of mixing method and clay content whereas the TMSA-MMT having quaternized hydrophobic groups in PNVCz has more homogeneous dispersion only for 17 hours magnetic stirring. These results are also consistent with the XRD patterns, DSC thermograms and SEM micrographs described above.

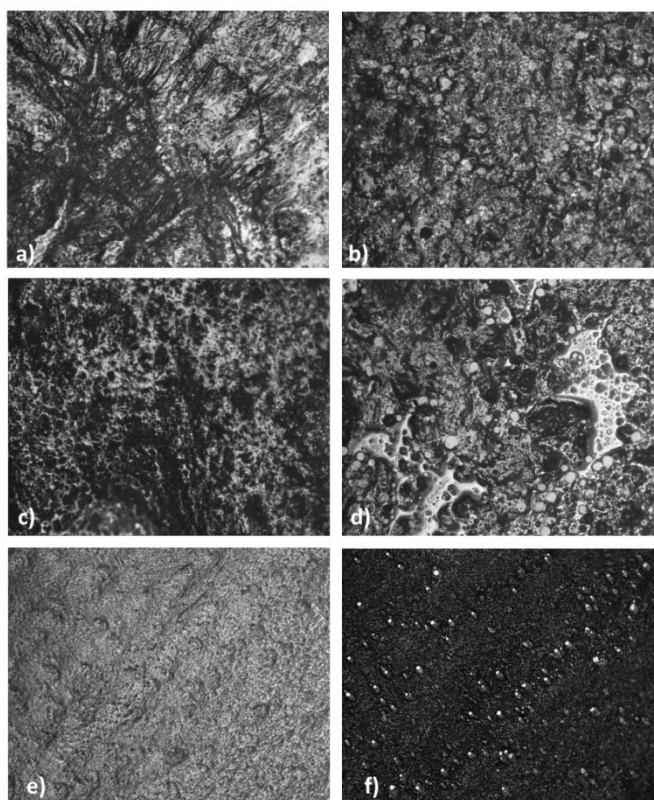


Figure 4.11: Optical microscope images for PNVCz/MMT composites containing (a, c) 15.0 wt % ODA-MMT and TMSA-MMT, respectively ; for 17 hours magnetic stirring, (b, d) 15.0 wt % ODA-MMT and TMSA-MMT, respectively ; for 5 min ultrasonic agitation, (e, f) 1.0 wt % ODA-MMT ; for 5 min ultrasonic agitation. Image (f) is the same position with the others but under cross-polarized light condition.

4.4.4. Electrochemical properties

The influence of the preparation methods on the electrochemistry of Pt and GC electrodes coated with PNVCz/MMT composites in ACN was examined using 0.1 mol/L NaClO₄, which is known to be a relatively inert electrolyte. Cyclic voltammograms of the working electrodes were obtained from 0.5 to 1.5 V. The counter electrode was a Pt wire while Ag wire was used as a pseudo reference electrode.

The CVs of both during and after the electrochemical deposition process of Pt and GC electrodes coated with chemically polymerized PNVCz composite containing 5.0 wt % of TMSA-MMT (based on monomer concentration in the feed) are shown in Figures 11 and 12. The voltammograms recorded on Pt and GC electrodes during the deposition of PNVCz/TMSA-MMT composite in CH₃CN + NaClO₄ (0.1 mol/L) solution at 50 mV/s exhibited two peaks. First one around 1.1 V corresponds to electrooxidation and crosslinking between carbazole rings on the nonconductive-white PNVCz chains while the second peak centered at 0.8 V and formed after the second cycle refers polymer deposition on the electrode surface. Their intensities increase with increasing cycle number. For composite coated on Pt and GC disc electrodes, the cyclic voltammograms at three different scan rates also indicated the formation of electroactive-green polymer films because of two different electron transfer at 0.9 V and 1.2 V (Insets in Figures 4.12 and 4.13).

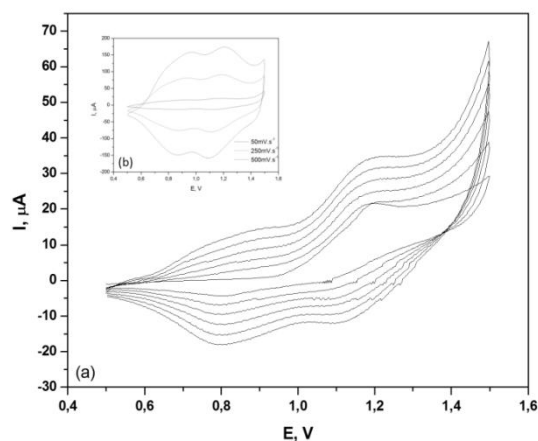


Figure 4.12: Cyclic voltammograms of GC electrode during electrochemical deposition of chemically synthesized PNVCz/TMSA-MMT composite (Sample 22 in Table III) in ACN + NaClO₄ solution. Scan rate: 50 mV / s. **Inset:** Cyclic voltammograms of PNVCz/TMSA-MMT coated GC electrode in three different scan rates (50, 250 and 500 mV/s). Supporting electrolyte: NaClO₄ in ACN.

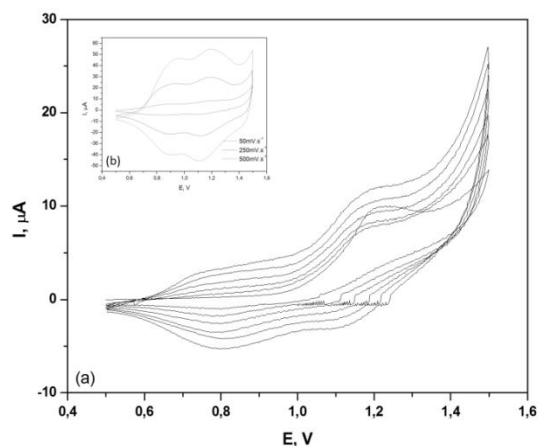


Figure 4.13: Cyclic voltammograms of Pt electrode during electrochemical deposition of chemically synthesized PNVCz/TMSA-MMT composite (Sample 18 in Table III) in $\text{NaClO}_4 + \text{ACN}$ solution. Scan rate: 50 mV / s. **Inset:** Cyclic voltammograms of PNVCz/TMSA-MMT coated Pt electrode in three different scan rates (50, 250 and 500 mV/s). Supporting electrolyte: NaClO_4 in ACN.

The peak potentials and currents for the composite coated electrodes prepared by electrodeposition of PNVCz/ Na^+MMT , PNVCz/ODA-MMT and PNVCz/TMSA-MMT composites on Pt and GC disc electrodes together with the yields for the formation of PNVCz/MMTs in the presence of CAN with Na^+MMT , ODA-MMT and TMSA-MMT during the chemical polymerization are given in Tables 3.12-3.14. The results indicate that polymerization yields in the present system varied between 50 and 98, depending upon both the type and amount of silicate layers taken in the initial feed, and clay-dispersing methods used for oxidative polymerization of NVCz.

Further, it is clearly seen that both mixing methods and the structures of cationic surfactants which are used to synthesize the composite materials and organically modified layered silicates, respectively, are mainly affected on the voltammetric behaviors of these composite materials (Tables 3.12-3.14). In the case of ODA-MMT dispersed by using sonic tip, it was observed that there is an inverse relation between the intensities of anodic / cathodic peak currents and the yields, and clay content whereas the peak intensities and yields of PNVCz/ODA-MMT composites prepared by homogenizator increased with increasing clay content for 1.0 and 5.0 wt %. After that, the further addition of ODA-MMT slightly decreased the peak currents. On the other hand, the composite films of PNVCz with TMSA-MMT exhibited a direct

relation between current intensities/yields and increasing amount of MMT for both of the mixing method.

For the same amounts of three different MMT clay, the following relationships between mixing method/surfactant structure/electrode material and current intensities/yields can be indicated. In the case of magnetic stirring and Pt electrode, peak intensities of anodic/cathodic currents and polymerization yields decreased with the order of $\text{Na}^+\text{MMT} > \text{ODA-MMT} > \text{TMSA-MMT}$. For dispersions and coatings obtained with sonication and on GC electrodes, respectively ($\text{TMSA-MMT} > \text{ODA-MMT} \approx \text{Na}^+\text{MMT}$), peak currents of GC electrode coated with PNVCz/TMSA-MMT composite were stronger than the others. On the other hand, the composite indicated above could not deposited by electrooxidation process on Pt electrode while the current intensity of PNVCz/ Na^+MMT coated Pt electrode was higher than PNVCz/ODA-MMT and PNVCz/TMSA-MMT composites. From this comparison, it can be seen that the results obtained with voltammetric measurements have similar tendency with the ones of gravimetric method.

As a summary, the voltammetric data collected in Tables 3.12-3.14 along with FTIR spectra, XRD diffractograms, DSC thermograms, XRD patterns and SEM/POM images exhibited that the mixing with a sonic tip and using ODA-MMT, having a long hydrophobic chain with 18 unit of CH_2 were the most preferable method to prepare highly intercalated PNVCz/MMT composites.

4.4.5. Electrochemical impedance spectroscopy (EIS) measurements

EIS is an effective method to study the interfacial properties of surface-modified electrodes. Bode and Nyquist plots are constructed, and appropriate equivalent circuit model is used to correlate the impedance measurements with the capacitance and the resistance of the film. Special attention is paid to obtain a relationship between the type of conductivity (electronic and/or ionic) and the shape of impedance spectra.

Electrical properties were measured by electrochemical impedance spectroscopy (EIS) in the frequency range from 10 mHz to 10 kHz. EIS measurements were performed in order to characterize the Pt-solution, GC-solution, Pt-PNVCz/MMT-solution and GC-PNVCz/MMT-solution interfaces.

Bode plots of EIS measurements of GC disc electrodes coated with PNVCz and PNVCz/ TMSA-MMT composites containing 15.0 wt % of silicate layers are shown in Figure 4.14. The peak profile was dependent on both the polymerization mechanism of PNVCz (b and c) and the preparation conditions of PNVCz/TMSA-MMT composites (d, e and f). The obtained Bode plots for impedance characterization of the interfaces indicated the existence of mainly two regions. After a dominant peak in the phase angle at low frequencies, a second peak developed at high frequencies. It is believed that the low frequency peak represents bulk conduction while the second peak refers ionic conduction.

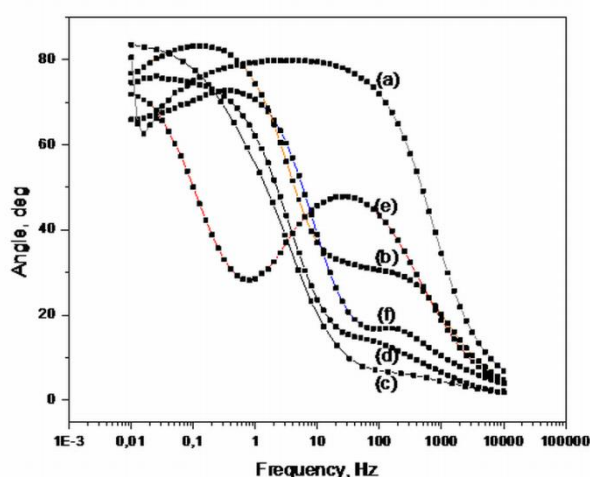


Figure 4.14: Bode plots showing change in phase angle of bare GC disc electrode (a) and GC electrode coated on PNVCz polymerized chemically (b) and electrochemically (c), PNVCz / TMSA-MMT composites mixed with sonicator (d), homogenizator (e) and magnetic stirrer (f) (Samples 6, 11 and 3, respectively, in Table 4.1) during dispersion of silicate layers.

Nyquist plots of PNVCz/ODA-MMT composites prepared using sonicator with three different clay content (1.0, 5.0 and 15.0 wt % of ODA-MMT based on NVCz concentration in the feed) at room temperature are shown in Figure 3.25. All three plots exhibit a semicircular arc in the high frequency region and an oblique line in the low frequency region. In another word, these Nyquist plots are characterized by two regions: a semicircle at high frequencies associated with charge transfer (R_{dl}) at the polymer/solution interface and a second region consisting of an oblique line indicating a diffusion-controlled process at the electrode, i.e., R_{pol} (or R_b). The interactions between solution - PNVCz/ODA-MMT - Pt interfaces were modeled as an equivalent circuit which consists parallel combination of double-layer constant

phase element (CPE- Q_{dl}) and charge transfer resistance (R_{ct}) in series with parallel circuit of bulk-polymer constant phase element (CPE- Q_{pol}), the bulk-polymer resistance (R_{pol}) and Warburg impedance (W). The impedance values (Z) in Figure 4.15 also depend on the solution resistance (R_s) and, the capacitance (C_{el}) and resistance (R_{el}) of Pt electrode.

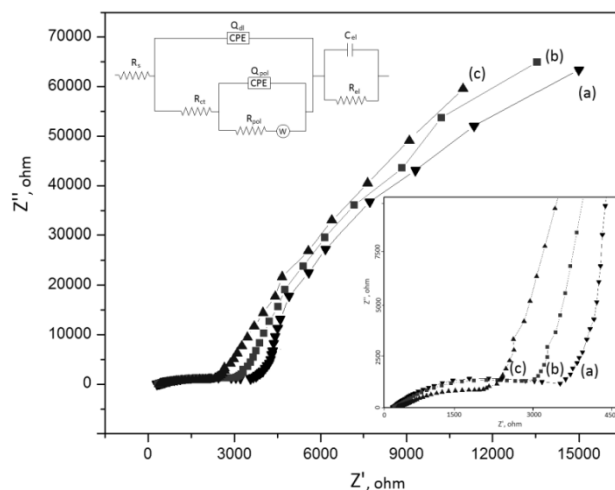


Figure 4.15: Nyquist plots of PNVCz / ODA-MMT composites containing 15.0 (a), 5.0 (b) and 1.0 (c) wt % of layered silicate (Samples 5, 12 and 13, respectively, in Table II) coated on Pt electrode. Their corresponding equivalent circuit and the enlarged data in high frequency are shown in insets. Symbols Z' and Z'' refer to the real and imaginary components.

The constant phase element (CPE) instead of capacitance was introduced to account for the nonideality of the interfaces between the electrode – polymer/clay – electrolyte in the impedance spectra. In addition, the equivalent circuit in Figure 3.25 includes a Warburg impedance, to explain diffusion-controlled process between PNVCz/ODA-MMT – electrode interface that corresponds to second region. The bulk-polymer resistances (R_{pol}) were determined from the low frequency parts of Nyquist plots. Then, the conductivities of PNVCz/ODA-MMT composites were obtained from R_{pol} , A and l , using the relation $\text{Conductivity} = l / R_{pol} A$, where l and A are the thickness of PNVCz/ODA-MMT composite and area of Pt disc electrode. The results are given in Table 4.4. Conductivity values of composites were remarkably improved relative to that for PNVCz homopolymer. It was seen that the variations in the conductivities calculated from EIS data had similar tendency with the ones obtained from DC-measurements. The numerical values obtained with two different methods reflect the effects of measuring techniques on data. As to the capacitances and conductivities increased in the presence of silicate layers, it can be

said that the intercalated composite structures for PNVCz chains associated with MMT particles may facilitate the ion conduction within the materials.

Table 4.4: Conductivity results.

Sample	Conductivity ^b (S/cm)	R _{ct} (Ω)	Q _{dl} ^d (μS.s ⁻ⁿ)	R _{pol} (Ω)	Q _{pol} ^d (μS.s ⁻ⁿ)	Conductivity ^c (S/cm)
PNVCz ^a	1.00 x 10 ⁻¹⁵	-	-	-	-	2.26 x 10 ⁻¹¹
5	1.74 x 10 ⁻⁸	3389	10.64 (0.71)*	57.31x10 ⁶	17.45 (0.85)*	1.02 x 10 ⁻¹⁰
12	5.77 x 10 ⁻⁷	3097	11.44 (0.74)	1.73 x 10 ⁶	57.43 (0.90)	6.80 x 10 ⁻⁸
13	1.92 x 10 ⁻⁵	2517	35.38 (0.74)	52.08 x 10 ³	160.90 (0.96)	3.21 x 10 ⁻⁷

^a initiated with CAN

^b calculated from EIS measurements

^c calculated from DC measurements

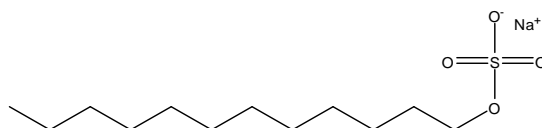
^d best fitting parameters obtained from equivalent circuit and impedance data on Pt electrode

*n value in the paranthesis indicates the type of capacitor. The impedance for non-ideal condenser can be represented as $Z = 1/Q(j\omega)^n$, where $n < 1$.

5. POLY(N-VINYL CARBAZOLE) (PNVCz) BASED COMPOSITE MATERIALS: ELECTRICAL PROPERTIES, MORPHOLOGICAL AND THERMAL CHARACTERIZATION OF PNVCz / MULTIWALLED CARBON NANOTUBES AND PNVCz / GRAPHITE SYSTEMS

5.1 Experimental

The monomer, N-vinylcarbazole (NVCz; Aldrich) was used without further purification. Monocetyl itaconate, MCEI chosen as comonomer has been synthesized in another work, according to the general methods previously reported by Gargallo (27, Yalçın). Cerium ammonium nitrate ((NH₄)₂Ce (NO₃)₆, CAN; BDH Chemicals Ltd.) was chosen as initiator. In this study, two types of MWCNTs were used. The first one was obtained from Aldrich (diameter < 15 nm and length range: 0.1–10 μm; purity ≥ 90%; density: 2.1 g/cm³) while the second one used in the composites were prepared with oxidation of MWCNTs purchased from Aldrich and the product was named as o-MWCNTs. Graphite powder (product code: G/0900/60; density: 2.1 g/cm³) purchased from Fisher Scientific. The carbon nanotubes and graphite layers were dispersed in tetrahydrofuran (THF, Merck) and acetonitrile (ACN, Merck) via energetic agitation (after the sonication in an ultrasound bath cleaner (Elma Transsonic 460/H, 35 kHz) for 4 h, they were mixed with a high power sonic tip (Sonopuls HD 2200, 200W/20kHz) for 15 min.) in order to achieve stable dispersions. In some cases, they were dispersed in ACN/water (9:1 v/v %) mixtures containing surfactant followed by ultrasonication. The surfactant was sodium dodecyl sulfate (SDS, C₁₂H₂₅SO₄⁻ Na⁺, Merck) and used as supplied.



Sodium Dodecyl sulphate

Figure 5.1: Schematic illustration of used chemicals.

5.1.1 Free radical polymerization of PNVCz and P(NVCz-co-MCEI)

Copolymer of NVCz with MCEI (5.0 mol %, in the feed) was synthesized by free radical solution polymerization in 1,4-Dioxane with AIBN (1.0 x 10⁻³ mol / L) at

50°C under nitrogen atmosphere (30). The polymerization mixture was introduced into large glass tube with ~30 mm diameter equipped with a rubber cap and a syringe. Solution was degassed by bubbling nitrogen for about 30 min. After 4 d polymerization mixture was poured into hexane to precipitate the copolymer (Figure 5.2). The homopolymer of NVCz (1.0 mol/L) was also synthesized under identical experimental conditions.

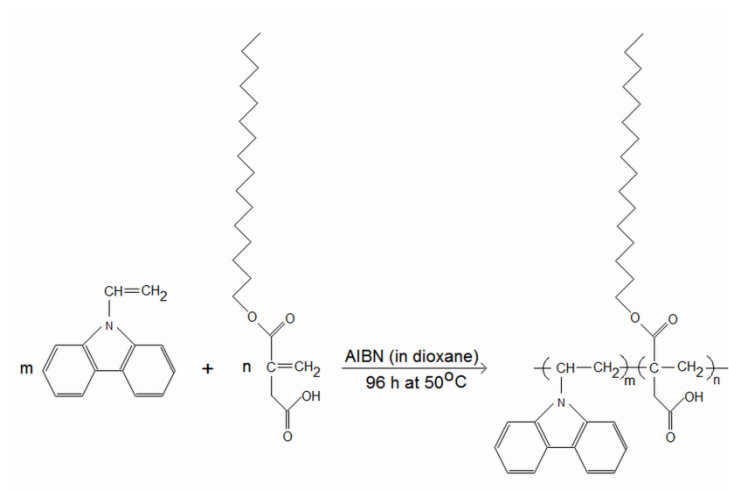


Figure 5.2: Polymerization reaction of P(NVCz-co-MCeI) copolymer.

5.1.2 Oxidative polymerization of PNVCz

The heterogeneous solution process was as follows: NVCz monomer with a known weight was dissolved in ACN. Then, CAN as an oxidizing agent was added into the NVCz/ACN solution to initiate the polymerization. The mole ratio of monomer to oxidizing agent was kept at 200:1. 1.0 mol /L concentration of NVCz was used. The synthesis was carried out at 25°C under atmospheric conditions. After completed reaction period, the white product was santrifugated and washed with ACN at least 3 times to remove any unreacted NVCz, and then nonconductive PNVCz was dried to constant weight under vacuum at room temperature (Figure 5.3). Another PNVCz sample was synthesized under identical experimental conditions but in the presence of SDS (10.0 wt %, based on NVCz in the feed).

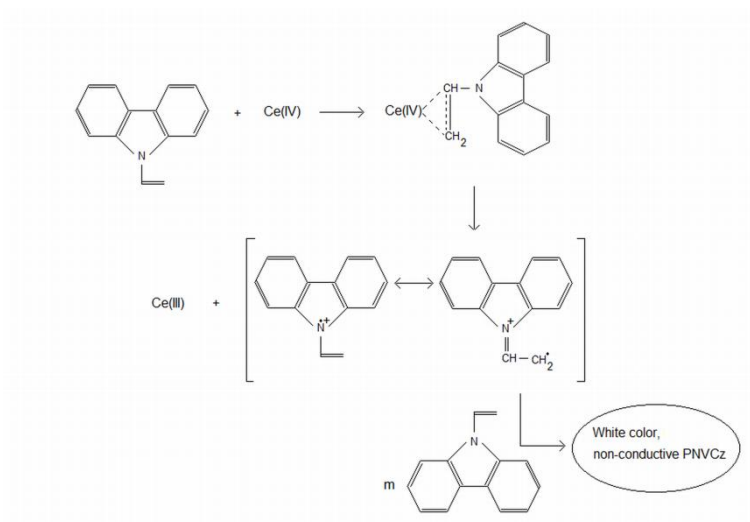


Figure 5.3: Possible mechanism for the polymerization of NVCz by Ce (IV) ion.

5.1.3 Oxidation of GLs and MWCNTs

Ten grams of graphite powder were suspended in 200 mL of concentrated H_2SO_4 in a 1 L round bottomed flask under vigorous stirring at 0°C . KMnO_4 was then added gradually with stirring and cooling, so that the temperature of the mixture was maintained around 20°C . The stirring was continued at room temperature for 30 min.

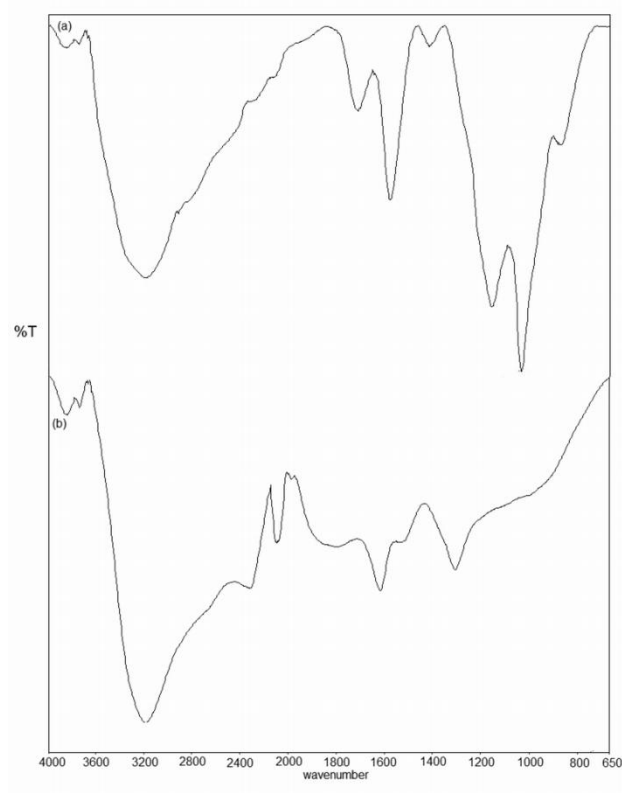


Figure 5.4: FTIR spectra of o-GLs (a) and o-MWCNT (b).

After the slowly addition of 250 mL of deionized water, the graphite/H₂SO₄/KMnO₄/water mixture was stirred for another 15 min, by keeping its temperature below 98°C. Finally, the content of the flask was poured into 1 L of deionized water, and 100 mL of a 30 % H₂O₂ solution was added to destroy the excess KMnO₄. The oxidized graphite layers (o-GLs) were isolated by filtration through a sintered glass funnel, washed successively with 5 % HCl and dried in a vacuum oven at 60°C for 48 h (31- 32).

The surfaces of MWCNTs were oxidized by refluxing with 5.0 M nitric acid (HNO₃) at 75°C for 2 h. Then, the HNO₃/MWCNTs mixture was washed several times with distilled water and finally, oxidized MWCNTs were filtered and left to dry in a vacuum oven at 60°C for 3 d [33, 34].

The acid-treatment, reflux and sonication procedures can introduce functional groups that promote the adsorption of polymer chains and monomer molecules on the pores and surfaces of graphite layers and carbon nanotube walls [35]. Figure 3.26a shows the FTIR spectrum of o-GLs. The most characteristic features of graphite oxide are the broad, intense band around 3400 cm⁻¹ assigned to O-H stretching vibrations, the band at 1730 cm⁻¹ attributed to C=O stretching vibrations from carbonyl/carboxylic groups and the band centered at 1620 cm⁻¹ from the skeletal vibrations of unoxidized graphitic domains along with the strong bands at 1230 cm⁻¹ and 1060 cm⁻¹ assigned to C-OH and C-O stretching vibrations, respectively. The FTIR spectrum of o-MWCNTs are shown in Figure 3.26b. The broad bands in the range of 3200-2400 cm⁻¹ and 1800-1600 cm⁻¹ can be attributed to O-H and C=O stretching vibrations of hydrogen bonded-hydroxyl and -carboxyl groups which present on the o-MWCNTs.

All the bands were attributed to the carboxylic acid groups generated at the surfaces of the graphite layers and MWCNTs after acid treatments. In addition, the o-MWCNTs were analyzed quantitatively by acid-base titration to support the presence of carboxylic groups on the surfaces of the acid-treated MWCNTs. In a typical experiment, 50 mg of the o-MWCNTs were added into 10 ml of 0.05 N NaOH solution and stirred for 24 h to reach the equilibrium state at room temperature. Then, the mixture was titrated with a 0.05 N HCl solution to determine the excess NaOH in the solution and, the concentration of the carboxyl groups on o-MWCNTs was found as 2.0 mmol/g. The value of 0.63 mmol/g for untreated-

MWCNTs also supports the formation of –COOH groups on tube surfaces treated with nitric acid.

5.1.4 Preparation of PNVCz / graphite composites

PNVCz/graphite composites were prepared by both the solution blending and in-situ polymerization method.

In order to obtain homogeneous dispersions of o-GLs, the solutions were prepared in THF for solution blending process and in ACN/water mixture (9:1, v/v %) containing 1.0 or 10.0 wt % SDS (based on NVCz content) for in-situ polymerization process by sonicating for 15 min using a high-power sonic tip processor and for 4 h using an ultrasound bath. Each 1 h in a sonic bath was followed by 5 min with a sonic tip.

PNVCz and P(NVCz-co-MCeI) synthesized with CAN and AIBN as initiator, respectively, were added to the o-GLs / THF dispersions and the mixtures were stirred using magnetic stirrer until the entire polymers were dissolved. The solutions were then transferred into glass petri dishes. The solvent, THF was first evaporated at room temperature for 1 d and then in a vacuum oven at 25° C for 2 d to yield a well dispersed PNVCz/o-GLs and P(NVCz-co-MCeI)/o-GLs composites.

o-GLs (in the range of 0.05 -0.40 wt % for PNVCz obtained by in-situ polymerization method) were dispersed in 10 mL of ACN/water mixture containing SDS and stirred by ultrasonication to obtain homogeneous dispersions. Before addition of a known amount of CAN, 1.0 mol /L of NVCz was dissolved in the o-GLs/SDS/ACN/water dispersion with magnetic stirring. The in-situ polymerization mixture was continuously stirred at room temperature after addition of CAN as oxidant. The precipitate was washed with ACN at least 3 times to remove any unreacted NVCz, placed into a glass dish and allowed to stand at room temperature for 1 d. The black composite was further vacuum-dried at 25°C for 2 d to remove the residual solvent.

In the case of 10 wt % of SDS, a known amount of NVCz was added to the SDS/o-GLs (0.40 wt %)/ACN/water dispersion with magnetic stirring. The reaction mixture was polymerized without CAN during the magnetic stirring process at room temperature. It was assumed that during stirring, NVCz and SDS molecules were adsorbed on the surface of graphite layers (Figure 5.5).

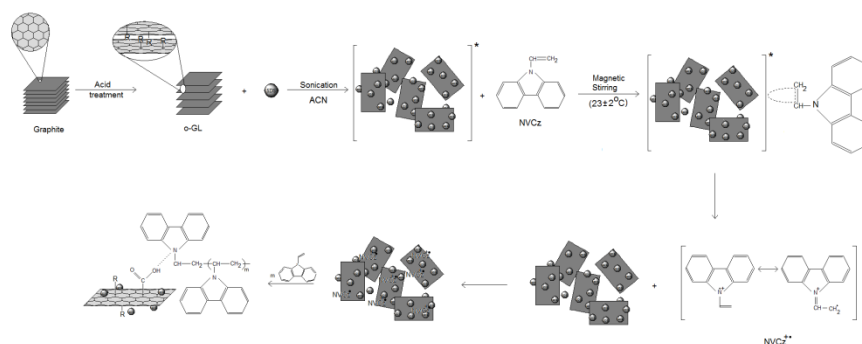


Figure 5.5: Proposed mechanism for the in situ polymerization of NVCz without CAN by sonicated o-GLs in ACN/water/SDS (10.0 wt % of NVCz) mixture at room temperature.

5.1.5 Preparation of PNVCz / MWCNT composites

The PNVCz/MWCNTs and PNVCz/o-MWCNTs composites were also synthesized using both solution blending and in-situ polymerization methods.

In a beaker, 10 ml of THF and a certain amount of MWCNTs (to yield the desired loading of MWCNTs from 0.5 to 2.0 wt % in 100 mg of PNVCz and P(NVCz-co-MCeI)) were mixed and dispersed by sonication. Then, 0.1 g of PNVCz and its copolymers, P(NVCz-co-MCeI) were dissolved in the MWNT/THF dispersions and stirred using magnetic stirrer for 1 h. After that, PNVCz/MWCNT/THF and P(NVCz-co-MCeI)/MWCNT/THF mixtures were transferred into glass petri dishes. Remaining THF was first evaporated in the petri dishes at room temperature for 1 d and then in a vacuum oven at 25° C for 2 d to yield PNVCz /carbon nanotube composites prepared by solution blending process.

In the case of in-situ polymerization process in the presence of 10 wt % of o-MWCNT, a known amount of NVCz was added to both SDS (10 wt %)/o-MWCNT/ACN/water and o-MWCNT/ACN dispersions, and SDS(10 wt %)/MWCNT/ACN/water and MWCNT/ACN dispersions with magnetic stirring (Table 5.1). The NVCz/o-MWCNT/ACN mixture was polymerized without initiator, CAN during magnetic stirring at room temperature whereas the others produced PNVCz/carbon nanotube composites only after the addition of a known amount of CAN (Figure 5.6). The black composites were decanted into glass dishes and dried in a vacuum oven at 25°C for 2 d to remove the residual solvents.

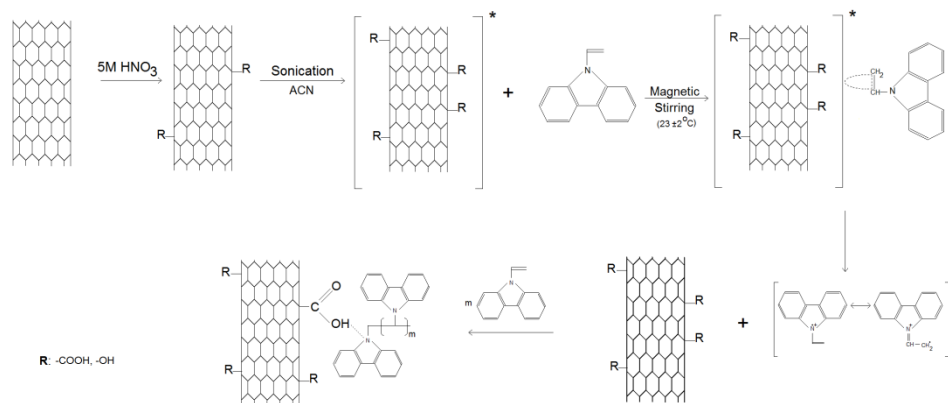


Figure 5.6: Proposed mechanism for the in situ polymerization of NVCz without CAN by sonicated o-MWCNTs in ACN at room temperature.

Table 5.1: Reaction possibilities between NVCz and conducting fillers.

reaction media	in-situ polymerization without CAN
o-GLs (0.2 g/100 g NVCz) /10 wt% SDS	+
o-GLs (0.2 g/100 g NVCz)/5.0 wt% SDS	-
o-GLs (0.2 g/100 g NVCz) /1.0 wt% SDS	-
o-MWCNTs (5.2 g/100 g NVCz)	+
o-MWCNTs (5.2 g/100 g NVCz)/10 wt % SDS	-
MWCNT (5.2 g/100 g NVCz)	-
MWCNT (5.2 g/100 g NVCz) / 10 wt % SDS	-

5.2 Analysis and characterization techniques

PNVCz/o-GL, PNVCz/MWCNT and PNVCz/o-MWCNT composites were analyzed and characterized by using Fourier transform infrared spectroscopy (FTIR), X-ray diffractometer (XRD), differential scanning calorimetry (DSC), thermogravimetric analysis (TGA), polarized optical microscope (POM) and direct current (dc) conductivity measurements. FTIR, XRD, DSC and TGA measurements were carried out using dried and milled samples of polymers and composites in order to describe their structural properties. For POM studies, PNVCz/graphite and PNVCz/carbon nanotube composites were dissolved in dichloromethane to give the 4.0 g/L solutions. After casting onto a microscope slide glass, they were dried under vacuum to obtain coatings for polarizing microscope observations. All the samples used for dc electrical-conductivity measurements were in the form of compressed pellets (13 mm in diameter and about 0.2 mm in thickness) obtained by applying a hydraulic pressure of about 10 MPa. The pellets were placed between two identical

Pt electrodes in a conductivity cell. The slope of the potential vs current plots in the range of 1.0 – 10.0 V yields the resistance (Keitley picoammeter Model 6487). The conductivities of PNVCz matrix and its composites with graphite layers and carbon nanotubes were evaluated from the surface resistance by means of Meter Scan Scientific software. The conductivity measurements were evaluated as a function of conducting filler type and content along with preparation method and the type of organic matrix in the composite.

FTIR spectra of the samples were recorded on Perkin Elmer Spectrum One (FTIR-reflectance, Universal ATR with diamond and ZnSe) spectrophotometer using the samples in powder form. XRD patterns were obtained by Bruker X-ray diffractometer (XRD), a conventional copper target X-ray tube set to 40 kV and 40 mA. The X-ray source was CuK α radiation ($\lambda = 0.154$ nm). Data were collected from 2θ of 2.00° to 40.00° (θ being the angle of diffraction) with a step width of 0.02° and step time of 12 s, scanning speed of $0.1^\circ/\text{min}$. Optical micrographs were taken with a Leica DM-2500P model polarized optical microscope, under cross-polarized light conditions. DSC was performed on a Metler Toledo DSC-821 under a continuous flow of nitrogen (60 mL/min). All the samples (about 10 mg in weight) were heated from 40°C to 250°C and the thermograms were recorded at a heating rate of $10^\circ\text{C}/\text{min}$. After cooling to 40°C , heating procedure was repeated. The glass transition temperatures (T_g) of the samples were selected as the middle point of the transition region at the respective curves. The thermal stability was investigated by TGAQ600 instrument (TA Instrument) at a heating rate of $10^\circ\text{C}/\text{min}$ under dry air atmosphere. In each case, the sample was examined at an air flow rate of 100 ml/min at temperatures ranging from 40°C to 700°C .

5.3 Results and discussion

5.3.1 XRD patterns of PNVCz/ graphite and PNVCz/carbon nanotube composites

X-ray diffraction patterns of o-GLs, MWCNT and their composites prepared by in-situ preparation and solution blending processes are shown in Figures 5.7 and 5.8, respectively.

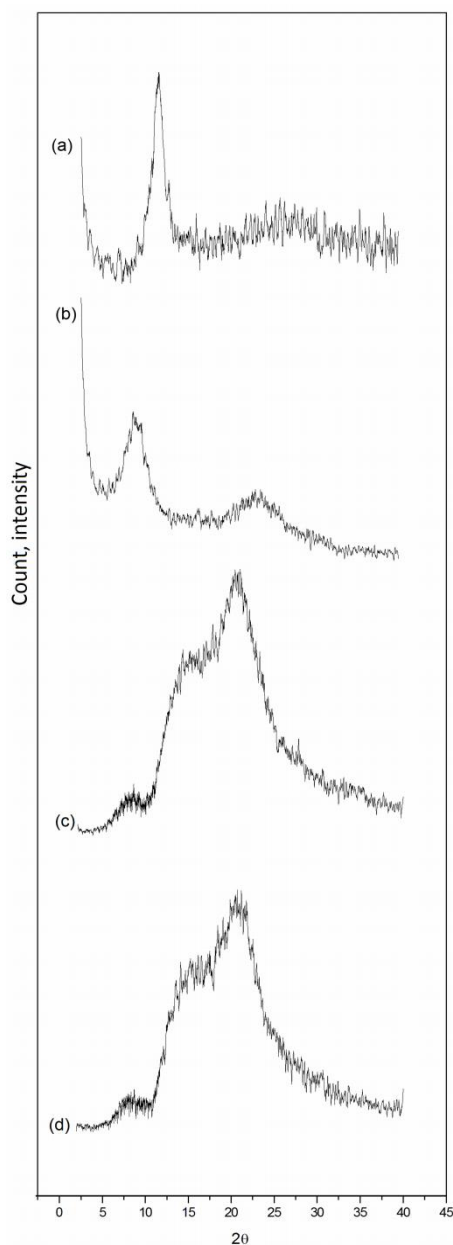


Figure 5.7: XRD patterns of (a) o-GLs, (b) PNVCz initiated with CAN and, PNVCz/o-GLs composites prepared by in-situ polymerization (c) without CAN and (d) with CAN as oxidant, respectively.

The characteristic diffraction peak of o-GLs appears at around 2θ value of 10° as shown in Figure 5.7a. It can be seen from Figure 5.7c and 6. 7d that the sharp peak of o-GLs shifts to ca. 14° . On the other hand, the one of the peaks of PNVCz (Figure 5.7b) shifts to lower degree while the other becomes very weak . It supports the presence of the electrostatic interactions between functional groups of o-GLs and NVCz that polymerize around and/or on the layers in ACN/water mixture containing SDS molecules. In another words, the broad peak from 10° to 22°

indicates that most of the NVCz adsorbed onto the oxidized graphite layers and was polymerized in situ to form composite materials (Figure 5.6).

XRD patterns for MWCNT, PNVCz, P(NVCz-co-MCeI) and their composites prepared by solution blending in THF (carbon nanotube content = 1.0 and 15.0 wt %, based on polymer) are shown in Figure 3.28. Both homopolymer and copolymer of NVCz clearly illustrated two diffraction peaks at $2\theta = 7.5^\circ$ and 23.5° , while the MWCNT demonstrated the diffraction peak at $2\theta = 26^\circ$. The three peaks appeared at different locations ($2\theta = 12.5^\circ$, 17.5° and 22.5°) in the PNVCz/MWCNT composites (Figure 5.8c and 5.8e) also clearly support that the introduction of PNVCz affects the structure of both MWCNTs and PNVCz chains. These three diffraction peaks may be an indication of the crystalline behavior of PNVCz.

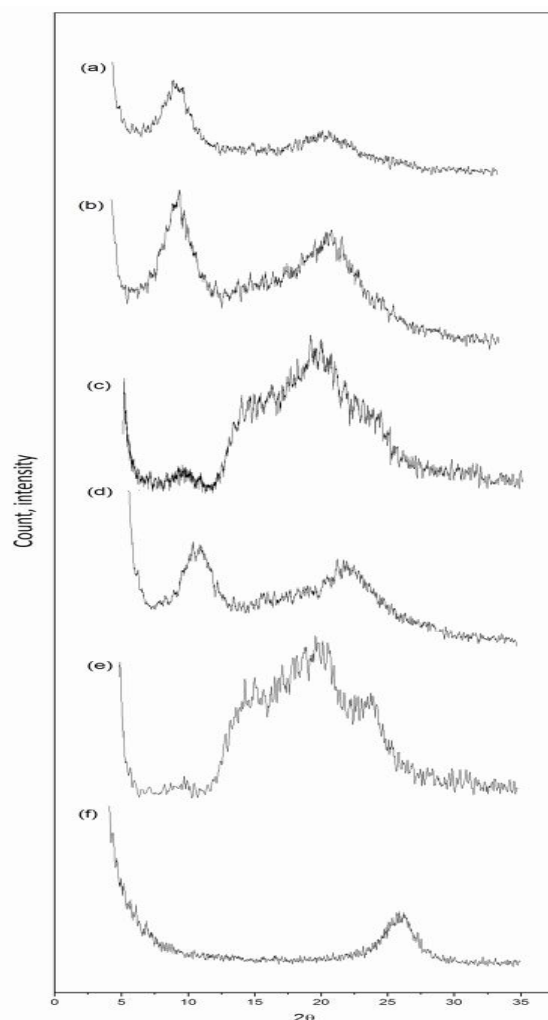


Figure 5.8: XRD patterns of (a) P(NVCz-co-MCeI), (b) and (c) P(NVCz-co-MCeI)/MWCNT (1.0 and 15.0 wt %, respectively) composites prepared by solution blending, (d) and (e) PNVCz(initiated with CAN)/MWCNT (1.0 and 15.0 wt %, respectively) composites prepared by solution blending and (f) MWCNT.

5.3.2 Morphological image studies of PNVCz/graphite and PNVCz/carbon nanotube composites

Figures 5.9 and 5.10 show the POM micrographs of the PNVCz /o-GLs and PNVCz / MWCNT composites from the cross polarized views. It is understood that the type of composite preparation method is an important parameter for the dispersion and orientation of filler particles in the composites. In these experiments, both ultrasonic bath and high power sonic tip was employed to promote their optimal dispersion in the composites prepared by in-situ polymerization (Figure 5.9) and solution blending (Figure 5.10) processes.

SDS is an anionic surfactant containing a sulphate hydrophilic group and a long hydrocarbon chain as hydrophobic segment. The alkane groups of SDS prefer to adsorb on the o-GL surfaces while the repulsive forces between the oxidized functional groups increase the interlayer distances and so, the charge transfer between oxidized layers and NVCz monomer may be possible to create cation radical and initiate in-situ polymerization without an additional oxidant in the SDS-adsorbed o-GL dispersions (Scheme 5.6). Insufficient surfactant (in this study, SDS < 10 wt %) can reduce the electrostatic repulsion between the same charged groups and consequently, an inefficient SDS adsorption on the oxidized graphite layers prevents the in-situ polymerization of NVCz without CAN in ACN/water mixture (Table 3.16).

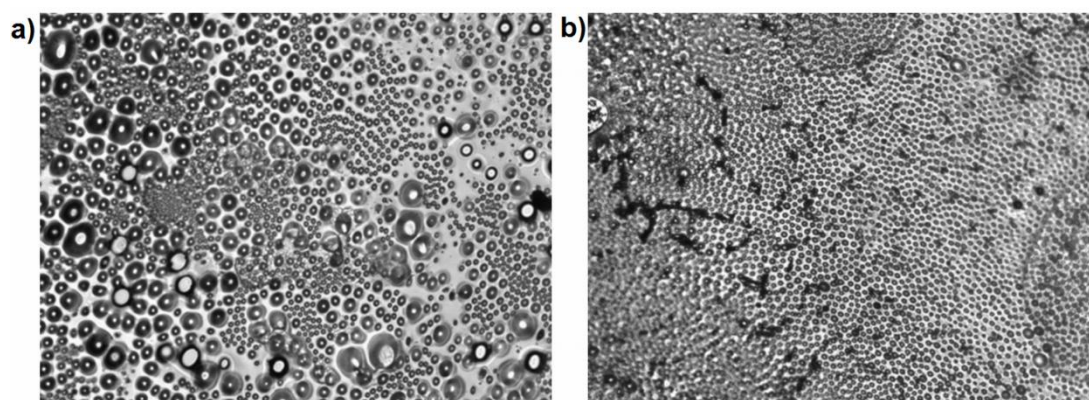


Figure 5.9: Polarizing microscope images of PNVCz/o-GLs composites prepared by in situ polymerization method in ACN/water mixture (a) without CAN in the presence of 10.0 wt % of SDS and (b) with CAN in the presence of 1.0 wt % of SDS, respectively.

Images of PNVCz/o-GL composites taken with POM are shown in Figures 4a and 4b. It is seen that their morphologies are different from those of the PNVCz/

MWCNT composites prepared by solution blending method in the absence of SDS in THF (Figure 5.10).

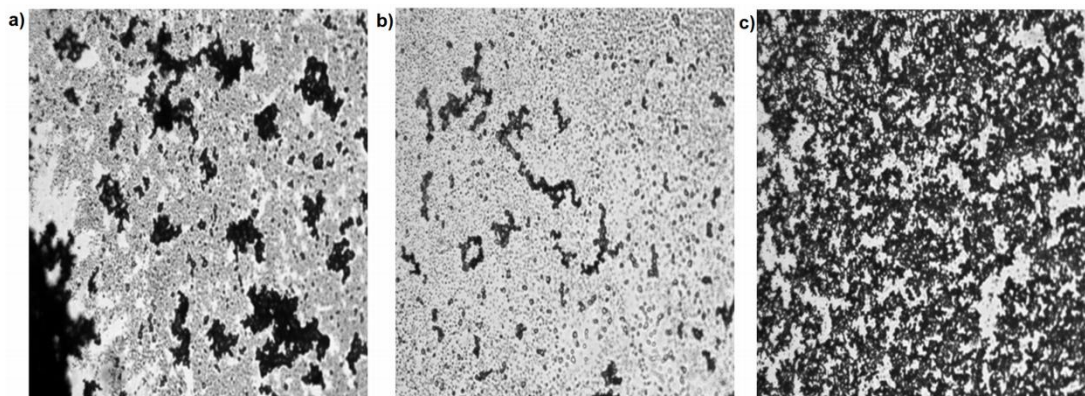


Figure 5.10: Polarizing microscope images of (a) PNVCz/MWCNT, (b) P(NVCz-co-MCeI)/MWCNT and (c) P(NVCz-co-MCeI)/o-GLs composites prepared by solution blending method in THF containing 1.0 wt % o-GLs.

In the case of Figure 5.9a, NVCz polymerizes without the addition of an oxidant in the presence of o-GLs containing 10 wt % SDS. It can be considered that the solubilization of NVCz in the areas surrounded by SDS molecules stabilize its cationic radicals because catalytic efficiency of SDS increase with increase in SDS concentration. The formation of PNVCz chains in the absence of CAN proceeds only for 10 wt % of SDS but not for 1.0 and 5.0 wt % and, this observation also supports the effect of SDS concentration on the stability of NVCz radicals. However, the image (a) in Figure 5.9 exhibits that the higher content of SDS and absence of CAN during in-situ polymerization results in the formation of much more heterogeneous globular structure compared with the one initiated with CAN in the presence of 1.0 wt % of SDS.

The POM images in Figure 5.10 of the PNVCz/MWCNT, P(NVCz-co-MCeI)/MWCNT and P(NVCz-co-MCeI)/o-GLs composites containing 1.0 wt % of MWCNT and o-GLs reflect the positive effect of the long alkyl chain on the compatibility, and the micrographs support the discussions based on their T_g results in Figure 5.12. The white phases indicate PNVCz or its copolymer with MCeI. It is clearly seen that the polymer/MWCNT composite containing MCeI with long hydrophobic tail has more homogeneous morphology as compared to the others. It might be resulting from the strong hydrophobic interactions between the surfaces of unoxidized MWCNTs and the cetyl groups that promote the formation of more

homogeneous structures. The long alkane groups also provide external steric repulsion to help the particles overcome the attractive van der Waals force at contact (36). As a conclusion, the copolymer containing a straight hydrophobic chain and a hydrophilic $-\text{COOH}$ group can modify the interfaces in the dispersion medium of the untreated MWCNTs and prevent their aggregation.

On the other hand, the graphite content in Figure 5.9c seems to be much higher than the polymer content in the P(NVCz-co- MCEI)/ MWCNT composite in Figure 5.9b, where black areas represents graphite layers. As to the cross-polarized views, the bottom of the composite film contains much higher graphite layers than its upper portion. It may be attributed to that the electrostatic repulsive interactions between carboxyl groups of monocetyl itaconate and oxidized graphite layers are stronger than the hydrophobic interactions resulting from the cetyl groups on the copolymer chains.

5.3.3 Glass transition behavior of PNVCz/ graphite and PNVCz/carbon nanotube composites

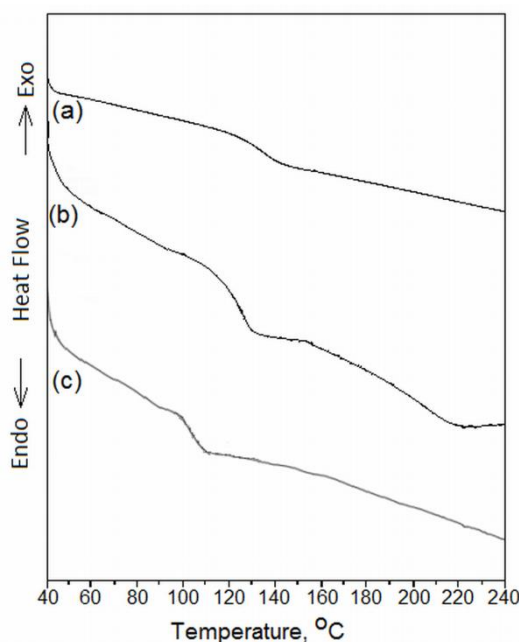


Figure 5.11: DSC thermograms of (a) PNVCz prepared by oxidative polymerization, (b) and (c) PNVCz/o-GLs composites prepared by in situ polymerization method in ACN/water mixture with CAN in the presence of 1.0 wt % of SDS and without CAN in the presence of 10.0 wt % of SDS, respectively.

In Figure 5.11, the difference between the DSC thermograms of PNVCz initiated with CAN(a) and PNVCz/o-GLs composites prepared by in-situ polymerization in the presence of SDS with and without CAN (b and c, respectively) are compared. The glass transition temperatures of PNVCz, PNVCz/o-GLs/SDS/CAN (b) and PNVCz/o-GLs/SDS (c) are 136, 104 and 122° C, respectively. The reason for the increase in T_g of the composite (c) as compared to the composite (b) might be the influence of both the chain length increase of PNVCz and the strong hydrogen bonds between PNVCz chains and o-GLs.

Figure 5.12 shows the DSC curves of PNVCz/MWCNT composites prepared by solution blending process in THF. It was found that the T_gs of PNVCz after being added a 1.0 wt % of MWCNTs strongly decreased comparing with pristine polymer whereas the T_g of the composite based on the copolymer of NVCz with monocetyl itaconate slightly increased. These results were attributed to the characteristics of the composites and indicated that the quality of dispersion shifted T_g but the direction of shifts were dependent on the intermolecular interactions between the MWCNTs and polymer chains. As to the DSC thermograms in Figure 5.12, the compatibility between PNVCz and MWCNT were highly improved by the addition of 5.0 mol % of MCEI, bearing a long hydrophobic chain and a hydrophilic group, to the PNVCz chains. In another words, there are repulsive interactions between MWCNTs and the homopolymer of NVCz and therefore, an increase in free volume and chain mobility are created near the MWCNTs. Consequently, The T_gs of the homopolymers of NVCz shift to lower temperatures with the addition of carbon nanotubes because it takes less energy to transition from the glassy state to the rubbery one.

Both the T_g values of the PNVCz/o-GLs composites prepared by in-situ polymerization method and the thermograms of the PNVCz/MWCNT composites prepared by solution blending process (Figures 5.11 and 5.12) indicates that the T_g depression origin is not only the dispersion state of the conducting fillers in the PNVCz matrix. The molecular structure of PNVCz chains and the initiation mechanism of in-situ polymerization process during the preparation of composite materials also have an important role on their thermal characteristics.

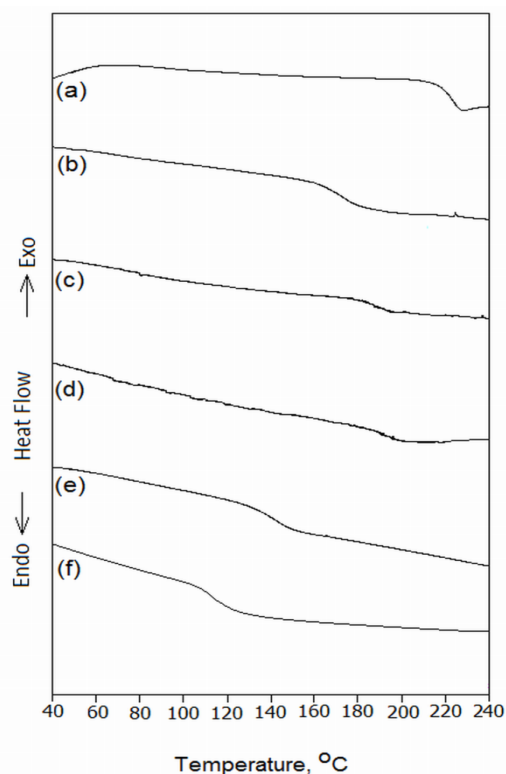


Figure 5.12: DSC thermograms of PNVCz initiated with AIBN and PNVCz/MWCNT composite (a,b), P(NVCz-co-MCeI) initiated with AIBN and P(NVCz-co-MCeI)/MWCNT composite (c, d), PNVCz initiated with CAN and PNVCz/MWCNT composite (e, f) (preparation method = solution blending in THF; filler content = 1.0 wt %).

5.3.4 Thermal Stability of PNVCz/carbon nanotube and PNVCz/ graphite composites

A series of thermal tests on PNVCz, its copolymer and composites with MCeI and two type of conducting fillers, respectively were performed. The TGA curves for PNVCz, PNVCz/MWCNT and PNVCz/o-GL composites under air flow are shown in Figures 5.13 and 5.14.

TGA thermograms of PNVCz/o-GLs composites synthesized by in-situ polymerization process in the presence and absence of CAN as initiator are illustrated in Figure 5.13. They show weight loss as a function of temperature under air atmosphere. The major weight losses for PNVCz/o-GLs initiated with CAN are observed in the range of 200-480°C while in the case of the PNVCz/o-GLs and PNVCz obtained without and with CAN as oxidant, respectively, the onset degradation temperatures shift toward a higher temperature and, their weight loss in

the range of 280-480°C are slower than the ones synthesized with CAN. This may be due to the molecular weight decrease of PNVCz in the PNVCz/o-GLs materials initiated with CAN.

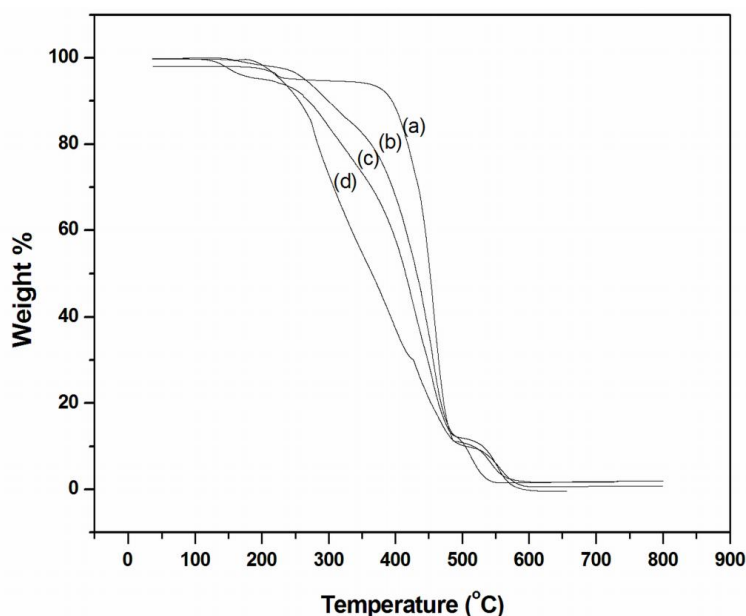


Figure 5.13: TGA thermograms of poly(N-vinyl carbazole)s initiated with AIBN and CAN (a, b), PNVCz/o-GLs composites prepared by in situ polymerization method in ACN/water mixture without CAN in the presence of 10.0 wt % of SDS (c) and with CAN in the presence of 1.0 wt % of SDS (d), respectively, under air atmosphere.

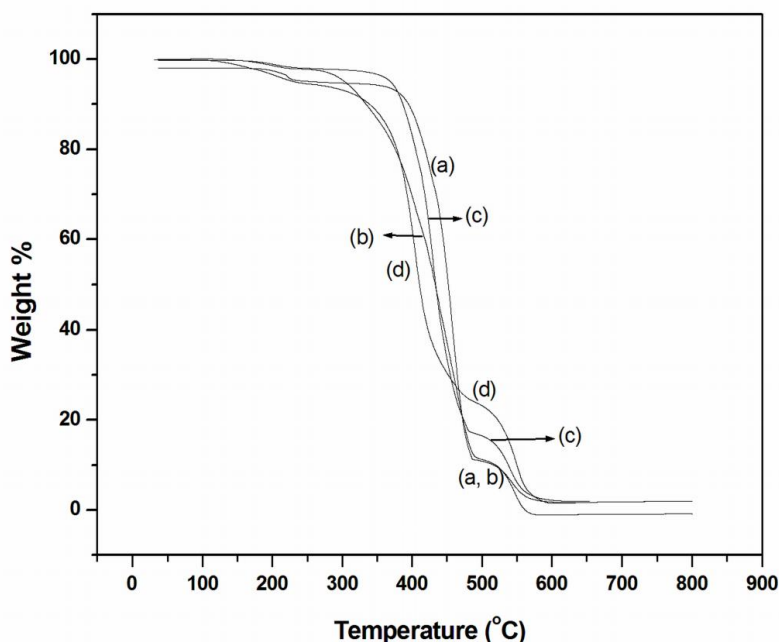


Figure 5.14: TGA thermograms of PNVCz and P(NVCz-co-MCeI) initiated with AIBN (a, b) and, PNVCz/MWCNT and P(NVCz-co-MCeI)/MWCNT composites under air atmosphere (preparation method = solution blending in THF; filler content = 1.0 wt %).

The onset degradation temperatures of PNVCz and P(NVCz-co-MCeI) polymers initiated with AIBN (450°C) were higher than the one synthesized in the presence of CAN (280°C). This may be due to the formation of high molecular weight polymer chains with AIBN as initiator in dioxane at 50°C. On the other hand, the lower onset degradation temperatures of the composites prepared by solution blending process compared to the pure PNVCz and P(NVCz-co-MCeI) may be due to the weak intermolecular interactions between PNVCz chains and unmodified MWCNTs. However, the higher thermal stability of P(NVCz-co-MCeI) /MWCNT composite than pristine polymers and PNVCz/MWCNT composite, in the higher temperature region (above 480°C), is related to the presence of P(NVCz-co-MCeI) chains, being strongly interacted with thermally stable MWCNTs.

5.3.5 Electrical conducting properties of PNVCz/carbon nanotube and PNVCz/graphite composites

Figure 5.15 shows the electrical conductivity of PNVCz/o-GL and PNVCz/MWCNT composites versus filler content. At low filler content less than 0.05 wt % for o-GLs and 0.50 wt % for MWCNTs, the conductivity was lower than 10^{-8} S/cm, resembling that of an insulator. At slightly higher filler concentration, the composites change from an insulator to nearly a semiconductor. This means that by varying the conducting filler content in PNVCz composites their electrical conductance behaviors can be controlled and conductivities are enhanced by 6 orders of magnitude with the increase in MWCNT content from 0 to 2.0 wt %, except the ones containing o-GLs.

The electrical conductivity of PNVCz prepared by chemical oxidative polymerization using CAN as initiator in ACN/water mixture containing 1.0 wt % of SDS was higher than the ones synthesized by using AIBN and CAN as initiator in dioxane and in ACN, respectively, in the absence of SDS. Therefore SDS, which is used to obtain homogeneous dispersions of o-GLs in ACN/water media, was considered as dopant for PNVCz chains and by addition of 0.24 vol. % of o-GLs, its conductivity increased to 10^{-6} S/cm. The electrical conductivity of PNVCz/o-GLs composite prepared by in-situ polymerization process without initiator in ACN/water/SDS (10.0 wt %) mixture also had nearly same value with the one synthesized with CAN (Figure 5.15c).

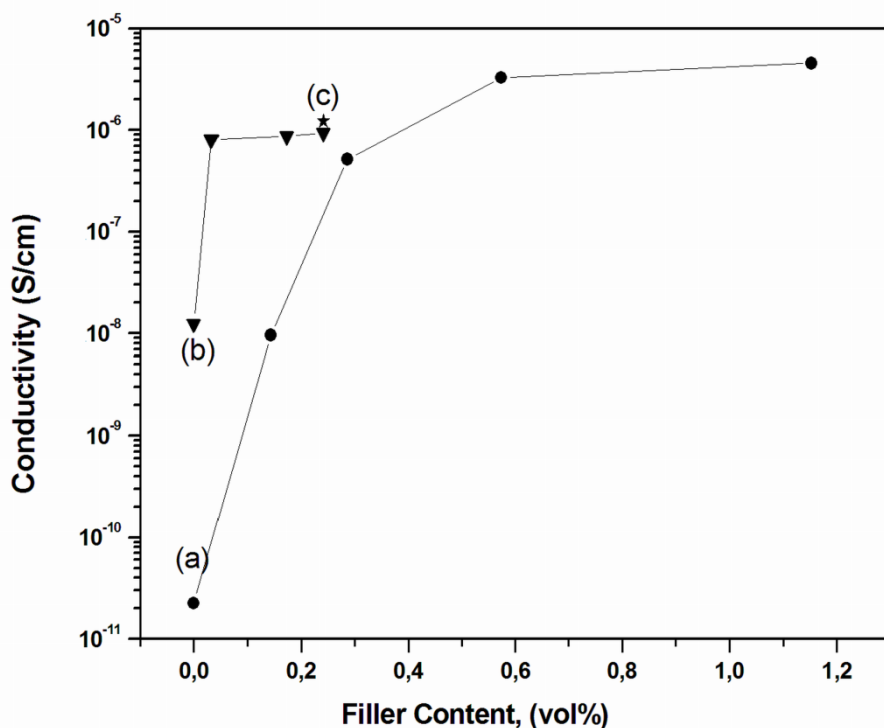


Figure 5.15: Electrical conductivities plotted as a function of filler volume fraction: (a) PNVCz/MWCNT composites prepared by solution blending, (b) PNVCz/o-GLs/SDS/CAN composites prepared by in situ polymerization and (c) PNVCz/o-GLs/SDS composite prepared by in situ polymerization.

The conductivity at room temperature of the PNVCz/MWCNT composites prepared by solution blending is shown in Figure 5.15 as a function of the weight fraction of the MWCNTs. The conductivities of PNVCz initiated with AIBN (a) and CAN (c), and P(NVCz-co-MCcl) initiated with AIBN (b) are 2.1×10^{-13} , 2.3×10^{-11} and 3.2×10^{-10} S/cm, respectively. According to the percolation theory, the percolation threshold corresponds to the onset of the transition from an insulator to a semiconductor (37, 38). At low MWCNT content less than 0.12 vol %, the conductivities resemble to that of an insulator. Between 0.24 and 0.95 vol % of filler, the composites exhibit smooth transition from insulator state to semi-conducting region and then at higher concentrations than 0.95 vol %, their conductivities reach 10^{-6} - 10^{-5} S/cm and steady-state region occurs, which are consistent with that of a semiconductor.

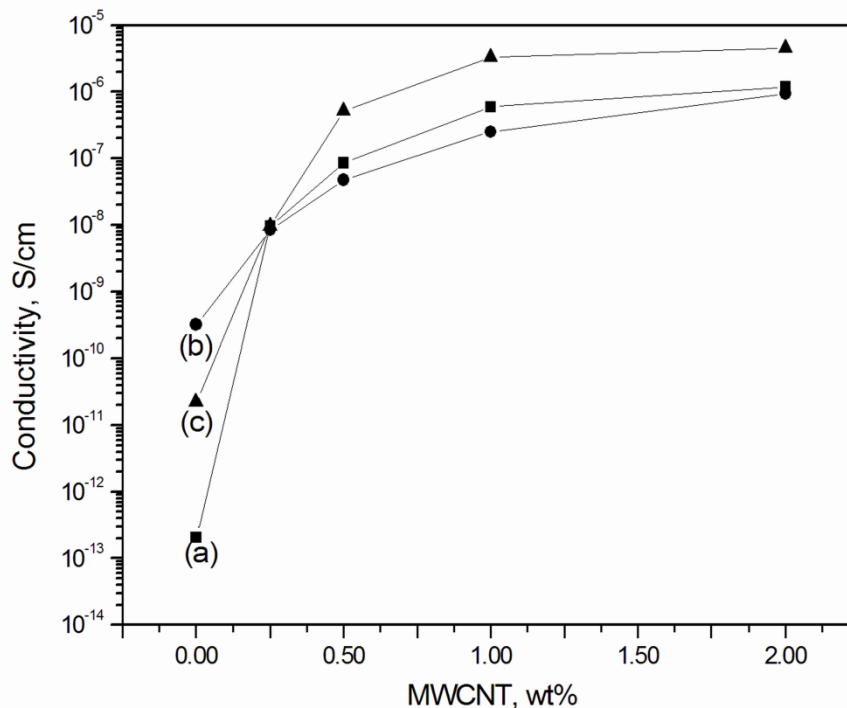


Figure 5.16: Electrical conductivities plotted as a function of MWCNT weight fraction: (a) PNVCz (initiator: AIBN) /MWCNT, (b) P(NVCz-co-MCeI) (initiator: AIBN)/MWCNT and (c) PNVCz (initiator: CAN) /MWCNT composites prepared by solution blending method in THF.

5.3.6 Proposed polymerization mechanisms for PNVCz/o-GL and PNVCz/o-MWCNT composites

The oxidized graphite is a strongly oxygenated, highly hydrophilic layered material (Figure 5.16). In this study, it was dispersed in ACN/water mixture containing SDS. The oxidative polymerization of NVCz initiated with CAN in the presence or absence of SDS resulted in the formation of white-colored and insulating PNVCz chains (Scheme 5.3) while NVCz monomer and o-GLs/ACN/water/SDS(10 wt %) dispersion at room temperature produced PNVCz/o-GLs composite by in situ polymerization method without oxidant. In the last case, the polymerization mechanism between the dispersion of o-GLs and NVCz in the presence of 10.0 wt % of SDS is not clear. The ratio of SDS molecules with oxidized graphite layers seems to be a critical condition to initiate the in-situ polymerization without CAN. To check the effect of SDS concentration on the NVCz polymerization in the presence of oxidized graphite layers, polymerization was repeated for both 1.0 and 5.0 wt % of SDS, under the same experimental conditions. However, there was no observed precipitation of PNVCz in o-GLs/ACN/water mixture, suggesting that SDS content

has effected to initiate the polymerization of NVC monomer. It is assumed that during sonication, SDS molecules help to disperse o-GLs, and afterwards they are adsorbed on the surfaces of o-GLs and prevent the aggregation of graphite layers by repulsive forces and then, the direct interaction of NVCz, being an electron donor molecule with the graphite layers (sonicated and so strongly activated, and decorated with functional groups) creates charge transfer between them (Scheme 5.5).

FTIR spectra of the composites prepared by in-situ polymerization of NVCz with oxidized fillers in the absence of CAN are shown in Figure 5.17. Apart from the characteristic bands of PNVCz (1600 –1450 cm^{-1} for aromatic stretching and aromatic –CH in plane bending, and 750 cm^{-1} for aromatic –CH out of plane bending), the presence of the peaks around 1750 cm^{-1} and 3450 cm^{-1} , which are attributed to the o-GLs also confirms the formation of PNVCz/o-GLs composite without CAN (Figure 5.17c).

A similar mechanism is proposed for NVCz-acid treated o-MWCNT pairs in the absence of both SDS and CAN.

The oxidation of the MWCNTs also generates polar groups such as O–H and C=O on the tube surfaces (Figure 3.36b). Due to the strong electron-withdrawing ability of o-MWCNTs, they can form charge transfer complexes with NVCz molecules. It is considered that the activation of o-MWCNTs by means of sonication rather than the functional groups on the walls has a driving force to initiate the in-situ polymerization without the addition of an oxidant. Further, acid-treated MWCNTs form strong intermolecular interactions, based on mainly hydrogen bonding along with van der Waals force, with the polymer chains. Therefore, after the formation of PNVCz chains, the possible intermolecular interactions between the carbazole groups of PNVCz chains and the carboxyl groups of o-MWNTs may cause PNVCz polymer chains to be adsorbed at the surfaces of the o-MWNTs (Scheme 5.5).

Figure 5.6a and 5.6b show the FTIR spectra of PNVCz/o-MWCNT composite prepared by in-situ polymerization process and mainly PNVCz portion extracted from PNVCz/o-MWCNT composite after the polymerization without both SDS and CAN, respectively. From these spectra, it is seen that the intensities of the characteristic peaks of o-MWCNT in the case of the PNVCz/o-MWCNT composite are higher than those of the extracted portion. This observation indicates the heterogeneous distribution of weakly-coated PNVCz/o-MWCNTs and strongly-interacted PNVCz/o-MWCNTs systems.

6. ELECTROCHEMICAL IMPEDANCE SPECTROSCOPY AND IN-SITU UV-vis SPECTROELECTROCHEMISTRY STUDIES OF POLY DIMETHYL SILOXANE / POLY(N-VINYL CARBAZOLE) COMPOSITE SYSTEMS

6.1. Experimental

N-vinylcarbazole (NVCz; Aldrich) was used as received. Acetonitrile (ACN, LabScan), tetrabutyl ammonium tetrafluoroborate (TBABF₄), tetrahydrofuran (THF), dichloromethane (DCM) and hydroxyl terminated polydimethylsiloxane (PDMS; 1,800-2,200 cSt and 35,000 g/mol) were purchased from Sigma-Aldrich.

6.1.1 Electrochemical Polymerization and EIS Measurements

Cyclic voltammograms (CVs) of the working electrodes were obtained between 0.0 to 1.2 V at the scan rate 50 mV/s by using a Gamry Reference 600 potentiostat (Gamry Instruments, Warminster, PA, USA). A three-electrode cell containing Pt or GC disc electrodes that have geometric surface areas of 0.02 and 0.07 cm², respectively, as the working electrodes, a Pt wire as the counter electrode, and a silver (Ag) wire as the pseudo-reference electrode were used for all electrochemical characterizations.

PNVCz was deposited on Pt and GC electrodes by electropolymerization from ACN + 0.1 mol/L TBABF₄ system containing 5.2 x 10⁻² mol/L NVCz. All solutions were purged with nitrogen just before coating experiments.

The 5.0, 10.0 and 15.0 wt % solutions of PDMS in THF at 25°C were deposited on GC bare electrode. To prepare spin-coated electrodes by dropwise method, the solution drops were placed onto the electrodes using Pasteur pipette and then fixed by spin-coating with a rotation rate of 2500 rpm. The electrodes were dried under vacuum for 12 hours. Then, the GC/PDMS electrodes were electrochemically coated with NVCz. The obtained bilayer (or composite) electrodes were referred as GC/PDMS/PNVCz.

Pt / PDMS / PNVCz electrodes were prepared by PDMS coating at both 25°C and -15°C, and then NVCz electropolymerization at three different temperatures (-15°C, 0°C and 25°C) to observe the temperature effect on the bilayer-coating efficiency.

Pt/PNVCz, GC/PNVCz, Pt/PDMS/PNVCz and GC/PDMS/PNVCz electrodes in monomer-free (MF) ACN containing 0.1mol/L NaClO₄ were studied by potentiostatic EIS set to 0.0 V as open circuit potential. EIS measurements were conducted using a Gamry Reference 600 potentiostat in a frequency range from 10 kHz to 10 mHz and, the voltage amplitude was equal to 10 mV. It was assumed that at this offset, there would not be any current due to dc polarization and, in the case of bilayer coatings, the frequency dispersion was modeled as a constant phase element (Q_{CPE}) due to surface inhomogeneity.

In situ UV-vis spectroelectrochemistry studies were carried out using a HITACHI U-0080D model spectrometer and an electrochemical analyzer (CH Instruments). In order to study the electronic structures of the obtained PNVCz and PDMS/PNVCz coatings, they were oxidized from 1.0 x 10⁻³ g/ mL NVCz solution in ACN + 0.1 M NaClO₄ system, by using indium-tin oxide (ITO) coated glass electrode and Ag wire as working and reference electrodes, respectively. PNVCz films were polymerized potentiostatically at 1.2 V. After the PNVCz films coated on ITO and ITO/PDMS electrodes were rinsed with MF electrolyte solution, in-situ UV-vis spectra were recorded in MF electrolyte solution between 0.0 V and 2.0 V.

6.2 Results and discussion

Electrochemical impedance spectroscopy (EIS) is an effective method for the characterization of semiconductors, corrosion, solid-state devices and electrochemical power sources.

A semiconducting polymer synthesized or characterized by an electrochemical method uses an electrochemical cell with an appropriate electrolyte and necessary electrodes. EIS method uses three electrode system: reference electrode, working electrode and counter electrode. Supporting electrolyte is added to the test solution to ensure sufficient conductivity. The combination of the solvent, electrolyte and specific working electrode material determines the range of the potential. The reactions taking place across the electrode/electrolyte interfaces are interpreted in terms of an equivalent circuit.

In this work, two types of working electrodes were used to observe the effect of electrode material. GC and Pt electrodes were chosen as working electrodes. Ag and Pt wires were used as reference and counter electrodes, respectively. TBABF₄ and NaClO₄ were chosen as supporting electrolytes during the electropolymerizations and EIS measurements of NVCz monomer, PDMS/NVCz mixtures and PNVCz, PDMS/PNVCz coated electrodes in ACN, respectively. The frequency range was extended from 10 mHz to 10 kHz at an amplitude of 10 mV. The real and imaginary components of the EIS in the complex plane were analyzed using the ZsimpWin (version 3.10) software to estimate the parameters of the equivalent electrical circuit.

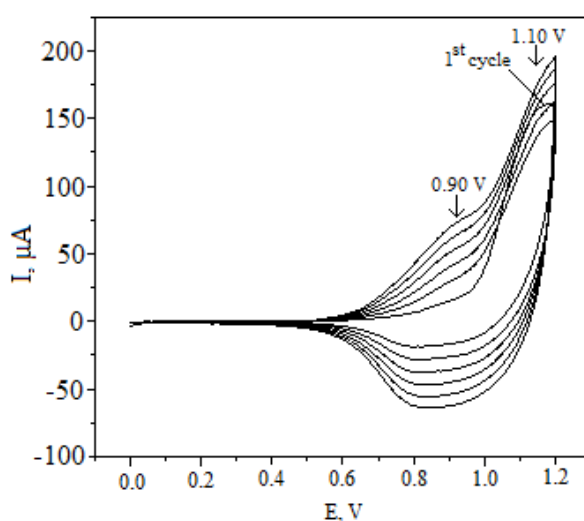


Figure 6.1: Cyclic voltammogram of NVCz in 0.1mol/L TBABF₄+ACN at 50mV/s scan rate on PDMS (5.0 wt %) coated Pt electrode.

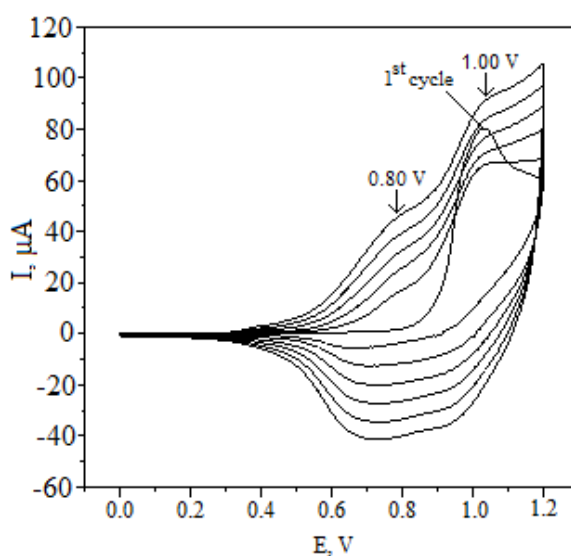


Figure 6.2: Cyclic voltammogram of NVCz in 0.1mol/L TBABF₄+ACN system at 50mV/s scan rate on PDMS (5.0 wt %) coated GC electrode.

The electrochemical behaviors of PNVCz/PDMS composite electrodes were recorded by cyclic voltammetry. Typical CVs of the electropolymerizations of NVCz on PDMS/Pt and PDMS/GC electrodes are shown in Figures 6.1 and 6.2.

Despite the insulating property of PDMS, NVCz was polymerized electrochemically on the PDMS/Pt and PDMS/GC disc electrodes. As can be seen from the indicated Figures, in the presence of PDMS coating, the oxidation peak in the first cycle was appeared at about 1000 mV, being higher anodic potential than that of pure PNVCz at 800 mV. Then, it was replaced with two reversible peaks recorded at 800 mV and 1000 mV for PDMS/GC electrode and at 900 mV and 1100 mV for PDMS/Pt electrode. In both voltammograms, current responses of the polymer redox processes increased upon repeated scanning. In addition, as PNVCz was being polymerized, the transparent PDMS films on Pt and GC disc electrodes turned to green and, the electrochemical processes were proceeded to form electroactive films, including conductive form of PNVCz. Further, in the case of PNVCz/PDMS/Pt electrode, the anodic peaks appeared at slightly higher potentials than that of the electropolymerization of NVCz on PDMS coated GC electrodes indicated that the electron transfer processes were dependent on the electrode material (27).

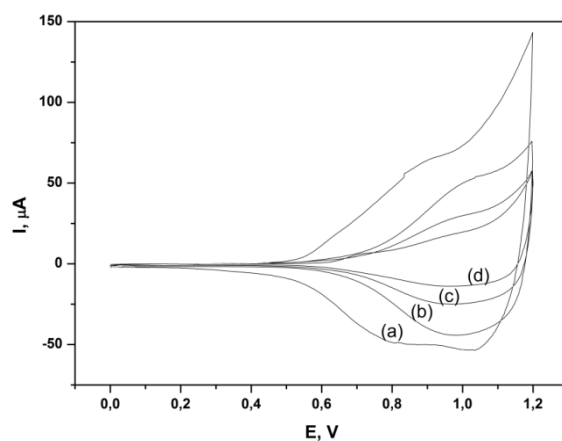


Figure 6.3: Cyclic voltammograms of (a) GC/PNVCz, (b) GC/PDMS(5.0 wt %)/PNVCz, (c) GC/PDMS(10.0 wt %)/PNVCz and (d) GC/PDMS(15.0 wt %)/PNVCz electrodes in MF solution at 50mV/s scan rate (0.1mol/L NaClO₄+ACN system; 25°C was chosen as PDMS coating and NVCz electropolymerization temperatures).

Figures 6.3 and 6.4 illustrate the electrochemical behaviours of PNVCz/PDMS/Pt and PNVCz/PDMS/GC composite electrodes in MF solution. It can be seen that in

the cases of the PNVCz/PDMS layers coated on Pt and GC disc electrodes, the peak current intensities are lower than those of the PNVCz/Pt and PNVCz/GC electrodes.

This means that the presence of the insulating PDMS layer does not completely prevent the interaction between the PNVCz chains and electrode, and the diffusion of ions. It proceeds through the pores and/or interlayer interactions between PDMS and PNVCz (21).

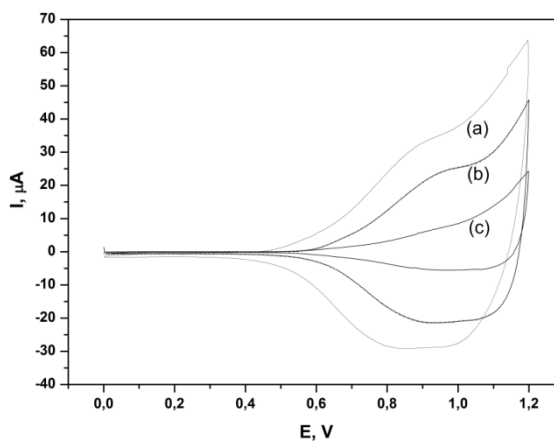


Figure 6.4: Cyclic voltammograms of (a) Pt/PNVCz, (b) Pt/PDMS (5.0 %; 25°C)/PNVCz (25°C) and (c) Pt/PDMS (5.0 %; -15°C)/PNVCz (-15°C) electrodes in MF solution (0.1mol/L NaClO₄+ACN) at 50mV/s scan rate.

Table 1 summarizes the charge, thickness and the weight of the electrochemically active layer, i.e., PNVCz in the PNVCz/PDMS films, depending on the coating temperature of PDMS, electropolymerization temperature of PNVCz and PDMS concentration (in wt/v %). They were calculated from the CVs of both the films obtained with electrochemical polymerization in TBABF₄/ACN and the deposits in an electrolyte solution of 0.1 mol/L NaClO₄ in MF acetonitrile after 6 and 2 cycles, respectively.

The results which are given in Table 6.1 show that in the case of the electrochemical polymerization of NVCz on PDMS coated Pt electrodes there is a direct relation between PDMS content and the film thickness/charge density while for GC electrodes, charge densities are reduced with increasing PDMS concentration at 25°C. The observed inverse relation between PDMS concentration (in wt/v %) and the charges on the coated GC electrode indicates the presence of PNVCz layer coated onto more homogeneous PDMS layer, even if the preparations of the composite electrodes were carried out at 25°C. On the other hand, both the weights and the

charges of the bilayers on Pt electrode was increased with decreasing electropolymerization temperature from 25°C to -15°C, for 5.0 wt % of PDMS whereas when the concentration of PDMS was increased in two times the charge amounts and weights of the films decreased with decreasing electropolymerization temperatures, for PDMS-coating temperature at 25°C, except the ones prepared at -15°C (for both PDMS-spincoating and PNVCz-electropolymerization). PDMS, which is a strongly hydrophobic and viscous material, can interact with both polar and hydrophobic materials either through hydrogen bonding or van der Waals forces (21, 28, 29). Therefore, the increase in both secondary physical interactions indicated above between electrode material and bilayer coatings, and a decrease in the viscosity of PDMS with increasing electropolymerization/coating temperature result in the formation of heterogeneous PDMS layers on Pt electrode.

Table 6.1: The effect of the coating temperature of PMDS, electropolymerization temperature of PNVCz and PDMS concentration on the charge, thickness and weight of the films.

Electrode	Coating Temperature (°C)	PDMS (wt %)	Charge (μC)	Thickness (μm)	Weight (μg)	MF Charge (μC)
Pt	25	-	1551	55.46	1.22	565
Pt	25	5.0	652	23.31	0.51	87
Pt	0	5.0	741	26.49	0.58	194
Pt	-15	5.0	773	27.64	0.61	204
Pt	25	10.0	728	26.03	0.57	96
Pt	0	10.0	708	25.32	0.56	132
Pt	-15	10.0	664	23.74	0.52	158
Pt	-15	5.0	580	20.74	0.46	226
Pt	-15	10.0	837	29.93	0.66	443
GC	25	-	4451	45.47	3.50	779
GC	25	5.0	3644	37.23	2.87	499
GC	25	10.0	3177	32.46	2.49	465
GC	25	15.0	1284	13.12	1.00	252

Scan rate: 50mV/s; Cycle number: 6 (for electropolymerization)

Scan rate: 50mV/s, Cycle number: 2 (for MF solution)

Electrochemical impedance spectroscopy (EIS) measurements were represented with both Bode and Nyquist plots and, appropriate equivalent circuit model was used to correlate the impedance with the capacitance and the resistance of the films.

Figures 6.5-6.8 show Bode and Nyquist plots of bare Pt and GC disc electrodes, PNVCz and PNVCz/PDMS (5.0, 10.0 and 15.0 wt %) coated Pt and GC electrodes. The obtained Bode plots for impedance characterization of the interfaces indicated

the existence of mainly two regions: After a dominant peak in the phase angle at low frequencies, a second peak developed at high frequencies. The Bode phase angles in the intermediate-frequency range for the Pt/PDMS/PNVCz and GC/PDMS/PNVCz composite electrodes show the influence of PDMS layer between electrode surface and PNVCz layer. The peak profiles were dependent on the PDMS content, the coating temperatures of PDMS on electrode surface and the electropolymerization temperature of NVCz on PDMS/Pt electrode.

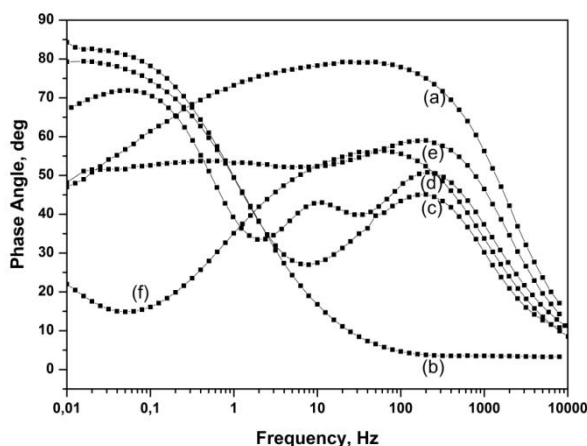


Figure 6.5: Bode phase plots of (a) Pt and (b) Pt/PNVCz , (c) Pt/PDMS (5.0 wt/v % ; 25°C)/PNVCz (25°C), (d) Pt/PDMS (5.0 wt/v % ; 25°C)/PNVCz (0°C), (e) Pt/PDMS(5.0 wt/v % ; 25°C)/PNVCz (-15°C) and (f) Pt/PDMS(5.0 wt/v % ; -15°C)/PNVCz (-15°C) composite electrodes in ACN containing 0.1 mol/L NaClO₄.

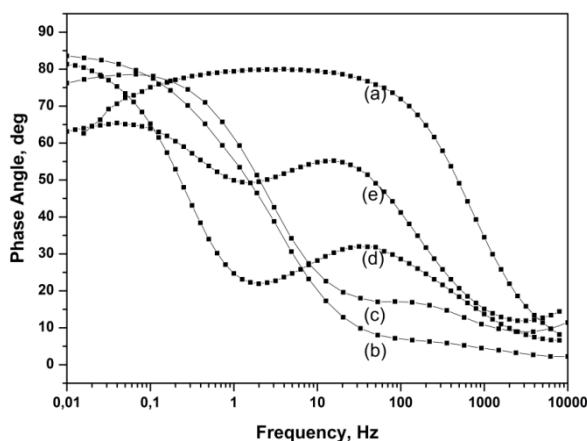


Figure 6.6: Bode phase plots of (a) GC and (b) GC/PNVCz , (c) GC/PDMS (5.0 wt %) /PNVCz, (d) GC/PDMS (10.0 wt %) /PNVCz and (e) GC/PDMS(15.0 wt %) /PNVCz electrodes in ACN containing 0.1 mol/L NaClO₄ at 25°C.

The Bode phase angles of Pt/PDMS/PNVCz and GC/PDMS/PNVCz electrodes prepared at 25°C had limit values at nearly 80° (except GC/PDMS/PNVCz

electrode containing 15.0 wt % of PDMS) in the low frequency region (below 0.10 Hz) while at higher frequencies than 1.0 Hz, the second peak regions, which exhibit the phase angles between 15° and 55° , were observed. It is seen that there is an indirect relation between PDMS content in coating solution and phase angles. These lower phase angles in the first resist and second capacitive regions, which correspond to intermediate frequencies, were probably due to increasing inhomogeneity above the electrodes. The single capacitive region in the case of Pt/PNVCz and GC/PNVCz electrodes was disrupted by a resistive region and so PDMS layered electrodes exhibited two-step capacitive behavior (100-1000Hz and <1Hz). The spectra of the bare electrodes in Figures 6.5 and 6.6 show the phase angles lower than 90° in the 0.10 Hz - 100 Hz region and a plateau that corresponds to a single capacitive behaviour while the Bode plots of bilayer coated electrodes exhibit a second resistor region, indicating electrolyte resistance (R_{sol}) at higher frequency region ($>10^3$ Hz) along with charge transfer resistance R_{ct} in the first resistor region. The first resistive behaviour in the range of 1-100Hz is attributed to the formation of PDMS/PNVCz bilayers that have mainly insulating character. It can also be explained as decrease in the electrolyte penetration through PDMS/PNVCz layers and contact the Pt and GC electrode surfaces.

Bode phase plot in Figure 6.5 show the effect of coating temperature on the electrochemical behaviours of bilayer electrodes. As seen from the indicated plots, Pt/PDMS/PNVCz electrodes form more homogeneous structures, having lower phase angles and higher resistive property with decreasing temperature due to increasing viscosities of the coating solutions containing 5.0 and 10.0 wt/v % concentration of PDMS in THF.

In addition, Figures 6.5 and 6.6 indicate the effect of electrode material together with coating temperature on the composite films. The presence of lower phase angles and more concentrated upper limit for PDMS solutions at 25°C support that the hydrophobic interactions between GC electrode and PDMS layer are more stronger than that of the Pt electrode at the same experimental conditions. The results, calculated by using the CVs in Figures 6.1-6.4 and summarized in Table I, also have similar tendency with the discussions based on phase angles.

The Nyquist plots of PNVCz films and PDMS/PNVCz bilayers coated on Pt and GC disc electrodes are shown in Figures 6.7 and 6.8. Interpretation of the Nyquist

diagrams is usually done by fitting the experimental impedance spectra to an electrical equivalent circuit. That is, an electric circuit combined by some physical elements can be built that has an impedance spectrum identical to that of the electrochemical system under investigation.

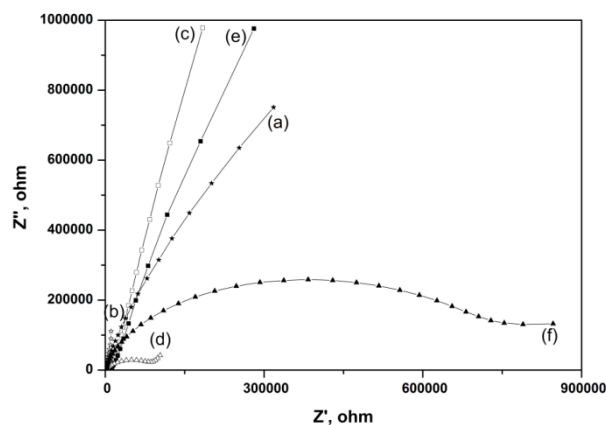


Figure 6.7: Nyquist plots of (a) Pt, (b) Pt/PNVCz, (c) Pt/PDMS(5.0 wt/v % ; 25°C)/PNVCz (25°C), (d) Pt/PDMS(5.0 wt/v % ; -15°C)/PNVCz (-15°C), (e) Pt/PDMS(10.0 wt/v % ; 25°C)/PNVCz (25°C), (f) Pt/PDMS(10.0 wt/v % ; -15°C)/PNVCz (-15°C) electrodes in ACN containing 0.1 mol/L NaClO₄. The points denote the experimental data while the line represents the fitting obtained using the equivalent circuit in Figure 6.9.

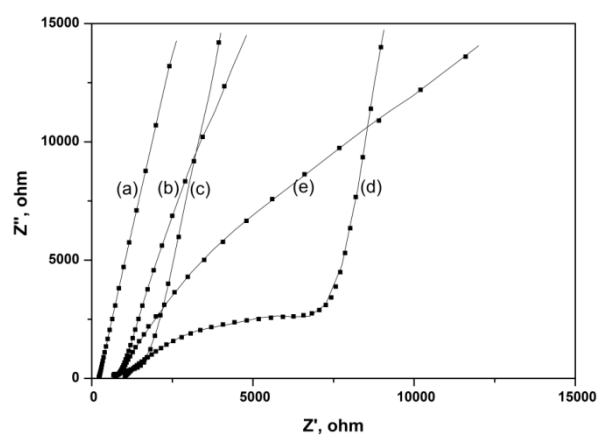


Figure 6.8: Nyquist plots of (a) GC, (b) GC/PNVCz (c) GC/PDMS (5.0 wt %)/PNVCz, (d) GC/PDMS (10.0 wt %)/PNVCz and (e) GC/PDMS(15.0 wt %)/PNVCz electrodes in ACN containing 0.1 mol/L NaClO₄ (25°C was chosen as PDMS coating and NVCz electropolymerization temperatures). The points denote the experimental data while the line represents the fitting obtained using the equivalent circuit in Figure 6.9.

The equivalent circuit in Figure 6.9 represents the Nyquist diagrams in Figures 6.7 and 6.8. In this circuit, R_{sol} is the electrolyte solution resistance, R_{pol} is interpreted as

the resistance of the PNVCz/PDMS bilayer (resulting from the penetration of the electrolyte), $Q_{CPE,pol}$ is the capacitance of the PNVCz/PDMS bilayer-electrode interface, R_{ct} denotes the charge transfer resistance and $Q_{CPE,dl}$ is the double layer capacitance related to the PNVCz/PDMS film-electrolyte interface. The constant phase elements instead of capacitances were introduced to account for the nonideality of the interfaces between bilayer coating and electrode and, between bilayer coating and electrolyte in the impedance spectra because they expressed the distribution of the current density along the bilayer polymeric coatings as a result of surface inhomogeneity.

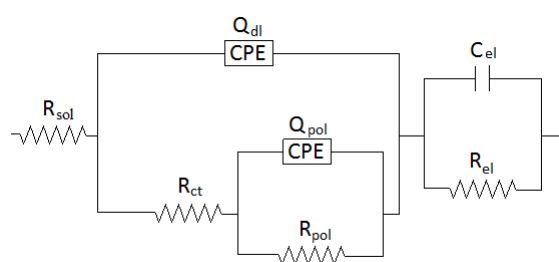


Figure 6.9: Equivalent circuit for PDMS / PNVCz composite electrodes: R_{el} / R_{pol} refer electrode resistance (bare electrode)/bulk resistance (polymer coated electrode). R_{sol} / R_{ct} denote solution/charge-transfer resistances.

The solution resistance R_{sol} , being the first circuit element is placed with a parallel combination of the double-layer capacitance and resistance, Q_{CPE-dl} and R_{ct} . The charge transfer resistance appears in series with the parallel combination of the capacitance ($Q_{CPE-pol}$) and the resistance (R_{pol}) for the interactions between PNVCz/PDMS bilayer coating and electrode material.

In the case of the Nyquist plots in Figures 6.7 and 6.8, the high frequencies semicircle characterizes the PNVCz/PDMS-solution interface while the low frequencies semicircle corresponds to the behaviour of the PNVCz/PDMS-electrode interface. As there was an uncompleted semicircle in the low frequencies part of the spectra, the accuracy of R_{pol} and Q_{pol} values, which correspond to the bulk phase of PDMS/PNVCz bilayers, should be less reliable than R_{ct} and C_{dl} values (Tables 6.2 and 6.3).

The mean error (χ^2) of the fits for impedance spectra of all PNVCz and PDMS modified PNVCz films at 0.0 V along with the GC/PDMS/PNVCz electrode

prepared with 15.0 wt % of PDMS at 25°C and measured at 0.60 V was in the range of 10^{-4} .

Table 6.2: EIS fitting data of PDMS/PNVCz bilayers coated on Pt disc electrode and tested in 0.1 mol/L NaClO₄ + ACN system.

Electrode type	PDMS content (in wt)	Coating temperature (°C)	R _{ct} (Ω)	Q _{dl} (μS.s ⁻ⁿ)	n _{dl}	R _{pot} (Ω)	Q _{pol} (μS.s ⁻ⁿ)	n _{pot}	R _{el} (Ω)	C _{el} (μF/cm ²)	Mean error
PNVCz	-	25	85.3	0.62 μF/cm ^{2*}	-	6.89 x10 ¹²	457.2	0.50	1.35 x 10 ⁶	143.1	8.34 x 10 ⁻⁵
PDMS / PNVCz	5.0	PDMS, 25 PNVCz, 25	1.16 x10 ⁴	1.33	0.79	4.17 x10 ⁵	22.21	0.75	9.99 x 10 ⁶	23.7	1.63 x 10 ⁻⁴
PDMS / PNVCz	5.0	PDMS, 25 PNVCz, 0	8.46 x10 ³	1.30	0.81	8.98 x10 ⁵	9.65	0.69	3.43 x 10 ⁴	24.6	1.88 x 10 ⁻⁴
PDMS / PNVCz	5.0	PDMS, 25 PNVCz, -15	6.64 x10 ³	1.28	0.85	6.49 x10 ⁶	6.69	0.58	4.14 x 10 ³	24.6	3.79 x 10 ⁻⁵
PDMS / PNVCz	10.0	PDMS, 25 PNVCz, 25	1.13 x10 ⁴	1.33	0.79	9.47 x10 ⁵	34.22	0.70	7.82 x 10 ⁶	15.9	1.61 x 10 ⁻⁴
PDMS / PNVCz	10.0	PDMS, 25 PNVCz, 0	1.66 x10 ⁴	2.18	0.82	1.32 x10 ⁶	32.15	0.64	2.97 x 10 ⁶	30.6	3.61 x 10 ⁻⁴
PDMS / PNVCz	10.0	PDMS, 25 PNVCz, -15	1.40 x10 ⁴	1.10	0.87	1.34 x10 ⁶	4.97	0.56	1.54 x 10 ⁶	44.2	3.12 x 10 ⁻⁵
PDMS / PNVCz	5.0	PDMS, -15 PNVCz, -15	1.03 x10 ⁵	0.59	0.94	8.07 x10 ⁵	0.96	0.46	38.2	1.66	4.98 x 10 ⁻⁵
PDMS / PNVCz	10.0	PDMS, -15 PNVCz, -15	4.82 x10 ²	0.77	0.47	9.11 x10 ⁵	0.51	0.95	46.5	2.91	5.13 x 10 ⁻⁵

* It behaves like an ideal capacitor (C_{dl}) in the case of Pt/PNVCz electrode

** The equivalent circuit in Figure 9 was used for data analysis. The value of exponent *n* is related to the roughness of electrode surfaces. *n* = 1 refers an ideal capacitor while its values between 0 and 0.5 denote a resistance and Warburg behavior.

From the EIS fitting data in Tables 6.2 and 6.3, it is seen that the charge transfer resistance, R_{ct} increases while the constant phase element, Q_{CPE-pol} decreases with increasing PDMS content for the GC/PDMS/PNVCz composite electrodes prepared with spincoating and electropolymerization processes at 25°C and, in the case of the

PDMS-coatings at 25°C for the Pt/PDMS/PNVCz composite electrodes when the electropolymerization temperatures decrease, the capacitive behaviour tends to decrease. Q is a constant combining the resistance and capacitance properties of the electrode, and n takes values between 0 and 1.

Table 6.3: EIS fitting data of PDMS/PNVCz bilayers coated on GC disc electrode and tested in 0.1mol/L NaClO₄ + ACN system.

Electrode type	PDMS content (in wt)	Coating temperature (°C)	R _{ct} (Ω)	Q _{dl} (μS.s ⁻ⁿ)	n _{dl}	R _{pol} (Ω)	Q _{pol} (μS.s ⁻ⁿ)	n _{pol}	R _{ct} (Ω)	C _{el} (μF/cm ²)	Mean error
PNVCz	-	25	58.9	0.45 μF/cm ² *	-	2.48 x10 ¹¹	670.7	0.62	6.92 x 10 ⁵	263.0	2.79 x 10 ⁻⁴
PDMS / PNVCz	5.0	PDMS, 25 PNVCz, 25	1.33 x10 ³	23.64	0.59	1.00 x10 ¹⁰	79.39	0.79	1.15 x 10 ⁶	66.7	2.27 x 10 ⁻⁴
PDMS / PNVCz	10.0	PDMS, 25 PNVCz, 25	7.90 x10 ³	10.99	0.64	1.71 x10 ⁶	299.50	0.92	2.97 x 10 ¹⁴	95.6	2.23 x 10 ⁻⁴
PDMS / PNVCz	15.0	PDMS, 25 PNVCz, 25	3.48 x10 ⁴	6.46	0.75	4.62 x10 ⁵	13.51	0.81	9.99 x 10 ¹⁹	47.9	4.37 x 10 ⁻⁴

* It behaves like an ideal capacitor (C_{dl}) in the case of Pt/PNVCz electrode

** The equivalent circuit in Figure 9 was used for data analysis. The value of exponent n is related to the roughness of electrode surfaces. n = 1 refers an ideal capacitor while its values between 0 and 0.5 denote a resistance and Warburg behavior.

The regular decrease in n_{pol} values along with the changes in Q_{CPE-pol} also supports the formation more resist coatings with increasing PDMS concentration and decreasing electropolymerization temperature. However, there is an exceptional case for the Pt/PDMS/PNVCz electrodes coated first with 5.0 and 10.0 wt % of PDMS in THF at -15°C and then with the electropolymerization of the solution of 5.2 x 10⁻² mol/L of NVCz in ACN at -15°C. In those cases, Q_{CPE-dl} and Q_{CPE-pol} moves to Warburg behaviour from nearly ideal capacitor or, just reverse by depending on the PDMS content under identical coating conditions (last two rows in Table 6.3). The values of n_{dl} and n_{pol} that change between 0.5 (that behaves like a Warburg impedance) and 0.95 (nearly ideal capacitor behaviour) might also be associated with the charging of the double-layer on the external surfaces or inside the pores on the bilayer coatings, depending on the PDMS content at -15°C. Further, the lower values of the bulk resistances (R_{pol}) of bilayer electrodes as to PNVCz coated

electrodes indicate that the mobility of ions within the PDMS/PNVCz bilayers are higher than that of PNVCz.

The real impedance, Z' at 10 mHz, where the capacitive behaviour dominates, is a reflection of the combined resistance of the electrolyte and the PDMS/PNVCz film including both electronic and ionic contributions (Table 6.4).

Table 6.4: Effect of PDMS content, PNVCz and PDMS coating temperatures, and electrode material on the impedance and capacitance values of Pt/PDMS/PNVCz and GC/PDMS/PNVCz bilayer electrodes

Coating temperature	Pt								GC			
	PNVCz, 25°C PDMS, 25°C		PNVCz, 0°C PDMS, 25°C		PNVCz, -15°C PDMS, 25°C		PNVCz, -15°C PDMS, -15°C		PNVCz, 25°C PDMS, 25°C			
PDMS (in wt %)	5.0	10.0	5.0	10.0	5.0	10.0	5.0	10.0	PDMS (in wt%)	5.0	10.0	15.0
Z'' (Ω)	1.8 $\times 10^5$	2.8 $\times 10^5$	1.8 $\times 10^5$	4.3 $\times 10^5$	1.8 $\times 10^5$	2.8 $\times 10^5$	1.1 $\times 10^5$	8.5 $\times 10^5$	Z' (Ω)	7.3x 10^4	2.6x 10^4	2.6x 10^5
C_{if}^b (F/g)	37.2	29.8	47.5	85.1	59.6	71.2	0.15	0.002	C_{if} (F/g)	18.9	18.9	33.0

- the value of real impedance, Z' at 10 mHz
- The absolute impedance magnitude by $|Z| = (Z'^2 + Z''^2)^{1/2}$
- obtained by using the slopes of Z'' vs $1/2\pi f$ plots

The capacitances in the low frequency region of Pt/PDMS/PNVCz and GC/PDMS/PNVCz bilayer electrodes were calculated from the slope of the linear relation between Z'' and $1/2\pi f$, according to the following equation

$$C_{if} = (Z'' 2\pi f)^{-1} \quad (1)$$

where Z'' is the imaginary part of impedance and f refers the frequency. The maximum value of the imaginary impedance at intermediate frequencies, Z''_{max} was used to calculate the double layer capacitance.

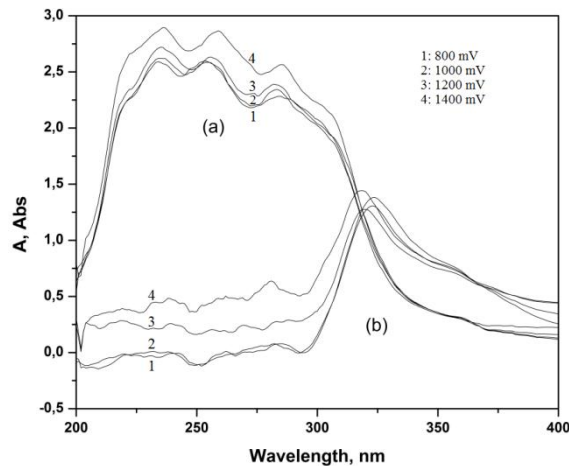


Figure 6.10: In-situ UV spectra of PDMS (5.0 wt/v % in THF) / PNVCz composites coated on ITO, at four different potentials between 800 mV and 1400 mV.

It is seen that the PDMS/PNVCz bilayer electrodes prepared with higher PDMS content at lower temperatures have significantly higher resistance than both PNVCz

films and the ones obtained with lower PDMS/higher temperature conditions. The capacitance values of the bilayer electrodes also show that in the cases of the same temperatures for both coating and electropolymerization solutions, the capacitive behavior of equivalent circuit decreased with increasing PDMS content in coating solution (from 5.0 to 10.0; in wt/v %) and with decreasing coating temperatures of PDMS (from 25°C to -15°C) and PNVCz and, more resist PDMS layers formed on GC electrode at 25°C as to the Pt electrode at the identical process conditions.

Spectroelectrochemistry also is an effective method to follow the spectral changes of conducting polymer films during their electrochemical growth.

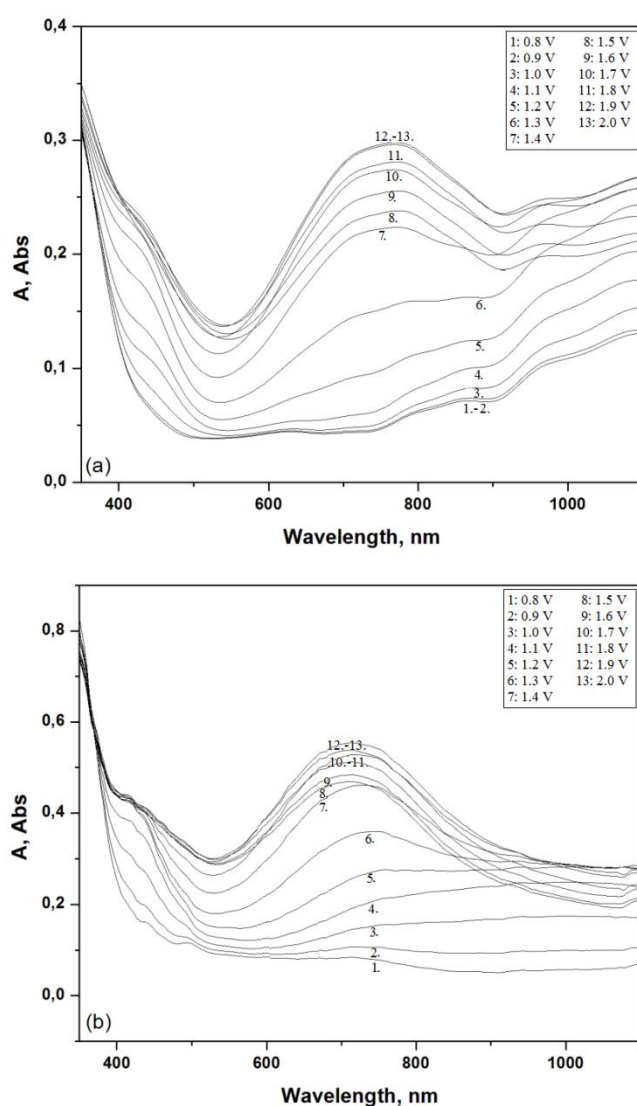


Figure 6.11: Absorption spectra of (a) PNVCz and (b) PNVCz/PDMS films at different potentials.

The change of the UV-vis spectra of PDMS/PNVCz bilayers as a function of potential are shown in Figures 6.10 and 6.11. In these absorption spectra, the absorption bands developed at around 410 and 720 nm indicate the formation of polarons and bipolarons in conducting polymers, while the π - π^* transitions of the neutral polymer appear in higher energies ($\lambda < 350$ nm; four absorption bands observed at 345, 295, 262, and 237 nm). In the case of the spectroelectrochemistry of PDMS/PNVCz films coated on ITO, the peaks in the range of 200-300 nm, which characterize the neutral polymer, disappeared, the ones at 410 nm and nearly 950 nm, corresponding to the possible electronic transitions from polaron bonding level to the π^* conduction band, were stabilized and/or decreased continuously as the doping proceeds (Figure 6.11) whereas the bipolarons at 720 nm in the formation of charged states increased with increasing potential.

The peak absorbances (below about 350 nm) of PNVCz film disappeared since ITO electrodes absorb photons in the ultraviolet region but a new peak, being independent of applied potential, appeared nearly 350 nm for PDMS/PNVCz films. It was attributed to the intermolecular interactions between PDMS and PNVCz, as it is reported in the cases of single walled and multi walled carbon nanotubes (21, 30). In addition, these PDMS/PNVCz films freed from an applied potential preserved their green colors even under atmospheric conditions. The spectra containing both bipolaron and neutral characteristics may mean that the doped bilayer coatings are partially stable and the PNVCz portions inserted into the pores of PDMS layer convert slowly back to the insulating state.

7. CONCLUSION

PNVCz, PIA, PAA and PNIPAAm homopolymers and, NVCz/IA, NVCz/AA and NVCz/NIPAAm copolymers having different compositions were synthesized by free radical polymerization in solution, using AIBN as initiator. These homopolymers and copolymers were characterized by calorimetric (DSC) and spectroscopic (FTIR and UV) methods.

- Analysis of the data by the extended Kelen-Tüdös (for high conversion) yields $r_1 = 0.29$ and $r_2 = 0.12$, $r_1 = 0.84$ and $r_2 = 0.12$, $r_1 = 0.86$ and $r_2 = 0.31$ by UV (for NVCz/NIPAAm, NVCz/IA and NVCz/AA copolymers, respectively), $r_1 = 0.32$ and $r_2 = 0.07$ by FTIR (for NVCz/NIPAAm copolymers).

- From these results, it was observed that in the case of NVCz-IA and NVCz-AA systems there is a tendency to obtain random copolymers while NIPAAm-NVCz system follows an alternative distribution of monomeric units. In addition, the relationship between T_g^{-1} (obtained from DSC thermograms and Fox equation) and w_{IA} supported that NVCz/IA copolymer chains have a random distribution of monomeric units.

- Electrochemical behavior of NVCz/IA and NVCz/NIPAAm coated electrodes was studied by CV measurements and found dependent on the type of comonomer.

- The present work provided useful data for biological application of new DA-sensitive materials based on copolymers of NVCz with IA and NIPAAm.

In this thesis the influence of both mixing methods which were used to obtain homogeneous dispersions of MMTs and the type of surfactants attached to MMT layers on the electrical and structural properties of PNVCz/MMT composites synthesized by one step oxidative polymerization in ACN using CAN as initiator has been investigated.

- The widened interlayer distances, more oriented silicate layers and ordered morphologies were obtained with both ODA-MMT and PNVCz/ODA-MMT

composites in ACN when intercalating agent octadecylamine, and sonication with high power sonic tip were applied for MMT modification and dispersion, respectively, according to FTIR, XRD, POM and SEM studies.

- Effects of intercalating agents, mixing methods and clay loading (in wt %) on thermal stability and the electrochemical/electrical properties of PNVCz/MMT composite materials consisting of unmodified and organomodified MMTs were also studied by means of DSC, CV, EIS and DC-measurements.

- The addition of the inorganic particles into the polymer matrix promoted not only an improvement on the thermal properties but also contributed to the increase in the conductivity of PNVCz. From EIS and DC-measurements, it has been shown that the conductivity of PNVCz in the presence of ODA-MMT between 15.0 and 1.0 wt % at room temperature increased from 10^{-13} S/cm to 10^{-5} S/cm.

PNVCz/MWCNT composites were synthesized by solution blending process in THF.

- POM, DSC and TGA observations show that the P(NVCz-co-MCeI)/MWCNT composites have more homogeneous and thermally stable structures than the ones containing homopolymer of NVCz as organic matrix because of the strong hydrophobic interactions between MCeI units and carbon nanotube walls.

In addition, the composites that consisted of PNVCz as organic matrix and o-GLs or o-MWCTs as conducting filler were prepared by in-situ polymerization with/without CAN in the presence of SDS in ACN/water mixture or without CAN in the absence of SDS in ACN, respectively.

- Both the broad peak on their XRD diffractograms and the appearance of the characteristic peak of carbonyl group in the FTIR spectra indicated that the NVCz adsorbed onto the oxidized graphite layers or carbon nanotubes formed composite materials by charge transfer mechanism between NVCz and filler, dispersed and activated by sonication.

- Their conductivities around 0.10 vol % resemble to that of an insulator while between 0.1 and 1.0 vol % of filler, the composites exhibit smooth transition from insulator state to semi-conducting region.

The capacitances at low frequencies of PDMS/PNVCz composite electrodes were estimated from EIS data.

-Their values in the range of 85 and 2×10^{-3} F/g were found to be related with electrode material, PDMS content and preparation temperature.

- An increase in PDMS content and decrease in coating temperature showed the influence of the PDMS-coating temperature on the capacitive behavior of composite electrodes. The lower coating/electrocoating temperature pairs resulted in more resist electrodes. Further, both the charge transfer resistance and Q_{pol} obtained from equivalent circuit for EIS data at 0.60 V, and in-situ spectroelectrochemical measurements between 0.0 V and 2.0 V indicated the effect of electrode potential on capacitive behavior of composite electrodes.

REFERENCES

- [1] Shirakawa, H., Louis, E. J., MacDiarmid, A. G., Chiang, C. K., Heeger, A. J., 1977. Synthesis of Electrically Conducting Organic Polymers: Halogen Derivatives of Polyacetylene, $(\text{CH})_x$, *Chem. Soc., Chem. Commun.*, **14**, 578-593.
- [2] Scott, H., Miller, G. A., Labes, M. M., 1963. A radical-cation initiated polymerization of N-vinyl carbazole. *Tetrahedron Lett.*, **17**, 1073-1098.
- [3] Skotheim, T. A., Elsenbaumer, R. L., Reynolds, J. R., 1997. *Handbook of Conducting Polymers*, Marcel Dekker: New York, **1-2**.
- [4] Chiang, C. K., Fincher, C. R., Park, Y. W., Heeger, A. J., Shirakawa, H., Louis, E. J. 1977. Electrical Conductivity in Doped Polyacetylene. *Phys. Rev. Lett.*, **39** 1098-1124.
- [5] Park S.-M. and Lee H. J., 2005. Recent Advances in Electrochemical Studies of π -Conjugated Polymers *Bull. Korean Chem. Soc.*, Vol. **26**, No. 5 697-706.
- [6] Scrosati, B. 1997. *Applications of Electroactive Polymers*, Chapman and Hall: London.
- [7] Paul, E. W., Ricco, A. J., Wrighton, M. S., 1985. Resistance of polyaniline films as a function of electrochemical potential and the fabrication of polyaniline-based microelectronic devices. *J. Phys. Chem.*, **89**, 1441-1451.
- [8] Hum P.W., 2006. Exploration of Large Scale Manufacturing of Polydimethylsiloxane (PDMS) Microfluidic Devices. Thesis - Massachusetts Institute of Technology, Dept. of Mechanical Engineering.
- [9] Naarmann H., 1993. *Polymers to the Year 200 and Beyond*, John Wiley & Sons, Chapter 4.
- [10] Salaneck W. R., Clark D. T., Samuelsen E. J., 1991. *Science and Application of Conducting Polymers*, **52** 108-121.
- [11] URL-1 < <http://www.maybachusa.com/index.php>>, accessed at 28.08.2010
- [12] Margolis J., 1989. *Conductive Polymers and Plastics*, Chapman and Hall, P. 33.
- [13] Klimisch H.J., Kieczka H., 1983. 4th ed. Ullmanns *Encyclopedie der technischen Chemie*, 23. Weinheim: Verlag Chemie., 597-765.
- [14] Pennwell, R. C., Gangully, B. N., Smith, T. W. 1976. Poly(N-vinylcarbazole): A selective review of its polymerization, structure, properties, and electrical characteristics. *J Polym Sci Macromol Rev*, **13**, 63-69.

- [15] **Pearson J.M., Stolka M.**, 1981: Poly(N-vinylcarbazole). *Polymer Monographs*, Vol. 61. New York: Gordon and Breach.
- [16] **Pennwell, R. C.; Ganguly, B. N.; Smith, T. W.** 1973. Poly(N-vinylcarbazole): A selective review of its polymerization, structure, properties, and electrical characteristics. *J Polym Sci Macromol Rev*, **13**, 63.
- [17] **Biswas, M.; Das, S. K.** 1982: Poly(N-vinylcarbazole), synthesis and characterization. *Polymer*, **23**, 1705-1723.
- [18] **Brindly SW, Brown G**, editors. 1980. Crystal structure of clay minerals and their X-ray diffraction. London: Mineralogical Society.
- [19] **Biswas, M.; Mitra, P.** 1991. Synthesis and thermal stability, dielectric and conductivity characteristics of some aromatic anhydride-modified carbazole polymers. *J Appl Polym Sci*, **42**, 1989.
- [20] **Pasquier A.D., Warren P.C., Culver D., Gozdz A.S., Amatucci G.G., Tarascon J.-M.**, 2000. *Solid State Ionics*, **135**, 249.
- [21] **Choi S.W., Jo S.M., Lee W.S., Kim Y.-R.**, 2003. An electrospun poly(vinylidene fluoride) nanofibrous membrane and its battery applications. *Adv. Mater.*, **15**, 2027-2038.
- [22] **Papez V., Josowicz M.**, 1994. Electrochemical preparation and study of poly(N-vinylcarbazole) as a sensing layer for propylamine vapour: *J. Electroanal. Chem.*, **365**, 139-144
- [23] **Sarac A.S., Sezer E., Ustamehmetoğlu B.**, 1997. Oxidative polymerization of N-substituted carbazoles. *Polym. Adv. Technol.*, **8**, 556
- [24] **Papež V., Inganäs O., Cimrová V. and Nešpůrek S.**, 1991. Electrochemical preparation and study of thin poly(N-vinylcarbazole) layers *Journal of Electroanalytical Chemistry*, **282(1-2)**, 123-139.
- [25] **Ambrose JF, Nelson RF.**, 1968. Anodic Oxidation Pathways of Carbazoles. *J Electrochem Soc*, **115**, 1159-1172.
- [26] **Mengoli G, Musiani MM, Schreck B, Zecchin S.**, 1988. Electrochemical synthesis and properties of polycarbazole films in protic acid media. *J Electroanal Chem* **246**, 73-78.
- [27] **Desbene-Morvernay A., Dubois J.E, Lacaze P.C.**, 1986. Study of substituent effects on the growth of poly(3-halogenated-N-vinylcarbazole) films obtained by oxidative electropolymerisation. *J Electroanal Chem*, **199**, 449-453.
- [28] **Compton R.G., Davis F.J., Grant S.C.**, 1986. The anodic oxidation of poly(N-vinylcarbazole) films. *J Appl Electrochem*, **16**, 239-246.
- [29] **Inzelt G.**, 2003. Formation and redox behaviour of polycarbazole prepared by electropolymerization of solid carbazole crystals immobilized on an electrode surface *J Solid State Electrochem*, **7**, 503–510.
- [30] **Sato M. A., Tanaka S., Kaeriyama K.**, 1986. Soluble conducting polythiophenes. *J. Chem. Soc., Chem. Commun.*, **12**, 873-898.

- [31] **Jen K. Y., Miller G. G., Elsenbaumer R. L.**, 1986.] Highly conducting, soluble, and environmentally-stable poly (3-alkylthiophenes). *J. Chem. Soc., Chem. Commun.*, **16**, 1346-1377.
- [32] **Sugimoto R., Takeda S., Gu H. B., Yoshino K.**, 1986. Preparation of soluble polythiophene derivatives utilizing transition metal halides as catalysts and their property. *Chem. Express*, **1** 635-647
- [33] **S. Hotta, S. D. D. V. Rughooputh, A. J. Heeger, F. Wudl**, 1987. Conducting polymer composites of soluble polythiophenes in polystyrene. *Macromolecules*, **20**, 212-221
- [34] **Roncali J., Garreau R., Yassar A., Marque P., Garnier F., Lemaire M.**, 1987. Effects of steric factors on the electrosynthesis and properties of conducting poly (3-alkylthiophenes). *J. Phys. Chem.*, **91**, 6706-6714.
- [35] **M. Leclerc, F. M. Diaz, G. Wegner**, 1989. Structural analysis of poly (3-alkylthiophene)s. *Makromol. Chem.*, **190**, 3105-3110.
- [36] **Yoshino, K., Onoda, M. and Kawai, T.**, 1990. *Optoelec. Devices Tech.*, **5**, 1-12.
- [37] **Hyodo, K.**, 1994. Electrochromism of conducting polymers. *Electrochim. Acta*, **39**, 265-271.
- [38] **Lyoo WS.** 2001. Synthesis of ultrahigh molecular weight poly (N-vinylcarbazole) with a high yield using low-temperature heterogeneous-solution polymerization. *J Polym Sci Part A: Polym Chem* **39** 539-547.
- [39] **Krongauz VV, Schmelzer ER, Yoahannan RM.** 1991. Kinetics of anisotropic photopolymerization in polymer matrix. *Polymer*, **32** 1654-1673.
- [40] **Ohoka M., Misumi S., Yamamoto M.**, 1999. Determination of propagation rate coefficient of free-radical polymerization of N-vinylcarbazole by pulsed-laser polymerization. *Polymer J*, **31(10)** 878-893.
- [41] **Lee C.J., Kim D.H., Oh J.M., Park K.H., Kim N., Ji B.C., Lyoo W.S.**, 2000. Solution polymerization behavior of N-vinylcarbazole by low-temperature azoinitiator. *J Appl Polym Sci*, **76** 1558-1563.
- [42] **Hort EV**, German Patent No: 2 111 293, assigned to GAF Corp
- [43] **Lyoo W.S., Oh J.M., Kim D.H., Kim J.H., Yoon W.S., Ji B.C., Ghim H.D., Lee C.J.**, 2000. Preparation of high molecular weight poly (N-vinylcarbazole) in high yield by low-temperature precipitation polymerization of N-vinylcarbazole. *Polym Int.* **49** 1324-1332.
- [44] **Davidge H**, British Patent No: 831 913, assigned to British Oxygen Comp
- [45] **Biswas M, Roy A.** 1993. Conductivity, thermal stability, dielectric and morphological characteristics of poly (N-vinylcarbazole) prepared in aqueous suspension. *Polymer* **34** 2903-2910.
- [46] **Obloj-Muzaj M, Kurowska H, Dudziak H, Moliak A.** 1996. In: Salamone JC, editor. Polymeric materials encyclopedia, 9. Boca Raton: CRC Press., 7107-7213.

- [47] **Solomon OF, Ciuta IZ, Cobiann N.** 1964. Spontaneous polymerization of N-vinylcarbazole in the presence of dilute aqueous solutions of perchloric acid. *J Polym Sci: Polym Lett*, **2**, 311-313.
- [48] **Wang, Chi-Hua.** 1964. *Chem. Ind.* (London), 751.
- [49] **Tazuke, S., Tjoa, T.B., and Okamura, S.** 1967. Effects of metal salts on polymerization. Part IV. Polymerization of N-vinylcarbazole initiated by oxidizing metal nitrates. *J. of Polym. Sci.: Part A1*, **5**, 1911-1925.
- [50] **Tsuji, K., Takakura, K., Nishii, M., Hayashi, K., Okamura, S.,** 1996. Synthesis and radical ring-opening polymerization behavior of vinylcyclopropane bearing six-membered cyclic acetal moiety *J. Polym. Sci., A-1*, **4**, 2028-2043.
- [51] **Gibson HW,** 1984. Control of electrical properties of polymers by chemical modification, *Polymer* **25**:3-27
- [52] **Solomon O.F., Ciuta I.Z. and Cobiann N.** 1965. Polymerization of some substituted Allyl-Carbazoles. *J Polym Sci: Polym Lett* **3**, 314-319.
- [53] **Atmaca L., Kayihan A and Yagci Y.** 2000. Photochemically and thermally induced radical promoted cationic polymerization using allyl phosphonium salts. *Polymer* **41**, 6035-6041.
- [54] **Jones G.D.,** 1963. In: P. Plesh, Editor, *The Chemistry of Cationic Polymerization*, Pergamon Press, Oxford p. 542.
- [55] **Heller J., Lyman D. J., Hewett W.A.,** 1964. The synthesis and polymerization studies of some higher homologues of 9-vinylcarbazole. *Die Makromolekulare Chemie*, **73**, 48-59.
- [56] **Jones GD. In: Plesh P,** editor. *The Chemistry of Cationic Polymerization*. Oxford: Pergamon Press, 1963. p. 542.
- [57] **Biswas MJ.** 1976. *Macromol Sci Part C: Rev Macromol Chem*, **14**, 1-7.
- [58] **Gandini A, Plesch P.** 1966. The polymerization of N-vinylcarbazole by electron acceptors:: Part I. Kinetics, equilibria and structure of oligomers. *J Chem Soc, Part B*, **3**, 7-17.
- [59] **Tsubukawa N, Yoshihara T.** 1991. Carbon whisker as an initiator of cationic polymerization of N-vinylcarbazole and N-vinyl-2-pyrrolidone. *Polym J*, **23**, 177-183.
- [60] **Tsubukawa N, Inagaki M, Kubota H, Endo T.** 1993. Grafting of polyesters from carbon whisker surface: Copolymerization of epoxides with cyclic acid anhydrides initiated by COOK groups introduced onto the surface. *J Polym Sci, Part A: Polym Chem*, **31**, 2459-2461.
- [61] **Topart PA, Josowicz M,** "Study of electrochemically deposited thin poly(N-vinylcarbazole) films" *Talanta* 1994; **41**.909-916
- [62] **Biswas M, Roy A,** "Conductivity, thermal stability, dielectric and morphological characteristics of poly(N-vinylcarbazole) prepared in aqueous suspension", *Polymer* 1993; **34**.2903-2906

- [63] **Gargallo L., Leiva A., Radic D., Leon A.**, 1998. Experimental Evidence of Aggregation Effects in Comblike Poly(mono-n-alkyl itaconates). *Langmuir*, **14**, 5314-5316.
- [64] **Domínguez E., Laborra C., Linaza A., Madoz A. and Katime I.A.** 1989. A series of mono and diesters of itaconic acid: Synthesis and structural determination. *Monatshefte für Chemie* **120**, 743-748.
- [65] **Biswas M, Ray SS**, 1998. Preparation and evaluation of composites from montmorillonite and some heterocyclic polymers. 1. Poly(N-vinylcarbazole)-montmorillonite nanocomposite system, *Polymer* **38**, 6423-6428.
- [66] **Biswas M, Ray SS, Liu Y**, 1999. Water dispersible conducting nanocomposites of poly(N-vinylcarbazole), polypyrrole and polyaniline with nanodimensional manganese (IV) oxide, *Synthetic Metals* **105**:99-105
- [67] **Biswas M, Ray SS**, 2001. A conducting nanocomposite of poly(N-vinylcarbazole) with buckminsterfullerene, *Synth. Met.* **123**, 135-139
- [68] **Ballav N, Maity A, Biswas M**, 2004, Preparation and characterization of a conducting nanocomposite of polyN-vinylcarbazole with acetylene black, *Mat. Chem. Phys.* **87**, 120-126
- [69] **Sanchis M. J., Díaz-Calleja R., Pelissou O., Gargallo L. and Radic D.**, 2004. Dynamic mechanical and dielectric relaxations in poly(di-n-chloroalkylitaconates). *Polymer*, **45**, 1845-1855.
- [70] **Higashika S, Kimura K, Matsuo Y, Sugie Y.**, 1999. Synthesis of polyaniline-intercalated graphite oxide, *Carbon* **37** 351–358.
- [71] **Ray SS, Okamoto M**, 2003. Polymer/layered silicate nanocomposites: a review from preparation to processing”, *Prog. Polym. Sci.* **28**:1539-1641
- [72] **Zhao Z, Tang T, Qin Y, Huang B**, 2003. Relationship between the Continually Expanded Interlayer Distance of Layered Silicates and Excess Intercalation of Cationic Surfactants”, *Langmuir* **19**, 9260-9265
- [73] **Stefanescu EA, Dundigalla A, Ferreira V, Loizou E, Porcar L, Negulescu I, Garnea J, Schmidt G**, 2006. Supramolecular structures in nanocomposite multilayered films” *PCCP* **8**, 1739-1746
- [74] **Erbil C., Yıldız Y. and Uyanık N.**, 2009. N-Isopropylacrylamide/monoalkyl itaconate copolymers and N-isopropylacrylamide/itaconic acid/dimethyl itaconate terpolymers. *Polym. Adv. Technol.*, **20** 926–933
- [75] **Yu YH, Lina CY, Yeha JM, Linb WH**, 2003. Preparation and properties of poly(vinyl alcohol)–clay nanocomposite materials. *Polymer*, **44**, 3553-3560.
- [76] **Odian, G.** 1991. *Principles of Polymerization*: 3rd Edition, John Wiley and Sons Inc.: New York.
- [77] **Fineman M. and Ross S. D.**, 1950. Linear method for determining monomer reactivity ratios in copolymerization. *J. Polym. Sci.*, **5**, 259-262.

- [78] **Kelen T. and Tudos F.**, 1975. Analysis of the Linear Methods for Determining Copolymerization Reactivity Ratios. I. A New Improved Linear Graphic Method . *J. Macromol. Sci. Chem. A*, **9**, 1-27.
- [79] **Alfery, T. and Goldfinger, G.J.**, 1944. The Mechanism of Copolymerization. *J. Chem. Phys.*, **12**: 205-209.
- [80] **Tudos F., Kelen T., Foldes–Bereznich T., and Turcsanyi B.**, 1976: Analysis of Linear Methods for Determining Copolymerization Reactivity Ratios. III. Linear Graphic Method for Evaluating Data Obtained at High Conversion Levels. *J. Macromol. Sci. Chem.A*, **10**, 1513-1540.
- [81] **Mao R. and Huglin M. B.**, 1993. A new linear method to calculate monomer reactivity ratios by using high conversion copolymerization data: terminal model. *Polymer*, **34**, 1709-1715.
- [82] **Tidwell P. W. and Mortimer G. A.**, 1965. An improved method of calculating copolymerization reactivity ratios. *J. Polym. Sci., Polym. Chem.*, **3**, 369-387.
- [83] **Mayo F. R. and Lewis F. M.**, 1944. Copolymerization. I. A Basis for Comparing the Behavior of Monomers in Copolymerization; The Copolymerization of Styrene and Methyl Methacrylate. *J. Am. Chem. Soc.*, **66**, 1594-1601.
- [84] **Yezrielev A. I., Brokhina E., and Roskin Y. S.**, 1969. *Vysokomol. Soedin.*, **11**, 1670-1677.
- [85] **Barson C. A. and Fenn D. R.**, 1992. Binary copolymerizations of N-antipyryl acrylamide with methyl methacrylate, butyl methacrylate, acrylonitrile and vinyl acetate. *Eur. Polym. J.*, **28**, 1405-1410.
- [86] **Dube M. A., Sanayei R. A., Penlidis A., O’Driscoll K. F., and Reilly P. M.**, 1991. A microcomputer program for estimation of copolymerization reactivity ratios. *J. Polym. Sci., Polym. Chem.*, **29**, 703-710.
- [87] **Wightman R.M., May L.J. and Michael A.C.**, 1988. Detection of dopamine dynamics in the brain, *Anal. Chem.* **60**, 769A–779A
- [88] **Smith T.E.**, In: T.M. Devlin, Editor, 1992. *Textbook of Biochemistry with Clinical Correlations*, Wiley-Liss, New York, 929.
- [89] **Mo J.W., Ogorevc B.**, 2001. Simultaneous measurement of dopamine and ascorbate at their physiological level using voltammetric microprobe based on overoxidized poly(1,2-phenylenediamine)-coated carbon fiber, *Anal. Chem.* **73**, 1196–1202.
- [90] **Sarre S., Michotte Y., Herregodts P., Deleu D., De Klippel N., Ebinger G.**, 1992. High-performance liquid chromatography with electrochemical detection for the determination of levodopa, catecholamines and their metabolites in rat brain dialysates, *J. Chromatogr.* **575**, 207–212.
- [91] **Guan C.L., Ouyang J., Li Q.L., Liu B.H., Baeyens W.R.G.**, 2000. Simultaneous determination of catecholamines by ion chromatography with direct conductivity detection, *Talanta* **50**, 1197–1203.

- [92] **Zetterstrom T., Sharp T., Marsden C.A., Ungerstedt U.**, 1983. In vivo measurement of dopamine and its metabolites by intracerebral dialysis: change after d-amphetamine, *J. Neurochem.* **4**, 11769–1773.
- [93] **Malem F., Mandler D.**, 1993. Self-assembled monolayers in electroanalytical chemistry: application of N-mercapto carboxylic acid monolayers for the electrochemical detection of in the presence of high conc. of ascorbic acid, *Anal. Chem.* **65**, 37–41.
- [94] **Gonon F., Buda M., Cespuglio R., Jouvet J., Pujol J.F.**, 1981. Voltammetry in the striatum of chronic freely moving rats: detection of catechols and ascorbic acid, *Brain Res.* **223**, 69–80.
- [95] **Saraceno R.A., Pack J.G., Ewing A.G.**, 1986. Catalysis of slow charge transfer reactions at polypyrrole-coated glassy carbon electrodes, *J. Electroanal. Chem.* **197**, 265–278.
- [96] **Ciszewski A., Milczarek G.**, 1999. Polueugenol-modified platinum electrode for selective detection of dopamine in the presence of ascorbic acid, *Anal. Chem.* **71**, 1055–1061.
- [97] **Zhao H., Zhang Y.Z., Yuan Z.B.**, 2001. Electrochemical determination of dopamine using a poly(2-picolinic acid)-modified glassy carbon electrode, *Analyst* **126**, 358–360.
- [98] **Zhao H., Zhang Y.Z., Yuan Z.B.**, 2001. Study on the electrochemical behavior of dopamine with poly(sulfosalicylic acid)-modified glassy carbon electrode, *Anal. Chim. Acta* **441**, 117–122
- [99] **Downard A.J., Roddick A.D., Bond A.M.**, 1995. Covalent modification of carbon electrodes for voltammetric differentiation of dopamine and ascorbic acid, *Anal. Chim. Acta* **317**, 303–310.
- [100] **Zhang Y., Cai Y., Su S.**, 2006. Determination of dopamine in the presence of ascorbic acid by poly(styrene sulfonic acid) sodium salt/single-wall carbon nanotube modified glassy carbon electrode *Analytical Biochemistry* **350**, 285–291
- [101] **Zhao H., Zhang Y.Z., Yuan Z.B.**, 2002. Determination of dopamine in the presence of ascorbic acid using poly(hippuric acid) modified glassy carbon electrode, *Electroanalysis* **14**, 1031–1035.
- [102] **Zhang Y.Z., Jin G.Y., Wang Y.L., Yang Z.S.**, 2003. Determination of dopamine in the presence of ascorbic acid using poly(acridine red) modified glassy carbon electrode, *Sensors* **3**, 443–450.
- [103] **Jin G., Zhang Y., Cheng W.**, 2005. Poly(*p*-aminobenzene sulfonic acid) modified glassy carbon electrode for simultaneous detection of dopamine and ascorbic acid, *Sensors Actuat. B Chem.* **2**, 528–534.
- [104] **Zhang Y., Jin G., Yang Z.**, 2004. Determination of dopamine in the presence of ascorbic acid using poly(amidosulfonic acid) modified glassy carbon electrode, *Microchim. Acta* **4**, 225–230.
- [105] **Zhang Y., Jin G., Chen W.**, 2005. Poly(*o*-aminobenzoic acid) modified glassy carbon electrode for electrochemical detection of dopamine in the presence of ascorbic acid, *Front. Biosci.* **1**, 23–29.

- [106] **Zhao H., Zhang Y.Z., Yuan Z.B.**, 2001. Electrochemical determination of dopamine using a poly(2-picolinic acid)-modified glassy carbon electrode, *Analyst* **126**, 358–360.
- [107] **Pierson R, Basavaraja C, Kim NR, Jo EA, Huh DS**, 2009. Microstructure and Electrical Properties of Poly-N-isopropylacrylamide-N-vinylcarbazole Copolymers. *Bull. Korean Chem. Soc.*; **30**, 2057-2060.
- [108] **Zhao Z, Tang T, Qin Y, Huang B**, 2003. Relationship between the Continually Expanded Interlayer Distance of Layered Silicates and Excess Intercalation of Cationic Surfactants, *Langmuir*; **19**, 9260-9265.
- [109] **Kalaycioglu, E.; Toppare, L.; Yagci, Y.; Harabagiu, V.; Pintela, M.; Ardelean, R.; Simionescu, B. C.** 1998. Synthesis of conducting H-type polysiloxane-polypyrrole block copolymers. *Synth Met*, **97**, 7-12.
- [110] **Olinga, T.; Francois, B.** 1991. Synthesis of soluble polystyrene-graft-polythiophene comblike copolymers: a new precursor for polythiophene film preparation. *Macromol Chem Rapid Commun*, **12**, 575-582.
- [111] **Hallensleben, M. Stanke, D , Toppare L.**, 1995. Poly(methyl methacrylate) containing pyrrole moieties in the side chains. *Macromol Chem Phys*, **7**, 75-83.
- [112] **Stanke D.; Hallensleben M. L.; Toppare L.** 1993. Electrically conductive poly(methyl methacrylate-g-pyrrole) via chemical oxidative polymerization. *Synth Met*, **55**, 1108-1113.
- [113] **Wang, H. L.; Toppare, L.; Fernandez, J. E.** 1990. Conducting polymer blends: polythiophene and polypyrrole blends with polystyrene and poly (bisphenol A carbonate). *Macromolecules*, **23**, 1053-1059.
- [114] **Axial F., Brosteaux D., De Leersnyder E., Bossuyt F., Gonzalez M., N. De Smet, E. Schacht, Rymarczyk-Machal M., Vanfleteren J.**, Low Cost, Biocompatible Elastic And Conformable Electronic Technologies Using Mid Instretchable Polymer Proceedings of the 29th Annual International Conference of the IEEE EMBS Cité Internationale, Lyon, France August 23-26, 2007.
- [115] **Yilmaz E. and Kucukyavuz Z.**, 1993. Monomer reactivity ratios of styrene-4-vinylpyridine copolymers at low and high conversions. *Polymer*, **34**, 145-149.
- [116] **Cakmak G, .Kucukyavuz Z., Kucukyavuz S., Cakmak H.**, 2004. Mechanical, electrical and thermal properties of carbon fiber reinforced poly (dimethylsiloxane)/polypyrrole composites. *Composites: Part A*, **35**, 417-421.
- [117] **Sankır M., Kücükyavuz Z., , Kücükyavuz S.**, 2003. Synthesis and Characterization of Poly(dimethylsiloxane)Polythiophene Composites *Journal of Applied Polymer Science*, **87**, 2113–2119.
- [118] **Gangopadhyay R. and Amitabha D.**, 2000. Conducting Polymer Nanocomposites: A Brief Overview *Chem. Mater.*, **12**, 608-614.

- [119] **Jana S.C., Jain S.**, 2001. Dispersion of nanofillers in high performance polymers using reactive solvents as processing aids. *Polymer*, **42**, 6897–905.
- [120] **Saujanya C, Radhakrishnan S.** 2001. Structure development and crystallization behaviour of PP/nanoparticulate composite. *Polymer*, **42**, 6723–6731
- [121] **Calvert P.** Potential applications of nanotubes. In: Ebbesen TW, editor. Carbon nanotubes. Boca Raton, FL: CRC press, 1997.
- [122] **Favier V, Canova GR, Shrivastava SC, Cavaille JY.** 1997. Mechanical percolation in cellulose whiskers nanocomposites. *Polym Eng Sci*, **37**, 1732–1739.
- [123] **Theng BKG.** The chemistry of clay-organic reactions. New York: Wiley, 1974.
- [124] **Chen GH, Wu DJ, Weng WG, Yan WL.** 2001. Preparation of polymer/graphite conducting nanocomposite by intercalation polymerization. *J Appl Polym Sci*, **82**, 2506–2513.
- [125] **Pan YX, Yu ZZ, Ou YC, Hu GH.** 2000. New process of fabricating electrically conducting nylon 6/graphite nanocomposites via intercalation polymerization. *J Polym Sci Part B: Polym Phys*, **38**, 1626–33.
- [126] **Maity, A., Biswas, M.** 2006. Recent progress in conducting polymer, mixed polymer-inorganic hybrid nanocomposites. *J Ind Eng Chem*, **12**, 311-351.
- [127] **Ray, S. S., Liu, Y., Biswas, M.** 1999. Water dispersible conducting nanocomposites of poly(N-vinylcarbazole), polypyrrole and polyaniline with nanodimensional manganese (IV) oxide. *Synth Met*, **105**, 99-105.
- [128] **Maity, A., Biswas, M.,** 2003. A nanocomposite of poly (N-vinylcarbazole) with nanodimensional alumina. *J Appl Polym Sci*, **88**, 2233-2237.
- [129] **Ray, S. S., Biswas, M.** 1998. Preparation and evaluation of composites from montmorillonite and some heterocyclic polymers. 1. Poly (N-vinylcarbazole)-montmorillonite nanocomposite system. *Polymer*. **39**, 6423-6428.
- [130] **Ray, S. S., Biswas, M.** 1999. Preparation and evaluation of composites from montmorillonite and some heterocyclic polymers. II. A nanocomposite from N-vinylcarbazole and ferric chloride-impregnated montmorillonite polymerization system. *J Appl Polym Sci*, **73**, 2971-2976.
- [131] **Maity, A., Ballav, N., Biswas, M.** 2006. Conducting composites of poly (N-vinylcarbazole), polypyrrole, and polyaniline with 13X-zeolite. *J Appl Polym Sci*, **101**, 913-921.
- [132] **Ray, A., Biswas, M.** 1993. Conductivity, thermal stability, dielectric and morphological characteristics of poly (N-vinylcarbazole) prepared in aqueous suspension. *Polymer*, **34**, 2903-2906.

- [133] **Ballav, N., Maity, A., Biswas, M.** 2004. Preparation and characterization of a conducting nanocomposite of poly(*N*-vinylcarbazole) with acetylene black. *Mat Chem Phys*, **87**, 120-126.
- [134] **Ray, S. S., Biswas, M.** 2001. A conducting nanocomposite of poly(*N*-vinylcarbazole) with buckminsterfullerene. *Synth Met*, **123**, 135-139.
- [135] **Topart PA, Josowicz M,** 1994. Study of electrochemically deposited thin poly(*N*-vinylcarbazole) films. *Talanta*, **41**, 909-916
- [136] **Meincke, O., Kaempfer, D., Weickmann, H., Friedrich, C., Vathauer, M., Warth, H** 2004. Mechanical properties and electrical conductivity of carbon-nanotube filled polyamide-6 and its blends with acrylonitrile/butadiene/styrene *Polymer.*, **45**, 739-747.
- [137] **Badaire, S., Poulin, P., Maugey, M., Zakri, C.** 2004. Mechanical properties and electrical conductivity of carbon-nanotube filled polyamide-6 and its blends with acrylonitrile/butadiene/styrene. *Langmuir*, **20**, 10367-10370.
- [138] **Islam, M. F., Rojas, E., Bergey, D. M., Johnson, A. T., Yodh, A. G.** 2003. High weight fraction surfactant solubilization of single-wall carbon nanotubes in water. *Nano Lett.*, **3**, 269-273.
- [139] **Barrau, S., Demont, P., Perez, E., Peigney, A., Laurent, C., Lacabanne, C.** 2003. Effect of Palmitic Acid on the Electrical Conductivity of Carbon Nanotubes–Epoxy Resin Composites. *Macromolecules*. **36**, 9678-9680.
- [140] **Bryning, M. B., Milkie, D. E., Islam, M. F., Kikkawa, J. M., Yodh, A. G.** 2005. Thermal conductivity and interfacial resistance in single-wall carbon nanotube epoxy composites. *Appl. Phys. Lett.*, **87**, 161909/1-161909/3.
- [141] **Yano K., Usuki A. and Okada A.,** 1997. Synthesis and properties of polyimide-clay hybrid films, *J Polym Sci Part A: Polym Chem* **35**, 2289–2294.
- [142] **Okamoto M.,** 2006. Recent advances in polymer/layered silicate nanocomposites: an overview from science to technology *Materials Science and Technology* **22**, 756-779.
- [143] **Biswas M, Roy A,** 1993. Conductivity, thermal stability, dielectric and morphological characteristics of poly(*N*-vinylcarbazole) prepared in aqueous suspension *Polymer* **34** 2903-2906.
- [144] **Brindly SW, Brown G,** editors. Crystal structure of clay minerals and their X-ray diffraction. London: Mineralogical Society, 1980.
- [145] **Aranda P, Ruiz-Hitzky E.** 1992. Poly(ethylene oxide)-silicate intercalation materials. *Chem Mater* **4**, 1395–403.
- [146] **Greenland DJ.** 1963. Adsorption of poly(vinyl alcohols) by montmorillonite. *J Colloid Sci* **18**, 647–664.
- [147] **Blumstein A.** 1965. Polymerization of adsorbed monolayers: II. Thermal degradation of the inserted polymers. *J Polym Sci A* **3**, 2665–73.

- [148] **Theng BKG.** Formation and properties of clay–polymer complexes. Amsterdam: Elsevier, 1979.
- [149] **Blumstein A.** 1965. Polymerization of adsorbed monolayers: II. Thermal degradation of the inserted polymers. *J Polym Sci A*, **3** 2665–2673.
- [150] **Leszczynska A., Njuguna J., Pielichowski K., Banerjee J. R.,** 2007. *Themochimica Acta*, Vol. **43-2**, 75-96.
- [151] **Hay N. and Shaw S.J.** 2000. a review of nanocomposites.
- [152] **Giannelis E.P.,** 1996. Polymer layered silicate nanocomposites. *Adv Mater*, **8** 29–35.
- [153] **Giannelis EP, Krishnamoorti R, Manias E.** 1999. Polymer-silicate nanocomposites: model systems for confined polymers and polymer brushes. *Adv Polym Sci*, **138** 107–147.
- [154] **LeBaron PC, Wang Z, Pinnavaia TJ.** 1999. Polymer-layered silicate nanocomposites: an overview. *Appl Clay Sci*, **15** 11–29.
- [155] **Giannelis EP.,** 1998. Polymer-layered silicate nanocomposites: synthesis, properties and applications. *Appl Organomet Chem*, **12** 675–80.
- [156] **Xu R, Manias E, Snyder AJ, Runt J.** 2001. New biomedical poly(urethane uera)-layered silicate nanocomposites. *Macromolecules*, **34** 337–339.
- [157] **Bharadwaj RK.** 2001. Modeling the barrier properties of polymerlayered silicate nanocomposites. *Macromolecules*, **34** 1989–1992.
- [158] **Messersmith PB, Giannelis EP.** 1995. Synthesis and barrier properties of poly(1-caprolactone)-layered silicate nanocomposites. *J Polym Sci, Part A: Polym Chem* **33**, 1047–57.
- [159] **Yano K, Usuki A, Okada A, Kurauchi T, Kamigaito O.** 1993. Synthesis and properties of polyimide–clay hybrid. *J Polym Sci, Part A: Polym Chem*, **31** 2493–2498.
- [160] **Gilman J.W., Kashiwagi T., Lichtenhan J.D.,** 1997. Flammability studies of polymer-layered silicate nanocomposites. *SAMPE J*, **33** 40–45.
- [161] **Gilman J.W.,** 1999. Flammability and thermal stability studies of polymer-layered silicate (clay) nanocomposites. *Appl Clay Sci* **15** 31–49.
- [162] **Bourbigot S, LeBras M, Dabrowski F, Gilman JW, Kashiwagi T.,** 2000. PA-6 clay nanocomposite hybrid as char forming agent in intumescent formulations. *Fire Mater*, **24** 201–208.
- [163] **Ray S.S, Yamada K., Okamoto M., Ueda K.,** 2002. New polylactide/layered silicate nanocomposite: a novel biodegradable material. *Nano Lett*, **2** 1093–1096.
- [164] **Hackett E., Manias E., Giannelis E.P.,** 1998. Molecular dynamics simulations of organically modified layered silicates. *J Chem Phys*, **108** 7410–7415.
- [165] **Hackett E, Manias E, Giannelis E.P. ,** 2000. Computer simulation studies of PEO/layered silicate nanocomposites. *Chem Mater*, **12** 2161–2167.

- [166] **Anastasiadis S.H., Karatasos K., Vlachos G., Manias E., Giannelis E.P.**, 2000. Nanoscopic-confinement effects on local dynamics. *Phys Rev Lett*, **84** 915–918.
- [167] **Zax D.B., Yang D.K., Santos R.A., Hegmann H., Giannelis E.P., Manias E.**, 2000. Dynamical heterogeneity in nanoconfined poly(styrene) chains. *J Chem Phys*, **112** 2945–2951.
- [168] **Manias E., Kупpa V.**, 2001. Relaxation of polymers in 2-nm slitpores: confinement induced segmental dynamics and suppression of the glass transition. *Colloids Surf., A* **187** 509–521.
- [169] **Blumstein A.**, 1965. Polymerization of adsorbed monolayers: II. Thermal degradation of the inserted polymers. *J Polym Sci A* **3** 2665–2673.
- [170] **Theng BKG.** 1979. Formation and properties of clay–polymer complexes. Amsterdam: Elsevier.
- [171] **Okada A, Kawasumi M, Usuki A, Kojima Y, Kurauchi T, Kamigaito O.**, 1990. Synthesis and properties of nylon-6/clay hybrids. In: Schaefer DW, Mark JE, editors. Polymer based molecular composites. MRS Symposium Proceedings, Pittsburgh, vol. **171**, 45–50.
- [172] **Kojima Y., Usuki A., Kawasumi M., Okada A., Kurauchi T., Kamigaito O.**, 1993. Synthesis of Nylon 6 – Clay Hybrid by Montmorillonite Intercalated with ϵ -Caprolactam. *Journal of Polymer Science: Part A: Polymer Chemistry* **31** 983 – 986.
- [173] **Okada A., Kawasumi M., Usuki A., Kojima Y., Kurauchi T. and Kamigaito O.**, 1989. Nylon 6-Clay Hybrid. *Mat. Res. Soc. Symp. Proc.* **171**, 45-49
- [174] **Vaia R.A., Ishii H., Giannelis E.P.**; 1993. Synthesis and Properties of Two-Dimensional Nanostructures by Direct Intercalation of Polymer Melts in Layered Silicates. *Chem. Mater.* **5** 1694 – 1696.
- [175] **Ma J., Xu J., Ren J. H., Yu Z. Z., Mai Y. W.** 2003. A new approach to polymer / montmorillonite nanocomposites.” *Polymer*, **44**, 4619 – 4624.
- [176] **Harikrishnan G., Umasankar T., Khakhar D.V.**; 2006. Polyurethane Foam –Clay Nanocomposites: Nanoclays as Cell Openers. *Ind. Eng. Chem.Res.*, **45**, 7126 – 7134.
- [177] **Liu A., Xie T., Yang G.**, 2006 : Properties of Nylon-6/Na⁺- Montmorillonite Nanocomposites Obtained by Hydrolyzed Ring-Opening Polymerization. *Macromolecular Rapid Communication*, **27**, 1572 – 1577.
- [178] **Wilkinson A., Man Z., Stanford J., Matikainen P., Clemens M., Lees G., Liauw C.**, 2006. Structure and Dynamic Mechanical Properties of Melt Intercalated Polyamide 6 – Montmorillonite Nanocomposites.” *Macromol. Mater. Eng.* **291**, 917 – 928.
- [179] **He X., Yang J., Zhu L., Wang B., Sun G., Lv P., Phang I. Y., Liu T.**, 2006. Morphology and Melt Rheology of Nylon 11/Clay Nanocomposites. *Journal of Applied Polymer Science*, **102** 542 – 549.

- [180] **Lee E.C., Mielewski D.F., Baird R.J.**, 2004. Exfoliation and Dispersion Enhancement in Polypropylene Nanocomposites by In-Situ Melt Phase Ultrasonication. *Polymer Engineering and Science*, **44**, 1773 – 1782.
- [181] **Okamoto M., Morita S., Taguchi H., Kim Y. H., Kotaka T., Tateyama H.**, 2000. Synthesis and structure of smectic clay/poly(methyl methacrylate) and clay/polystyrene nanocomposites via in situ intercalative polymerization. *Polymer*, **41**, 3887 – 3890.
- [182] **Aphiwantrakul S., Srikhirin T., Triampo D., Putiworanat R., Limpanart S., Osotchan T., Udomkichdecha W.**, 2004. Role of the Cation-Exchange Capacity in the Formation of Polystyrene – Clay Nanocomposites by In Situ Intercalative Polymerization. *Journal of Applied Polymer Science*, **95** 785 – 789.
- [183] **Litina K., Miriouni A., Gournis D., Karakassides M., Georgiou N., Klontzas E., Ntoukas E., Avgeropoulos A.**, 2006. Nanocomposites of polystyrene – b-polyisoprene copolymer with layered silicates and carbon nanotubes. *European Polymer Journal*, **42**, 2098 – 2107.
- [184] **Kaynak C., Tasan C. C.**, 2006. Effects of production parameters on the structure of resol type phenolic resin/layered silicate nanocomposites. *European Polymer Journal*, **42** 1908 – 1921.
- [185] **Chen C., Khobaib M., Curliss D.**, 2003. Epoxy layered – silicate nanocomposites. *Progress in Organic Coatings*, **47**, 376 – 383.
- [186] **Jia Q., Zheng M., Cheng J., Chen H.**, 2006. “Morphologies and properties of epoxy resin/layered silicate-silica nanocomposites.” *Polymer International*, **55**, 1259 – 1264.
- [187] **Meneghetti P., Qutubuddin S.** 2006. Synthesis, thermal properties and application of polymer – clay nanocomposites. *Thermochimica Acta*, **442**, 74 – 77.
- [188] **Lin K. F., Lin S. C., Chien A. T., Hsieh C. C., Yen M. H., Lee C. H., Lin C. S., Chiu W. Y., Lee Y. H.**, 2006. Exfoliation of Montmorillonite by the Insertion of Dislike Micelles via the Soap-Free Emulsion Polymerization of Methyl Methacrylate. *Journal of Polymer Science Part A: Polymer Chemistry*, **44**, 5572 – 5579.
- [189] **Ratinac K. R., Gilbert R. G., Ye L., Jones A. S., Ringer S. P.**, 2006. The effects of processing and organoclay properties on the structure of poly(methyl methacrylate) – clay nanocomposites. *Polymer*, **47**, 6337 – 6361.
- [190] **Yu Y.H., Yeh J.M., Liou S.J., Chen C.L., Liaw D.J., Lu H.Y.**; 2004. Preparation and Properties of Polyimide – Clay Nanocomposite Materials for Anticorrosion Application.. *Journal of Applied Polymer Science*, **92**, 3573 – 3582.
- [191] **Yeh J.M., Chen C.L., Kuo T.H., Su W.F., Huang H.Y., Liaw D.J., Lu H.Y., Liu C.F., Yu Y.H.**, 2004. Preparation and Properties of (BATB-ODPA) Polyimide – Clay Nanocomposite Materials. *Journal of Applied Science*, **92**, 1072 – 1079.

- [192] **Delozier D.M., Orwoll R.A., Cahoon J.F., Johnston N.J., Smith J.G., Connell J.W.**, 2002. Preparation and characterization of polyimide/organoclay nanocomposites. *Polymer*, **43**, 813 – 822.
- [193] **Lee S.H., Kim J.E., Song H.H., Kim S.W.**, 2004. Thermal Properties of Maleated Polyethylene/Layered Silicate Nanocomposites. *International Journal of Thermophysics*, **25**, 1585 – 1595.
- [194] **Zhang G., Shichi T., Takagi K.**, 2003. PET – clay hybrids with improved tensile strength.” *Materials Letters*, **57**, 1858 – 1862.
- [195] **Biswas M., Sinha Ray S.**, 1998. Preparation and evaluation of composites from montmorillonite and some heterocyclic polymers. 1. poly(N-vinylcarbazole)–montmorillonite system. *Polymer*, **39** 6423–6428.
- [196] **Ray S.S., Biswas M.**, 1999. Preparation and evaluation of composites from montmorillonite and some heterocyclic polymers. II. A nanocomposite from N-vinylcarbazole and ferric chloride-impregnated montmorillonite polymerization system. *Journal of Applied Polymer Science*, **73** 2971–2976.
- [197] **Maertens C., Dubois P., Jerome R., Blanche P.A. and Lemaire P.C.**, 2000. Synthesis and polarized light-induced birefringence of new polymethacrylates containing carbazolyl and azobenzene pendant groups. *J. Polym. Sci., Part B, Polym. Phys.* **38** 205-210.
- [198] **Theng B.K.G.**, 1974. The chemistry of clay-organic reactions. , Wiley, New York.
- [199] **Chen G.H., Wu D.J., Weng W.G. and Yan W.L.**, 2001. Preparation of polymer/graphite conducting nanocomposite by intercalation polymerization. *J Appl Polym Sci.* **82** 2506–2513.
- [200] **Pan Y.X., Yu Z.Z., Ou Y.C. and Hu G.H.**, 2000. New process of fabricating electrically conducting nylon 6/graphite nanocomposites via intercalation polymerization. *J Polym Sci Part B: Polym Phys* **38** 1626–1633
- [201] **Kojima Y., Usuki A. and Kawasami M.**, 1993. Mechanical properties of nylon-6-clay hybrid. *J Mater Res.* **6** 1185–1189.
- [202] **Uhl F.M., Yao Q., Nakajima H., Manias E., Wilkie C.A.**, 2005. *Polym Degrad Stab* **89** 70-77.
- [203] **Jacob J., Anil G., Bhowmick K.**, 2008. Ethylene vinyl acetate/expanded graphite nanocomposites by solution intercalation: preparation, characterization and properties *J Mater Sci* **43** 702–708.
- [204] **Lalancette J.M., Roussel R.**, 1976. *Can J Chem*, **54**.2110-2115.
- [205] **Zois H., Apekis L., Omastova M.** 1999. Electrical properties and percolation phenomena in carbon black filled polymer composites. Proceedings—International Symposium on Electrets, 10th International Symposium on Electrets (ISE 10),. 529–532.
- [206] **Gabriel P, Cipriano LG, Ana JM.** 1999. Polymer composites prepared by compression molding of a mixture of carbon black and nylon 6 powder. *Polym Comp*, **20** 804–808.

- [207] **Zheng W., Wong S.-C.**, 2003. Electrical conductivity and dielectric properties of PMMA/expanded graphite composites *Composites Science and Technology* **63** 225–230.
- [208] **Stauffer, D.**, Introduction to Composite Materials, Cambridge University Press, London 1981
- [209] **Kirkpatrick, S.**, 1973. Percolation and conduction. *Rev. Mod. Phys.* **45**, 574-578.
- [210] **Wang, W.-P., Pan, C.-Y.** 2003. Cationic polymerization of styrene on the surface of graphite expanded. *J Polym Sci Part A: Polym Chem* **41**, 2715-2721.
- [211] **Daoulas, K.C., Terzis, A. F., Mavrantzas, V.G.** 2002. Detailed atomistic Monte Carlo simulation of grafted polymer melts. I. Thermodynamic and conformational properties. *J Chem Phys*, **116**, 11028-11036.
- [212] **Cao, N., Shen, W., Wen, S., Liu, Y.** 1996. *Chem Bull*, **4**, 37-41.
- [213] **Wang W., Liu Y., Li X., You Y.**, 2006. Synthesis and characteristics of poly (methyl methacrylate)/expanded graphite nanocomposites. *Journal of Applied Polymer Science*, Vol. 100, 1427–1431 ()
- [214] **Usuki, A., Kojima, Y., Kawasumi, M., Okada, A., Fukushima, Y., Kurauchi, T., Kamigaito, O.** 1993. Synthesis of nylon 6–clay hybrid. *J. Mater Res*, **8** 1179-1188.
- [215] **Ezquerra, Y. A., Kulescza, M., alta-Calleja, F. J.** 1991. Electrical transport in polyethylene-graphite composite materials. *Synth Met* **41**, 915-924.
- [216] **Chen, G.-H., Wu, C.-L., Wang, W.-G., Wu, D.-J., Yan, W.-L.**, 2003. Preparation of polystyrene/graphite nanosheet composite. *Polymer*, **44**, 1781-1784.
- [217] **Cao, N. Z., Shen, W. C., Wen, S. Z.** 1996. *Acta PhysichoChimica Sinica*, **12**, 766–768.
- [218] **Zhou, Q., Cao, N. Z., Shen, W. C., Wen, S. Z.** 1996. *New Carbon Materials (China)*, **11**, 42–45.
- [219] **Saini P., Choudhary V., Dhavan S.K.**, 2007. LiSIPA doped polyaniline-colloidal graphite composites: Synthesis and characterisation *Ind. J. Eng. Mat. Sc.* **14**, 436-442.
- [220] **Zheng W., Wong S.C. and Sue H.J.**, 2002. Transport behavior of PMMA/expanded graphite nanocomposites, *Polymer*, **73**, 6767–6773
- [221] **Cheng G., Weng W., Wu D. and Wu C.**, 2003. PMMA/graphite nanosheets composite and its conducting properties, *Europ Polym J* **39**, 2329–2335.
- [222] **Zheng G., Wu J., Wang W. and Pan C.**, 2004. Characterizations of expanded graphite/polymer composites prepared by in situ polymerization, *Carbon* **42**, 2839–2847.
- [223] **Li J., Kim J. and Sham M.**, 2005. Conductive graphite nanoplatelet/epoxy nanocomposites: effects of exfoliation and UV/ozone treatment of graphite, *Scripta Materialia* **53**, 235–240

- [224] **Zheng W. and Wong S.**, 2003. Electrical conductivity and dielectric properties of PMMA/expanded graphite composites *Composites Science and Technology*, **63**, 225-235.
- [225] **Iijima, S.** 1991. Helical microtubules of graphitic carbon. *Nature.*, **354**, 56-58.
- [226] **Dresselhaus MS, Dresselhaus G, Eklund PC**, 1996. editors. Science of fullerenes and carbon nanotubes. San Diego: Academic Press.
- [227] **Iijima S., Ichihashi T.**, 1993. Single-shell carbon nanotubes of 1-nm diameter. *Nature* 363, 603-605.
- [228] **E.W. Wong, P.E. Sheehan, C.M. Lieber**, Science 277 (1997) 1971
- [229] **M.S. Dresselhaus, G. Dresselhaus, P. Avouris**, Top. Appl. Phys. 80 (2001)
- [230] **P.M. Ajayan and O.Z. Zhou**, Application of carbon nanotubes. In: M.S. Dresselhaus, G. Dresselhaus and P. Avouris, Editors, Carbon nanotubes synthesis, structure, properties and applications, Springer-Verlag, Berlin (2000), pp. 391–425.
- [231] **Soutar I, Swanson L, Davidson K, et al.** “Photophysics of Carbazole-Containing Systems. 2. Fluorescence Behavior of Poly(N-Vinyl Carbazole) and N -Vinyl Carbazole/Methyl Acrylate Copolymer Films”, High Performance Polymers 1997; 9.353-367
- [232] **Holzinger M., Abraham J., Whelan P., Graupner R., Ley L. and Hennrich F. et al.**, 2003. Functionalization of single-walled carbon nanotubes with (R-)oxycarbonyl nitrenes, *J Am Chem Soc* **125** , 8566–8580.
- [233] **Peng H., Alemany L.B., Margrave J.L. and Khabashesku V.N.**, 2003. Sidewall carboxylic acid functionalization of single-walled carbon nanotubes, *J Am Chem Soc* **125**, 15174–15182
- [234] **Jiang L., Gao L. and Sun J.**, 2003 Production of aqueous colloidal dispersions of carbon nanotubes, *J Colloid Interface Sci* **260**, 89–94.
- [235] **Zhu J., Kim J.D., Peng H., Margrave J.L., Khabashesku V.N. and Barrera E.V.**, 2003. Improving the dispersion and integration of single-walled carbon nanotubes in epoxy composites through functionalization, *Nano Lett* **3**, 1107–1113.
- [236] **Kuzmany H., Kukovecz A., Simon F., Holzweber M., Kramberger Ch. and Pichler T.**, 2004. Functionalization of carbon nanotubes, *Synth Metals* **141**, 113–122.
- [237] **Z.H. Yu and L.E. Brus**, 2000. Reversible oxidation effect in Raman scattering from metallic single-wall carbon nanotubes, *J Phys Chem A*, **104**, 10995–10999.
- [238] **A. Kuznetsova, I. Popova, J.T. Yates, M.J. Bronikowski, C.B. Huffman and J. Liu et al.**, 2001. Oxygen-containing functional groups on single-wall carbon nanotubes: NEXAFS and vibrational spectroscopic studies, *J Am Chem Soc* **123**, 10699–10704.
- [239] **Kukovecz A., Kramberger C., Holzinger M., Kuzmany H., Schalko J. and Mannsberger M. et al.**, 2002. On the stacking behavior of functionalized single-wall carbon nanotubes, *J Phys Chem B*, **106**, 6374–6380.

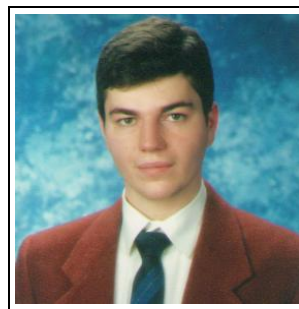
- [240] **Mawhinney D.B., Naumenko V., Kuznetsova A., Yates J.T., Liu J. and Smalley R.E.**, 2000. Surface defect site density on single walled carbon nanotubes by titration, *Chem Phys Lett* **324**, 213–216.
- [241] **Hu H., Bhowmik P., Zhao B., Hamon M.A., Itkis M.E. and Haddon R.C.**, 2001. Determination of the acidic sites of purified single-walled carbon nanotubes by acid–base titration, *Chem Phys Lett* **345**, 25–28.
- [242] **Rosca I. D., Watari F., Uo M. and Akasaka T.** 2005. Oxidation of multiwalled carbon nanotubes by nitric acid. *Carbon*, **43**, 3124–3131.
- [243] **Li Y.H., Xu C., Wei B., Zhang X., Zheng M. and Wu D. et al.**, 2002. Self-organized ribbons of aligned carbon nanotubes, *Chem Mater* **14**, 483–485.
- [244] **Kim B. and Sigmund W.M.**, 2003. Self-alignment of shortened multiwall carbon nanotubes on polyelectrolyte layers, *Langmuir* **19**, 4848–4851.
- [245] **Chen J., Hamon M.A., Hu H., Chen Y., Rao A.M. and Eklund P.C. et al.**, 1998. Solution properties of single-walled carbon nanotubes, *Science* **282**, 95–98.
- [246] **Liu Y., Rinzler A.G., Dai H., Hafner J.H., Bradley R.K. and Boul P.J. et al.**, 1998. Fullerene pipes. *Science* **280**, 1253–1256.
- [247] **Balasubramanian K. and Burghard M.**, 2005. Chemically functionalized carbon nanotubes, *Small* **1**, 180–192.
- [248] **Ramanathan T., Fisher F.T., Ruoff R.S. and Brinson L.C.**, 2005. Amino-functionalized carbon nanotubes for binding to polymers and biological systems, *Chem Mater* **17**, 1290–1295.
- [249] **Baibarac M., Gómez-Romero P.**, 2006. Nanocomposites based on conducting polymers and carbon nanotubes: from fancy materials to functional applications. *J Nanosci Nanotechnol.* **6**, 289–302.
- [250] **Bertoncello P., Notargiacomo A., Erokhin V. and Nicolini C.**, 2006. Functionalization and photoelectrochemical characterization of poly[3-3(vinylcarbazole)] multi-walled carbon nanotube (PVK-MWNT) Langmuir–Schaefer films. *Nanotechnology* **17**, 699–705.
- [251] **Liu G., Ling Q., Teo E. Y. H., Zhu C.-X., Chan D. S.-H., Neoh K.-G., and Kang E.-T.**, 2009. Electrical Conductance Tuning and Bistable Switching in Poly(Nvinylcarbazole) Carbon Nanotube Composite Films *ACS NANO*, **3**, 1929–1937.
- [252] **Fan, J., Wan, M., Zhu, D., Chang, B., Pan, Z., Xie, S.** 1999. Synthesis and properties of carbon nanotube-polypyrrole composites. *Synth. Met.*, **102**, 1266–1267.
- [253] **Cochet, M., Masser, W. K., Benito, A. M., Callejas, M. A., Martinez, M. T., Benoit, J. M., Schreiber, J., Chauvet, O.** 2001. Synthesis of a new polyaniline/nanotube composite: “in-situ” polymerisation and charge transfer through site-selective interaction. *Chem. Commun.*, 1450–1451.

- [254] **Natori I**, 2006. Anionic Polymerization of *N*-Vinylcarbazole with Alkylolithium as an Initiator. *Macromolecules*, **39**, 6017-6024.
- [255] **M. Baibarac, I. Baltog, S. Lefrant, J. Y. Mevellec, O. Chauvet**, 2003. Polyaniline and carbon nanotubes based composites containing whole units and fragments of nanotubes, *Chem. Mater.*, **15**, 4149–4156.
- [256] **Martin, C. A., Sandler, J. K. W., Shaffer, M. S. P., Schwarz, M. K., Bauhofer, W., Schulte, K., Windle, A. H.** 2004. Formation of percolating networks in multi-wall carbon-nanotube–epoxy composites. *Compos. Sci. Technol.* **64**, 2309-2316
- [257] **Tamburri, E., Orlanducci, S., Terranova, M. L., Valentini, F., Palleschi, G., Curulli, A., Brunetti, F., Passeri, D., Alippi, A., Rossi, M.** 2005. Modulation of electrical properties in single-walled carbon nanotube/conducting polymer composites. *Carbon*, **43**, 1213-1221.
- [258] **Shaffer M. S. P., Fan X. and Windle A. H.**, 1998. Dispersion and packing of carbon nanotubes. *Carbon*, **36**, 1603-1612.
- [259] **Bae J., Jang J. and. Yoon S.-H**, 2002. Cure behavior of the liquid-crystalline epoxy/carbon nanotube system and the effect of surface treatment of carbon fillers on cure reaction. *Macromol. Chem. Phys.*, **203**, 2196-2204.
- [260] **Gandini A. and Plesch P.**, 1966. Spectroscopic studies on carbonium ions derived from aromatic olefins. Part II. Acenaphthylene, *N*-vinylcarbazole, and tetraphenylethylene. *J Chem Soc, Part B*, **14**, 7-10.
- [261] **Tsubokawa N. and Yoshihara T.**, 1991. Carbon Whiskers as an Initiator of Cationic Polymerization of *N*-vinylcarbazole and *N*-vinyl-2-pyrrolidone. *Polym J*, **23**, 177-183.
- [262] **Tsubokawa N., Inagaki M., Kubota H. and Endo T.** 1993. γ -poly (glutamic acid) as an initiator of cationic polymerization of *N*-vinylcarbazole and *N*-vinyl-2-pyrrolidone. *J Polym Sci, Part A: Polym Chem* **31**, 3193-3198.
- [263] **Maity A., Ray S.S.** 2009. The effect of the carbon nanotubes surface oxidation on the morphology and properties of poly(*N*-vinylcarbazole) coated multi-walled carbon nanotube nanocables *Synthetic Metals* **159**, 1158–1164.
- [264] **Aharoni, S. M.** 1972. Electrical Resistivity of a Composite of Conducting Particles in an Insulating Matrix. *J Appl Phys*, **43**, 2463–2465.
- [265] **Ishigure, Y., Iijima, S., Ito, H., Ota, T., Unuma, H., Takahashi, M., Hikichi, Y., Suzuki, H.** 1999. Electrical and elastic properties of conductor-polymer composites. *J Mater Sci*, **34**, 2979–2985.
- [266] **Feng, J., Chan, C.-M.** 1998. Carbon black-filled immiscible blends of poly(vinylidene fluoride) and high density polyethylene: Electrical properties and morphology. *Polym Eng Sci*, **38**, 1649–1657
- [267] **Semko, L. S., Popov, R. E., Chernysh, I. G.** 1997. Electrical properties of composites based on polypropylene and thermally expanded graphite. *Int Polym Sci Technol*, **24**, 71–74.

- [268] **Wu, G., Asai, S., Sumita, M.** 1999. A self-assembled electric conductive network in short carbon fiber filled poly (methyl methacrylate) composites with selective adsorption of polyethylene. *Macromolecules* **32**, 3534–3536.
- [269] **D’Ilario, L., Martinelli, A.** 1991. Electrical behaviour of poly (p-phenylene sulphide) conducting composites. *J Mater Sci Lett*, **10**, 1465–1467
- [270] **Xu, C., Bin, Y., Agari, Y., Matsuo, M.** 1998. Morphology and electric conductivity of cross-linked polyethylene–carbon black blends prepared by gelation/crystallization from solutions. *Colloid Polym Sci*, **276**, 669–679.
- [271] **Miyasaka, K., Watanabe, K., Jojima, E., Aida, H., Sumita, M., Ishikawa, K.** 1982. Electrical conductivity of carbon-polymer composites as a function of carbon content. *J Mater Sci*, **17**, 1610–1616.
- [272] **Sumita, M., Abe, H., Kayaki, H., Miyasaka, K.,** 1986. Effect of melt viscosity and surface tension of polymers on the percolation threshold of conductive-particle-filled polymeric composites. *J Macromol Sci Phys*, **25**, 171–184.
- [273] **Lundberg, B., Sundqvist, B.** 1986. *Resistivity of a composite conducting polymer as a function of temperature, pressure, and environment: Applications as a pressure and gas concentration transducer.* *J Appl Phys*, **60**, 1074–1079
- [274] **Semko, L. S., Popov, R. E., Chernysh, I. G.** 1997. Electrical properties of composites based on polypropylene and thermally expanded graphite. *Int Polym Sci Technol*, **24**, 71–74.
- [275] **Pan, Y., Yu, Z., Ou, Y., Hu, G.** 2000. A new process of fabricating electrically conducting nylon 6/graphite nanocomposites via intercalation polymerization. *J Polym Sci Part B: Polym Phys* **38**, 1626–1633.
- [276] **PAN Y.X., YU Z. Z., OU Y.C. and FENG Y. P .,** *Polym. Acta (Chinese)* **1** (2001) 42.
- [277] **Sandler, J. K. W.; Kirk, J. E.; Kinloch, I. A.; Shaffer, M. S. P.; Windle, A. H.** 2003. *Polymer*, **44**, 5893-5899.
- [278] **Nair S.S. and Khadar M.A.** 2008. Dc conductivity of consolidated nanoparticles of zinc sulfide *Sci. Technol. Adv. Mater.* **9**, 1-4.
- [279] **Samuel P. Kounaves** Chapter 37 Voltammetric Techniques Tufts University Department of Chemistry.
- [280] **Li Z, Yu G, Dong S, Wu W, Liu Y, Ye C, Qin J, Li Z,** “The role of introduced isolation groups in PVK-based nonlinear optical polymers: Enlarged nonlinearity, improved processibility, and enhanced thermal stability”, *Polymer* 2009; **50**.2806-2814
- [281] **Biswas M, Ray SS,** 1998. Preparation and evaluation of composites from montmorillonite and some heterocyclic polymers.1.Poly(N-vinylcarbazole)-montmorillonite nanocomposite system. *Polymer*; **39**, 6423-6428

- [28] **Sitaramaiah G, Jacobs D**, 1970. Solution properties of poly-N-vinyl carbazole” *Polymer*; **11**, 165-176.
- [282] **Lu X.L., Mi Y.L.**, 2005. Characterization of the Interfacial Interaction between Polyacrylamide and Silicon Substrate by Fourier Transform Infrared Spectroscopy” *Macromolecules*; **38**, 839-843.
- [283] **Park, S.-M.; Yoo, J.-S.** 2003. Electrochemical Impedance Spectroscopy for Better Electrochemical Measurements. *Anal. Chem.*, **75**, 455-461.
- [284] **Bard A.J., Faulkner L.R.**, 1980. *Electrochemical Methods: Fundamental and Applications*, Wiley, New York, USA.
- [285] **Wang J.**, 2000. *Analytical Electrochemistry*, 2nd ed., Wiley/VCH, New York,.
- [286] **Bockris J.O.M., Reddy A.K.N., Gamboa-Aldeco M.**, 2000. *Modern Electrochemistry 2A: Fundamentals of Electrode Processes*, vol. 2, 2nd ed., Kluwer Academic/Plenum Publishers, New York.
- [287] **Bard A.J., Faulkner L.R.**, 2001. *Electrochemical Methods: Fundamentals and Applications*, 2nd ed., John Wiley & Sons, New York.
- [288] **Macdonald J.R.** 1987. (Ed.), *Impedance Spectroscopy Emphasizing Solid Materials & Systems*, John Wiley & Sons, New York.

CURRICULUM VITAE



Candidate's full name: Argun Talat GÖKÇEÖREN
Place and date of birth: 19.07.1975
Permanent Address: Güzelkent Hukukçular Sitesi, Huzur sok No:2,
Büyükcemece - İstanbul

Universities and

Colleges attended: Istanbul Technical University (ITU)

Publications:

- Erbil C., **Gökçeören A. T.**, Sezer E., (2007): "Binary and ternary Copper(II) complexes with NIPAAm/IA copolymers and aminoacids: Interpretation of UV-visible spectra and cyclic voltammograms", J. of Macromolecular Sc. Part A: Pure&App. Chem. 44, 525-534
- Erbil C., **Gökçeören A. T.** & Polat Y. O., (2007): "N-isopropylacrylamide-acrylamide copolymer initiated by ceric ammonium nitrate in water", Polymer International, 56, 547-556
- **Gökçeören A. T.**, Erbil C., Sezer E. (2007): "Voltammetric Investigation of Polyelectrolyte-Cu(II) Complexes" J. App. Electroch., 37, 941-948
- Erbil C., Terlan B., Akdemir Ö., **Gökçeören A. T.**, (2009): "Monomer reactivity ratios of N-isopropylacrylamide-itaconic acid copolymers at low and high conversions, Eur. Pol. J. 45, 1728-1737
- **Gökçeören A. T.**, Erbil C., Sezer E., Saraç A. S. (2009) "Copolymers of N-vinylcarbazole with Acrylic Acid, Itaconic Acid, and N-isopropylacrylamide: Synthesis, Determination of Monomer Reactivity Ratios, and Electrochemical Properties" 14, 140-159
- Yumakgil K., **Gökçeören A. T.**, Erbil C., (2010): "Effects of TEMED and EDTA on the Structural and Mechanical Properties of NIPAAm / Na⁺MMT Composite Hydrogels" J. Pol. Sc. Part B: Pol. Phys. 48, 1256-1264.
- Erbil C., Topuz D., **Gökçeören A. T.** ve Şenkal F. "Network parameters of poly(N-isopropylacrylamide)/ montmorillonite hydrogels: effects of accelerator and clay content", Pol. Adv. Tech. (in press)
- **Gökçeören A. T.** and Erbil C. "Morphological characterization and electrochemical/electrical properties of poly(N-vinyl carbazole) / montmorillonite composites" J. Pol. Sc. Part B: Pol. Phys. (submitted)
- **Gökçeören A. T.** and Erbil C. "Electrochemical impedance spectroscopy and in-

situ UV-vis spectroelectrochemistry studies of Poly(N-vinyl carbazole) / Polydimethylsiloxane composite electrodes” Surf. Int. Anal. (submitted)

▪ **Gökçeören A.T.**, Yumakgil K. and Erbil C. “ Poly(N-vinyl carbazole) (PNVCz) based composite materials: electrical properties, morphologic and thermal characterization of PNVCz/ multiwalled carbon nanotube and PNVCz/graphite systems” J. Pol. Sc. Part B: Pol. Phys. (submitted)